Inspection and monitoring techniques for bridges and civil structures

Related titles:

Analysis and design of plated structures, Volume 1: Stability
(ISBN-13: 978-1-85573-967-3; ISBN-10: 1-85573-967-4)
Steel-plated structures are used in a variety of marine and land-based applications such as ships, off-shore platforms, power and chemical plants, box-girder cranes and bridges. This major new book will provide the first authoritative survey on the stability, analysis and design of plated structures particularly laminated plates, tapered steel members, concrete-filled tubular columns and stiffened composite structures. It will be a valuable source of reference for all those in mechanical, civil and structural engineering.

Corrosion in reinforced concrete structures
(ISBN-13: 978-1-85573-768-6; ISBN-10: 1-85573-768-X)
In this authoritative new book the fundamental aspects of corrosion in concrete are analysed in detail. An overview of current monitoring techniques together with a discussion of practical applications and current numerical methods that simulate the corrosion process provides the civil and structural engineer with an invaluable guide to best practice when it comes to design aimed at minimising the effects of corrosion in concrete. The corrosion protective properties of concrete and modified cements are also discussed.

The deformation and processing of structural materials
(ISBN-13: 978-1-85573-738-9; ISBN-10: 1-85573-738-8)
This new study focuses on the latest research in the performance of a wide range of materials used in the construction of structures, particularly structural steels. It considers each material's processing and its deformation behaviour in structural applications. This book will be the first to give such comprehensive coverage to the deformation and processing of all types of structural materials and will be a valuable resource for researchers in mechanical, civil and structural engineering.

Details of these and other Woodhead Publishing materials books and journals, as well as materials books from Maney Publishing, can be obtained by:

- visiting our web site at www.woodheadpublishing.com
- contacting Customer Services (e-mail: sales@woodhead-publishing.com; fax: +44 (0) 1223 893694; tel.: +44 (0) 1223 891358 ext. 30; address: Woodhead Publishing Ltd, Abington Hall, Abington, Cambridge CB1 6AH, England)

If you would like to receive information on forthcoming titles, please send your address details to: Francis Dodds (address, tel. and fax as above; email: francisd@woodhead-publishing.com). Please confirm which subject areas you are interested in.

Maney currently publishes 16 peer-reviewed materials science and engineering journals. For further information visit www.maney.co.uk/journals.

Inspection and monitoring techniques for bridges and civil structures

Edited by

Gongkang Fu

Woodhead Publishing and Maney Publishing
on behalf of
The Institute of Materials, Minerals & Mining

CRC Press
Boca Raton Boston New York Washington, DC

WOODHEAD PUBLISHING LIMITED
Cambridge England

Woodhead Publishing Limited and Maney Publishing Limited on behalf of
The Institute of Materials, Minerals & Mining

Published by Woodhead Publishing Limited, Abington Hall, Abington
Cambridge CB1 6AH, England
www.woodheadpublishing.com

Published in North America by CRC Press LLC, 6000 Broken Sound Parkway, NW,
Suite 300, Boca Raton, FL 33487, USA

First published 2005, Woodhead Publishing Limited and CRC Press LLC
© 2005, Woodhead Publishing Limited, except Chapter 1 which is © The Crown in Right of Canada.
The authors have asserted their moral rights.

This book contains information obtained from authentic and highly regarded sources. Reprinted material is quoted with permission, and sources are indicated. Reasonable efforts have been made to publish reliable data and information, but the authors and the publishers cannot assume responsibility for the validity of all materials. Neither the authors nor the publishers, nor anyone else associated with this publication, shall be liable for any loss, damage or liability directly or indirectly caused or alleged to be caused by this book.

Neither this book nor any part may be reproduced or transmitted in any form or by any means, electronic or mechanical, including photocopying, microfilming and recording, or by any information storage or retrieval system, without permission in writing from Woodhead Publishing Limited.

The consent of Woodhead Publishing Limited does not extend to copying for general distribution, for promotion, for creating new works, or for resale. Specific permission must be obtained in writing from Woodhead Publishing Limited for such copying.

Trademark notice: Product or corporate names may be trademarks or registered trademarks, and are used only for identification and explanation, without intent to infringe.

British Library Cataloguing in Publication Data
A catalogue record for this book is available from the British Library.

Library of Congress Cataloging in Publication Data
A catalog record for this book is available from the Library of Congress.

Woodhead Publishing ISBN-13: 978-1-85573-939-0 (book)
Woodhead Publishing ISBN-10: 1-85573-939-9 (book)
Woodhead Publishing ISBN-13: 978-1-84569-095-3 (e-book)
Woodhead Publishing ISBN-10 1-84569-095-8 (e-book)
CRC Press ISBN 0-8493-9544-5
CRC Press order number: WP9544

The publishers' policy is to use permanent paper from mills that operate a sustainable forestry policy, and which has been manufactured from pulp which is processed using acid-free and elementary chlorine-free practices. Furthermore, the publishers ensure that the text paper and cover board used have met acceptable environmental accreditation standards.

Typeset by SNP Best-set Typesetter Ltd., Hong Kong
Printed by TJ International Limited, Padstow, Cornwall, England

Contents

	Contributor contact details	ix
1	Testing steel corrosion in reinforced concrete S. Qian, National Research Council Canada, Canada	1
1.1	Introduction	1
1.2	Electrochemical techniques	1
1.3	Physico-chemical techniques	15
1.4	Conclusions	18
1.5	References	18
2	Alkali–silica reaction (ASR) testing of deterioration in concrete V. Jensen, Norwegian Concrete and Aggregate Laboratory Ltd, Norway	22
2.1	Introduction	22
2.2	Understanding the reaction	23
2.3	Diagnosis, investigation and monitoring	26
2.4	Case histories	40
2.5	Trends in analysing and preventing ASR	54
2.6	Conclusions	57
2.7	Sources of information	58
2.8	References	59
3	Acoustic testing of concrete bridge decks R.D. Costley, Miltec Corporation, USA	64
3.1	Introduction	64

3.2 Manual techniques 65
3.3 Electro-mechanical sounding 68
3.4 Automated chain drag system (ACDS) 69
3.5 Conclusions 80
3.6 Acknowledgements 80
3.7 References 81

4 Electrical impedance testing of wood components 83
M. Tiitta, University of Kuopio, Finland

4.1 Introduction 83
4.2 Background 83
4.3 Advantages and limitations 87
4.4 Equipment and procedure 88
4.5 Wood moisture gradient inspection 91
4.6 Wood decay inspection 94
4.7 Future research and development 96
4.8 Conclusions 97
4.9 References 97

5 Detecting decay in wood components 100
R.J. Ross, USDA Forest Products Laboratory, USA and X. Wang and B.K. Brashaw, Natural Resources Research Institute, USA

5.1 Introduction 100
5.2 Conventional methods 101
5.3 Stress wave propagation method 105
5.4 Case studies 111
5.5 Future research and development 113
5.6 Conclusions 113
5.7 References 114

6 Testing timber pile length in bridges 115
A.K. Pandey, EDM International Inc., USA and R.W. Anthony, Anthony & Associates Inc., USA

6.1 Introduction 115
6.2 Background 115
6.3 Use of longitudinal stress waves 117
6.4 Pile length determination 120
6.5 Case studies 124
6.6 Future research and development 129

6.7 Conclusions 131
6.8 References 131

7 Ultrasonic testing of structural timber components 133
T.L. Shaji, College of Engineering – Trivandrum, India

7.1 Introduction 133
7.2 Properties of wood 134
7.3 Wood deterioration 135
7.4 Ultrasonic pulse velocity technique 136
7.5 Laboratory investigations 138
7.6 In-service evaluation 140
7.7 Future research and development 145
7.8 Conclusions 145
7.9 Acknowledgements 146
7.10 References 147

8 Digital radioscopy analysis of timber structures 149
R.W. Anthony, Anthony & Associates Inc., USA

8.1 Introduction 149
8.2 Physics of X-rays 150
8.3 History of wood building radiography 152
8.4 Equipment for investigating timber structures 153
8.5 Case studies 156
8.6 Future research and development 163
8.7 Conclusions 163
8.8 References 164

9 Visual inspection techniques for bridges and other transportation structures 166
B.M. Phares, Iowa State University Bridge Engineering Center, USA

9.1 Introduction 166
9.2 History of structural inspection in the USA 166
9.3 Types of visual inspection 169
9.4 Qualifications of inspectors 171
9.5 Inspection tools 172
9.6 Reliability and accuracy of visual inspection of highway bridges 174
9.7 Conclusions 180

9.8	Acknowledgements	181
9.9	References	181
10	Acoustic emission testing of bridges K.M. Holford and R.J. Lark, Cardiff University, UK	183
10.1	Introduction	183
10.2	The role of acoustic emission in bridge monitoring	183
10.3	Acoustic emission theory	189
10.4	Practical techniques	199
10.5	Sources of information and advice	210
10.6	Conclusions	212
10.7	Acknowledgements	212
10.8	References	213
11	Bridge inspection using virtual reality and photogrammetry D.V. Jáuregui and K.R. White, New Mexico State University, USA	216
11.1	Introduction	216
11.2	Bridge inspection via virtual reality	217
11.3	Bridge monitoring via photogrammetry	226
11.4	Potential impact and future developments	240
11.5	References	244
12	Discontinuity in masonry walls M. Pieraccini, University of Florence, Italy	247
12.1	Introduction	247
12.2	Impact echo	248
12.3	Sonic tomography	250
12.4	Thermography	252
12.5	Penetrating radar	253
12.6	Thermal, mechanical or electromagnetic: what kind of energy for detecting discontinuity in masonry?	260
12.7	References	263
	Index	265

Contributor contact details

(* indicates main point of contact)

Editor
Professor Gongkang Fu
Director, Center for Advanced Bridge Engineering
Department of Civil and Environmental Engineering
Wayne State University
Detroit
Michigan
MI 48202-3939
USA

E-mail: gfu@eng.wayne.edu

Chapter 1
Dr Shiyuan Qian
Institute for Research in Construction
National Research Council of Canada
1200 Montreal Road
Ottawa
Ontario
K1A 0R6
Canada

E-mail: shiyuan.qian@nrc-cnrc.gc.ca

Chapter 2
Dr Viggo Jensen
Norwegian Concrete and Aggregate Laboratory Ltd
Osloveien 18B
N-7018 Trondheim
Norway

E-mail: viggo.jensen@nbtl.no

Chapter 3
Dr R. Daniel Costley
Miltec Corporation
Oxford Enterprise Center
9 Industrial Park
Oxford
MS 38655
USA

E-mail: dcostley@miltecresearch.com

Chapter 4
Dr Markku Tiitta
University of Kuopio
PO Box 1627
Savilahdentie 9

70211 Kuopio
Finland

E-mail: Markku.Tiitta@uku.fi

Chapter 5

Dr Robert J. Ross*
USDA Forest Products Laboratory
1 Gifford Pinchot Drive
Madison
WI 53707-2398
USA
E-mail: rjross@fs.fed.us

Dr Xiping Wang and Brian K. Brashaw
Natural Resources Research Institute
University of Minnesota Duluth
Duluth
MN 55811-1442
USA

Chapter 6

Dr Arun K. Pandey
EDM International Inc
4001 Automation Way
Fort Collins
CO 80525-3479
USA

E-mail: apandey@edmlink.com

Ronald W. Anthony*
Anthony & Associates Inc.
PO Box 271400
Fort Collins
CO 80527-1400
USA

E-mail: woodguy@anthony-associates.com

Chapter 7

Prof. T.L. Shaji
Department of Architecture
College of Engineering
Trivandrum-695016
Kerala
India

E-mail: tlshaji@hotmail.com

Chapter 8

Ronald W. Anthony
Anthony & Associates Inc.
PO Box 271400
Fort Collins
CO 80527-1400
USA

E-mail: woodguy@anthony-associates.com

Chapter 9

Prof. Brent M. Phares
Iowa State University
Bridge Engineering Center
2901 South Loop Drive, Suite 3100
Ames, IA 50010-8632
USA

E-mail: bphares@iastate.edu

Chapter 10

Dr K.M. Holford* and R.J. Lark
Cardiff School of Engineering
Cardiff University
Queens Buildings
5 The Parade
Cardiff
CF24 3AA
UK

E-mail: Holford@cardiff.ac.uk

Chapter 11
Prof. David V. Jáuregui* and
Prof. Kenneth R. White
Department of Civil Engineering
New Mexico State University
PO Box 30001, MS 3CE
Las Cruces
NM 88003
USA

E-mail: jauregui@nmsu.edu

Chapter 12
Prof. Massimiliano Pieraccini
Department of Electronics and
Telecommunications
University of Florence
Via Santa Marta, 3
50139 Florence
Italy

E-mail: massimiliano.pieraccini@
unifi.it

1

Testing steel corrosion in reinforced concrete

S. QIAN
National Research Council Canada, Canada

1.1 Introduction

Corrosion of reinforcing steel is the main cause of deterioration of reinforced concrete structures and has received increased attention because of its widespread occurrence and the high costs of repair associated with it. The total cost of corrosion in reinforced concrete structures amounts to billions of dollars annually. Effective condition assessment techniques are necessary to detect corrosion in its early stages, evaluate its extent and implement appropriate and cost-effective protection and repair measures. A number of techniques or devices have been developed to facilitate the assessment of corrosion in reinforced concrete structures. They can provide rapid, cost-effective and non-destructive evaluation of reinforcement corrosion and very important information regarding the corrosion damage in existing concrete structures. In order to obtain an accurate and reliable assessment of the state of corrosion damage, engineers and bridge inspectors often have to gather information from different corrosion evaluation techniques. The selection and application of different techniques to identify corrosive environments and active corrosion in concrete structures with non-prestressed reinforcement depend upon the resources available and the specific condition of the structure. These techniques and methods will be discussed in the following two sections: (1) electrochemical techniques and (2) physico-chemical techniques.

1.2 Electrochemical techniques

1.2.1 Corrosion of steel in concrete structures

The corrosion of steel in concrete is an electrochemical process that involves the transfer of electrons from one chemical species to another. The reactions involving consumption of metal and release of electrons are referred to as anodic:

$$Fe \rightarrow Fe^{2+} + 2e^{-} \quad [1.1]$$

The Fe^{2+} ions react with OH^{-} to form ferrous hydroxide:

$$Fe^{2+} + 2OH^{-} \rightarrow Fe(OH)_2 \quad [1.2]$$

The $Fe(OH)_2$ can further react with oxygen to form various oxide species such as hydrated ferric oxide ($Fe_2O_3 \cdot H_2O$) and hydrated magnetite ($Fe_3O_4 \cdot H_2O$), depending on pH and oxygen availability:

$$4Fe(OH)_2 + O_2 \rightarrow 2Fe_2O_3 \cdot H_2O + 2H_2O \quad [1.3]$$

$$6Fe(OH)_2 + O_2 \rightarrow 2Fe_3O_4 \cdot H_2O + 4H_2O \quad [1.4]$$

Reactions involving consumption of electrons and dissolved chemical species are referred to as cathodic. They probably incorporate the following steps depending on the availability of oxygen, pH of the cement paste pore solution, and electrochemical potential:

$$2H_2O + O_2 + 4e^{-} \rightarrow 4OH^{-} \quad [1.5]$$

$$2H_2O + 2e^{-} \rightarrow 2OH^{-} + H_2 \quad [1.6]$$

Whenever spontaneous corrosion occurs, all the electrons released in the anodic reaction are consumed in the cathodic reaction; no excess or deficiency is found. Therefore no net current can be measured externally. Moreover, the metal normally takes up a more or less uniform electrode potential, often called the corrosion or mixed potential (E_{corr}). The corresponding rate of metal dissolution at this potential is referred to as the corrosion rate (i_{corr}).

1.2.2 Corrosion potential mapping

Since the early 1980s, the corrosion potential measurement method for identifying corrosion in reinforcing steel bars in concrete has been widely used owing to its simplicity and cost effectiveness[1,2] and growing confidence in the success of bridge deck corrosion surveys. This method allows evaluation of the probability of corrosion activity through the measurement of the potential difference between a standard portable reference electrode (RE), normally a copper/copper sulphate reference electrode (CSE), and the reinforcing steel. The results can be represented as equipotential lines that allow the location of corroding rebars at the most negative values. This work formed the basis of the ASTM standard C876-91, which provides general guidelines for evaluating corrosion in concrete structures as described in Table 1.1. These criteria were developed empirically in the USA for concrete bridges[3] and have been found applicable in Europe where there has been exposure to de-icing salts.[4]

Table 1.1 Probability of corrosion according to corrosion potentials

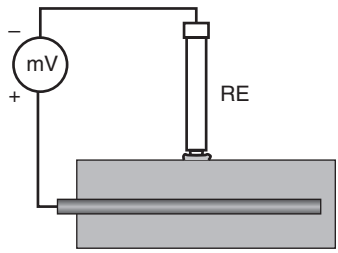
Corrosion potential *vs* CSE	Corrosion activity
Less negative than –0.2 V	90% probability of no corrosion
Between –0.2 and –0.35 V	Corrosion activity is uncertain
More negative than –0.35 V	90% probability of corrosion

The procedure for corrosion potential measurement is quite simple. The voltage between a portable CSE placed on the surface of the concrete and the reinforcing steel bar located below the surface is measured and plotted as an equipotential contour map, which is compared with values that have been empirically developed to indicate relative probabilities of corrosion. A sponge wetted by a 1% solution of detergent is attached to the tip of the portable reference electrode to reduce the contact resistance as shown in Fig. 1.1. A voltmeter or data logger with input impedance between 10^7 ohms (for normal outdoor concrete) and 10^{10} ohms (for dry concrete) should be used for the corrosion potential measurement.

Corrosion potential surveys should be carried out on a regular interval grid depending on the size of the structure. Before starting the potential survey, the electrical continuity of the reinforcing steel in the structure needs to be established for each surveyed area. A common ground point can be established by exposing an area on the reinforcing steel and drilling a hole in the bar. A self-tapping screw is then driven into the hole and the test lead wire is clamped to the screw to achieve a good connection. Attach any pair of the reinforcement connections to an ohmmeter, and if the continuity is good, the resistance should be less than 1 ohm. The measured corrosion potential should be steady or drifting steadily in one direction. The common reading should be in the range of –700 mV and 0 mV *vs* CSE. If a reading falls outside this range or fluctuates randomly, it is probably caused by a loss of electrical continuity and should be investigated.

Several commercial instruments that record and store multiple potential readings simultaneously can speed up corrosion potential surveys over large areas. For some devices equipped with wheel electrodes, potentials are recorded in a data logger as the wheels are rolled along the concrete surface.[5]

Theoretical considerations and practical experience on a large number of structures have shown that the results of potential mapping on existing structures require careful interpretation because many conditions can affect the measured corrosion potentials, which include: (1) water saturation in concrete (availability of oxygen); (2) electrical discontinuity of the reinforcing steel grid; (3) presence of stray currents; (4) carbonated concrete; (5)



1.1 Illustration of the corrosion potential measurement in reinforced concrete.

epoxy-coated or galvanized reinforcing steel; (6) chloride concentration; (7) electrical resistance; and (8) cover thickness of the concrete. In addition, the development of concrete and application of new repair technologies such as dense material, concrete sealers, corrosion inhibitors, concrete admixtures and the application of cathodic protection systems, etc. further complicates the interpretation of corrosion potentials. Hence, successful interpretations require extensive knowledge and experience under many complicated conditions. A simple comparison of corrosion potential data with the ASTM C876-91 guideline could lead to invalid interpretations.

When large areas have been surveyed and a sufficient number of potential readings have been taken, the potential values can be examined statistically. These values are represented as cumulative frequency distributions,[6] which give an indication of the amount of passive and active potential. This type of plot is particularly suitable for comparison purposes. Differences in corrosion potentials across a structure or in specific areas are often better indicators of the level of corrosion activity than the absolute potential values. For instance, a 1 m^2 area that has a potential variation of 100 mV is more active than a similar area with a 30 mV variation.

Studies on European bridge decks,[7] where waterproofing membranes were used or where de-icing salts were applied less frequently, have resulted in a different set of interpretive guidelines. Completely water saturated concrete can have 200–300 mV more negative potential values due to oxygen starvation.[8,9] Studies on carbonated concrete[10] have shown that the typical measured potential was in the range of –200 and –500 mV but with much lower potential gradients.

The best approach to the interpretation of corrosion potentials is to plot equipotential contours, estimate the background potential and potential gradient, and then look for areas with a higher potential gradient that are 200 mV more negative than the background potential value. In many cases, this method should be verified by other techniques such as the tests of corrosion rate, concrete cover and carbonation depth, analysis of resistivity and chloride content of the concrete, even taking cores in some representative

areas to verify the assessment results on the state of reinforcing steel corrosion.

1.2.3 Corrosion rate measurements

The corrosion rate of reinforcing steel can be determined by measuring the rate at which electrons are removed from steel in the anodic reactions. In many cases oxygen is not freely available at the metal surface, especially at the interface of steel and concrete; the cathodic reaction rate is often controlled by the rate of arrival of oxygen at the surface, referred to as mass transfer control, and attains a limiting value. The corrosion rate then approximates the limiting current for oxygen reduction.

As mentioned before, when spontaneous corrosion occurs, all the electrons released in the anodic reaction are consumed in the cathodic reaction. Therefore no net current can be measured externally. Several electrochemical techniques can be used for quantitative assessment of the corrosion rate in concrete including linear polarization resistance (LPR), AC impedance, galvanostatic pulse and Tafel extrapolation. Among these methods, LPR and galvanostatic pulse have been successfully used for corrosion rate measurements in the field.

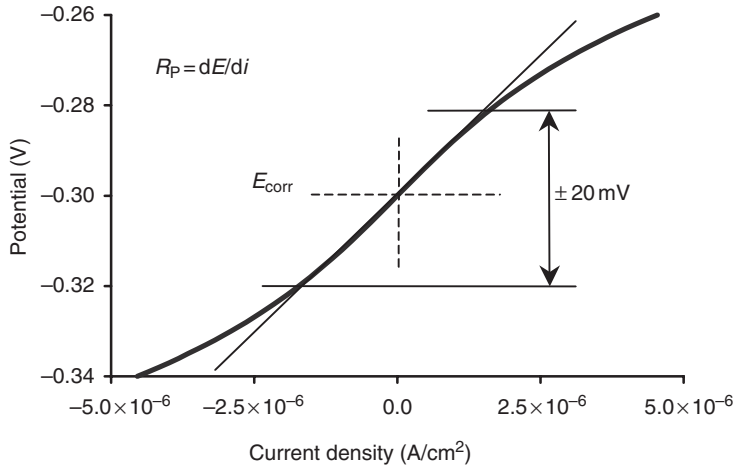
Linear polarization resistance (LPR)

The most extensively used method for evaluating rebar corrosion rates in concrete is the LPR measurement. This measurement can be performed by using permanently embedded reference electrodes (RE) and counter electrodes (CE)[2,11] or external electrodes placed on the concrete surface.[12] The LPR device applies a slow potential scan at a rate of 0.1–0.02 mV/s, from –20 to +20 mV versus corrosion potential, E_{corr}, to the steel via the CE and records the response current density or vice versa. The polarization resistance (or electrochemical resistance), R_P, of the measured steel is defined as the slope of a potential current density plot (as shown in Fig. 1.2) at the E_{corr} based on the Stern–Geary equation:

$$R_P = \left(\frac{\Delta E}{\Delta i}\right)_{E_{corr}} = -\frac{b_a b_c}{2.303 i_{corr}(b_a + b_c)} \quad [1.7]$$

$$\text{with} \qquad i_{corr} = K / R_P \quad [1.8]$$

where: R_P is expressed in ohm cm^2; ΔE and Δi are the changes of potential and current density (in V and A/cm^2, respectively) over a small potential range near the corrosion potential; E_{corr} and i_{corr} are the corrosion potential and corrosion current density, respectively; b_a and b_c are the Tafel slopes of anodic and cathodic polarization curves, respectively, and can be deduced by correlating the values of $\Delta E/\Delta i$ measured on the steel sample;



1.2 A linear polarization plot at $E_{corr} = -0.3$ V.

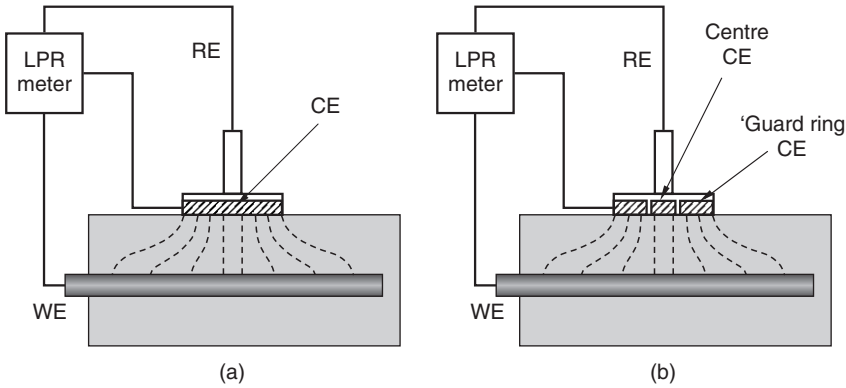
and K is a function of b_a and b_c (often a value from 0.026 to 0.052 is used for steel corrosion in concrete).

If uniform corrosion and a constant corrosion rate over time are assumed, i_{corr} can be converted to a rate of thickness loss (R_{TL}) according to Faraday's law as follows:

$$R_{TL}(\mu m / year) = \frac{3.3 i_{corr} M}{z d} \quad [1.9]$$

where i_{corr} is in μA/cm^2, z = ionic charge (2 for iron), M = atomic weight of metal (55.8 for iron) and d = density of steel (7.9 g/cm^3).

When reinforcing steel is polarized by a CE that is placed on the surface of the concrete, the polarized area is much larger than that of the CE and the current distribution on the steel is not precisely defined, as shown in Fig. 1.3(a). Therefore, it is difficult to calculate the effective polarized area and the corrosion current density. A 'guard ring' has been developed to define the current paths. A controlled current or potential was applied on the second CE (guard ring) which surrounded the first one to confine the current paths between the central CE and the steel working electrode (WE) as shown in Fig. 1.3(b). Thus, only the area polarized by the central CE is involved in the corrosion rate measurement and calculation.[13,14] Measurements made using the instrument equipped with 'guard ring' were found to be more accurate, especially when the corrosion rates were low.[15] However, it takes a longer time (2–5 min) to perform one measurement.



1.3 Experimental set-ups of LPR measurements with a normal CE (a) and the centre and 'guard ring' CE (b).

Several devices for measuring the corrosion rate of reinforcing steel in concrete based on the LPR technique are commercially available, such as Gecor (Qualitest International Inc.), PR Monitor (Cortest Columbus Technologies Inc.) and 3LP (K.C. Clear, Inc.). The first two are equipped with a 'guard ring' CE to confine the polarization current. The 3LP does not confine polarization current, but uses a large rectangular counter electrode (approximately 17.1 cm by 5 cm). The PR monitor applies a potential scan on the WE, while the other two apply current scans on the WE.

The investigation carried out by Flis and co-workers[16] showed that the values of corrosion rate measured by 3LP were larger than that measured by Gecor. They attributed this discrepancy to differences in the current confinement and the CE sizes. It has been reported in a separate investigation[15] that in the aggressive medium of chloride-containing specimens, the deviations from the average R_P for the Gecor device were below 100% and were about 2200% for the 3LP device, and in chloride-free specimens the deviations were about 1000% for the Gecor device and 6000–15 000% for the 3LP device. The large deviation from the average R_P indicates that even the use of a 'guard ring' does not guarantee confinement of the signal, especially for high-resistance concrete or passive reinforcing steel.

In addition there are still some difficulties associated with this technique including the following:

- When the steel surface is passivated, the Tafel slope is often difficult to determine. As a result the K value is very likely to be inaccurate and/or to change markedly as the steel surface condition changes.
- The electrochemical current at the fixed potential should be constant during the entire polarization period (steady state).

Table 1.2 Criteria of corrosion rate ($\mu A/cm^2$) for estimation of extent of corrosion for different devices

Extent of corrosion	i_{corr} applied to device with guard ring	i_{corr} applied to device without guard ring
Passive	$i_{corr} < 0.1$	$i_{corr} < 0.22$
Low to moderate	$0.1 < i_{corr} < 0.5$	$0.22 < i_{corr} < 1.08$
Moderate to high	$0.5 < i_{corr} < 1$	$1.08 < i_{corr} < 10.8$
High	$i_{corr} > 1$	$i_{corr} > 10.8$

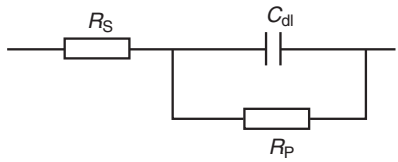
- The current distribution should be uniform around the steel bar.
- The effect of high electrical resistance of concrete should be precisely corrected.

However, these conditions are often difficult to achieve. Moreover, this technique measures only the instantaneous corrosion rates of the reinforcement; it does not necessarily reflect the long-term corrosion rate, which can fluctuate or change significantly in a very short time,[17] owing to changes in temperature, oxygen content and moisture content. It has been reported[18] that in the case of localized pitting, corrosion rates can be five to ten times greater than regular corrosion rates. The broad criteria for corrosion have been developed from field and laboratory investigations[17,19] with the different devices as shown in Table 1.2.

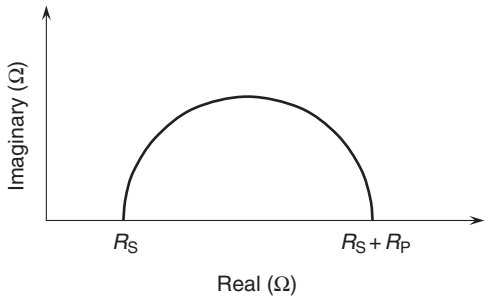
After laboratory and field testing and comparison, it can be concluded that even with the previously mentioned difficulties and an ineffective 'guard ring' CE under some conditions, the LPR technique is one of the most successful non-destructive, cost-effective and quantitative approaches in field assessment of reinforcing steel corrosion to date. It can locate active corrosion areas with good accuracy and estimate the extent of corrosion damage in reinforced concrete structures. These LPR measurements can be used in conjunction with corrosion potential measurements to validate and better define corroded areas in reinforced concrete structures.[9,15]

AC impedance spectroscopy

AC impedance spectroscopy has been widely used in fundamental and applied studies in electrochemistry for a long time. This technique has also been used extensively for studying corrosion mechanisms in the laboratory and determining the corrosion rate of reinforcing steel in concrete.[20–24] This method applies small amplitude sinusoidal signals over a range of frequencies to a system and records the impedance response. The complex plane



1.4 Simple equivalent circuit for modeling steel/concrete interface.



1.5 Impedance plot in the complex plane from simple equivalent circuit.

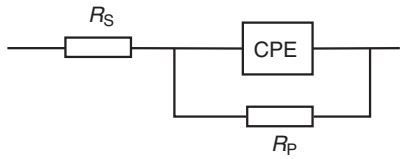
(imaginary *vs* real) and bode plots (phase and amplitude *vs* frequency) can be obtained for data analysis, which can be used to provide information about corrosion kinetics and insights into corrosion mechanism.

A simple electrochemical interface between liquid (pore solution) and solid (steel) can be modelled with an equivalent circuit as shown in Fig. 1.4. The impedance of the circuit can be described by the following equation:

$$Z(\omega) = R_S + \frac{R_P}{1 + (\omega C_{dl} R_P)^2} - j\frac{\omega C_{dl} R_P^{\,2}}{1 + (\omega C_{dl} R_P)^2} \qquad [1.10]$$

where R_S is the solution (concrete) resistance between the RE and measured reinforcing steel, C_{dl} is the double layer capacitance at the steel–concrete interface, R_P is the polarization resistance, $\omega = 2\pi f$ and $j = \sqrt{-1}$. A plot of equation 1.10 in the complex plane yields a perfect semicircle, which intercepts on the real axis at R_S and $R_S + R_P$ with R_P as its diameter (Fig. 1.5). Therefore, the corrosion rate can be calculated according to the Stern–Geary equation (1.7).

In practice, an ideal semicircle is not observed for most systems. Instead, a depressed semicircle with its centre located below the real axis by an angle α is observed. This behaviour is normally associated with a spread of relaxation times and can be accounted for by an equivalent circuit with a frequency-dependent element called a constant phase element (CPE)[25,26] instead of a fixed double layer capacitance as shown in Fig. 1.6. In situations



1.6 Equivalent circuit containing CPE.

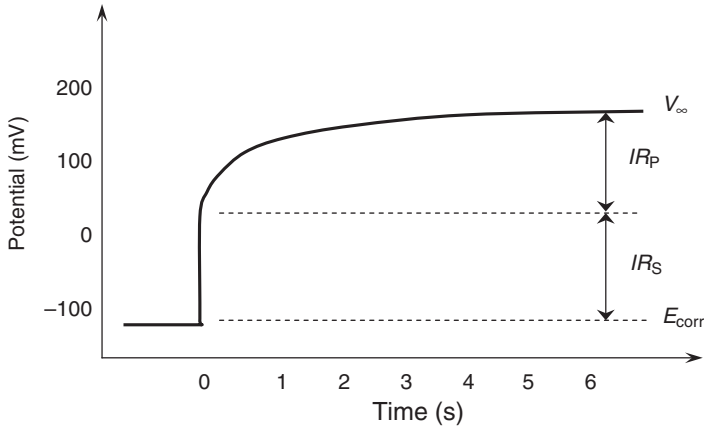
where oxide films and interfacial films are present, the impedance spectra become more complicated, mandating a more complex equivalent circuit to model the steel–concrete interface. In these cases the R_P can be obtained by simulation of the frequency-response behaviour by means of a suitable equivalent circuit using commercially available AC impedance simulation software. Usually, a fairly reliable R_P value can be obtained using an equivalent circuit simulation method based on the entire impedance spectrum.

A potentiostat coupled with a frequency response analyser (Solartron) can perform complicated tests for different systems. Its software can provide simulations for evaluating the parameters of components in various equivalent circuit models. It is a very powerful instrument for the laboratory; however, a complete frequency scan is simply too time-consuming (often taking hours for a single measurement) and the equipment is overly expensive. By using an NSC device (Nippon Steel Corp.), which applies only a high-frequency pulse of 1280 Hz to determine the concrete resistance, R_S, and a low-frequency pulse of 0.02 Hz to determine the R_P value, the time required to conduct these tests is greatly reduced. However, the low frequency varies significantly from system to system and is often not low enough to cover the whole low frequency $R_P C_{dl}$ loop, leading to a lower estimated R_P value and a higher estimated corrosion rate. At this point, there is still no AC impedance instrument suitable for field tests over the entire frequency range.

Galvanostatic pulse

A technique that has been developed to study the dynamic response of a corrosion interface to evaluate the corrosion rate of the reinforcing steel is the galvanostatic pulse transient response method. A small current perturbation is applied to a steel bar using an auxiliary electrode placed on the surface of the concrete and the resulting potential transient of the reinforcing steel is recorded with respect to a reference electrode. The analysis of this transient response allows the corrosion rate of steel to be determined.

Figure 1.7 shows a typical potential response for a corroding reinforcement. Under galvanostatic conditions, the potential response of an electro-



1.7 Typical galvanic pulse charging curve.

chemical system, approximated by a simple Randles circuit to a current pulse I is given by:

$$V_t = IR_S + IR_P\left[1 - \exp\left(-\frac{t}{C_{dl}R_P}\right)\right] \qquad [1.11]$$

where V_t is the total change in the potential of the steel WE, IR_S is the ohmic drop in the concrete between the RE and WE, IR_P is the effective polarization potential during a charging (or discharging) period, R_P is the polarization resistance of the rebar, C_{dl} is the double layer capacitance of the metal/concrete interface and $C_{dl}R_p$ is the time constant for the corrosion process. After a long period of equilibration, the transient response reaches a steady-state potential (V_∞) where:

$$V_\infty = IR_S + IR_P \qquad \text{as } t \to \infty \qquad [1.12]$$

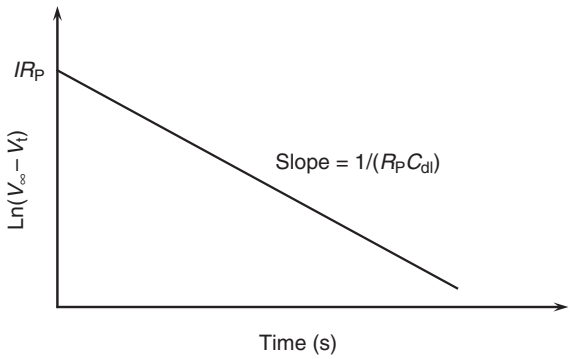
therefore:

$$V_\infty - V_t = IR_P \exp\left(\frac{-t}{R_P C_{dl}}\right) \qquad [1.13]$$

thus:

$$\log(V_\infty - V_t) = \log(IR_P)\left(\frac{-t}{R_P C_{dl}}\right) \qquad [1.14]$$

From this equation it can be seen that a plot of $\log(V_\infty - V_t)$ against t will illustrate a linear relationship with a slope of:



1.8 Transformation for calculating $\ln(IR_P)$ and $1/(R_P C_{dl})$.

$$\frac{1}{R_P C_{dl}} \qquad [1.15]$$

and an intercept at $\log(IR_P)$ on the y-axis as shown in Fig. 1.8.

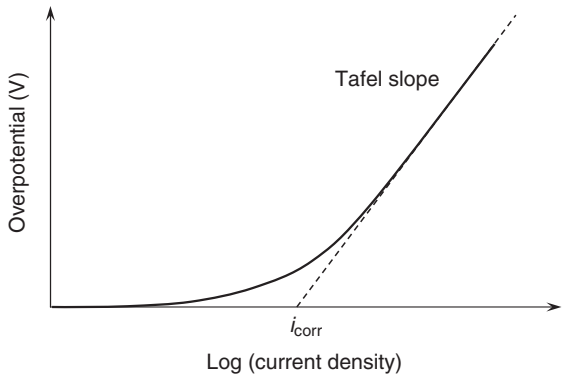
C_{dl} can be determined by dividing the current by the slope of the potential decay as shown in the following equation:

$$C_{dl} = \frac{I}{dV/dt} \qquad [1.16]$$

The corrosion rate can then be calculated by the measured R_P based on the Stern–Geary equation (1.7) assuming C_{dl} is independent of the polarization potential.

The transient galvanostatic pulse technique can be used to evaluate the polarization resistance with a reasonable degree of resolution, in spite of the errors that can be associated with semi-logarithmic plots. Results of this analysis carried out in the laboratory provided the confidence to use this technique to evaluate the corrosion state in concrete structures.

The galvanostatic pulse technique was first introduced for field application in 1988,[27] and the equipment (GP-5000 GalvaPulse System made by Germann Instruments) specifically designed for these field applications recently became commercially available. The instrument applies an anodic galvanic pulse current in the range of 5–400 μA for 5–10 s, and is equipped with a guard ring CE to confine the polarization current to an area of the reinforcement below the central CE. It can also be connected to a PC for easy documentation and reporting as long as the Windows-based GalvaPulse Viewing and Reporting software has been installed. Besides estimating the corrosion rate, the system simultaneously measures the corrosion potential



1.9 Schematic plot of a Tafel curve.

and the electrical resistance of the concrete cover layer, with each test taking only about 5–10 s.

Tafel extrapolation

This method has been widely used in electrochemical laboratories for the study of corrosion of different metals. A slow anodic potential (or current) scan is applied to the reinforcing steel and the current (or potential) is recorded. The results are plotted on a potential versus logarithmic current density to yield what is called a Tafel plot as shown in Fig. 1.9. The linear portion of the curve, which is usually around 100 mV above the corrosion potential, follows the Tafel relationship:

$$\eta = a + b \log i \qquad [1.17]$$

where η is the overpotential, $E–E_{corr}$ and b is referred to as the Tafel slope. The intercept of this linear line at the log current density axis is the corrosion current density.

This method is quite simple but a relatively large anodic polarization has to be applied on the reinforcing steel resulting in the increase of corrosion of the metal, and the destruction of steel concrete bonding. The Tafel relation is usually observed on corroded steel; however, it may not exist on a passive steel. Another difficulty is the high concrete resistance, which causes a large iR drop, leading to inaccuracy in the determination of the intercept on the logarithmic current density axis.

It is important to emphasize that the corrosion rate is an instantaneous value for the measured area of the reinforcement under the specific conditions during the time of testing. For service life assessment of concrete structures, more detailed knowledge of the daily and seasonal changes of

corrosion rate is required in order to obtain meaningful corrosion damage evaluation in concrete structures. It is necessary to combine the corrosion rate measurements with a number of other non-destructive techniques or limited invasive methods to provide reliable corrosion condition assessment of concrete structures.

1.2.4 Electrochemical noise measurements

Electrochemical noise measurements allow the polarization resistance to be measured passively, i.e. without external polarization. This technique involves measurement and analysis of the random fluctuations in corrosion potential and corrosion current. Methods for analysis of the electrochemical noise include statistical analysis and frequency domain transforms. A correlation between the spectral noise resistance and corrosion rate has been reported in laboratory investigations.[28] Electrochemical noise measurements can also provide insights into the nature of localized corrosion events. The advantage is that such measurements do not perturb the system. However, the accuracy of this technique depends on the length of the data recording period and requires the corrosion rate to be constant during this period of time. It also requires substantial experience to interpret the results correctly and therefore has yet to see extensive use in the field.

1.2.5 Remote monitoring techniques

In order to monitor changes of the corrosion state of reinforcing steel with time, a remote corrosion monitoring system was developed to assess the corrosion of reinforced concrete structures and to conduct condition surveys. This corrosion monitoring system can provide a range of parameters from probes cast into new concrete structures to those retrofitted into existing structures.

A typical remote corrosion monitoring system consists of various types of sensors, a data acquisition system, a cellular modem with a telescopic antenna for data transfer, a power supply and a 12V battery for power failure back-up. The sensors that can be installed in concrete structures include manganese dioxide (MnO_2) electrodes[29] or silver/silver chloride (Ag/AgCl) reference electrodes for corrosion potential monitoring, embedded LPR sensors for corrosion rate measurements,[30] and two or four pin probes embedded in the concrete at different depths to monitor moisture movement and changes that may be associated with chloride ingress. These sensors have been used in some concrete structures and have shown promise; however, most systems have been used in the field for only a few years, which is too short a period for long-term corrosion moni-

toring. Some systems are still at the research stage and there are still some technical problems that need to be solved, such as the effects of seasonal and temperature variations, the slow shifting on the reference electrode due to the changing of environmental conditions and the reliability of the sensors and systems.

1.2.6 Galvanic corrosion test

This test is used to characterize the galvanic corrosion behaviour of two dissimilar metals in electrical contact in electrolytes (ASTM G71-81) or embedded in concrete with different chloride environments (ASTM G109-92[31]). For galvanic corrosion tests in concrete, specimens are made with two layers of rebar: the top layer with a single rebar and bottom layer with two rebars. A plastic dam is placed on the top of the specimen for chloride solution ponding. The two layers of rebar should be electrically joined by a zero resistance ammeter or a 100 Ω precision resistor. Control specimens (same alloy, shape, size and conditions as the materials in the couple) should also be tested to provide the corrosion rates of the individual metals and alloys in the absence of coupling for comparison purposes. The prime considerations are that the electrical bond to the rebar must not corrode (i.e. the method of joining will not in itself be a galvanic couple or introduce other corrosion mechanisms) and that the resistance of the electrical path be small compared with the concrete resistance or polarization resistance of the coupled materials.

Galvanic coupling currents and potentials of the coupled and control rebars (*vs* reference electrode) should be recorded during the exposure time. One of the advantages of this technique is that it can be set up for long-term monitoring of reinforcing steel macrocell corrosion caused by changes in the environmental conditions or the coupling effect due to the different metals used. However, it is important to point out that the recorded galvanic current is only a portion of the corrosion current, which is caused by the coupling effect. The spontaneous micro-corrosion reactions occurring in the metals cannot be measured externally.

1.3 Physico-chemical techniques

1.3.1 Concrete resistivity measurements

The electrical resistivity of concrete, which is a function of the moisture, microstructure of the matrix and conductivity of the pore solution, has a significant effect on the rate of corrosion of embedded reinforcing steel. Several studies have shown that measured resistivity values are closely related to the actual corrosion rates in a structure.[32–34] High concrete

resistivity implies a high electrolyte resistance, which limits the rate of corrosion.

Concrete resistivity can be measured using a modification of the four-electrode Wenner resistivity meters commonly used for measuring soil resistivity (ASTM G57-78). The four probes are placed in a straight line on the concrete with a conductive sponge on the tips to overcome the high contact resistance. The resistivity is a function of the voltage drop between the two centre probes with current flowing between the two outside probes. Table 1.3 provides guidelines for interpreting resistivity measurements from the Wenner four-probes when referring to corrosion of reinforcing steel embedded in concrete.[11]

Other concrete resistivity measuring instruments include hand-held 'two probe' types, as well as some (Gecor) that use a single electrode placed on the concrete surface, with a voltmeter connected to the reinforcing steel in the concrete. Both techniques require the use of AC or pulse signals to perform the measurement to reduce or eliminate the error caused by the contact resistance and polarization resistance at the interface of steel and concrete.

The electrical resistivity of concrete is a function of moisture and ion content in the pores. It is affected by many factors, such as cement content, water/cement ratio, additives and salt content. Measuring concrete electrical resistivity is relatively simple and rapid. However, changes in the moisture and salt contents affect the resistivity measured at the concrete surface and therefore complicate evaluation of the corrosion rate. Therefore, analysis results should be verified using other measurements to ensure reliability.

1.3.2 Chloride ion content analysis

Chloride ions are a major contributing factor in the corrosion of steel in concrete, particularly in areas where structures suffer from the heavy use of de-icing salts or marine climates with saline ground conditions. When chloride ion concentration in concrete exceeds the chloride corrosion threshold, the steel passive film, which provides protection from corrosion, breaks down and localized corrosion is initiated. Chlorides may be absorbed from the surface or enter through cracks in the concrete. In some parts of the world, contaminated sand or aggregates may also present serious problems.

The profile of the chloride ion content is determined by analysis of powdered concrete samples, which are collected on site at various depths using a hammer drill or from cores sliced at different depths then ground/pulverized into powder. The latter provides better and more reliable results.

Table 1.3 Relationship between concrete resistivity and corrosion rate

Concrete electrical resistivity	Corrosion activity
>20 kΩ cm	Low corrosion rate
10–20 kΩ cm	Low to moderate corrosion rate
5–10 kΩ cm	High corrosion rate
<5 kΩ cm	Very high corrosion rate

The analysis of the chloride ion concentration is usually performed in the laboratory using chemical analysis methods described in ASTM C 1152, AASHTO T260 (for acid-soluble chloride content) and ASTM C 1218 (for water-soluble chloride content). For the acid-soluble test, a weighed portion of a ground or powdered sample is treated with hot nitric acid and then diluted and filtered to make the test solution. The acid-soluble chloride content is determined by the potentiometric titration of this solution with 0.05 N silver nitrate solution. The acid-soluble chloride analysis technique is more reproducible and less time consuming, therefore making it the more widely accepted method.

Field test kits (Germann RCT or James CL-1000) have been developed for chloride content analysis using specific ion selective electrodes. These kits are easy to use and require only 1.5–3 g powder samples; analysis can be performed rapidly on-site. However, some precautions need to be taken. For instance, it is important to avoid contamination during sampling. When the two chloride test kits were compared with the AASHTO T260 laboratory method, it was found that the two kits gave results that represented approximately 57–62% of the AASHTO values.[35] Thus corrections must be made to obtain accurate results.

The results of chloride content are usually reported in percentage chloride ion (Cl^-) by mass of cement (or mass of concrete). Studies carried out by the Federal Highway Administration (FHWA)[36] showed that the reinforcing steel corrosion is initiated at 0.2% acid-soluble chloride by mass of cement. Actually the initiation of the reinforcing steel corrosion depends on the ratio of the chloride concentration to the hydroxyl concentration. It also depends on the moisture conditions in concrete. The chloride content that can be tolerated is lower in wet concrete with lower pH values.

1.3.3 Carbonation testing

Carbonation of concrete is mainly caused by a reaction between atmospheric carbon dioxide and calcium hydroxide. Carbon dioxide dissolves in

the pore water and forms carbonic acid, which reduces the pH of the pore water to a level at which the passive layer on the steel reinforcement is no longer sustained. Sulphur dioxide and nitrogen dioxide in the air also significantly reduce the pH of the pore water and cause reinforced concrete to deteriorate. Carbonation of concrete is normally restricted to a surface layer thickness of only a few millimetres in good quality concrete but can be much deeper in poor quality concrete.

The extent of carbonation can be measured by exposing fresh concrete, roughly perpendicular to the external face, and applying a phenolphthalein–ethanol pH indicator solution. Phenolphthalein is a clear pH indicator that turns magenta (or purple-red) at or above a pH of approximately 9. Coloration will be obtained where the highly alkaline concrete has not been affected by carbonation, but no coloration will appear in carbonated areas.

This technique is simple and rapid for the determination of the front of concrete carbonation but is only a qualitative measurement. A number of practical difficulties may arise, which include freshly broken concrete showing an initial colour change boundary that may become obscured within a minute, and the presence of porous aggregates, voids and cracks that may cause difficulty in determining the front of the carbonation. Currently there is no standard for this test.

1.4 Conclusions

Corrosion of steel reinforcement used in concrete structures can lead to major problems in terms of reduced safety and serviceability and increased rehabilitation costs. Reliable evaluation of the level of reinforcement corrosion in concrete structures by non-destructive techniques is key to identification of cost-effective solutions to stop or delay its damaging effects. The assessment of reinforcement corrosion is a complex process and requires extensive experience and consideration of several interrelated factors. A better understanding of the factors causing reinforcing steel corrosion, the basic principles of corrosion and the advantages and limitations of the different techniques will significantly improve the accuracy and reliability of corrosion assessment of reinforced concrete structures.

1.5 References

1. Stratfull, R.F. (1973), 'Half-cell potentials and the corrosion of steel in concrete', *Highway Research Record*, p. 433.
2. Broomfield, J., Davies, K. and Hladky, K. (2002), 'The use of permanent corrosion monitoring in new and existing reinforced concrete structures', *Cement and Concrete Composites*, Vol. 24, No. 1 pp. 27–34.

3. Van Daveer, J. (1975), 'Techniques for evaluating reinforced concrete bridge decks', *ACI Journal*, Dec., pp. 697–704.
4. Vassie, P.R. (1991), 'The half cell potential method of locating corroding reinforcement in concrete structures', Application guide, Department of Transport and Road Research Laboratory report No. 9, Crowthorne, UK, pp. 1–30.
5. Sohanghpurwala, A.A., Scannell, W.T. and Jackson, D.R. (1994), 'Comparison of commercially available half-cell array units used in conducting surveys of reinforced concrete bridges', *Structural Materials Technology – An NDT Conference*, Technomic Publications, Lancaster, PA, p. 63.
6. Elsener, B., Andrade, C., Gulikers, J., Polder, R. and Raupach, M. (2003), 'Half-cell potential measurements – potential mapping on reinforced concrete structures', RILEM TC 154-EMC, *Materials and Structures/Matériaux et Constructions*, Vol. 36, August–September, pp. 461–471.
7. Raharinaivo, A. (1988), 'Contrôle de la corrosion des armatures dans les structures en béton armé', *Bulletin de liaison des Laboratoires des Ponts et Chaussés*, Vol. 158, Nov./Dec., pp. 29–38.
8. Arup, H. (1985), Electrochemical monitoring of the corrosion state of steel in concrete, *1st International Conference, Deterioration and repair of reinforced concrete in Arabian Gulf*, CIRIA/BSE, pp. 485–493.
9. Qian, S., Cusson, D. and Chagnon, N. (2003), 'Evaluation of reinforcement corrosion in repaired concrete bridge slabs – a case study', *Corrosion*, Vol. 59, No. 5, pp. 457–468.
10. Baker, A.F. (1986), 'Potential mapping techniques', *Proc. Seminar on Corrosion in Concrete*, London Press Centre, Global Corrosion Consultants, Telford, May, 3.1–3.21.
11. Broomfield, J. (1997), '*Corrosion of Steel in Concrete: Understanding, Investigation and Repair*', E&FN Spon, London.
12. Alonso, C., Andrade, C. and González, J.A. (1988), 'Relation between resistivity and corrosion rate of reinforcements in carbonated mortar made with several cement types', *Cement and Concrete Research*, Vol. 18, pp. 687–698.
13. Feliu, S., Gonzalez, J.A., Escudero, M.L., Feliu, Jr S. and Andrade, C. (1990), 'Possibilities of the guard ring for electrical signal confinement in the polarization measurements of reinforcements', *Corrosion*, Vol. 46, pp. 10–15.
14. Andrade, C., Macias, A., Feliu, S., Escudero, M.L. and Gonzalez, J.A. (1990), 'Quantitative measurement of the corrosion rate using a small counter electrode in the boundary of passive and corroded zones of a long concrete beam', in *Corrosion Rate of Steel in Concrete*, ASTM STP 1065, ASTM, West Conshohocken, PA, pp. 134–142.
15. Flis, J., Sehgal, A., Li, D., Kho, Y., Sabol, S., Pickering, H., Osseo-Asare, K. and Cady, P. (1992), 'Condition Evaluation of Concrete Bridges Relative to Reinforcement Corrosion, Volume 2: Method for Measuring the Corrosion Rate of Reinforcing Steel', Report, Strategic Highway Research Program, National Research Council, Washington, DC, p. 43.
16. Flis, J., Sabol, S., Pickering, H.W., Sehgal, A., Osseo-Asare, K. and Cady, P.D. (1993), 'Electrochemical measurements on concrete bridges for evaluation of reinforcement corrosion rates', *Corrosion*, Vol. 49, No. 7, pp. 601–613.
17. Broomfield, J. (1996), 'Field measurement of the corrosion rate of steel in concrete using a microprocessor controlled guard ring for signal confinement', in

Techniques to Assess the Corrosion Activity of Steel Reinforced Concrete Structures, ASTM STP 1276, Berke, N.S. *et al*., eds, ASTM, West Conshohocken, PA.

18. González, J., Andrade, C., Alonso, P. and Feliú, S. (1993), 'Effect of corrosion current on the degradation of reinforced concrete structures', in *Progress in the understanding and prevention of corrosion*, Costa, J. and Mercer, A., eds, The Institute of Materials, London, p. 629.
19. Gu, P., Ramachandran, V.S. and Beaudoin, J.J. (1997), 'Corrosion of steel in concrete: assessment techniques', in *Testing and Quality Control in Cement Industry*, Vol. 3, Ghosh, S.N., Mathur, V.K., Saketharaman, J. and Kumar, A., eds, Akademia Books International, New Delhi, pp. 334–381.
20. Wenger, F. and Galland, J. (1990), 'Analysis of local corrosion of large metallic structures or reinforced concrete structures by electrochemical impedance spectroscopy', *Electrochimica Acta*, Vol. 35, pp. 1573–1578.
21. John, D.G., Searson, P.C. and Dawson, J.L. (1981), 'Use of AC impedance technique in studies on steel in concrete in immersed conditions', *Br. Corrosion Journal*, Vol. 16, pp. 102–106.
22. Somuah, S.K., Boah, J.K., Leblanc, P., Al-Tayyib, A.H.J. and Ai-Mana, A.I. (1991), 'Effect of sulphate and carbonate ions on reinforcing steel corrosion as evaluated using ac impedance spectroscopy', *ACI Materials Journal*, Vol. 88, pp. 49–55.
23. Macdonald, D.D., El-Tantawy, Y.A., Rocha-Filho, R.C. and Urquidi-Macdonald, M. *Evaluation of Electrochemical Impedance Techniques for Detecting Corrosion on Rebar in Reinforced Concrete*, National Research Council, Washington, DC, SHRP-ID/UFR-91-524.
24. Hachani, L., Fiaud, C., Triki, E. and Raharinaivo, A. (1994), 'Characteristics of steel/concrete interface by electrochemical impedance spectroscopy', *British Corrosion Journal*, Vol. 29, pp. 122–127.
25. Cole, K.S. and Cole, R.H. (1941), 'Dispersion and absorption in dielectrics I. Alternating current characteristics', *Journal of Chemistry and Physics*, Vol. 9, pp. 341–351.
26. Sluyters-Rehbath, M. and Sluyters, J.H. (1970), 'On the impedance of galvanic cell. The potential dependence of the Faradaic parameters for electrode processes with coupled homogeneous chemical reactions' in *Electroanalytical Chemistry*, Vol. 4, Bard, A.J. and Dekker M., eds, Marcel Dekker, New York, pp. 1–125.
27. Elsener, B. (1988), 'Elektrochemische Metoden Zur auwerksüberwachung', Zerstörungsfreie Prüfung an Sthalbetonbauwerken, SIA Dokumentation D020, Schweizer Ingenieur-und Architektverein, Zürich, 27.
28. Hardon, R.G., Lambert, P. and Page, C.L. (1988), Relationship between electrochemical noise and corrosion rate of steel in salt contaminated concrete, *British Corrosion Journal*, Vol. 23, No. 4, pp. 225–228.
29. Cusson, D. and Mailvaganam, N. (1999), 'Monitoring and evaluation techniques for corrosion inhibiting systems in reconstructed bridge barrier walls', *Concrete International*, Vol. 21, No. 8, pp. 41–47.
30. Broomfield, J., Davies, K. and Hladky, K. (2000), 'Permanent corrosion monitoring in new and existing reinforced concrete structures', *Materials Performance*, Vol. 39, No. 7, pp. 66–71.

31. ASTM (1992), *Annual Book for ASTM Standards*, Vol. 03.02, Wear and Erosion: Metal Corrosion, G109-92, American Society for Testing and Materials, Philadelphia, PA.
32. Alonso, C., Andrade, C. and Gonzalez, J.A. (1988), 'Relation between resistivity and corrosion rate of reinforcements in carbonated mortar made with several cement types', *Cement and Concrete Research*, Vol. 8, No. 5, pp. 687–698.
33. Polder, R. (2001), 'Test methods for on site measurement of resistivity of concrete – a RILEM TC-154 technical recommendation', *Construction and Building Materials*, Vol. 15, pp. 125–131.
34. McCarter, W.J., Emerson, M. and Ezirim, H. (1995), 'Properties of concrete in the cover zone: developments in monitoring techniques', *Magazine of Concrete Research*, Vol. 47, pp. 243–251.
35. Jackson, D.R., Soh, F.W., Scannell, W.T., Sohanghpurwala, A.A. and Islam, M. (1995), 'Comparison of Chloride Content Analysis Results Using the AASHTO T260 Test Method and Two Field Test Kits', Paper No. 520, *Corrosion/95*, NACE International, Houston, TX.
36. Clear, K.C. (1976), 'Time to corrosion of reinforcing steel in concrete slabs, V. 3: Performance after 830 Daily Salt Applications', Report No. FHWA-RD-76–70, Federal Highway Administration, Washington, DC, p. 64.

2

Alkali–silica reaction (ASR) testing of deterioration in concrete

V. JENSEN
Norwegian Concrete and Aggregate Laboratory Ltd, Norway

2.1 Introduction

The main aim of the chapter is to give a brief description of the alkali–silica reaction (ASR) and how to diagnose this problem and the damage it causes in structures. Sections 2.1 and 2.2 give background information on ASR and the conditions necessary for ASR to occur in concrete structures. Section 2.3 gives information on how to carry out the correct diagnosis of ASR by field inspection and laboratory investigation using selected methods. Long-term monitoring of expansion and relative humidity (RH) is important for assessment of future damage and risk of failure. Section 2.4 gives case histories on condition assessment and monitoring of ASR damage on individual structures and in survey investigations. Examples of the effects of surface treatments on structures are also given. Section 2.5 discusses the importance of implementation of knowledge and use of correct methods and the need for research. Section 2.6 gives a short conclusion.

ASR was first mentioned in the literature by Thomas Stanton in 1940, who explained the causes of the map cracking that first occurred in King City Bridge and several structures situated in California. Laboratory tests carried out by Stanton revealed that expansion and cracking in mortar samples were caused by a reaction between alkalis from the cement paste and opaline flint from the Oro Fino sand used as concrete aggregate in structures with map cracking. After a few years of intensive research Stanton and co-workers described the fundamental knowledge of ASR which is still valid, though today more comprehensive information is available. During intensive research in the 1940s, structures with ASR were discovered in several other places in the USA, and other types of alkali–reactive aggregate were identified by petrographical investigations and laboratory tests.

During the following years worldwide research on ASR was carried out and ASR was identified in several places in the world, e.g. in Denmark in the 1950s (Nerenst 1957), in the UK in 1971 (Nixon 1990) and in Australia in the 1980s (Cole and Lancucki 1981, 1983). ASR has today been reported

in numerous countries around the world, e.g. the USA, Australia, England, Denmark, Canada, Iceland, Germany, New Zealand, South Africa, Japan, India, Italy, France, Belgium, Sweden and Norway. Recently, Turkey and Brazil recognized ASR.

2.2 Understanding the reaction

2.2.1 Raw materials

The inherent properties of raw materials used for concrete, namely sand, gravel or crushed rock, and the cement, depend on the geological processes and history in the area/country of withdrawal. Normally sand, gravel and crushed rocks are taken locally and for certain areas these might react in concrete. The raw materials for cement production, which normally are also taken locally, can be of such a type that only cement with high alkali content can be produced (contributes with alkalis to the reaction). However, cements can be produced or mixed with pozzolanes (fly ashes, silica dust) or blast furnace slag which prevents the reaction in concrete. In existing structures, the concrete consists of aggregates and cements that cannot be changed. If the structure or part of the structure is exposed to water, and alkali-reactive aggregates in sufficient amounts have been used together with a high alkali cement, ASR may develop.

2.2.2 Classification

Alkali aggregate reaction (AAR) is the name given to a group of reactions between certain types of aggregate–mineral and the alkaline pore solution of the cement paste. Two major types are termed alkali silica reaction (ASR) and alkali carbonate reaction (ACR). ASR is the dominant reaction type found in most countries and dealt with in this chapter. ACR is today only accepted to occur in China, Canada, Austria and possibly in Spain.

ASR can be subdivided into the following:

- Fast expansive reactions caused by metastable silicates (e.g. opal, Mielenz 1947 black list). Cracking and serious damages due to ASR are often observed a few years after construction.
- Slow/late expansive reactions caused by crypto-microcrystalline silicates and certain chemical unstable rock types as sandstones and granite. The slow/late reaction is distinguished from the fast expansive reaction ('classical' ASR) by a delayed onset of expansion of concrete test prism and the very long time span (which may be up to 20 years) before cracking becomes evident in concrete structures. Over a long time, damage is more serious than from the fast expansive reaction.

The reactive constituent of ACR (Gilliot 1964) is dolomitic limestone. The exact reaction mechanism that causes the expansion of carbonate rocks has still not been satisfactorily explained, and many researchers do not accept that the reaction occurs. The reaction is rather fast and structures are often seriously damaged after few years. No remedial measures such as low alkali cement, slag cement or pozzolanes seem to stop the reaction. Therefore the Canadian strategy is to avoid the use of such aggregates in concrete. Some recent but rather limited research suggests that ASR and ACR occur simultaneously in certain limestone aggregates. This may explain the observation of a very low amount of reaction products (gel) and very expansive damage in concrete.

The third major reaction type formerly named alkali silicate reaction and suggested by Gilliot (1975) and mentioned in many publications and books is today generally agreed not to exist by most researchers around the world.

2.2.3 Conditions of ASR

ASR is a complex chemico-physical reaction between alkalis and alkali-reactive aggregates in the concrete. The reaction forms a swelling gel (the chemical reaction), and following the uptake of water, the gel exerts pressure (the physical process) that can crack the concrete. For the slow/late expansive reaction, research suggests that the expansive pressure is first caused by internal expansion of reacted aggregates owing to crystallization pressure of reaction products between minerals/grains and then expansion of gel (Jensen 1993). The reaction may lead to local volume expansion, cracking, loss of strength and, in extreme cases, the complete 'destruction' of the concrete. The reaction mechanism has been described by Powers and Steinour (1955a,b) and Dent Glasser and Kataoka (1981a,b,c,d, 1982) but the role of calcium is disputed today.

Three major conditions have to be met before ASR can occur in concrete: (1) sufficient reactive aggregates, (2) adequate available alkalis and (3) water. If one of these conditions is not obtained, ASR cannot occur in concrete. Other parameters that influence or determine the occurrence and extent of ASR are the presence of calcium hydroxide from the cement paste, the temperature and time. Calcium hydroxide is believed by some researchers to play a significant role in breaking down silica minerals and in the production of gel. High temperature is known to increase chemical reactions and influence the rate of ASR but because ASR is not designated as just a chemical reaction, high temperature in the long term can also have a negative effect on the expansion of concrete (Diamond *et al*. 1981). For slow/late aggregates low temperature and long time will have a more damaging effect on the structure than for fast-reacting aggregates. For a chemico-

physical process such as ASR, time plays a determining role before ASR affects concrete and becomes visible.

Aggregate

A black list of alkali-reactive aggregates and minerals has been published by Mielenz *et al*. (1947). These alkali-reactive aggregates contained one or more of the following components: opal, chalcedony, volcanic glass, devitrified glass, tridymite and possible hydromica. This group of aggregates and minerals are related to the fast-reacting type of ASR.

In the late 1950s and 1960s some reports about unidentified cement–aggregate reactions considered to be different from traditional ASR were published (Bredsdorff *et al*. 1963). Two different aggregate types seem to be involved in the reaction, namely (1) predominantly siliceous aggregates and (2) dolomitic limestone. For siliceous aggregates the alkali reactive constituents are suggested to be crypto/microcrystalline quartz, strained/granulated quartz and/or possible certain feldspar and the rock types as argillite, phyllite, greywacke, granite, quartzite, schist and sandstone. These aggregates are today designated to be slow/late expansive ASR. Dolomitic limestone is today designated to be alkali carbonate-reactive ACR (but not all types). An updated list of potentially alkali reactive aggregates and minerals is published by RILEM (Rilem AAR-1 2003). Limit values of alkali reactive aggregates vary from country to country and should be assessed based on national or regional regulations and practice.

Cement

The cement's alkali content is another major factor for the occurrence of ASR. For Portland cements and when the cement's total equivalent alkali content is less than 0.6 weight% Na_2O (low-alkali cement) ASR should not occur. However, some cases of deleterious ASR with use of low-alkali cements have been reported. In Canada ASR generally occurs only in the eastern part of the country owing to the use of high-alkali cements. In western Canada only few cases of ASR damage have been reported because the cements here generally have low alkali content. Use of blast furnace slag cement and cements containing pozzolanes, e.g. fly ash, also lowers the risk of ASR.

Humidity

Water is essential for ASR and if the concrete does not contain sufficient water, ASR cannot occur. However, rather limited research has been carried out on this matter. Relative humidity (RH) is the measure used for assess-

ing the influence of humidity on ASR and limit values have been established. Water content, water percentage or degree of saturation by drying and weighing of the concrete are other methods for humidity but limit values for these methods do not exist for ASR and probably never will. Moreover, these methods are destructive because core material has to be taken from the concrete. Today it is generally accepted that relative humidity higher than 80% is sufficient for ASR and more damages occur in the concrete in case RH is high, e.g. 95–100% (Nilsson 1981, 1983; Stark 1991a; Stark *et al*. 1993). RH is a measure of the thermodynamic state of the pore water, and not of the amount of water in the concrete. At a given moisture content, the RH will be a function of the pore structure, the temperature, the chemical composition of the pore solution and the moisture history of the concrete. Long-term measurements in many Norwegian concrete structures at various depths have shown that temperature does not influence RH in the concrete (Jensen 1998, 2000a,b, 2003a). It is important to know that RH measurements in concrete cannot be compared with RH measurements in atmospheric air, which are strongly influenced by temperature – this is not the case for concrete. Water can be transported into the concrete by capillary suction from surrounding ground and water exposure. In many concrete structures and structural elements rain water is the most important source of water into the concrete. The different exposures of water in, for example, a concrete bridge will therefore cause varying RH in the structural elements and rates of ASR. The remedial measure of lowering of humidity to less than a critical level (80% relative humidity) is one method to reduce the damaging effect of ASR.

2.3 Diagnosis, investigation and monitoring

2.3.1 Condition assessment – diagnosis

Correct diagnosis of the deterioration processes in the concrete structures is essential to determine the type of measurement and long-term monitoring programme (Larbi *et al*. 2004). Diagnosis and appraisal of concrete structures affected by ASR often involve complex damage caused by a combination of more than one deterioration process, such as ASR in combination with frost and/or sulphate attack. An example of coexistence between two significant different deterioration processes is that of reinforcement corrosion caused first by ASR, which cracks the concrete cover and opens the concrete for successive ingress of aggressive constituents (chloride, carbon dioxide, water) to the reinforcement. A reliable analysis to identify and determine the extent of the damage and to make a prognosis of its effect on the structure therefore requires a clear and thorough understanding of the mechanisms and processes of damage. Like many other

Table 2.1 Inventory stages and analyses for assessment of ASR

Stage	Investigation	Information and examples of type of testing
1	Inventory of existing records	Background information and history of damage
2	Field inspection of structure	Visual inspection, overview of the problem Registration of cracks, crack type(s), efflorescence Measurement of cracks and expansions Uranyl acetate testing Other tests when necessary Photo documentation and written record
3	Coring of samples	Use sufficient number of cores and core sizes Cores taken in most damaged areas and 'less' damaged areas
4	Laboratory investigations	Very important to use relevant methods: such as microstructural analysis (visual examination of cores, optical microscopy on polished core slabs and thin sections (fluorescence impregnated)); crack counting, damage rate index; electron microscopy when necessary; mechanical tests (compressive and tensile strength)
5	Assessment of field and laboratory results	Results from field inspection and laboratory results to give a correct diagnosis of the problem and variation on ASR intensity in the structure
6	Monitoring programme	Monitoring of cracks, expansions and relative humidity over a long time for assessment of future damage
7	Assessment of service life and safety	Based on long-term measurement and damage history

causes of damage in concrete, diagnosis and appraisal of ASR and other types of damage in concrete structures rely to a large extent on the judgement and the level of expertise of the personnel involved and it is very important to use correct and suitable analysis methods valid for the existing structure and deterioration processes. Before a monitoring programme is planned and established, correct diagnosis of the problem(s) has to be documented. This is normally based on several different inventory stages and analyses as shown in Table 2.1.

2.3.2 Field inspection and laboratory investigations

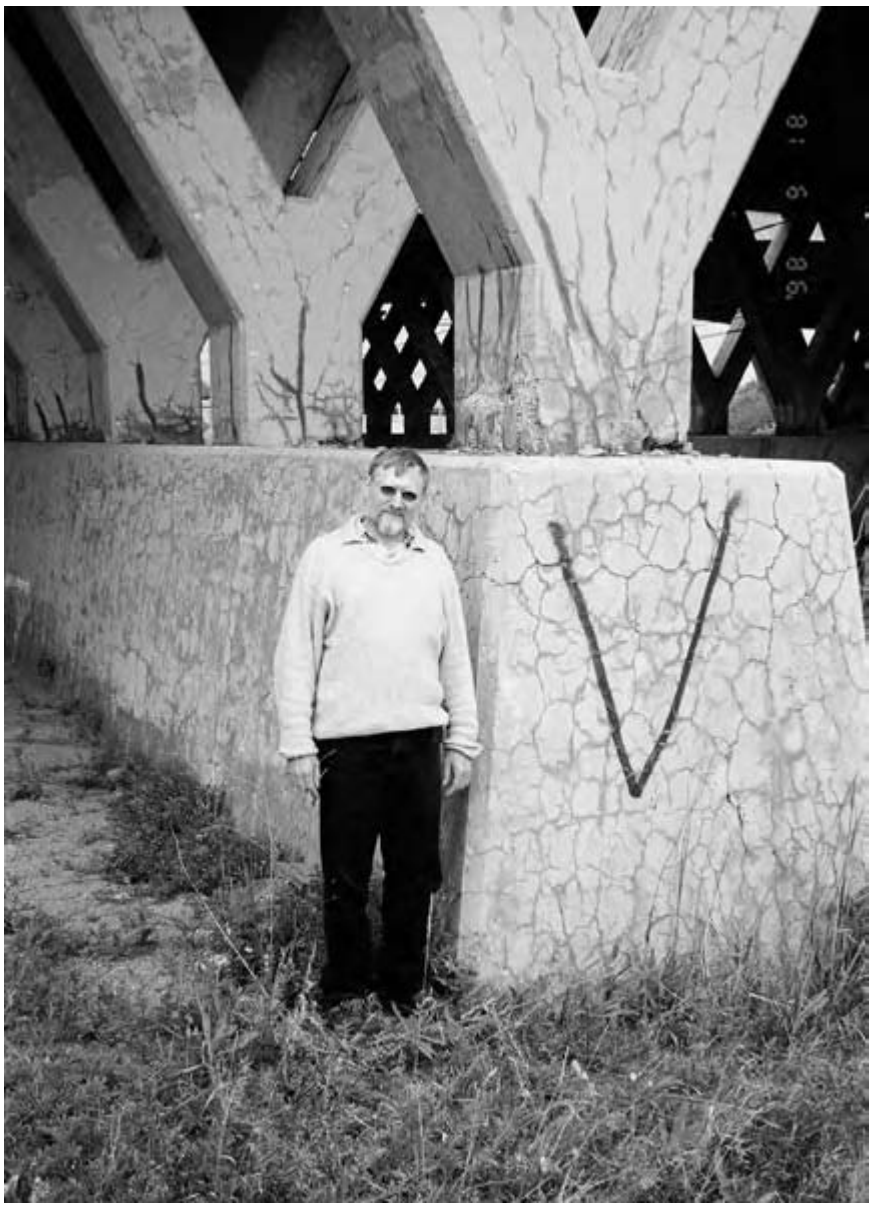
Field inspection

Before a field inspection is carried out, all information and background material about the structure and the problems and history of damage should be analysed. Visual inspection of the structure gives an overview of the problem. Important signs of ASR are map cracking, longitudinal cracking, pop-outs and movement of structural elements caused by volume expansion and deformation of concrete members. Figure 2.1 shows map cracking in a bridge foundation and columns suggesting the occurrence of ASR which also has been documented by microstructural analyses. Reduction or closing of expansion joints between structural elements also indicates the occurrence of expanding ASR. However, map cracking can be caused by other processes, e.g. drying shrinkage, sulphate attack and even freeze–thaw processes. Sometimes, exudation of ASR gel (which is water soluble) can be observed on the surface of the concrete not exposed to water. Cracking due to ASR will be influenced by the reinforcement. Therefore longitudinal cracks parallel with the principal reinforcement can often be observed on beams, plates and columns. Steel reinforcement can be extended by ASR with consequence of reduced carrying capacity. In some cases, ASR occurs in concrete without any sign of map cracking, expansion or deformation and can be identified only by laboratory examinations.

Registration of cracks and crack type(s), pop-outs, surface discoloration along cracks, efflorescence and precipitations, measurement of crack widths and sign of expansions should always be carried out together with photo documentation and a written record. Photographs of ASR damages in bridge structures have been published by the Strategic Highway Research Program (Stark 1991b, 1994). In cases where gel has been precipitated, the gel can be verified by use of uranyl acetate testing.

Uranyl acetate test

The uranyl acetate (uranium) fluorescence method detects sodium and indirectly verifies the occurrence of ASR. By applying an uranyl acetate solution to the concrete surface containing gel, the uranyl ion substitutes for sodium in the gel, producing a fluorescing constituent visible in ultraviolet light. However, some gels contain only minor amounts of sodium (potassium-rich or calcium-rich types) and these will not be detected. The uranyl acetate test should be used only as a supplement to microstructural analyses and ASR should not be diagnosed solely by this method. ASR gel is water soluble and in most cases has been washed away by rain-water.



2.1 Map cracking in a bridge foundation and Y-columns in Canada.

Uranyl acetate is moderately hazardous and precautions should be taken. UV light will damage sight, and protective glasses should be used. Further information on the method is given by the Strategic Highway Research Program (Stark 1991b, 1994).

Surface mapping of cracks

Measurement of cracks due to ASR is probably the most important way to assess ASR damage in a structure. Two methods for crack measurements are given in the following which can be used to assess individual structures or for survey investigation.

The Institution of Structural Engineers suggests crack summation for initial appraisal of ASR damage in structures (Institution of Structural Engineers 1992). A rough indication of the expansion in the structure is provided by measuring the widths of all cracks crossed by at least five straight lines with a minimum length of 1 metre and equal distance at least 250 mm. The lines should be perpendicular to the principal crack orientation on the most severely damaged concrete element. The expansion can be assumed to be equal to the sum of the widths of the cracks divided by the length of the lines drawn on the concrete expressed as mm/m.

The Norwegian map cracking system measures cracks by use of a crack width gauge and estimates the percentage of cracking in structural elements (Jensen 1993). It is an easy and fast method to get information on the extent of surface cracking in concrete structures. The largest cracks (maximum cracks) are easy to identify in the structural elements and these should be the target cracks to be measured. Cracks with occurrences in map cracking or cracks thought to be caused by ASR (e.g. longitudinal cracks in beams, columns or end faces of plates and walls) should be measured and registered. This should be done in all the structural elements in the structure, depending on type of structure and availability to do so. A crack width gauge, magnifying glass with measurement scale or a crack microscope can be used. Crack widths as small as 0.05 mm can be observed by the naked eye.

In addition to crack measurements, the area percentage in the structural element where map cracking or other ASR-related crack occurs should be estimated or, if possible, measured. This should be done in all the structural elements of the structure. This part of the investigation is more subjective and uncertain than the crack measurement but will give important information on the extent of the cracking between the elements. Other information important for the condition of the structures should be reported, too, and both overview and detail photographs should be taken at each structure. Observations should be registered in a scheme as well as in photographs. An example of surface mapping of cracks is given in Section 2.4.1.

Taking cores

To obtain information on the ASR and the reacted aggregates, it is necessary to drill cores from the structure and investigate the concrete under the microscope (microstructural analysis). It is recommended to drill a minimum of two cores from each structure. The cores should be long enough to

permit concrete more than 10 cm beneath the original outer to be examined and to allow the dimensions of any overall crack pattern to be studied. Appropriate precautions should be taken during core sampling and subsequent sample preparation to ensure that evidence of ASR is retained.

Laboratory investigation – microstructural analysis

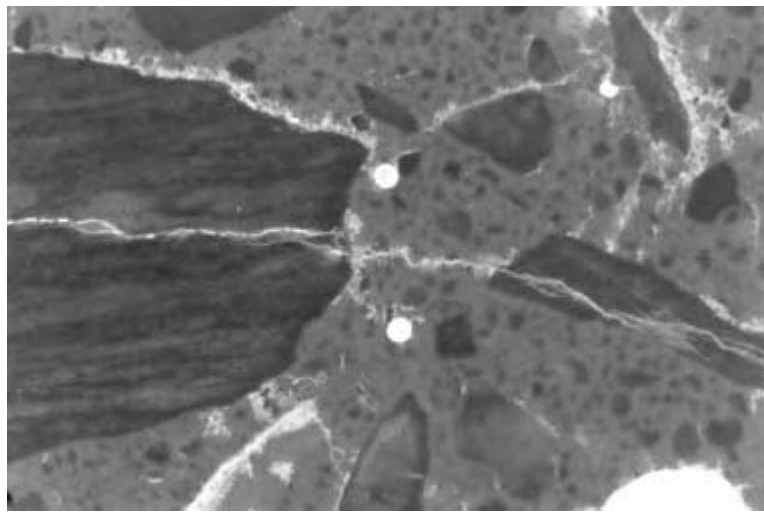
It is strongly recommended to use microscopic techniques, e.g. microstructural analyses, to diagnose ASR. Microstructural analysis is the visual examination of cores, polished half cores (sawn along the length axes) and thin sections (0.03 mm thin slice of concrete mounted on a 3 cm × 5 cm glass plate). It is advantageous to impregnate the concrete with epoxy containing fluorescent dye (e.g. Hudson Yellow) to highlight the microcracks and porosity. For the examination of polished half cores, a low-power stereomicroscope can be used. Examination with fluorescent light can be done using a UV-lamp. Figure 2.2 shows a polished fluorescence impregnated core slab photographed in UV light. Thin sections can be examined by use of a petrographic microscope mounted with polarizing filters and a UV filter. Figure 2.3 shows a micrograph from a thin section of a reacted aggregate with gel in a crack. Microstructural analyses should always be carried out by experienced personnel with petrographic experience and knowledge of ASR. Important observations on ASR and reacted aggregates are given in Table 2.2.

Microstructural analysis can be further supplied by scanning electron microscopy (SEM) mounted with an EDX analyser, WDX analyser or a micro probe microanalyser (EPMA). By these techniques the composition and nature of reaction products can be verified together with other microstructural changes of the concrete. It is very important not to use SEM investigation without other microscopic techniques because of the limitations of these techniques and because the investigation area is only a few millimetres square, which is not necessarily representative of the concrete in the structure.

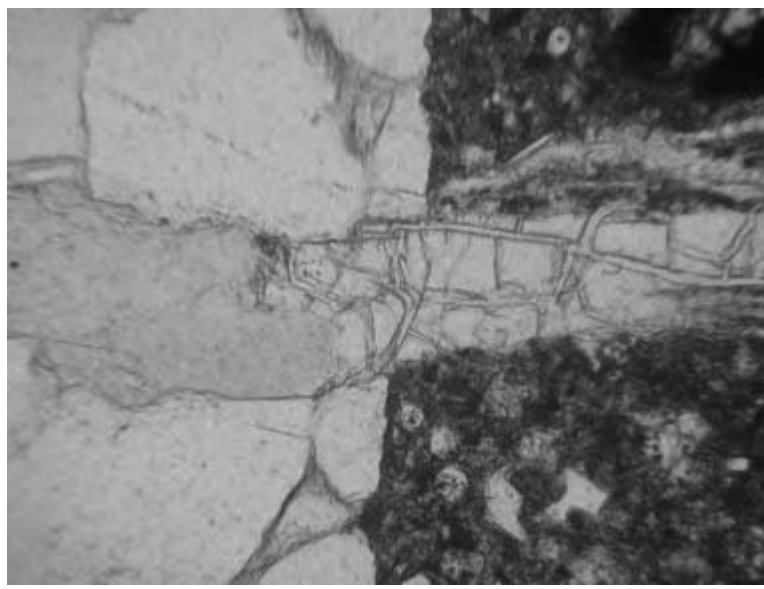
It should be noted that the occurrence of alkali–silica gel confirms the existence of ASR in the concrete; it does not necessarily mean that the reaction causes or has caused any damage to the concrete. This can be evaluated by studying the crack pattern in core materials from the structure as described in the following. Unless involved with the site investigation and the selection of core drilling locations, a petrographer should be careful not to reach unqualified conclusions from the laboratory study of concrete.

Laboratory investigation – assessment of damage

To assess the rate of damage in the concrete the crack pattern can be studied under the microscope on polished slabs of cores taken from the



2.2 Polished fluorescence impregnated core slab photographed in ultraviolet light. Note that cracks and porosities appear whitish. Length of photo is 40 mm.



2.3 Micrograph from a thin section of a reacted aggregate. Note the internal dissolution of constituents in the aggregate, the reaction products and that a crack filled with gel runs out into the cement paste. Plane polarized light. Length of photo is 1 mm.

Table 2.2 Signs of ASR by microstructural analysis

Gel and aggregates	Observations
ASR gel may occur as:	Gel exudations on the surface of cores and on the sawn and polished surfaces of samples
	Reaction rims around the aggregates on broken surfaces of samples
	Gel fillings in air voids and cracks in the concrete (normally whitish colour in ordinary light)
	Gel impregnation of the cement paste around porous reacted aggregates and cracks filled with gel
	Gel in cracks inside aggregates (often cryptocrystalline)
Identification of reactive aggregates:	Gel situated at the margin of aggregates and reaction rims in the aggregates (Note that dark rims can be observed around some gravel particles that can be related to weathering and have nothing to do with ASR)
	Reaction products located within the aggregate
	Cracks originating from within the aggregate and penetrating the surrounding cement paste together with reaction product
	Gel impregnation of the cement paste around reacted aggregates (observed e.g. in porous flint and opal)

structures under investigation. To make a relationship between observations from the laboratory investigation and field investigation, cores should be taken in areas where surface mapping has been carried out. There are two methods to assess the damage rate in cores: the damage rate index and the Norwegian crack counting method.

Damage in cores can be registered by examining polished cores under the microscope. A method called ‘damage rate index (DRI) method’ has been published and used around the world (Grattan-Bellew and Danay 1992; Grattan-Bellew 1995). The DRI method registers defects by use of a binocular microscope (16× magnification) over a minimum area of 180 cm^2. Defects are coarse cracks, coarse particles with cracks and gel, debonded coarse particles, reaction zones, cracks in the cement paste, cracks and gels in the cement paste, air voids with gel and coarse particles with ‘wide’ cracks. Each parameter is multiplied by a factor, normalized to 100 cm^2 and summarized.

By conducting the DRI method on concrete from various portions of the investigated structure, the variable extent of ASR damage is better characterized. The method has been used with success on several structures and has given important quantified information on the current condition of concrete affected by ASR (Rivard *et al*. 2000; Shrimer and Jones 2000). According to Lindgaard and Wigum (2003) the DRI method is rather time consuming and inaccurate owing to the use of 'undefined factors' and the Norwegain crack counting method was preferred.

A simpler and faster method than the DRI method was developed during the first national alkali project in Norway (Jensen 1993). The Norwegian crack counting method uses fluorescence impregnated polished cores examined under UV light where cracks and porosities (e.g. gel) are very visible, e.g. cracks as small as few micrometres can be observed without use of a microscope. Before the test, aggregate particles with cross-sections >4 mm visible on the plane section have to be counted and the area of the plane section (in cm^2) measured. Three parameters examined under UV light should be registered and counted: (1) aggregates (with cross-sections >4 mm) with internal cracks, (2) aggregates (with cross-sections >4 mm) where cracks run into the cement paste (significant for ASR) and (3) the number of cracks in the cement paste. Parameters for aggregates should then be normalized to the percentage of aggregates with cross-section >4 mm and cracks in the cement paste to cracks/cm^2. Gel should be registered too. Examples of the use of the Norwegian crack counting method are given in Section 2.4.1.

Other test methods

ASR influences the mechanical parameters of concrete, sometimes significantly when large expansions occur in the concrete or ASR is in an advanced stage. Compressive strength can be reduced by up to 25% and tensile strength even more. The stiffness of the concrete (elastic modulus) is influenced significantly and can be reduced up to 50% depending on the expansion in the concrete (Hobbs 1988).

The ultrasonic pulse velocity (UPV) technique can be used to assess the quality of the concrete damaged by ASR. The UPV depends on the presence of open cracks and absence of gel in cracks. Cracking caused by ASR will therefore reduce the UPV compared with uncracked concrete. The UPV technique is described in more detail in Chapter 7. The impact echo test is another method for detecting cracks in ASR damaged concrete and is further described in Chapter 12.

The rest expansion test on cores has been used to predict the future expansion of concrete. The method is described by the Institution of Structural Engineers (1992) and has been used widely in the UK. However, lack of information on the correlation between core testing and expansion

of the structure means the core expansion result will be of limited value. The method is therefore not recommended for assessing future expanding due to ASR (Sims 1992).

2.3.3 Long-term monitoring methods

Two monitoring methods are recommended to assess future damage and remaining service life of structures damaged by ASR: expansion/crack measurements and RH. Expansion and/or crack measurement measures the effect of deleterious ASR on the structure and gives information on the future damage. For assessment of ASR it is important to know how the concrete expands and that cracks are 'alive,' and how the increment will grow over time. If cracks or the concrete do not expand it is possible that ASR has become innocuous (dormant), but only a few examples of this have been published internationally. However, only long-term measurements over many years should be used for such an assessment. Measurement of RH in different locations and depths in the concrete structure gives information on the variations of ASR throughout the structure. Higher RH will over time produce more damage to the concrete than lower RH. RH is not always uniform through the concrete and should therefore be measured at different depths. Long-term measurements of cracks/expansions and RH are therefore recommended methods for assessment of remaining service life, future damage and effects of rehabilitation on structures damaged by ASR.

Crack and expansion measurements

Expansion of concrete and cracks can be done in several ways. Expansion of the concrete can be monitored by use of electrical strain gauges, whose electrical resistance varies in proportion to the amount of strain in the device. Several commercial types are available. Use of vibrating wire sensors has given promising results on the expansion in two ASR-damaged structures in the Netherlands, but the long-term durability of the tests has yet to be assessed (Borsje *et al*. 2002; Bakker and Postemar 2003).

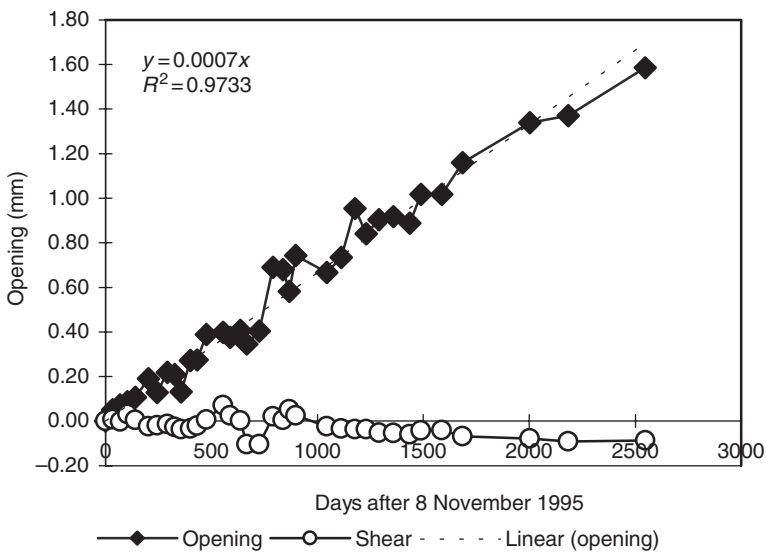
Expansion on the concrete surface can also be monitored manually by mounting two or several steel discs with centred conical holes along a line at equal distances, depending on the type of strain gauge to be used. The distance between locating discs is measured by use of a demountable strain gauge, e.g. Demec gauge, and the expansion is calculated by incremental increases by time relative to total measurement length in mm/mm or %.

Expansions through or in the concrete element can be measured by use of a sliding micrometer in a hole drilled into the concrete. Since 1987 sliding micrometer – ISETH – measurements have been carried out in a Norwegian foundation damaged by ASR through the reaction of rhyolite aggregates. The measuring hole is 6 m deep. Over four years, the accumulated

expansion is 1.35 mm/6 m, or the concrete foundation has increased 0.023% during four years. Measurements also show that the expansion in the top of the bore hole is larger relative to the bottom of the bore hole (Winsnes 1991; Jensen 1993).

More accurate results than those attained by use of the crack width gauge or crack microscope can be obtained by use of three points measurements. Expansion of cracks is measured on three triangularly arranged measuring discs (A, B, C) with equal distances, e.g. 50 mm, drilled into the surface and hereafter epoxy glued. The distances A–B (always along the crack), A–C and C–B are manually measured by a strain gauge (Demec gauge). Calculation of expansion (opening of crack) and shear (movement parallel to the crack) is by use of simple trigonometric calculations. All results have to be corrected by use of a theoretical temperature coefficient (10^{-5}/°C). Average expansion from many measurements is calculated by use of regression analysis. The advantage of using three point measurement is that the expansion/reduction perpendicular to the crack and parallel to the crack can be measured (Jensen and Haugen 1996).

Figure 2.4 shows the expansion of a crack (initially 2.5 mm) in a pier from a concrete dam over a period of seven years. Note that the yearly expansion rate (opening) is about 0.25 mm, which is the highest expansion rate measured in Norway. Expansions parallel with the crack (shear) are in this case



2.4 Expansion of a crack (opening) in a concrete dam over seven years. Shear is movement along the crack.

nearly zero. Measurements over many years on different locations of the dam have shown large variations in the expansion rate (opening) between cracks from 0.01 mm to 0.25 mm yearly (Jensen 2002a).

Relative humidity

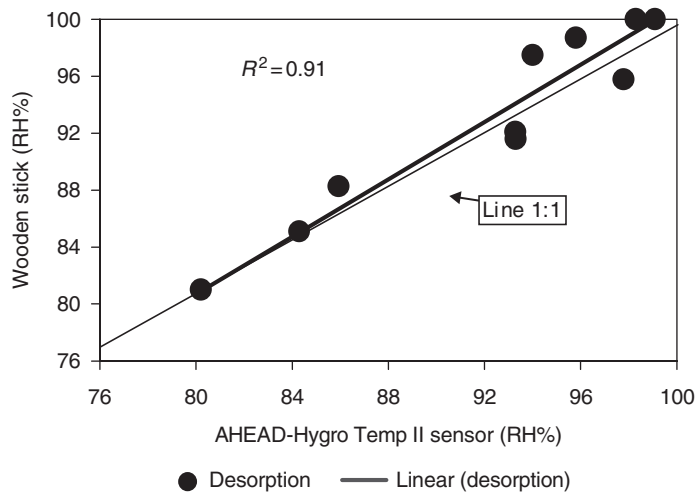
Relative humidity is the measure normally used to assess ASR. The limit is around 80% RH, with some variations due to temperature and concrete type. It is important to know that higher RH gives more damage relative to lower RH and therefore RH is the main parameter for variation of ASR damages in structures. Theoretically RH will never reach 100% in the concrete because of the influence of salts in the pore solution and capillary pores in the concrete. In practice, RH measurements in real structures damaged by ASR often measure 100%. RH measurements in structures are difficult and are often reported to give confusing results. This is in many cases caused by insufficient mounting in the structure (allowing admission of atmospheric air) and non-durable humidity sensors. Moreover, most electrical humidity sensors are not suitable for measurements of relative humidity higher than 95–98%.

Humidity can be measured in several ways. Drilling cores from structures and testing in the laboratory is a destructive method used for measurement of water content and RH, and is not described further. Electrical humidity sensors of different types are frequently used to measure RH. Normally a hole is drilled into the concrete and the sensor is put into the hole and isolated from the atmospheric air. When equilibrium with the concrete has been obtained, after 8–24 hours, the RH can be recorded by use of a humidity meter. Sometimes humidity sensors permanently are mounted into the concrete. Experience has shown that many electrical sensors break down within a few years in structures located in humid environments (outdoors in most countries) and are not very successful on a long-term basis (Bakker and Postemar 2003). Research in Norway has concluded that electrical sensors should be calibrated after two months (Sellevold 1997). The humidity can also be measured indirectly by the electrical resistance of the concrete or by use of, for example, autoclam and multi-ring methods, where the electrical conductivity is measured. Long-term monitoring tests with multi-ring in Dutch and Norwegian structures have been reported to be unsuccessful because the system has broken down after a short time (Steen 1998; Bakker and Postemar 2003). Generally, one can say that humidity measurements often give uncertain and confusing results and are not stable over the long term.

Measurement of relative humidity by use of wooden sticks of the species Ramin (*Gonystylus macrophyllum*) drilled into the concrete is a reliable

method with long-term durability: wooden sticks mounted in Norwegian concrete structures in 1995 are still reliable and in use. The method is not commercial today, but wooden sticks can easily be prepared and calibrated, and inexpensive measurement equipment can be bought commercially in most places. Guidance on preparation and calibration of wooden sticks and measurements has been given by Jensen and Haugen (1996) and Jensen (1998, 2000a). Measurement of relative humidity by use of wooden sticks drilled into the concrete has been used in the UK and Denmark. In the UK, one company has used this method on several structures with AAR (Wood 1985, 1990). In Denmark one company has used the method in a few structures and for laboratory testing (APM 106, 1989). The method has been successfully used since 1995 on several concrete structures damaged by ASR in Norway. Documentation of the wooden stick method has been published in Norway and internationally (Jensen and Haugen 1996; Jensen 1998, 2000a,b, 2003a,b). Correlation tests with two commercial humidity sensors (the Norwegian AHEAD Hygro Temp II and the Swedish Humi Guard) have shown that wooden sticks still are in good condition and reliable after nine years (Jensen 2003a). Figure 2.5 shows the correlation between the wooden sticks which have been in continuous use for three years and AHEAD hygrotemp sensors (sensors from the company Rotronic). Note the acceptable correlation between the two methods (Jensen 1998).

In Esboenderup Hospital in Denmark wooden sticks were used together with five other methods to measure humidity. The sensors were mounted on access balconies damaged by ASR and after the balconies were surface



2.5 Correlation between wooden sticks and AHEAD hygrotemp II sensors (Rotronic).

protected. After 2.5 years the average RH was reduced from 100% to 81% measured by wooden sticks and 88% by the Finnish Vaisala probes. The other methods, water percentage in cores, electrical resistance with resistance nails, HUM sensors (a year's results – a new method developed by Force Technology, Denmark) and GANN Hydromette, all showed reductions in the humidity. It was concluded that all the sensors have the same tendency, namely decreasing values of moisture content in the balcony after renovation (Kofoed 2004; Poulsen 2004).

For many concrete structures, e.g. bridges, the humidity exposure varies between the different structural elements and the orientation of the structure. For concrete located in water or in the ground, e.g. foundations, abutments and piers, capillary suction from the surroundings is important. However, capillary suction and the transportation height in the concrete are normally not very high and depend on the porosity and permeability of the concrete. Water ingress from the surroundings (suction height) could not be measured 1 m above ground level/high water level in bridge columns with a water : cement ratio of 0.45–0.5 located in the river bed and in the river (Jensen 1998). For most structural elements, e.g. columns, beams, plates and girders, rain water and water spray (marine structures, dams) are the major sources of water into the concrete. The amount of water exposure depends on the climatic conditions and orientation of the structure, e.g. exposure to the prevailing wind direction (rain water) or sun. When the structural element or part of the element is sheltered from the ingress of water, the humidity in the concrete is determined by the humidity in the air. The annual average RH in air at the location can then be a measure of the maximum RH in the concrete. However, an RH equilibrium between the concrete and the surrounding air will take some time to become established after the construction period, depending on concrete type, dimensions and RH in the air. For massive concrete structures, e.g. dams and bridge members, remaining water from the concrete mix might be sufficient to hold an RH higher than 80% in the concrete even when the structure is located in an arid climate (Stark 1991a). For remedial measure where ingress of water from the surroundings is to be stopped or reduced (e.g. surface treatments), it can be hypothesized that the reduction of RH in the concrete cannot be lower than the annual average RH in the surrounding air (Jensen 2003a).

RH measurements at several different locations are needed to obtain the full scenario of the variability of RH and indirectly the rate of ASR in most concrete structures. The environmental exposure and different ways of water ingress require that RH is measured at different depths (not only near the surface) on the concrete member to provide a profile through the member. For assessment of surface treatment on ASR-damaged structures, RH measurements are important.

Table 2.3 Structures classified by risk category

Category	Type of structure/element
S1	• Non-load-bearing elements inside buildings • Temporary or short service life structures • Easily replacable elements • Most domestic structures
S2	Most building and civil engineering structures
S3	Long service life or highly critical structures where the risk of deterioration from AAR damage is judged unacceptable, such as: • Nuclear installations • Dams • Tunnels • Exceptionally important bridges or viaducts • Structures retaining hazardous materials • Monumental structures with high aesthetic requirement*

*Included after publication in 2004.

2.3.4 Assessment of field and laboratory results

Results from field inspection and laboratory results will give a diagnosis of the problem and variation on ASR in the structure when sufficient samples from different structural elements with different degrees of damage have been taken and analysed. Long-term measurements are important for the assessment of future damage and for appraisal of remedial and mitigating measures. The assessment of structural damage and the evaluation of future deterioration and reduction of functionality of the structure are very important.

The owner of the structure must take the decisions on which investigations and remedial measures should be carried out to assess the risk for failure of the structure. Rilem committee ARP-191 suggests structures to be categorized in three risk levels, S1 – low risk, S2 – normal risk and S3 – high risk. It is up to the owner, or authority responsible for the structure, to decide on the appropriate level of risk. The decision will be affected by the economic effects of possible failure or deterioration as well as engineering and safety considerations. Table 2.3 shows structures classified by risk category (Nixon *et al*. 2004).

2.4 Case histories

The following case histories give examples of inspection and monitoring of ASR damage on individual structures and as survey investigations. Examples of the effects of surface treatments on structures are also given.

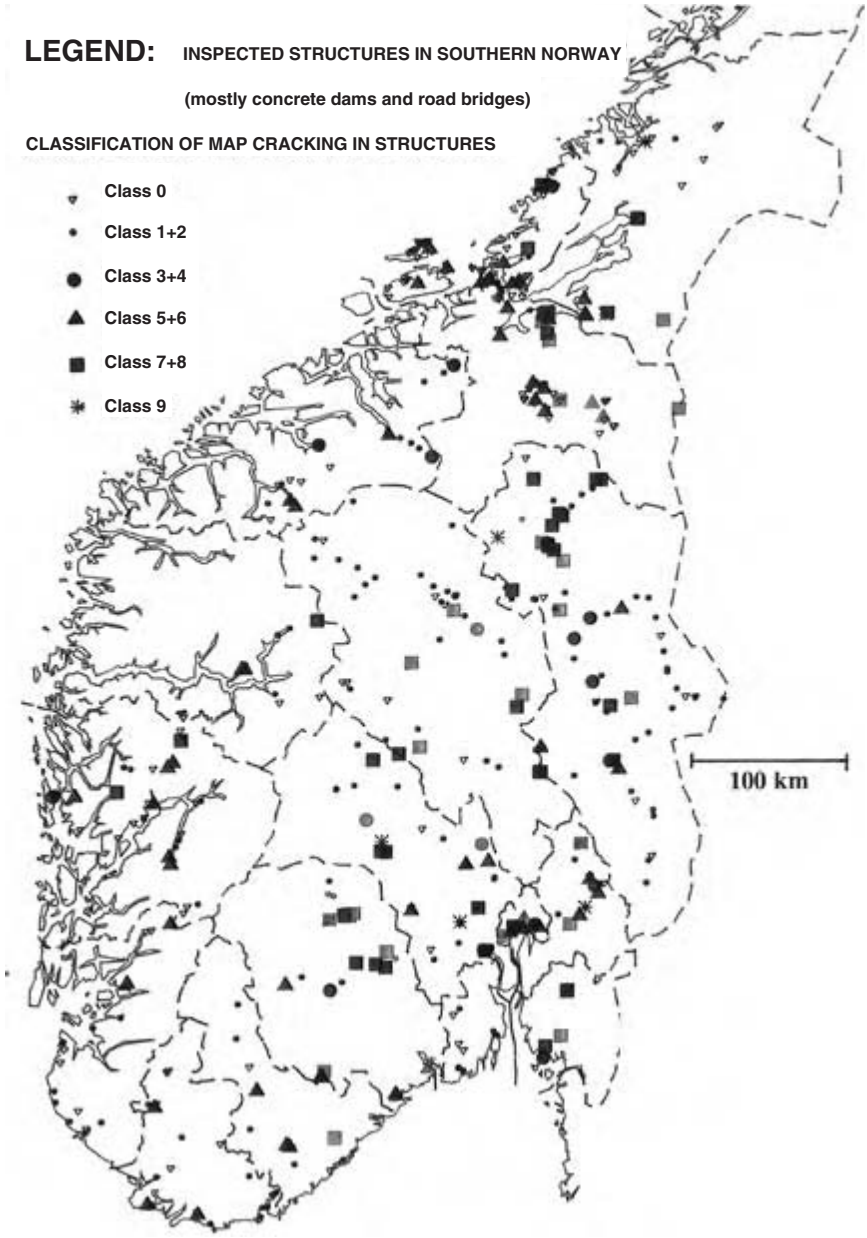
2.4.1 Survey investigation for ASR in Norway

To obtain information on the distribution of ASR in Norway, which was newly documented in the late 1980s, a simplified and fast surface mapping method was developed and a classification system was made (Jensen 1993, 1994). Common to most classification systems is that the damage and/or partial observations (e.g. degree of cracking) are grouped into one or several scoring system(s) by the investigator *in situ*. Therefore the reliability of the classification depends very much on the experience of the personnel and the calibration of assessments of observations and scores between personnel. To reduce subjective assessments by the investigators during the field inspections carried out in 1990, it was therefore decided not to classify damage *in situ*, but to measure maximum crack width and estimate the area distribution of map cracking from individual structural elements in the structure. Here the most subjective data is the estimate of the area of map cracking in the structural element. To help the classification, overview and detailed photographs of the structure and structural elements with map cracking were taken, figures were drawn and important information was reported and put into a database. Table 2.4 show the grouping of structural elements into classes.

Figure 2.6 shows the distribution of 468 investigated structures older than 10 years (mostly road bridges) in southern Norway. Microstructural analyses from 31 structures (86 cores) have confirmed that structures with crack

Table 2.4 Classification system based on maximum crack width and area distribution of map cracking in the structure

Class	Criteria
Class 0	No map cracking has been observed in the structure
Estimated area with map cracking is less than 30%:	
Class 1	maximum crack width less than 0.05 mm (not visible with the naked eye)
Class 2	maximum crack width 0.05–0.5 mm
Class 3	maximum crack width 0.5–1 mm
Class 4	maximum crack width larger than 1 mm
Estimated area with map cracking is larger than 30%:	
Class 5	maximum crack width less than 0.05 mm (not visible with the naked eye)
Class 6	maximum crack width 0.05–0.5 mm
Class 7	maximum crack width 0.5–1 mm
Class 8	maximum crack width larger than 1 mm
Class 9	The structure has not been evaluated according to the classification system



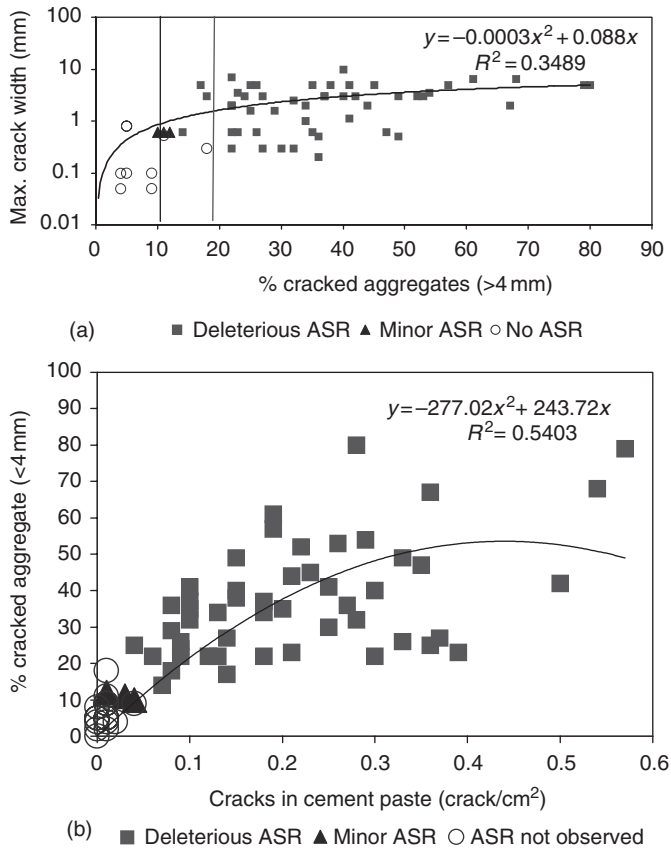
2.6 Map plot depicting the distribution of 468 investigated structures older than 10 years (mostly road bridges) in southern Norway. (Source: Viggo Jensen 1993)

widths larger than 0.5 mm (high-ranking classes) were generally damaged by ASR (Jensen 1993, 1994). The crack distribution shows that crack width is not related to construction age alone. More detailed statistical investigations have shown a tendency that structures built in the period 1950–1960 are more cracked compared with other periods, but the reason is unknown (Jensen 1993). In the period 1993–1996 a survey investigation in northern Norway was carried out using the same principles as in southern Norway (Jensen and Haugen 1996). The same conclusions were drawn, namely that map cracking observed and registered on the structure is a good measure for the occurrences of deleterious ASR (ASR was found in 36 structures). Many more structures damaged by ASR have today been identified and documented by microstructural analyses in Norway by other investigations, e.g. a resent research project investiging structures in southern Norway by Lindgaard and Wigum (2003).

Another import issue of the survey investigation was to document the relationship between damage in the concrete structures and core material analysed by the Norwegian crack counting method described in Section 2.3.2. Assessment of the relationship between cracking in cores and cracks on the concrete structures is shown in Fig. 2.7 (Jensen 2003b). The plot is based on 83 cores from structures located in southern Norway. The cores were first investigated by microstructural analysis and ranked as 'deleterious ASR', 52 cores, 'minor ASR', 7 cores, and 'ASR not observed', 24 cores. ASR was documented by examination of 112 thin sections. Because of the uncertainties in counting cracks in cores and measurements of maximum crack width in structure the correlation is rather low but real. Moreover, a 'grey zone area' between 10% and 18% cracked aggregates (see Fig. 2.7a) exists where 'deleterious ASR', 'minor ASR' and 'ASR not observed' plot together. It can be suggested that 10–18% 'cracked' aggregates is the limit for distinguishing between concrete suffering from ASR or not in Norwegian concrete structures. In cores, a low but acceptable correlation exists between 'percentage cracked aggregates' and 'cracks in paste' (Fig. 2.7b). Note also that a few cracks occur in cores where ASR has not been diagnosed. Therefore, it is likely that ASR has caused most of the cracks occurring in the cement paste. Very few cracks occur in samples where ASR has not been diagnosed.

2.4.2 Elgeseter Bridge in Trondheim

Elgeseter Bridge in Trondheim was built in 1949–1951 as a continuous 200 m long reinforced concrete bridge supported by eight rows with four columns, each having a diameter of 80 cm (Fig. 2.8). ASR was diagnosed by microstructural analysis in 1990 to be caused by the rock types mylonite, graywacke and argillite, this in columns, beams, girder and the road plate (Jensen



2.7 (a) Percentage cracked aggregates in cores related to maximum crack width in the structure. (b) Percentage cracked aggregates and cracks in cement paste in cores.

1990). In columns, several longitudinal vertical cracks up to 3 mm in width can be followed about 10 m from ground level to the underside of the supported beams. Some columns also contain map cracking. Inspection and measurement of cracks in columns show more cracking on the western faces than on the eastern faces owing to rain water (eastern faces of columns stay dry when it rains); see Fig. 2.9. Measurements have also shown that columns exposed more westerly and located in the middle of the river have more cracks.

The major problem besides cracking in columns is the movement of the bridge and the reduction of the only expansion joint in the bridge, which



2.8 Elgeseter Bridge in Trondheim, Norway.

was originally 20 cm but today is zero. Investigations have suggested that ASR had caused expansion of the 200 m long beams and the road plate calculated to be 0.1% after 50 years. Moreover, because columns are fastened to the beams, the upper part of the most northern of the columns has moved to the north (possibly by 15–18 cm) and are not vertical today. Where columns are inclined, the bearing capacity of the bridge is reduced. In 2003, the road directorate rehabilitated all the northern columns closest to the expansion joint. The major repair work was to move columns back to a vertical position. A special steel construction was made to support the beam before demolishing the uppermost metre of the column by 'mini-blasting', a Danish technique. Hereafter, the reinforcement was cut and the column moved back to the vertical position. New reinforcement was then welded to the beam and the upper part of the column remoulded with fresh concrete (Jensen 2003b).

In 1995, an *in-situ* system for measurement of RH by wooden sticks and expansion of cracks was initiated as a pilot project. Eight measurement locations were mounted in one beam and four columns with diameter 80 cm. Discs were mounted in each location for three point measurements across a crack and a specially made plastic tube with wooden sticks was drilled into the concrete for measurements of relative humidity 5 cm and 25 cm from the surface. Figure 2.10 shows a location with three point measurements along a crack and a neighbouring humidity location with the wooden stick pulled out of the plastic tube. Figure 2.11 shows a graph from a column

in Elgeseter Bridge where expansion measurements have been carried out over nine years. Note that the expansion rate after about three years has flattened out but still increases, although at a lower rate. Expansions in Elgeseter Bridge calculated from regression analysis from eight measurement locations give varying results: the openings in columns vary from

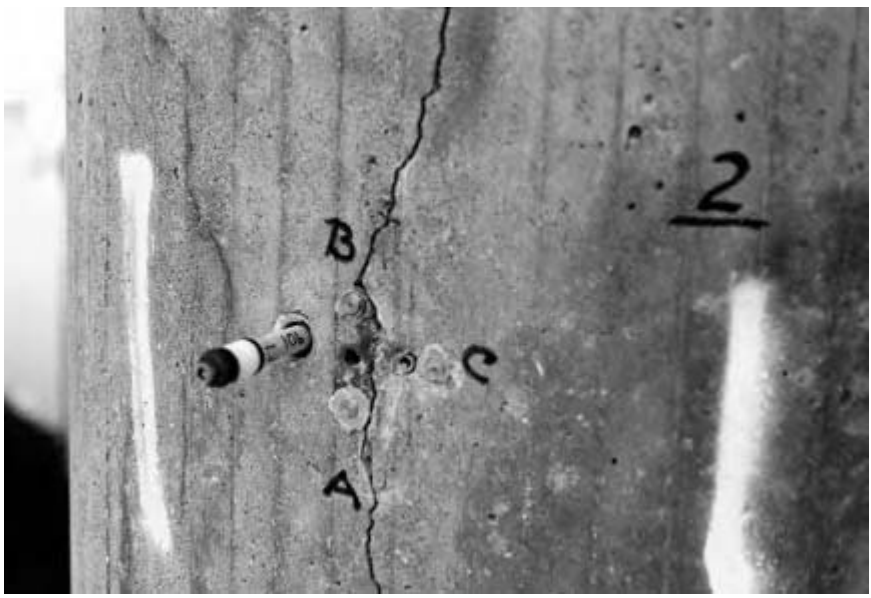


2.9 Column with vertical longitude cracks. Note that western face (near the man) is wet with rain water.

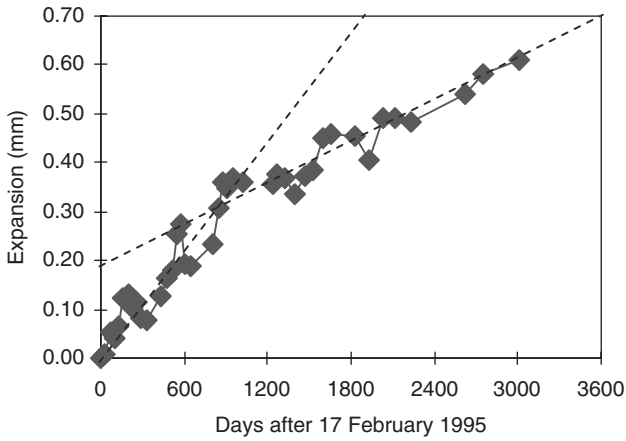
0.04 mm to 0.15 mm yearly. As shown in Fig. 2.11, the expansion rate has decreased over the past years. From 1998, in new measurement locations where several surface treatment products are tested, hardly any expansion has been measured.

Figure 2.12 shows RH and temperature in a measurement location over nine years. The column was silane impregnated after about 1600 days from the first measurement and RH 5 cm from the surface was decreased from about 100% to about 80% after about 2.5 years. This was not the case 25 cm from the surface where RH stayed stable (Jensen 2002b, 2003b). In untreated columns no decrease in RH has been measured.

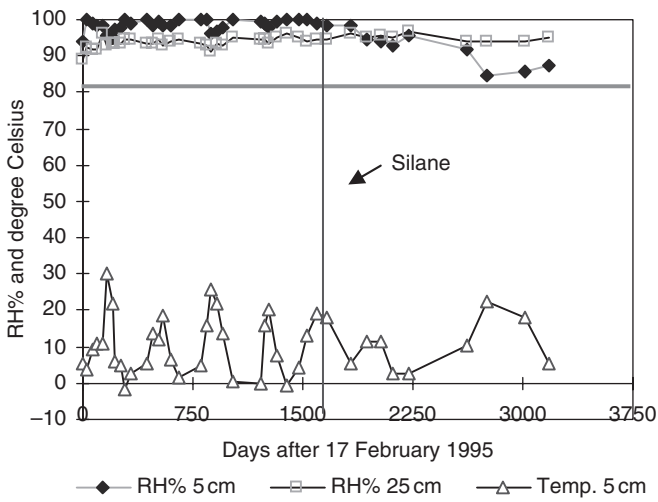
Rain water is an important source of water because western faces obtain higher RH than eastern faces (stay dry during rain), even when the columns are located in the river. Figure 2.13 shows RH profiles through two 80 cm columns located in the river about 1 m over high water level. Note that RH is significantly lower on eastern faces than on western faces. The results show that RH in the bridge varies from 100% to 87%, and is not significantly influenced by temperature fluctuations. Some 5 cm from the surface the RH is more or less stable. Measurement in the same column 20 cm over ground level and 1 m above ground level shows that capillary



2.10 Location with three point measurements along a crack and a neighbouring humidity location with the wooden stick pulled out of the plastic tube.



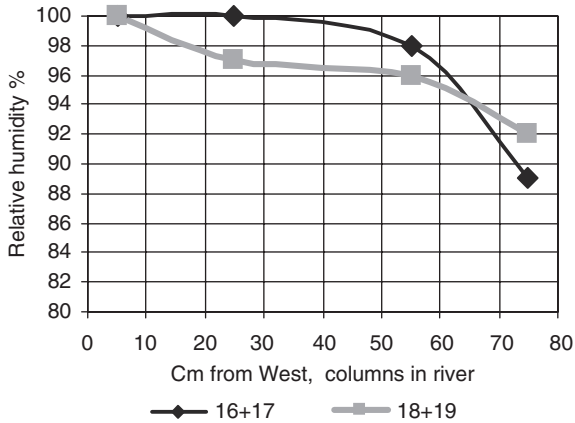
2.11 Expansion of a crack in a column, Elgeseter Bridge.



2.12 RH and temperature over nine years in a bridge column.

suction from the ground does not influence the RH 1 m above ground level.

With the aim of testing the effect of surface treatments and measuring the RH in other columns, both on land and in the river, 11 new measurement locations were mounted in 1999. Three different types of silanes were applied on three whole columns. Silane type A (100% isobutyl-tri-ethoxysilan) was applied by the road directory in July 2000. Silane type B (40% organosilan ester in isopropanol) and silane type C (80% not specified silane type, with creamy consistency) were applied by the product dealers



2.13 RH profiles through two columns with diameter 80 cm located in the river. The western face is 0 of the column and the eastern face is 80.

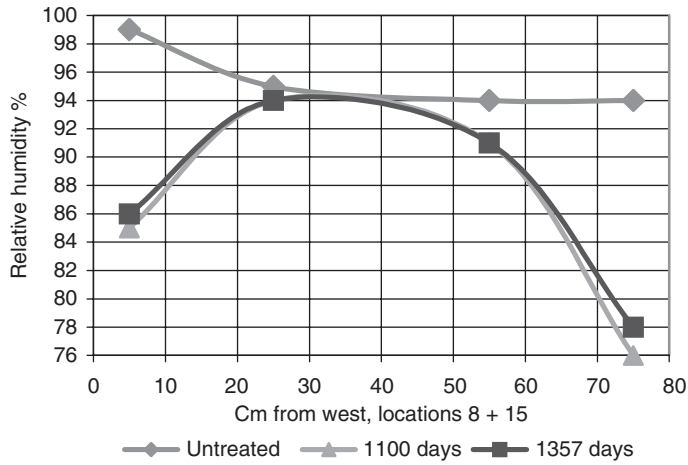
in September 1999. All the products were applied according to the producer's recommendations (Jensen 2000d).

Figure 2.14 show a cross-section through the column impregnated with silane type C (1357 days). Note that RH has been reduced significantly 5 cm from the surfaces 1100 days after impregnation and stayed stable after 1357 days. In the centre 25 cm from the surface some reduction in RH at the eastern face has apparently been obtained. Results from all the treated columns suggest that treatment with silane reduced the concrete's relative humidity 5 cm from the surface, most on the eastern 'dry' face but not in the middle of the columns.

Results of RH measured before treatment and 800 days and 1100 days respectively after silane impregnation of columns are given in Table 2.5. Results suggest that treatment with silane apparently reduces the concrete's relative humidity even when columns are massive and ASR is in an advanced stage. Moreover, one of the products apparently reduces the RH more efficiently compared with the other two products. The average annual RH in air in the nearest weather station to the bridge is 80%.

2.4.3 ASR in railway sleepers

In the period 1972–1992 about 3 million prestressed railway sleepers were produced in three concrete plants in Norway. In 1994 ASR was documented to occur in Norwegian railway sleepers and it was suggested that many of these were or would be damaged by ASR (Jensen *et al.* 2000). With the aim of obtaining information on the extent of the ASR problem,



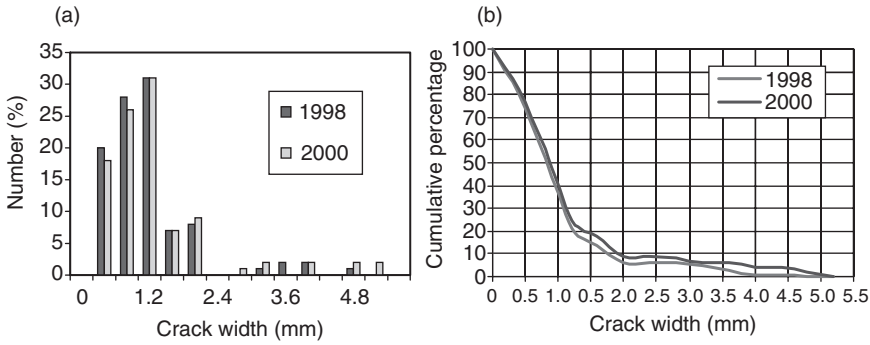
2.14 RH profiles through a column with diameter 80 cm. The western face of the column is 0 and the eastern face is 80. RH is measured before impregnation (untreated) and 1100 days and 1357 days after impregnation with silane type C.

Table 2.5 RH 5 cm from surfaces before and after impregnation, Elgeseter Bridge

	Western face		Eastern face	
	before	after	before	after
Silane A (800 days)	100	96	96	84
Silane B (1100 days)	99	91	95	82
Silane C (1100 days)	98	85	97	76

measurement areas located in different places in Norway were established. Each measurement area was located in the railway track and 100 concrete sleepers from the same production plant and production year were investigated (Jensen 2000d).

Figure 2.15 shows the distribution of cracks in one measurement area located in northern Norway. Cracks were measured by use of a crack width gauge at both end faces and in the centre of the sleeper. Measurements were carried out in 1998 and 2000. Note the large variations in crack widths (up to 5 mm) and the increase in crack widths from 1998 to 2000. The results suggest that crack width increases significantly for cracks wider than 1 mm. Three point measurements also suggest that 'wider' cracks have higher expansion rate than 'smaller' cracks as described in the following.



2.15 Crack distribution in 100 railway sleepers measured in 1998 and 2000.

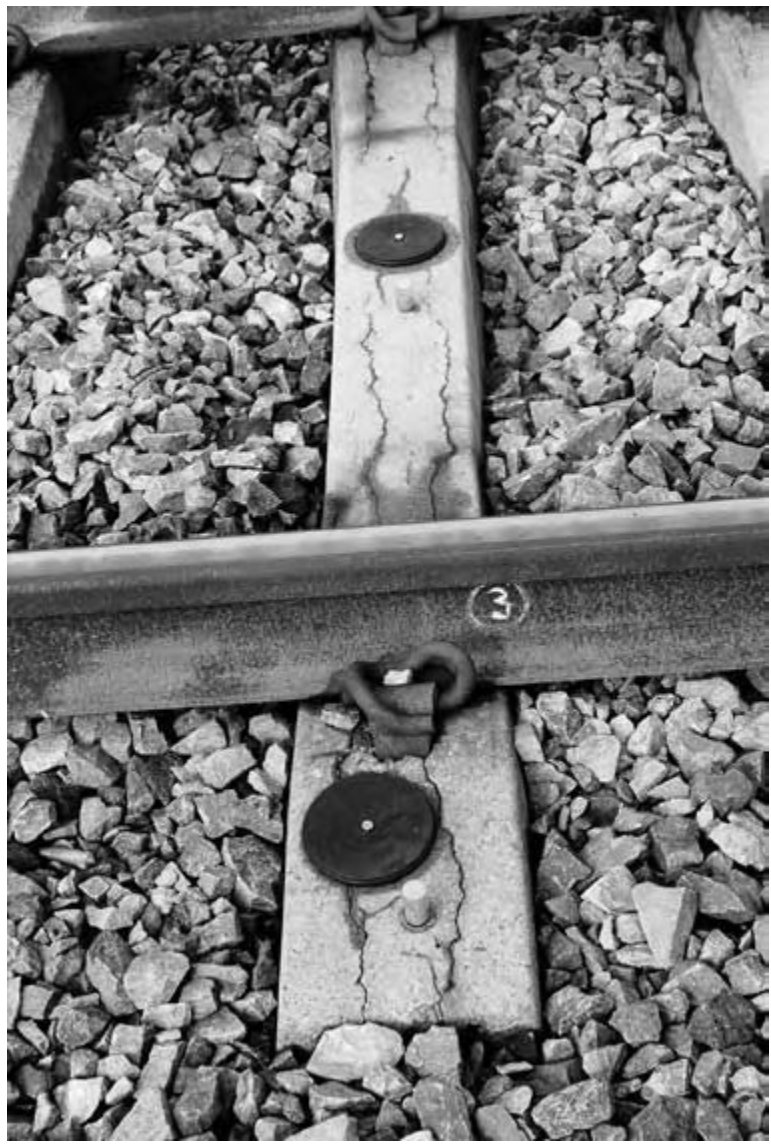
Two test areas, where 19 different surface products have been applied on individual sleepers, have been established. In one of the test areas, located in the railway track in northern Norway, the railway sleepers are significantly damaged by ASR. In the other test area, also located in northern Norway, ASR is in an initial stage but will probably become worse (Jensen 2000d). In each railway sleeper (21 in each test area), three point measurement locations have been mounted in upper surfaces at the end face and in the centre of the sleeper. RH was measured at locations with two wooden sticks mounted in each sleeper; see Fig. 2.16.

Figure 2.17 shows one and two year expansion results from one test area (end face) of railway sleepers cracked by ASR. The *y*-axis shows increase in crack width after one and two years and the *x*-axis shows the initial crack width measured in 1998. Note that cracks expand after one and two years, and that the expansion rate is apparently higher for wider cracks (suggested by the regression straight lines).

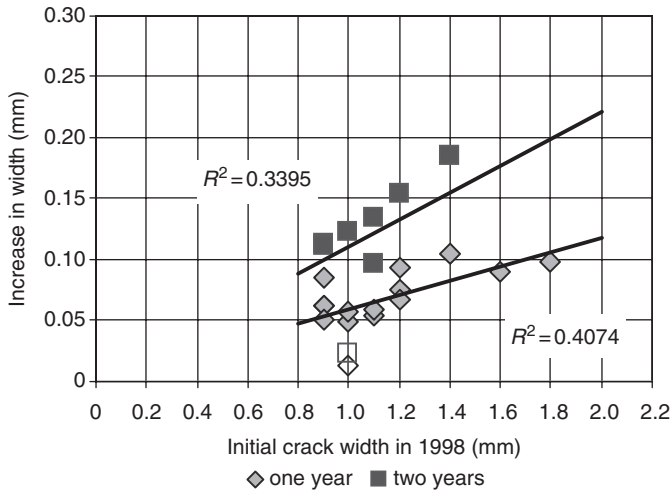
2.4.4 Veritas House in Oslo

The Norwegian Veritas House was built in the early 1970s using prefabricated columns, beams and plates. ASR has been diagnosed by microstructural analyses caused by impure limestone (metamarl), sandstone and mylonite. Delayed ettringite formation (DEF) due to high production temperature was diagnosed (Jensen 1996). *In-situ* measurements were established in September 1998. Relative humidity in 20 places was measured in beams and columns 5 cm from outer surface and in the middle of the elements (17 cm). In all the locations higher RH values have been recorded 5 cm from the outer surface relative to the centre (17 cm) of the prefabricated concrete elements which are 34 cm wide. The location of the elements

suggests that the only source of water in the elements is ingress of rain water in the outdoor exposed faces because inner faces stay dry due to indoor exposure. Expansion was measured in 11 places in the outer faces of beams and columns, but results have been difficult to interpret.



2.16 Railway sleeper damaged by ASR and mounted with locations for relative humidity and three point measurements (under the black cover).



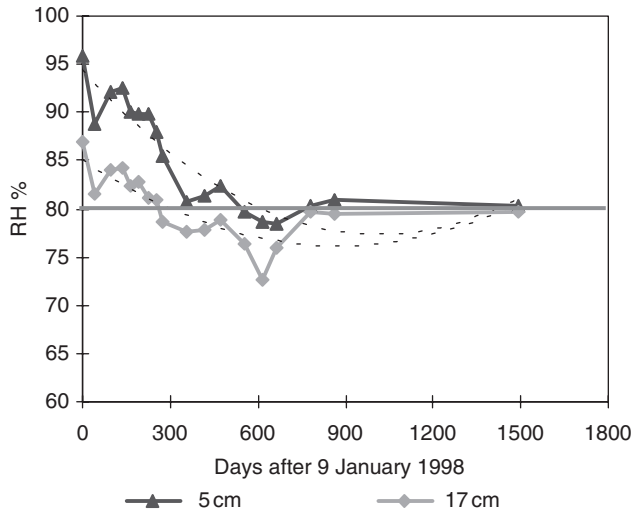
2.17 Expansion results of cracks on railway sleeper one and two years after mounting (end face).

Three types of surface treatments were applied in 1998, acrylic type (elastic acrylic dispersion), oligomer siloxane type (oligomer siloxan/silane + lazur paint) and silane type A (100% isobutyl-tri-ethoxysilan), the same as for Elgeseter Bridge. The product dealers applied the products on the whole of the outdoor exposed faces of columns or beams and according to specification. In addition, the owner (DNV) mounted 'ventilated' aluminium cladding on one column. Surface products were applied one or two months after initial measurement of RH (Jensen 2000c,d).

Figure 2.18 shows the distribution of relative humidity 5 cm and 17 cm from the surface in a column impregnated with silane type A. Note that the RH after about 900 days has been reduced to about 80% and then stays stable, both for measurements 5 cm from the surface and in the middle of the element. The same tendency that RH reduces over time has not been observed in reference locations.

Results (average of several location-regression analyses) of RH from surface-treated and untreated columns/beams from 1998 are given in Table 2.6. Note that the initial RH varies from 89% to 95%, which suggests that RH varies between the different elements. In sites from 1998, significant reductions in RH for all the products have been measured. This is not the case for references (except the ones accidentally impregnated with silane in 2001). The RH in the middle of elements is reduced with time for both untreated and treated elements. The average annual RH in air in the nearest weather station is 79%.

In June 2001 the whole building complex was impregnated with silane



2.18 Distribution of RH in a column impregnated with silane type A, DNV.

type A. Unfortunately, some or all of the reference locations (and treated test locations) were also impregnated with silane type A. Therefore, several of the reference locations show reduced RH today.

2.5 Trends in analysing and preventing ASR

2.5.1 Implementation of knowledge and methods

Correct diagnosis of the damage process in concrete structures is essential for the assessment of present and future damage and appraisal of remedial measures. For structures damaged by ASR no easy method exists to obtain the correct diagnosis. Field inspection, crack registration and cores drilled out for microstructural analyses should always be carried out as a minimum. In some cases, depending on the structure and the structural problem, other supplementary tests, e.g. mechanical tests, UPV technique or impact echo test, will improve the understanding of the problem.

Microstructural analysis is the only method to give the correct diagnosis of ASR and damage caused by ASR. Moreover, microstructural analysis will also diagnose other deterioration processes, e.g. sulphate attack, freeze–thaw, reacted aggregates if any and rate of damage in the concrete. However, the analysis should be carried out by an experienced petrographer with knowledge of ASR. Microstructural analysis of concrete, also named concrete petrography or concrete microscopy, is described in several international publications and proceedings. A handbook, *Concrete Petrography*,

Table 2.6 RH before and after treatment

	day 0	5 cm 1493 days	diff.	day 0	17 cm 1493 days	diff.
References* (avg.)	94	87	–7	85	81	–4
Aluminium	94	83	–11	84	82	–2
Oligomer S	95	81	–14	86	80	–6
Acrylic	89	78	–11	84	78	–6
Silane A	93	80	–13	84	80	–4

* Some or all the references were 'accidentally' impregnated with silane type A, June 2001.

includes detailed information on ASR and is recommended (St John *et al*. 1998). In the USA ASTM C 856 'Standard Practise for Petrographic Examination of Hardened Concrete' deals with concrete microscopy. However ASTM C 856 describes ASR only in a general way, which is insufficient for most petrographers without thorough knowledge of ASR. In SHRP-C-343 'Eliminating or Minimizing Alkali-Silica Reactivity' (Stark *et al*. 1993), microscopic examination is recommended but not described. In both publications the uranyl acetate method is included and it is stated that identification of the presence of alkali–silica gel using this technique must be confirmed by other petrographic techniques, such as microscopical examinations of thin sections. Microstructural analysis (concrete petrography) for assessment of ASR is widely used in Scandinavia, northern Europe, Canada and Japan, but its use is limited in the USA. Under the Strategic Highway Research Program (SHRP) a survey of use of microscopy techniques was carried out in the USA. Here only four states replied that microscopy was in use and three states that it was under evaluation (Springel in SHRP Product 2008 web page http://leadstates.transportation.org/car/SHRP_products/2008.stm). In recent years ASR has been found in many concrete structures in the USA, mostly caused by aggregate types of the slow/late expansive type formerly believed to be harmless in the USA (Glauz and Jain 2000; Lane 2000; Rangaraju 2000; Shrimer and Jones 2000).

The American standard ASTM C 295 'Standard Guide for Petrographic Examination of Aggregates for Concrete' gives a list of potentially alkali–silica reactive aggregates, including some slow/late expansive aggregates, but these are not included in ASTM C 33 'Standard Specification for Concrete Aggregates'. Moreover, the recommended test methods ASTM C 289 (chemical method) and ASTM C 227 (mortar bar test) are not suitable for testing of slow/late expansive aggregates (Stark *et al*. 1993; Jensen 1993). Slow/late expansive aggregates should be assessed for alkali reactivity by

use of the ASTM C 1260 (accelerated mortar bar test), the ASTM C 1293 (concrete prism test) methods or the new Rilem recommended test methods Rilem AAR-2 (ultra-accelerated mortar bar test), Rilem AAR-3 (concrete prism test) and Rilem AAR-4 (accelerated (60 °C) concrete prism test). For screening tests and classification of potentially alkali reactive aggregates the Rilem recommended test method AAR-1 'Detection of potential alkali-reactivity aggregates: petrographic method' should be used. This method is today implemented in several Scandinavian and northern European countries and is intended to become the European Standard and international method. Rilem Recommend Test Method AAR-0 gives guidance in the use of the Rilem methods.

2.5.2 Research needed

Long-term monitoring on existing concrete structures damaged by ASR has to a limited extent been reported internationally. Expansion measurements on test slabs under field conditions have been reported by e.g. Rogers *et al*. (2000) and Fournier *et al*. (1995). Long-term measurements on untreated and silane-impregnated highway girders located in Quebec City over a four year period (and longer) showed significant decrease of expansions (manually measured) and reductions of the relative humidity (measured in holes drilled into the concrete) in silane-impregnated girders relative to untreated girders. Moreover, the silane-impregnated girders obtained an improved aesthetic appearance compared to untreated girders (Berubé *et al*. 1996). Relative humidity on some existing structures in the USA has been measured on core materials (destructive method) and has given important information on the variation on RH in structural elements and among structures (Stark 1991a; Stark *et al*. 1993). Long-term measurements on ASR-damaged structures *in situ* are today carried out on only a few structures seen in a worldwide perspective, e.g. the Norwegian structures as mentioned in this chapter. No accepted recommendations and standardized methods for long-term monitoring of ASR damaged structures exist today to the author's knowledge.

More research and *in-situ* testing under field conditions are needed to improve our knowledge of damage caused by ASR. The existing methods should be improved according to functionality, reliability and durability and possibly new methods should be developed. Today the most promising remedial measure mitigating the damage of ASR is applying water repellent (mono-silane) and passively drying out the concrete aiming to render the ASR dormant. In the USA and Japan tests using lithium which replaces alkalis in the cement paste have given promising results and have in several cases been used commercially. More research, documentation and long-

term measurement on real structures are needed mitigating damaged structures due to ASR.

2.5.3 Resistance to ASR

The AASHTO transition plan of May 2000 concludes that although several key elements were successfully implemented in the USA 'There still is a resistance to accept ASR as a problem or a potential problem. As a result, the recommended mitigation methods have gone unaccepted and unimplemented'. The resistance to accept ASR as a real concrete problem has been experienced in many countries where ASR has been identified. History has shown that ASR will not be accepted as a real concrete problem unless sufficient convincing documentation has been produced, and ASR has been documented to be a real problem in concrete structures. Laboratory tests on aggregates and concrete mixes alone are not sufficient documentation for the existence of ASR.

In regions or countries where ASR has not been identified or accepted by the industry or the research society, it is strongly recommended to carry out survey investigations of the ASR problem on real concrete structures. All available information on ASR should be assessed and a strategy on how to carry out the survey investigation should be planned. Industry, especially the aggregate producers and cement industry, governmental institutions and research institutes, must be involved in the investigation. It is very important that investigations are carried out on several concrete structures and that damage due to ASR can be documented. The documentation should be based on microstructural analyses and field investigations and should be performed by qualified personnel with knowledge of ASR.

2.6 Conclusions

Correct diagnosis of the deterioration process and registration of damage over time are essential and decisive for assessment of risk for failure and appraisal of remedial measures mitigating damages by ASR. A thorough field inspection and sufficient microstructural analyses on various structural elements, eventually supplemented with other tests, will give an answer to the types of damage and how damaged the structure is. Long-term measurements of concrete/cracks expansion together with measurements of relative humidity in several locations will give an answer to the variation of present and future damage in the structure. Like many other causes of damage in concrete, diagnosis and appraisal of ASR and other types of damage in concrete structures rely to a large extent on the judgement and the level of expertise of the personnel involved and it is very important that correct and

suitable analysis methods valid for the existing structure and deterioration process are used.

2.7 Sources of information

The following institutions and organisations can be consulted for further information on ASR.

American Association of State Highway and Transportation Officials (AASHTO) are responsible for more than 4 million miles of streets and highways and 600 000 bridges in the US. The Technology Implementation Group (TIG) gives information on ASR on their web page: http://leadstates.transportation.org/

The Strategic Highway Research Program (SHRP) was a five year, $150-million program to develop and evaluate innovative technologies for roadway construction, maintenance, and operations. The program ended in 1993 and reports can be downloaded from the web page: http://www4.trb.org/trb/onlinepubs.nsf/web/shrp_publications

Canadian Strategic Highway Research Program (C-SHRP) is a dedicated programme of the Council of Deputy Ministers Responsible for Transportation and Highway Safety. Web page: http://www.cshrp.org/english/index.html

Institutution of Structural Engineers (IStructE) is the world's leading professional body for structural engineering. It is the appropriate source of relevant and considered opinion on all structural engineering and public safety issues in the built environment. Web page: http://www.istructe.org.uk/

Rilem is the International Union of Laboratories and Experts in Construction Materials, Systems and Structures. Rilem is a non-profit-making, non-governmental technical association whose vocation is to contribute to progress in the construction sciences, techniques and industries, essentially by means of the communication it fosters between research and practice. Rilem's activity therefore aims at developing the knowledge of properties of materials and performance of structures, at defining the means for their assessment in laboratory and service conditions and at unifying measurement and testing methods used with this objective. Web page: http://www.rilem.org/

Rilem committees TC 106 (now closed) and TC 191-ARP: 'Alkali-reactivity and prevention – assessment, specification and diagnosis of alkali-reactivity' have published several test procedures on ASR, Rilem recommended test methods AAR-0 (overview guide and reference materials), AAR-1 (petrographical examination method), AAR-2 (ultra accelerated mortar bar method), AAR-3 (concrete prism test). The following methods and reports will be published in the near future: AAR-4 (acceler-

ated (60 °C) concrete test), AAR-5 (assessing carbonate aggregates), AAR-6 (diagnosis and prognosis), AAR-7 (specification) and AAR-8 (methods for assessing releasable alkalis).

2.8 References

APM 106. (1989), 'Humidity measurements', Test method from the AEC-laboratory, Copenhagen, Denmark, November (in Danish).

ASTM C 33-01: 'Standard Specification for Concrete Aggregates', The American Society for Testing Materials, Philadelphia.

ASTM C 227-97a: 'Standard Test Method for Potential Alkali Reactivity of Cement-Aggregate Combinations (Mortar-Bar Method)', The American Society for Testing Materials, Philadelphia.

ASTM C 289-98: 'Standard Test Method for Potential Reactivity of Aggregates (Chemical Method)', The American Society for Testing Materials, Philadelphia.

ASTM C 295-98: 'Standard Practice for Petrographic Examination of Aggregates for Concrete', The American Society for Testing Materials, Philadelphia.

ASTM C 856-95: 'Standard Practise of Petrographic Examination of Concrete', The American Society for Testing Materials, Philadelphia.

ASTM C 1260-94: 'Standard Test Method for Potential Alkali Reactivity of Aggregates (Mortar-Bar Method)', The American Society for Testing Materials, Philadelphia.

ASTM C 1293-01: 'Standard Test Method for Determining of Length Change of Concrete Due to Alkali–Silica Reaction', The American Society for Testing Materials, Philadelphia.

Bakker, J. and Postemar, F. (2003), 'Monitoring of concrete structures on ASR: a "smart structure" project', *International Symposium (NDT-CE 2003) Non-Destructive Testing in Civil engineering 2003*, Deutse Gesellschaft fur Zerstoerungsfrei prufung e.V.

Berubé, M.A., Chouinard, D., Boisvert, L., Fregnette, J. and Pigeon, M. (1996), 'Influence of wetting and drying and freeze-thawing cycles, and effectiveness of sealers on ASR', *Proceedings 10th International Conference on Alkali–Aggregate Reaction in Concrete*, 18–23 August, Melbourne, Australia.

Borsje, H., Peelen, W.H.A., Postema, F.J. and Bakker, J.D. (2002), 'Monitoring alkali-silica reaction in structures', *HERON*, Vol. 47, No. 2, special issue on ASR.

Bredsdorff, P., Idorn, G.M., Kjaer, A., Plum, N.M. and Poulsen, E. (1963), 'Chemical Reactions in Concrete Involving Aggregate', special issue 128, *Chemistry of Cement, Proceedings Fourth International Symposium*, Washington, USA, pp. 749–806.

Cole, V.F. and Lancucki, C.J. (1981), 'Products formed in aged concrete', *Cement and Concrete Research*, Vol. 11, pp. 443–454.

Cole, V.F. and Lancucki, C.J. (1983), 'Products formed in aged concrete – the occurrence of okenite', *Cement and Concrete Research*, Vol. 13, pp. 611–618.

Dent Glasser, L.S.D. and Kataoka, N. (1981a), 'The chemistry of "alkali-aggregate" reactions', *Proceedings 5th International Conference on Alkali-Aggregate Reaction in Concrete*, Cape Town, South Africa, S252/23.

Dent Glasser, L.S.D. and Kataoka, N. (1981b), 'The chemistry of "alkali-aggregate" reaction', *Cement and Concrete Research*, Vol. 11, pp. 1–9.

Dent Glasser, L.S. and Kataoka, N. (198lc), 'Some observations on the rapid chemical test for potentially reactive aggregate', *Cement and Concrete Research*, Vol. 11, pp. 191–196.

Dent Glasser, L.S. and Kataoka, N. (198ld), 'A reply to J. Bensted's discussion of "The chemistry of alkali-aggregate reaction"', *Cement and Concrete Research*, Vol. 11, pp. 809–810.

Dent Glasser, L.S. and Kataoka, N. (1982), 'On the role of calcium in the alkali-aggregate reaction', *Cement and Concrete Research*, Vol. 12, pp. 321–331.

Diamond, S., Barneyback, R.S. and Struble, L.J. (1981), 'On the physics and chemistry of alkali-silica reactions', *Proceedings 5th International Conference on Alkali-Aggregate Reaction in Concrete*, Cape Town, South Africa, S252/22.

Fournier, B., Bilodeau, A. and Malhotra, V.M. (1995), 'CANMET/Industry research consortium on alkali-aggregate reactivity', *CANMET/ACI International Workshop on Alkali-Aggregate Reaction in Concrete*, Dartmount, Nova Scotia, 1–4 October.

Gilliott, J.E. (1975), 'Practical implications of the mechanisms of alkali-aggregate reactions', *Proceedings 3rd International Conference on Alkali-Aggregate Reaction*, *Preventive Measures*, Reykjavik, August.

Gilliot, J.E. (1964), 'Mechanism and kinetics of expansion in the alkali-carbonate rock reaction', *Canadian Journal of Earth Sciences*, Vol. 1, No. 2, p. 157.

Glauz, D. and Jain, V. (2000), 'California's experiences with reactive aggregates', *Proceedings 11th International Conference on Alkali–Aggregate Reaction in Concrete*, Quebec City, Canada, June.

Grattan-Bellew, P. (1995), 'Laboratory evaluation of alkali-silica reaction in concrete from Saunders Generator Station', *ACI Materials Journal*, Vol. 92, March–April, pp. 1–9.

Grattan-Bellew, P. and Danay, A. (1992), 'Comparison of laboratory and field evaluation of AAR in large dams', *Proceedings International Conference on Concrete AAR in Hydroelectric Plants and Dams*, CEA, Frederikston, Canada.

Hobbs, D.W. (1988), *Alkali–silica Reaction in Concrete*, Thomas Telford Ltd, London.

Institution of Structural Engineers (1992), *Structural Effects of Alkali-Silica Reaction: Technical Guidance on the Appraisal of Existing Structures*, ISE, London.

Jensen, V. (1990), 'Microstructural analysis on cores from Elgeseter Bridge', *Sintef test report* (in Norwegian).

Jensen, V. (1993), 'Alkali aggregate reaction in southern Norway', *doctoral thesis*, Technical University of Trondheim, NTH, Norway.

Jensen, V. (1994), 'Distribution and significance of alkali-aggregate reaction in southern Norway', *Proceedings 3rd International Conference on Durability of Concrete*, ACI, Nice, France, pp. 741–757.

Jensen, V. (1996), 'Microstructural analysis on cores from Veritas House in Høvik', *Sintef test report* (in Norwegian).

Jensen, V. (1998), 'Humidity and expansion measurements. Documentation of methods for long term measurement in a concrete bridge and a concrete dam', *SINTEF report* no. STF22 A97873 (in Norwegian).

Jensen, V. (2000a), '*In-situ* measurement of relative humidity and expansion of cracks in structures damaged by AAR', *Proceedings 11th International Conference on Alkali-Aggregate Reaction in Concrete*, Quebec, Canada, 11–16 June.

Jensen, V. (2000b), 'Relative humidity and expansion of cracks in protected and non

protected structures damaged by alkali reaction', *2000 International Conference – Repair, Rehabilitation and Maintenance of Concrete Structures, and Innovation in Design and Construction*, Seoul, Korea, 19–22 September.

Jensen, V. (2000c), 'The Norwegian Veritas house in Oslo: Assessment of surface treatment to reduce damage due to alkali aggregate reaction', *Postdoctoral project 1998–1999* (in Norwegian).

Jensen, V. (2000d), Postdoctoral project 1998–2000 financed by the Norwegian Research Council.

Jensen, V. (2002a), 'Embretsfoss Dam and hydro power plant: humidity and expansion measurements until 5th September 2002', *NBTL report* no R02001, November (in Norwegian).

Jensen, V. (2002b), 'Elgeseter Bridge: humidity and expansion measurements until 31st October 2002', *NBTL report* no R02003, December (in Norwegian).

Jensen, V. (2003a), 'Relative humidity measured by wooden stick method in concrete structures: long term measurements and reduction of humidity by surface treatment', *6th International Conference on Durability of Concrete*, ACI/CANMET, Thessaloniki, Greece.

Jensen, V. (2003b), 'Elgeseter Bridge in Trondheim damaged by alkali silica reaction: microscopy, expansion and relative humidity measurements, treatment with mono silanes and repair', *Proceedings 9th Euroseminar Applied to Buildings Materials*, 9–12 September, Trondheim, Norway.

Jensen, V. and Haugen, M. (1996), 'Alkali aggregate reaction in northern Norway, Report no. 3: In-situ measurement of humidity and expansion', *SINTEF-report* no. STF22 A96807 (in Norwegian).

Jensen, V., Gaasemyr, H. and Jensvik, K. (2000), 'Alkali reaction in railway sleepers', *Betongindustrien* Vol. 32, no. 2, pp. 10–12 (in Norwegian).

Kofoed, B.E. (2004), 'Repair of an access balcony according to DS/EN 1504 part 9', *Overhead presentation, Norecon Seminar 2004: Repair and Maintenance of Concrete Structures*, 19–20 April, Copenhagen, Denmark.

Lane, D.S. (2000), 'Alkali-silica reactivity in Virginia, USA: occurrences and reactive aggregates', *Proceedings 11th International Conference on Alkali–Aggregate Reaction in Concrete*, Quebec City, Canada June.

Larbi, J., Modry, S., Katayama, T., Blight, G. and Ballin, Y. (2004), 'Guide to diagnosis and appraisal of AAR damage in concrete structures: the Rilem TC 191-ARP approach', RILEM/TC ARP/04/17, *11th International Conference on Alkali Aggregate Reaction in Concrete*, 15–19 October, Beijing, China.

Lindgaard, J. and Wigum, B. (2003), 'Alkali reaction in concrete-field experience', *Sintef report* STF22 A02616 (in Norwegian).

Mielenz, R.C., McConnell, D., Holland, W.Y. and Greene, K.T. (1947), 'Cement-aggregate reaction in concrete', *J. Amer. Concrete Inst.*, Detroit, Vol. 19, No. 2, pp. 93–129.

Nerenst, P. (1957), 'General knowledge about alkali reaction in concrete', *Committee on Alkali Reactions in Concrete, The Danish National Insitute of Bui1ding Research and The Academy of Technica1 Sciences*. Progress Report Series A, No. 1, Denmark.

Nilsson, L.O. (1981), 'Pop-outs due to alkali-silica reaction – a moisture problem?', *Proceedings of the 5th International Conference on AAR in Concrete*, Cape Town, South Africa, S252/27.

Nilsson, L.O. (1983), 'Moisture effects on the alkali-silica reaction', *Proceedings 6th*

International Conference on AAR in Concrete, Copenhagen, Denmark, pp. 201–208.

Nixon, P., Hawthorn, F. and Sims, I. (2004), 'Developing an international specification to combat AAR. Proposal of Rilem 191-ARP', Rilem/TC ARP/04/13, *11th International Conference on Alkali Aggregate Reaction in Concrete*, 15–19 October, Beijing, China.

Nixon, P.J. (1990), *Review of United Kingdom Specifications, Test Methods and Guidance for Avoidance of Damage from Alkali-Aggregate Reactions*, *Report of the Proceedings of the Seminar on Alkali-Aggregate – The European Dimension*, The Geomaterials Unit, Queen Mary and Westfield College, University of London, pp. 93–99.

Poulsen, E. (2004), 'Repair of an access balcony according to DS/EN 1504 part 9', *Norecon Seminar 2004: Repair and Maintenance of Concrete Structures*, 19–20 April, Copenhagen, Denmark.

Powers, T.C. and Steinour, H.H. (1955a), 'An interpretation of some published researches on the alkali-aggregate reaction. Part 1 – The chemical reactions and mechanism of expansion', *J. Amer. Concrete Inst.*, Vol. 26, No. 6, Title No. 51–26, pp. 497–516.

Powers, T.C. and Steinour, H.H. (1955b), 'An interpretation of some published researches on the alkali-aggregate reaction. Part 2 – A hypothesis concerning safe and unsafe reactions with reactive silica in concete', *J. Amer. Concrete Inst.,* Vol. 26, No. 8, Title No. 51–40, pp. 785–812.

Rangaraju, P.R. (2000), 'A lab study on alkali-silica reactivity of quartzites used in concrete pavement of Minnesota', *Proceedings 11th International Conference on Alkali–Aggregate Reaction in Concrete*, Quebec City, Canada, June.

Rilem Recommended Test Method AAR-0. (2003), 'Detection of potential alkali-reactivity in concrete: Outline guide to the use of RILEM methods in assessments of alkali-reactivity potential', *Materials and Structures/Matériaux et Constructions*, August–September, Vol. 36, No. 261.

Rilem Recommended Test Method AAR-1. (2003), 'Detection of potential alkali-reactivity aggregates: Petrographic method', *Materials and Structures/Matériaux et Constructions*, August–September, Vol. 36, No. 261.

Rilem Recommended Test Method AAR-2. (2000), 'Detection of potential alkali-reactivity of aggregates – The ultra-accelerated mortar-bar test', Recommendations of Rilem TC 106-AAR: Alkali aggregate reaction, TC 106-2, *Materials and Structures/Matériaux et Constructions*, June, Vol. 33, No. 229.

Rilem Recommended Test Method AAR-3. (2000), 'Detection of potential alkali-reactivity of aggregates – Method for aggregate combinations using concrete prisms', Recommendations of Rilem TC 106-AAR: Alkali aggregate reaction, TC 106-3, *Materials and Structures/Matériaux et Constructions*, June, Vol. 33, No. 229.

Rilem Recommended Test Method AAR-4. (2000), 'Detection of potential alkali-reactivity – accelerated method for aggregate combinations and concrete mix designs using concrete prisms', committee draft November.

Rivard, P., Fournier, B. and Ballivy, G. (2000), 'Quantitative assessment of concrete damage due to alkali-silica reaction (ASR) by petrographic analysis', *Proceedings 11th International Conference on Alkali–Aggregate Reaction in Concrete*, Quebec City, Canada, June.

Rogers, C., Lane, B. and Hooton, D. (2000), 'Outdoor exposure for validation the

effectiveness of preventive measures for alkali-silica reaction', *Proceedings 11th International Conference on Alkali-Aggregate Reaction in Concrete*, Quebec City, Canada, June.

Sellevold, E.J. (1997), 'OFU Gimsøystraumen bridge: Humidity condition of the concrete', *Report nør. P–96-043*, *Statens vegvesen, Nordland Vegkontor*, Vegdirektoratet og RESCON (in Norwegian).

Shrimer, F. and Jones, D.M. (2000), 'AAR in Southern British Columbia and Western Washington', *Proceedings 11th International Conference on Alkali-Aggregate Reaction in Concrete*, Quebec City, Canada, June.

Sims, I. (1992), 'Alkali–silica reaction – UK experience', in Swamy R.N., *The Alkali–Silica Reaction in Concrete*, Blackie and Son Ltd, London.

St John, D.A., Poole, A.W. and Sims, I. (1998), *Concrete Petrography. A Handbook of Investigative Techniques*, Arnold, London.

Stanton, D.E. (1940), 'The expansion of concrete through reaction between cement and aggregate', *Proceedings American Society of Civil Engineers*, Vol. 66, pp. 1781–1811.

Stark, D. (1991a), 'The moisture condition of field concrete exhibiting alkali–silica reactivity', *Second International Conference on Durability of Concrete*, ACI Publication SP 126/52, pp. 973–987, Canada.

Stark, D. (1991b), 'Handbook for the Identification of Alkali–Silica Reactivity in Highway Structures', SHRP C-315, *Strategic Highway Research Program*, Contract C-202, ASR project developed by the National Research Council, 2101, Washington, DC.

Stark, D. (1994), 'Handbook for the Identification of Alkali–Silica Reactivity in Highway Structures', Revised Edition of SHRP C-315, *Strategic Highway Research Program*, Contract C-202, ASR project developed by the National Research Council, Washington, DC.

Stark, D., Morgan, B. and Okamoto, P. (1993), 'Eliminating or minimizing alkali–silica reactivity', *SHRP C-343*, National Research Council, Washington, DC.

Steen, P.E. (1998), 'Estimation of chloride penetration into concrete bridges in coastal areas', doctoral thesis, *Department of Structural Engineering, The Norwegian University of Science and Technology*, Trondheim, Norway.

Winsnes, H. (1991), 'Expansion measurement carried out in the period late 1987 to late 1991. Glidemikrometer – ISETH in a 6 m borehole from a turbine foundation, Saaheim power plant', *Results received by the author*, December 1991, Noteby A/S.

Wood, J.G.M. (1985), 'Methods of control of active corrosion in concrete', *Proceedings Deterioration of Reinforced Concrete in the Arabian Gulf*, October, Bahrain.

Wood, J.G.M. (1990), 'Physical effects of AAR: Structures as a laboratory', *International Workshop on AAR in Concretes: Occurrences, Testing and Control*, Halifax, Canada.

3

Acoustic testing of concrete bridge decks

R.D. COSTLEY
Miltec Corporation, USA

3.1 Introduction

The techniques discussed in this chapter are versions of the 'coin-tap' test. As the name implies, each part of a structure, such as a laminated panel, is tapped with a coin. The sound produced when tapping a delaminated area is distinct from that of an intact area. These methods, of which there are several variations, are local tests in that they detect defects only at the location of the tap. This is in contrast to a global test, in which the entire structure is tested with a single tap. Global tests are useful in identifying defective parts but are not as effective in identifying the location or type of defect. Local tests tend to be more sensitive to certain types of defects and are more effective in determining their location. However, local tests tend to be more time consuming in that each part of the structure will have to be tapped and the response recorded. Coin-tap tests are useful for the detection of delaminations, but are not suitable for the detection of cracks that are normal to the surface (Adams and Cawley, 1985).

Delaminations are a common defect that occur in concrete bridge decks. During construction, steel reinforcement bars, or rebar, are placed inside the bridge deck approximately 2 inches (5 cm) from the top surface, in a 1 foot (0.3 m) grid pattern. Another layer is placed close to the bottom surface, where the total thickness of the deck is on the order of 9 inches (23 cm). The top layer of rebar is susceptible to corrosion. Water from rain migrates through the porous concrete, which reacts with the steel rebar and causes corrosion. In many states salt is used to de-ice bridges. Salt exacerbates the problem and accelerates corrosion of the rebar. A delamination occurs when the corroding rebar expands, causing horizontal cracking in the plane of rebar. Horizontal cracks from adjacent corroding rebar combine to form areas of delaminations. 'Untreated, a delamination may increase in size and propagate to the surface, resulting in the chipping or spalling of the concrete' (Washer, 2004).

Several other methods, in addition to tapping methods, exist for detecting delamination in concrete decks, including impact echo, infrared thermography, and ground penetrating radar (GPR) (Khan, 2003; Washer, 2004). The impact echo technique involves striking the surface with a hard object, such as a steel ball, to generate stress waves that penetrate into the structure. The reflections are detected by a piezo-electric transducer. The technique is useful for finding other types of defects in addition to delaminations (Sansalone and Carino, 1991).

GPR systems, which are used for a wide variety of applications in addition to non-destructive testing, transmit microwave pulses into the concrete structure with an antenna, which is typically located 8–12 inches (0.2–0.3 m) from the bridge deck (Clemeña, 1991). Microwave energy is reflected at material discontinuities, such as a delamination, and detected by a receiving antenna, which may be the same as the transmitting antenna. These systems can be mounted on a vehicle so that a bridge can be scanned quickly. Another advantage of GPR is that it has the potential to be able to interrogate concrete decks below asphalt overlays (Khan, 2003; Washer, 2004).

Infrared thermography involves detecting temperature variations on the surface of a concrete structure with an infrared camera. Different types of defects, including delaminations, can affect the thermal transfer properties of a concrete structure, which will, in turn, cause temperature variations in the structure. Using infrared thermography, large areas of a structure can be inspected in a single image, but these images can be difficult to interpret (Khan, 2003; Washer, 2004).

The techniques discussed in this chapter are tapping, or acoustic methods, which are versions of the coin-tap methods. Also referred to as sounding methods, these methods are used to detect and locate delaminations in concrete bridge decks. Sounding methods, of which chain drag and hammer tap are the most common, are discussed in the next section. Automated versions of these methods are presented in the following section. The automated version of the chain drag method will be presented in greater detail than the other methods since the author has more experience with this technique than with the others. The last section summarizes the discussion from the other sections and contains a few concluding remarks.

3.2 Manual techniques

A popular technique for detecting and locating delaminations in concrete bridge decks involves tapping the structure with a hammer or dragging a chain across it and listening to the audible response. The technique, described in the standard ASTM D 4580, is not considered applicable 'on bridge decks that have been overlaid with bituminous mixtures.' The standard also states that the method should not be used on frozen concrete (ASTM, 2003).

Chain drag is probably the more popular of the two methods. Chain bars are typically 'homemade' devices and their design varies. A common implementation consists of a 3 foot (1 m) metal rod or tube welded to a 2 foot (0.6 m) metal rod to form a 'T'. Four or five short segments of 1 inch (25 mm) link chain of ¼ inch (6 mm) steel, approximately 18 inches (46 cm) in length, are welded to the short rod at the top of the 'T'. The worker will hold the chain bar so that the 'T' is upside down and the chains drag along the ground. Figure 3.1 shows a bridge inspector using a chain bar. He listens to the sound produced as he walks along the bridge deck sweeping the chains across the surface. A very distinctive, hollow sound occurs when the chains sweep over a delaminated area. When this occurs, the worker will mark the area with spray paint or lumber crayon. Hammer tap, or sounding, is similar to chain drag except that the inspector strikes the concrete surface with a masonry hammer and listens to the audible response.

When using a chain bar the inspector is able to stand upright as he walks over the bridge deck, sweeping the chains across the surface. When practicing the hammer tap method, the inspector will spend much of his time squatting or on his knees. This is probably one reason the chain drag is more popular. Also, with the hammer tap, the bridge is impacted at discrete points. It is easier and quicker to sweep the chains over a given area than it is to crawl over the bridge deck tapping discrete points with a hammer. Some inspectors will use chain drag to locate delaminations and then use hammer tap to determine their shape more precisely (Moore *et al*., 2001). In another application, striking soft concrete with a hammer produces 'a dampened tone that can be recognized by an inspector.' As a result, 'hammer sounding can also be useful for locating areas of severe damage to the cement matrix that correspond to reduced strength' (Washer, 2004).

In order to create an accurate map of the bridge, showing the locations of the delaminated areas, a grid system is created on the bridge surface. Distances are measured, and marked, from the end and sides of the bridge in 15–36 inches (38–91 cm) increments, depending on the resolution desired. The grid is drawn on the bridge from these measurements, typically using stringlines. The delaminations are plotted by hand on a map by referencing their positions with respect to the grid. The delaminated area is determined from this map (ASTM, 2003).

The Federal Highway Administration (FHWA), as part of a larger investigation, conducted a study to determine the reliability of sounding methods to detect delaminations in bridge decks (Moore *et al*., 2001). In conjunction with this study, the Nondestructive Evaluation Validation Center (NDEVC) conducted a sounding survey of a bridge deck in Northern Virginia, which had low traffic. Approximately two man-days were spent inspecting the bridge deck that was 182.6 feet (55.65 m) long and 20.0 feet (6.1 m) wide. A 2 foot (0.61 m) grid was marked on the bridge deck in order to create a



3.1 A bridge inspector with the Minnesota Department of Transportation is using a chain bar to look for delaminations in a bridge deck.

detailed delamination map. The detailed survey, which was more accurate than a typical chain drag survey, found the delaminated area of the center and southern spans of the bridge to be 19%. These results were confirmed by eight cores taken from the two spans.

As part of this study, 22 two-man teams of bridge inspectors conducted sounding surveys of the center and southern spans of the same bridge using either a steel chain and/or masonry hammer. The individual teams spent from 8 to 105 min performing their inspection, with an average time of 36 min. Since the inspectors were not allowed to make any marks on the bridge, this time did not include creating a grid on the deck surface. Their estimates of the delaminated area varied from 2% to 35%. Only 5 of the 22 teams produced delamination percentages within 5% of the NDEVC result. In addition, many of the delaminations indicated on the inspectors' maps were inaccurately located. However, none of the teams was allowed to make any marks on the bridge, either for marking the area of the delamination or for laying out a grid. This was probably so that the results of earlier surveys would not prejudice later surveys made by other teams. Many of the errors were probably the result of this imposed constraint.

In a separate study, the NDEVC sounding survey described above was compared with impact-echo and GPR inspections of the same bridge (Scott *et al.*, 2002, 2003). The impact echo results were generally consistent with those from the chain drag survey. While impact echo is more quantitative than chain drag sounding, the technique is more time consuming. In

addition, impact echo signals can be very complicated to interpret and may not always be conclusive. Neither of the two methods, chain drag or impact echo, is considered to be effective for inspecting decks with asphalt overlays. Neither of the GPR systems investigated in the study was as effective as either chain drag or impact echo in detecting and locating delaminations.

The rotary-percussion sounding system has recently been included into ASTM D 4580. As the device rolls over a concrete structure, two rotary percussion units strike the surface. A dull or hollow sound is generated when the device is rolled over delaminated concrete and a clear ringing sound when rolled over solid concrete. The device can be used on horizontal, vertical, or overhead surfaces. The delaminations detected with this device are marked with spray paint or lumber crayon, similar to the traditional chain drag and hammer sounding methods (ASTM, 2003; Khan, 2003).

Sounding techniques have the advantage of being simple and inexpensive. The workers who use these techniques intuitively understand how they work and have confidence in them. However, a disadvantage of these methods is that they rely on the subjective interpretation of the inspector, as the FHWA study demonstrated. That study was conducted in an environment where traffic noise was not an issue. However, inspectors are routinely required to inspect one lane of a bridge deck while traffic passes in the other. In noisy environments such as this, the chain drag sounds are more difficult to hear and the inspector is more likely to commit errors (Khan, 2003). As was also shown in the FHWA study, errors are also introduced when preparing the delamination map of the bridge from a sounding survey. In addition, the process of drawing this map can be inconvenient and time consuming.

3.3 Electro-mechanical sounding

An electro-mechanical sounding device essentially automates the hammer sounding method. The device electronically records the vibrations produced by hammer impacts with a contact transducer. A small, three-wheeled cart houses the device, which records data as the cart is rolled along the bridge deck (SIE, 1974; Smithson and Whiting, 1992; ASTM, 2003).

The hammer impacts are produced by two rigid tapping wheels, which have plungers that impact the bridge deck at a rate of 33 taps/s. The tapping wheels are mounted parallel to each other, approximately 6 inches (15.2 cm) apart. The impacts excite vibrations within the concrete that are detected by two piezo-electric hydrophones mounted inside two oil-filled soft tires, called receiving wheels. The receiving wheels are mounted outside the tapping wheels, approximately 3 inches (75 mm) from each. The hydrophones are mounted so that they do not rotate with the tire. The oil inside the tire serves as a couplant, or medium through which the vibrations are

transmitted from the concrete to the hydrophone in the form of pressure fluctuations. In order to distinguish between intact and delaminated concrete, the electronics unit gates the detected signal so that it accepts only that part that occurs within 3 ms of when the surface was tapped. In addition, the electronics unit filters the signal within the pass-band 300–1200 Hz. The unit rectifies and integrates this signal, which is then plotted on a strip chart recorder.

Since a receiving and tapping wheel must be above a delamination in order to detect it, the device interrogates a pair of 3 inch (75 mm) wide paths, separated by 6 inches (150 mm), as it traverses the bridge deck. The bridge is inspected by making parallel traverses along the length of the deck. The cart is pushed along the bridge deck so that the strip chart record represents predetermined travel distance. The records from successive traverses are placed side by side to create a map of the delaminated areas of the bridge. Spacing between parallel traverses will vary from 15 inches (380 mm) to 3 feet (910 mm), depending on the resolution required. Closer spacing intervals are required for in-depth analyses, while wider spacing intervals are suitable for general condition surveys.

The device requires calibration periodically. Calibration is accomplished by placing the device on top of a specially designed aluminum bar and recording the response. The sensitivities of each of the two channels are adjusted so that they are equal and at the proper levels.

Delamtect was a commercially available, electro-mechanical sounding device manufactured by SIE, Inc. The description of an electro-mechanical sounding device found in the ASTM standard is very similar to that found in the Delamtect Operator's Manual. The device, which is no longer available, may have been the only model to be sold commercially. The Iowa Department of Transportation still owns and uses four units. Three of these have been upgraded to include a laptop computer, which processes the signals detected by the receivers (Dunlay, 2000).

3.4 Automated chain drag system (ACDS)

The ACDS automates the chain drag method of inspection, resolving many of the issues associated with its manual execution. Sound produced by the dragging chains is recorded using a microphone, instead of the human ear, and processed on a computer to distinguish intact sections of the bridge deck from delaminated sections. The detection equipment is mounted on a hand-pushed cart with chains attached so that they drag along the surface of the concrete. Acoustic shielding and electronic filtering reduce external noise levels, such as that caused by passing vehicles in adjacent traffic lanes. These improvements make the technique operator independent and allow inspections to be made in noisy environments. In addition to detecting

defects in real time, this automated approach produces an objective record of the inspection, available both electronically and in hard copy. These permanent records can be compared with past and future inspections, allowing inspectors to monitor the health of the structure over time (Henderson *et al.*, 1999, 2000; Costley *et al.*, 2002, 2003).

3.4.1 System hardware

The detection equipment used on the ACDS includes a microphone with an amplifier, a band-pass filter, a data acquisition system, and a computer or microprocessor for processing the data. The current experimental system contains a pre-polarized microphone with a signal conditioner that converts the charge signal from the microphone to a voltage signal. The signal conditioner is battery powered and has adjustable gains of 1, 10, and 100. Normally, a gain of 10 is used to amplify the signals to fit within the dynamic range of the analog-to-digital converter without clipping.

From there the signal is fed to a low-pass filter with a 10 kHz cut-off. The selection of the cut-off frequency will be discussed later. The filter does not have any gain. It would be desirable to move the ×10 gain from the signal conditioner to the output of the filter. In that way, the undesirable frequency components of the signal would not be amplified before they are filtered. The amplified and filtered signal is then routed to a data acquisition card installed in a rugged laptop computer. The sample rate is 44.1 kHz, which provides CD quality sound and is a common playback rate on many computers.

A jogging cart served as the platform on which the equipment was mounted. This cart, shown in Fig. 3.2, is a large, three-wheel, single child carrier commonly used by recreational joggers. It is primarily made from aluminum tubing and rolls on 20 inch (0.5 m) diameter pneumatic tires. The original seat and vinyl covering were removed before the other equipment was mounted.

Attached to the underside of the carriage and behind the front wheel is a half-inch (13 mm) steel tube from which five 18 inch (46 cm) long chains hang. These chains drag along the concrete surface as the cart is pushed. Different size chains create noise with slightly different frequency characteristics, e.g. $\frac{3}{8}$ inch (9.5 mm) thick chain produces sound with lower frequencies than does $\frac{1}{4}$ inch (6.4 mm) chain. Most of the results presented here were obtained with a $\frac{5}{16}$ inch (7.9 mm) chain. The hardness of the steel also slightly affects the quality of the sound.

The microphone is mounted directly over the chains, within a box fastened to the cart frame. The purpose of the box is to shield the microphone from external noise sources, such as passing traffic. This box was made of R-board, a $\frac{3}{4}$ inch (18 mm) foam material that was coated with a thin layer



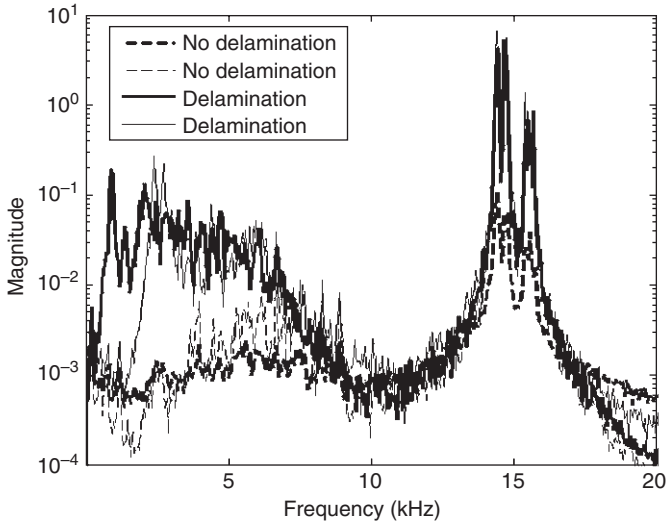
3.2 A side view of the ACDS experimental unit.

of fiberglass on both sides. It is a lightweight but relatively stiff construction material. The interior of the box is lined with textured foam which absorbs sounds that enter the box and provides additional sound shielding. Ideally, only those sounds produced by the chain and the concrete and traveling directly to the microphone should be detected. The addition of a 10 inch (250 mm) wide felt curtain around the base of the box and stretching to the ground completes the attempt to minimize the amount of external noise reaching the microphone.

An odometer, installed on the front wheel of the cart, measures the distance that the cart has traveled, making it possible to correlate the microphone signal with the position on the bridge where it was acquired. This signal is fed to a second channel of the data acquisition card and saved on the computer. In addition, the computer is capable of triggering a can of spray paint that marks the surface when a delamination is detected.

3.4.2 Signal processing

An acoustic signal is produced by the dragging chains as the device is pushed across a bridge deck. The frequency content of the sound can be determined by taking the power spectrum of the signal. One such signal was acquired while inspecting an overpass on the campus of Mississippi State University. Figure 3.3 shows the power spectra of 0.2 s duration segments of an acoustic signal acquired from a single pass of the ACDS across this bridge. Two of these spectra, indicated in the caption, were produced



3.3 Power spectra taken over 0.2 s duration segments of an acoustic signal acquired from a single pass of the ACDS. The spectra represented by the heavy and thin solid lines were taken from the delaminated areas. The spectra represented by dashed lines were acquired over regions of intact concrete. The large spikes at 15 kHz are produced by the ringing chains.

by dragging the chains over delaminated areas. The other two appear to come from regions of intact concrete. As can be seen in the figure, the spectra from intact and delaminated concrete have significant differences in the frequency band between 1 and 7 kHz.

The large spikes around 15 kHz in Fig. 3.3 are the dominant feature in each of the spectra. These were caused by the chains ringing as they bounced along the concrete surface. This component of the signal is fairly high in frequency and does not contain any useful information. It is over an order of magnitude louder than the noise from the delaminations and takes up most of the dynamic range of the system. A low-pass filter with a 10 kHz cut-off has since been added to the system to attenuate this noise.

The following is a qualitative explanation of the signals produced by scanning a delamination. As the chains drag over the deck surface, they excite vibrations on the top surface of the deck over a broad band of frequencies. The vibrations produce stress waves that propagate through the thickness of the deck. When the concrete is intact the stress waves are largely attenuated before they are reflected from the bottom surface and return to the top. When a delamination is encountered, the energy

is confined within the layer above the plane of the rebar. This layer will resonate at frequencies that depend on the area of the delamination and its thickness.

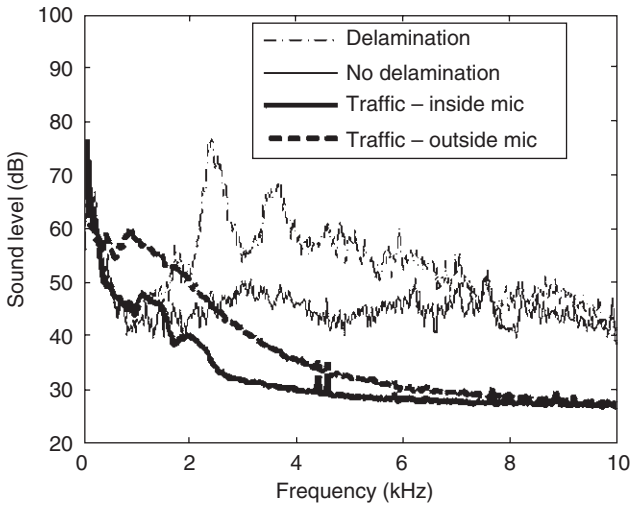
A simple model of a delamination is that of a circular plate clamped at its edges (Adams and Cawley, 1985). The resonance frequency of the fundamental mode is given by Adams and Cawley (1985) and Morse (1976)

$$f = \left(\frac{0.47h}{a^2}\right)\sqrt{\frac{E}{\rho(1-\mu^2)}} \qquad [3.1]$$

where h is the thickness of the layer above the delamination and a is the radius of the delamination. The symbol E represents the modulus of elasticity (3.5×10^6 psi or 25 GPa for concrete); ρ represents the density (162 lb/ft^3 or 2600 kg/m^3); and μ represents Poisson's ratio (0.15) (Jastrzebski, 1987). For example, the fundamental resonance of a two-inch (50 mm) thick circular, concrete plate with a diameter of 10 inches (250 mm) is roughly 4950 Hz. The resonance decreases to 550 Hz when the diameter increases to 30 inches (760 mm). However, the shapes of actual delaminations will be very complicated, not simple circles, and the thickness of the slab over the delamination will not be uniform. In addition, higher-order modes will be excited. As a result, their frequency responses will probably be very complicated, as seen in the spectra.

It may be that small defects will not be detected by this system. A 5 inch (120 mm) diameter delamination, which has a fundamental resonance of approximately 19 800 Hz, would excite frequencies above the noise of the ringing chains and the upper cut-off frequency of the filter. However, delaminations of this size are generally not considered a problem. Conversely, one might expect that the noise produced when scanning very large delaminations would be below the bandwidth of the system. This is not expected to be a problem because higher-order modes would be excited in the larger delaminations, which would radiate sound at higher frequencies that could be detected by the ACDS.

The effects of traffic noise on the performance of the system were investigated. The ACDS was placed on the side of a busy highway where the speed limit was 55 miles per hour (88 km/h). A calibrated microphone was mounted inside the ACDS and another was mounted outside and the sound of the passing traffic was recorded with the two microphones simultaneously. The spectra from each microphone from a single, representative event are plotted in Fig. 3.4. As can be seen in the figure, the microphone enclosure on the ACDS effectively attenuates traffic noise in the 1–6 kHz frequency band. Note the two small bumps in the spectrum of the inside microphone signal, at approximately 1 and 2 kHz. These are resonances within the enclosure. These can be reduced by properly

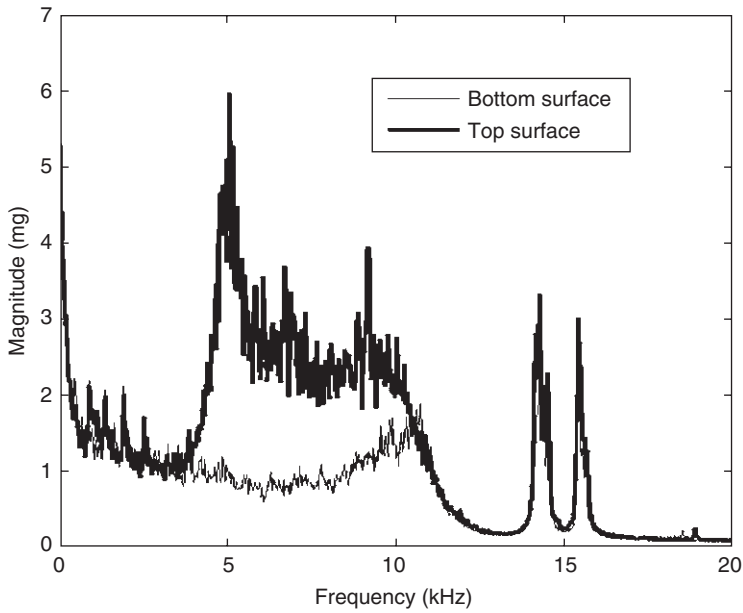


3.4 Comparison of sound levels from traffic and chain drag signals. This graph demonstrates the effectiveness of the sound enclosure in reducing traffic noise. It also shows that chain drag signals have higher frequency components than traffic noise.

redesigning the microphone enclosure so that it does not have parallel walls. For comparison, two chain drag signals are also plotted in Fig. 3.4: one from a delaminated area and the other from an area without a delamination. The figure shows that traffic noise recorded with the internal microphone does not interfere with the chain drag signal over most of the frequency band of interest for detecting delaminations, 1–8 kHz.

As mentioned earlier, the dragging chains cause the surface of the concrete deck to vibrate and stress waves to propagate into the concrete layer. Another simple test was conducted to investigate how far the stress waves penetrate into the layer. Accelerometers were mounted on the top and bottom surfaces of a 5 inch (125 mm) thick concrete ramp. The ACDS was pushed near the accelerometer locations. The spectra of these two signals are plotted in Fig. 3.5, which shows that these signals differ over the 4–10 kHz range. Both accelerometers detect the vibrations produced by the chains, but, as expected, the vibrations reaching the bottom surface have attenuated significantly.

These signals were recorded after the 10 kHz low-pass filter had been added to the system. The noise from the ringing chains, the peaks around 15 kHz, is no longer the dominant feature of the two spectra. Similar signals recorded with microphones show that the filter attenuates the noise from the ringing chains by an order of magnitude from that seen in Fig. 3.3.

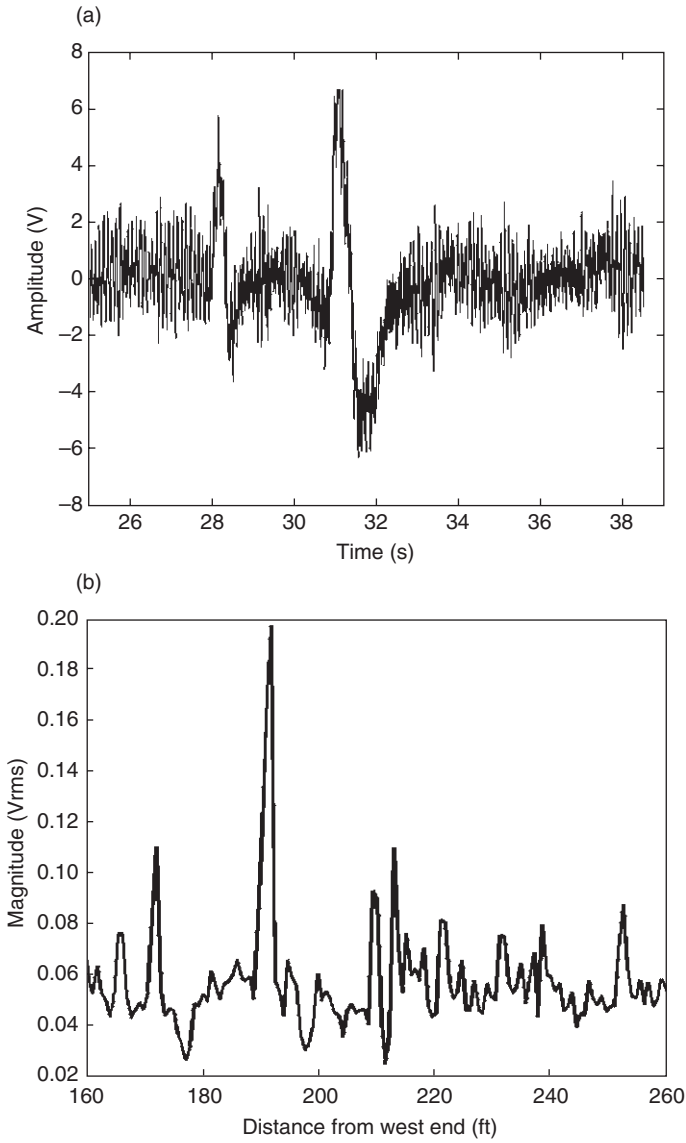


3.5 These signals were produced by accelerometers mounted on the top and bottom surfaces of a 5 in (125 mm) thick, concrete ramp used by pedestrians. The accelerometers detected the vibrations produced by the dragging chains as the ACDS was pushed along the ramp. The vibrations were greatly attenuated by the time they reached the bottom accelerometer.

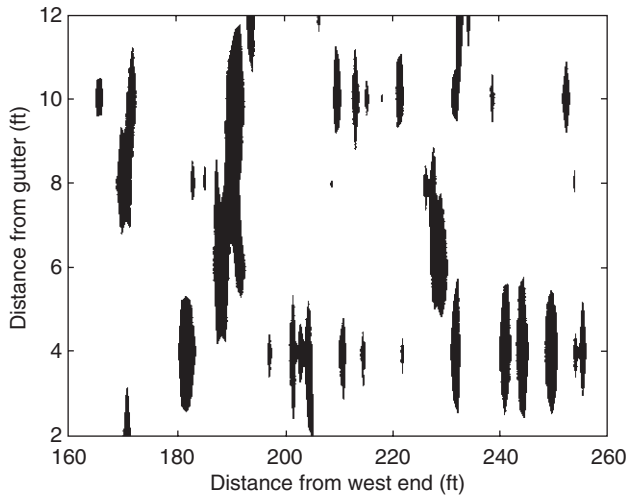
3.4.3 Creating delamination maps

The noise from the dragging chains is detected by the microphone and recorded onto a laptop computer as the ACDS traverses the length of the bridge. After making one pass across the bridge, the inspector moves over one width of the ACDS and pushes the cart across the bridge in the opposite direction. This is repeated until the entire lane is scanned.

An unprocessed microphone signal is shown in Fig. 3.6(a). After reading in the data, the program digitally filters this signal. Typically 1.4 and 8 kHz are the low and high-frequency cut-offs, which extract the ringing chain at the high frequencies and traffic noise at the low frequencies. It is a simple matter to change the cut-off frequencies in software. The two large, low-frequency excursions in the unfiltered signal were caused by passing automobiles or trucks. It appears that the second vehicle may have caused the signal to clip at +6 V. This could be remedied by replacing the 10 kHz low-pass hardware filter at the output of the microphone with a 100 Hz to 10 kHz band-pass filter.



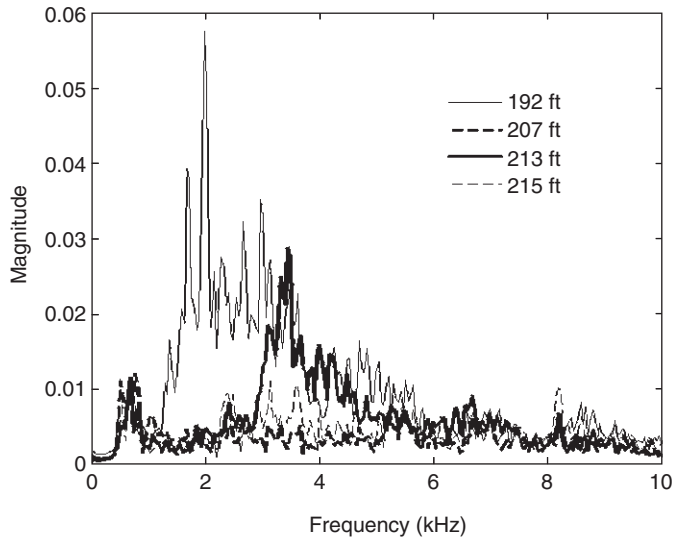
3.6 (a) The unprocessed microphone signal taken from part of a bridge scan. Passing automobiles caused the two large, low frequency excursions at 28 and 31 s. (b) The rms envelope of the signal calculated from part (a). All the peaks over 0.08 Vrms, and possibly 0.07 Vrms, indicate delaminations. (Data taken from east bound pass 5 of Minnesota Hwy 10 Bridge.) (1 foot = 0.3048 m.)



3.7 The section of a contour map of a bridge lane. The dark areas indicate the locations of delaminations. The inspector made six passes with the ACDS, in the horizontal direction, centered at distances 2, 4, 6, 8, 10, and 12 ft from the gutter. The data shown in Fig. 3.3a and b correspond to the scan at 10 ft, which was made from left to right. (1 ft = 0.3048 m.)

The data acquisition program buffers approximately 4500 samples from the microphone signal. The precise value can vary and depends on the speed at which the inspector pushes the ACDS across the deck. It calculates the root mean square voltage (Vrms) of this signal by squaring the individual samples, summing the values from the entire buffer, taking the square root of the sum, and dividing by the number of samples in the buffer. The result is one rms value for a predetermined travel distance, typically around 9 inches (230 mm). These values are referred to as the rms envelope of the signal. The rms envelope shown in Fig. 3.6(b) corresponds to the time domain signal in Fig. 3.6(a). Notice that the abscissa in Fig. 3.6(a) is Time whereas in Fig. 3.6b it is Distance. The spikes at approximately 172, 192, and 213 feet indicate the presence of delaminations. However, the passing cars are not detected.

A delamination map of a segment of a bridge is shown in Fig. 3.7. The dark areas on the map identify delaminations. A delamination map is made by assembling a large matrix in which the columns are rms envelopes from consecutive passes. The map is essentially a contour plot of this matrix. The minimum contour represents the threshold of detection and is selected by the inspector. This value will change slightly, depending on bridge surface,



3.8 Power spectra from segments of the signal shown in Fig. 3.6, which were taken from the pass centered at 10 ft from the gutter. The distances in the legend correspond to the abscissas in Figs 3.6b and 3.7. The spectra corresponding to 207 and 215 ft come from areas where there is no delamination. The spectra corresponding to 192 ft and 213 ft come from areas that are delaminated. (1 ft = 0.3048 m.)

microphone sensitivity, type of chain, and other factors. For this example, the threshold was set to 0.7 Vrms.

The ACDS made six passes to scan the lane in Fig. 3.7. The ACDS traveled from west to east (left to right in the figure) when making the passes 1, 3, and 5, centered at 2, 6, and 10 ft (0.61, 1.83, and 3.05 m) from the gutter. Passes 2, 4, and 6, centered at 4, 8, and 12 ft (1.22, 2.44, and 3.66 m), were made in the opposite direction. To compensate for this, the rms envelopes from the even numbered passes were flipped end to end before they were lined up with their neighbors when assembling the large matrix. Pass 5, centered at 10 ft from the gutter, corresponds to the signals shown in Fig. 3.6.

The spectra of four signals extracted from pass 5 are plotted in Fig. 3.8. Their labels in the legend identify the distance from the west end where they were acquired. The spectra corresponding to 207 and 215 ft come from areas where there is no delamination. The spectrum labeled 192 ft corresponds to the large spike in Fig. 3.6(b) and the largest delaminated area in Fig. 3.7. The spectrum at 213 ft comes from one of the smaller delaminations to the right of the largest one. It is interesting to note that the larger delamination produces sounds with lower frequency components. As discussed earlier, one would expect the larger delaminated area to have a lower resonance frequency.

The bridge supervisor would like to know the area of delamination. This number will aid him in estimating the materials and labor necessary to repair the bridge. A good estimate of this number is easily obtained by using the rms envelope to create a new function. Whenever the rms envelope exceeds the threshold value, the value of the new function is set to one. When the rms value is less than the threshold, the new function is set to zero. The area of delamination in one pass is determined by integrating the new function with respect to distance traveled over the length of the bridge, and multiplying by the width of the ACDS. The total area of delamination is determined by adding up these values from all the passes.

The pre-filtered microphone signal and odometer signal, collected as the unit is pushed along the bridge, are saved as one file for each pass, along with a file containing the rms envelope. The raw data files require approximately 1 megabyte of hard drive space for every 10 linear feet. If a bridge is 100 feet long and requires 10 passes to cover the surface, then the raw data alone will consume roughly 100 megabytes.

Although the data are currently archived to allow for post-processing and evaluation of other analysis methods, the device potentially will need only to save the much smaller envelope file, 10 kilobytes per 100 linear feet. However, hard-drives for laptop computers are available that can store tens of gigabytes. In addition, large amounts of data can be archived on writable CDs. Thus, the size of the raw data files and the amount of storage that they require does not seem to be a serious limitation.

3.4.4 Improvements and future development

A couple of improvements to the ACDS have already been suggested. By replacing the 10 kHz low-pass filter with a 100 Hz to 10 kHz band-pass filter, traffic noise could more effectively be filtered from the signal. In addition, the system gain should be moved from the output of the signal conditioner to the output of the band-pass filter. It was also mentioned that the microphone enclosure needs to be redesigned to minimize the effects of resonances.

It would be desirable to inspect one lane of a bridge in a single pass. This could be done by attaching several systems side by side. In this case, the system could be pulled slowly behind a vehicle on a trailer. With a system like this, it might be possible to inspect a lane of a bridge without shutting the lane off to traffic. It would also be interesting to investigate another type of excitation mechanism; for instance, recording the sound produced by tapper wheels, such as is used on the Delamtect, with a microphone.

Limited work has been performed to validate the results obtained with the ACDS. On the University Street overpass over Highway 12 in Starkville, Mississippi, the hammer tap method was used to confirm that the delaminations it detected were indeed delaminations. The entire bridge was

not surveyed using hammer sounding. Manual chain drag sounding was used to partially confirm the results of an ACDS survey of a bridge on Minnesota Highway 10 over the Mississippi River. A more complete comparison, such as the one discussed earlier between impact-echo, GPR, and chain drag (Scott *et al*., 2003), would be desirable.

In addition to the improvements and validation efforts discussed above, other signal processing techniques should be investigated. These could potentially be more effective and efficient in finding delaminations. Some work has been done to investigate several automated, or learning, techniques. The most promising of these involved the use of linear prediction coefficients (LPC), which is used extensively in speech recognition, to characterize chain drag signals (Dion, 1999; Henderson *et al*., 1999).

3.5 Conclusions

More sophisticated inspection techniques, such as impact echo, infrared thermography, and GPR, provide quantitative information about the structures on which they are being used. However, they require relatively high levels of education and training for equipment operation and data interpretation (Khan, 2003). Sounding techniques, such as chain drag and hammer tap, are simple and inexpensive to implement, require minimal training, and are intuitively easy to understand. However, these techniques are more limited in their application; they are basically used to detect delaminations. The results obtained with them are qualitative, not quantitative. Moreover, the techniques are very subjective and experience of the inspector can affect results (Moore *et al.*, 2001). In addition, archival of results is tedious and time consuming and another source of error. 'One of the serious limitations of these simple sounding techniques, however, is the lack of electronic data storage' (Khan, 2003).

Many of these shortcomings have been addressed in the development of the automated versions of these techniques, the Delamtect and the ACDS. These techniques generate more quantitative information, e.g. delamination maps, which can be stored electronically and used to monitor the health of a structure over several years. Perhaps more importantly, the subjectivity of the inspector is no longer a consideration.

3.6 Acknowledgements

The Bridge Division of the Mississippi Department of Transportation funded the initial work on the ACDS, which was performed at the Diagnostic Instrumentation and Analysis Laboratory at Mississippi State University (DIAL/MSU). Later work was supported by DIAL/MSU. The Minnesota Department of Transportation supported an inspection of the Highway 10

Bridge over the Mississippi River near Little Falls, Minnesota. The author acknowledges the significant contributions made by Gary M. Boudreaux, Gary N. Dion, and Mark E. Henderson in the development of the Automated Chain Drag System.

3.7 References

Adams, R.D. and Cawley, P. (1985), 'Vibration Techniques in Nondestructive Testing,' *Research Techniques in Nondestructive Testing, Volume VIII*, ed. R.S. Sharpe, 303–360, Academic Press, London.

ASTM D 4580-03 (2003), 'Standard Practice for Measuring Delaminations in Concrete Bridge Decks by Sounding,' ASTM International, West Conshohocken, PA.

Clemeña, G.G. (1991), 'Short-Pulse Radar Methods,' *CRC Handbook on Nondestructive Testing of Concrete*, ed. V. Malhotra and N. Carino, 253–274, CRC Press Inc., Boca Raton, FL.

Costley, R.D., Boudreaux, G.M., Kirkland, R. (2002), 'Automated Chain Drag Inspection of Concrete Bridge Decks,' *Structural Materials Technology V: An NDT Conference*, ed. S. Alampalli and G.A. Washer, 421–427, The American Society for Nondestructive Testing, Cincinnati, OH.

Costley, R.D., Henderson, M.E., Dion, G.N. (2003), 'Acoustic Inspection of Structures,' US Patent No. 6,581,466, June.

Dion, G.N. (1999), '*Acoustic Inspection of Concrete Bridge Decks*', Master's Thesis, Mississippi State University, May.

Dunlay, T. (2000), Assistant Bridge Maintenance Engineer, Iowa Department of Transportation, Office of Bridge and Structures, Private Communication.

Henderson, M., Dion, G.N. and Costley, R.D. (1999), 'Acoustic Inspection of Concrete Bridge Decks,' *SPIE's International Symposium on Nondestructive Evaluation Techniques for Aging Infrastructure & Manufacturing*, Newport Beach, CA, March.

Henderson, M., Costley, R.D. and Dion, G.N. (2000), 'Acoustic Inspection of Concrete Bridge Decks with the HollowDeck,' *Structural Materials Technology IV*, ed. Alampalli, S., 184–189, Technomic Publishing, Atlantic City, NJ.

Jastrzebski, Z. (1987), *The Nature and Properties of Engineering Materials*, Table 7-1, p. 203, Third Edition, John Wiley and Sons, New York.

Khan, M.S. (2003), 'Detecting Corrosion-Induced Delaminations,' *Concrete International*, 73–78, July.

Moore, M., Phares, B., Graybeal, B., Rolander, D. and Washer, G. (2001), *Reliability of Visual Inspection for Highway Bridges, Volume I: Final Report*, FHWA-RD-01-020, 423–449, Federal Highway Administration, McLean, VA.

Morse, M. (1976), *Vibration and Sound*, Chapter 5, 209–211, Second Edition, American Institute of Physics, for the Acoustical Society of America, New York.

Sansalone, M. and Carino, N.J. (1991), 'Stress Wave Propagation Methods,' *CRC Handbook on Nondestructive Testing of Concrete*, ed. Malhotra, V., Carino, N., 275–304, CRC Press Inc., Boca Raton, FL.

Scott, M., Rezaizadeh, A., Delahaza, A., Santos, C.G., Moore, M., Graybeal, B. and Washer, G. (2002), 'A Comparison of Nondestructive Evaluation Methods for Bridge Deck Assessment,' *Structural Materials Technology V: An NDT Conference*,

ed. Alampalli, S. and Washer, G.A., 111–118, American Society for Nondestructive Testing, Cincinnati, OH.

Scott, M., Rezaizadeh, A., Delahaza, A., Santos, C.G., Moore, M., Graybeal, B. and Washer, G. (2003), 'A Comparison of Nondestructive Evaluation Methods for Bridge Deck Assessment,' *NDT&E International*, vol. **38**, 245–255.

SIE, Inc. (1974), *Operators Manual for the SIE Delamtech*, Ft Worth, Texas.

Smithson, L.D. and Whiting, J.E. (1992), 'Rebonding Delaminated Bridge Deck Overlays,' *Concrete Repair Digest*, June/July.

Washer, G.A. (2004), 'Nondestructive Testing of Concrete,' *The NDT Technician*, vol. **3**, 1–4, American Society for Nondestructive Testing, April.

4

Electrical impedance testing of wood components

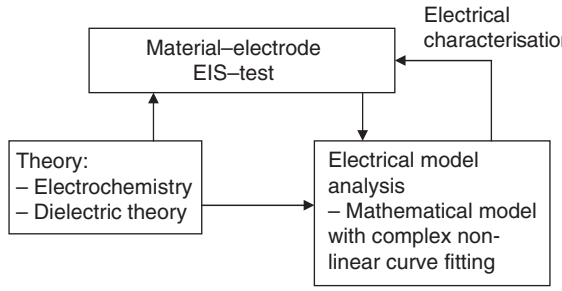
M. TIITTA
University of Kuopio, Finland

4.1 Introduction

Electrical impedance spectroscopy (EIS) and electrical impedance tomography (EIT) are quite novel methods for characterising and imaging electrical properties of materials. One of the main applications of EIS has been to study fundamental electrical properties of materials and correlate these properties with the structure and other material properties. It may be used to investigate the dynamics of bound or mobile charge in the bulk or interfacial regions of liquid or solid materials (e.g. ionic or insulator materials). Many different processes take place throughout the material when it is electrically stimulated and lead to the overall electrical response. In a test, electrodes are used to induce changing electric field into the material and the spectral responses are measured. Electrical model analyses are used to study the electrode–material interface and the material. Numerous successful applications include timber moisture gradient test, corrosion test, coating test, electrical impedance tomography, body composition test and many biomaterial applications. For further information on EIS and EIT, see Grimnes and Martinsen (2000), MacDonald (1987) and Webster (1990). This chapter introduces basic ideas of the EIS technique with applications for wood moisture gradient and decay inspection.

4.2 Background

In an EIS test (Fig. 4.1), both electrochemical and dielectric theories are used for analyses (Grimnes and Martinsen, 2000; MacDonald, 1987). Depending on the material, it is often necessary to apply both theories to the analyses when the material and interfaces have non-uniform structure and the electrical properties include dielectric and conductive regions. The equivalent circuit model may be based on the physical and electrochemical models or purely on the experimental data. The overall material–electrode response is then used for material characterisation using the electrical model parameters and the theories.



4.1 Electrical impedance test diagram.

One of the main differences between EIS analysis and dielectric analysis is that the electrical models are used to interpret the results and the analysis of electrode–material interface is emphasised in EIS. Also, temperature is often the main variable in the dielectric analysis, but frequency is the basic variable in EIS. The frequency range in EIS may include frequencies from μHz to MHz. In dielectric analyses microwave frequencies are also frequently used. In EIS, electrical parameters are used instead of dielectric parameters, but it is also possible to determine the dielectric parameters from the impedance measurements when the measurement configuration is known. As it is known that, in particular, the low-frequency spectrum range is predominated by the electrode–material interface, it is often very useful to use models that distinguish between material and interface properties. Electrical modelling using electrical parameters is an effective tool for this.

Electrical impedance (Z) can be represented by a complex quantity, which consists of a real part (resistance R) and an imaginary part (reactance X):

$$Z* = R + \mathrm{j}X \qquad [4.1]$$

Reactance can be represented in two forms, inductive ($X_L = 2\pi fL$) and capacitive ($X_C = 1/(2\pi fC)$), where f denotes frequency, L inductance and C capacitance. The modulus of impedance is represented by:

$$|Z| = \left(R^2 + X^2\right)^{1/2} \qquad [4.2]$$

and the phase as

$$\theta = \tan^{-1}(X/R) \qquad [4.3]$$

Electrical impedance can also be represented by admittance, which is the reciprocal of impedance ($Y = 1/Z$):

$$Y* = G + \mathrm{j}B \qquad [4.4]$$

where G is conductance and B susceptance. Admittance is especially useful

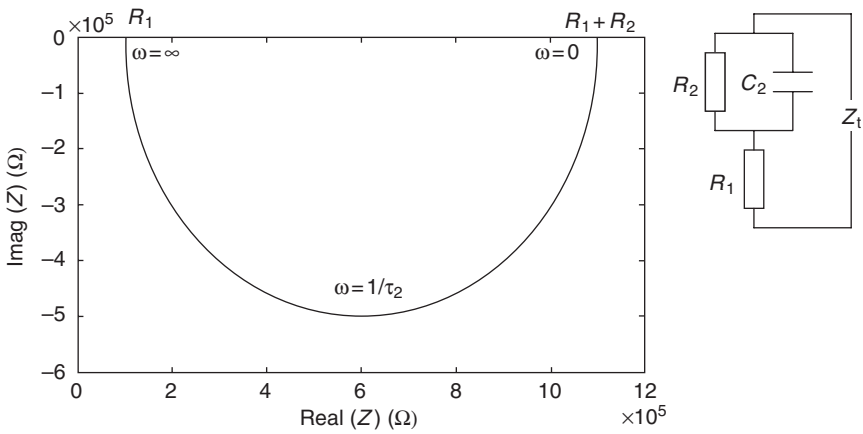
for representing parallel electrical connections and impedance for series connections. The unit for impedance is the ohm (Ω) and admittance is the siemens (S). Complex modulus M and capacitance C may also be used:

$$M^* = j\omega Z^* \quad [4.5]$$

$$C^* = (1/j\omega)Y^* \quad [4.6]$$

The impedance plane representation can be plotted as separated functions of frequency (e.g. capacitance and conductance spectra) or in a complex plane with frequency as the parametric variable. The measurements can be presented in impedance or in admittance plane plotting the imaginary part as a function of the real part. As an example, an impedance graph of a simple RC circuit is illustrated in Fig. 4.2. The plot for the circuit is a semicircle with its centre at $(R_1 + R_2/2, 0)$ and a radius of $R_2/2$. It can be seen that the direct current impedance ($\omega = 2\pi f = 0$) can be given by the sum of R_1 and R_2 as the C_2 is effectively an open circuit. Similarly, in infinite frequency ($\omega = \infty$), C_2 is effectively a short circuit, resulting in impedance of R_1.

Lumped and distributed models have been used for characterisation of materials. Lumped models are usually adequate approximations for lumped-constant resistor and capacitor systems, but an electrolytic cell or dielectric sample is always finite in extent. The circuit element is distributed and its impedance cannot be exactly expressed as the combination of a finite number of ideal circuit elements. One of the most efficient methods to analyse such a system is through the use of a constant phase element (CPE), in which the phase is independent of frequency. Typically resistors and capacitors are adequate additional components in the models to achieve



4.2 An impedance graph and an equivalent circuit (R_1 = 10 kΩ, R_2 = 1 MΩ and C_p = 1 nF). (Z_2 = total impedance.)

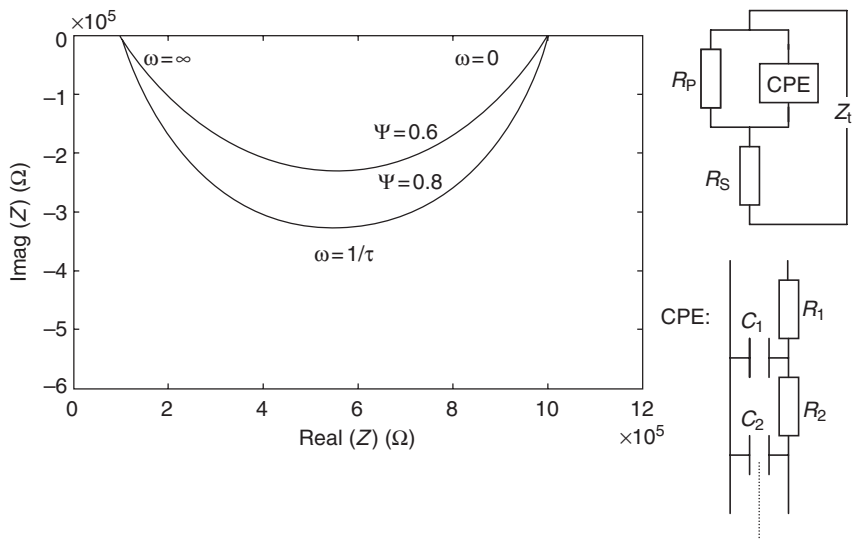
reasonably good results with the empirical measurements. CPE is a distributed model, which has been used to estimate the electrical properties of electrode/material interface. The admittance of the CPE may be represented by:

$$Y_{\mathrm{CPE}} = A_0(\mathrm{j}\omega)^{\Psi} = (\mathrm{j}\omega\tau)^{\Psi} \qquad [4.7]$$

where ψ and A_0 are real constants and τ is the time constant. The value of the fractional exponent ψ is between $0 < \psi < 1$ and it is frequently called as a distribution parameter because the distribution of relaxation times can be determined by ψ. The impedance of the CPE can be approximated by a distributed *RC* ladder network with constant resistors and capacitors for all stages. When a serial (R_S) and parallel (R_P) resistor are added into the model, the impedance can be calculated as:

$$\begin{aligned} Z_{\mathrm{ZARC}} &= R_S + \left[(R_P - R_S)/\left(1 + B_0(\mathrm{j}\omega)^{\Psi}\right)\right] \\ &= R_S + \left[(R_P - R_S)/\left(1 + (\mathrm{j}\omega\tau)^{\Psi}\right)\right] \end{aligned} \qquad [4.8]$$

where $B_0 = A_0(R_P - R_S) = \tau^{\psi}$. The equation is similar to the Cole–Cole dielectric response function. When the capacitor of the circuit (Fig. 4.2) is replaced by the CPE, the centre of the semicircle will be above the real axis in an impedance graph (Fig. 4.3).



4.3 An impedance graph and an equivalent circuit of a CPE-based model (R_S = 10 kΩ, R_P = 1 MΩ and ψ = 0.6/0.8).

Polarisation is, by general definition, the electric field-induced disturbance of the charge distribution in a region. Three major types of polarisation linked with the bound charges in biological materials can be typically found. Electronic polarisation is in the gigahertz region and is associated with the small translational displacements of the electronic cloud with respect to the single atoms or molecules. Oriental polarisation can be found with polar materials because of the rotational movement of the permanent dipoles. The slowest polarisation process is the ionic polarisation, which is the displacement of ions relative to each other. Relaxation and the corresponding frequency domain term dispersion are typically used to characterise the electrical properties of materials. Simple dispersions can be characterised by a permittivity with two different frequency-independent levels and a transition zone around the characteristic dispersion frequency.

Electrically complex materials typically exhibit a distribution of relaxation times. Thus, a simple Debye response or Cole model cannot be used to characterise the electrical properties of most materials. The building materials such as wood are typically very inhomogeneous dielectric materials in which the relaxation processes are linked to the interfaces and thus the interfacial polarisation is widely used to characterise the electrical properties of such materials.

4.3 Advantages and limitations

The quality of a wooden structure inspection depends on the level of experience of the inspector and the inspection tools available. Visual inspection and probing are the most frequently used methods for exterior deterioration (Ross *et al.*, 1999). Visual inspection cannot detect internal decay or decay in the early stages. An experienced inspector may analyse wooden structures for decay using hammer sounding. Widely used coring and drilling can be rather destructive and potentially open the interior of the member to decay attack. Stress wave technique can be used to detect internal decay. Typically the through-transmission method is applied, as measurements can be done in longitudinal or transverse directions. It is also possible to detect and analyse internal decay distributions using scanning techniques (Emerson *et al.*, 1999; Tiitta *et al.*, 1998, 2001a). Electrical methods including EIS can be used to detect regions in wood with high moisture content, which are damaged or potentially available for biodegradation (Skaar, 1988; Tiitta *et al.*, 1999). Also, EIS can be used to analyse decay from wood both in low and high moisture stage (Tiitta *et al.*, 2001b). One of the potential uses of the electrical methods is to serve as a complementary and fully non-destructive technique to quickly monitor the internal state of the visually suspicious region from wooden structures.

The commercially available electrical moisture content (MC) measurement methods include direct current (DC) resistance and dielectric (capacitance or power-loss) methods (Forsen and Tarvainen, 2000; Skaar, 1988). Existing resistance moisture meters are essentially DC megaohm meters, which are not fully non-destructive because of the electrode design (pin electrodes must be driven into the specimen). Surface-contact electrodes can be used in dielectric moisture meters. The lower practical limit for most electrical meters is in the order of 6–8%, and the highest limit is about 25–30%. The dielectric moisture meters are usually planned to measure the average MC of a wood sample though it is obvious that moisture gradient (MG) also has a huge influence on meter readings. It has been shown that dielectric moisture meters are predominantly affected by the surface MC (James, 1986; Mackay, 1976). The measurement of the internal moisture gradient in wood can be improved with the EIS method (Tiitta *et al.*, 1999; Tiitta and Olkkonen, 2002). The method is fully non-destructive and can detect internal high moisture regions. The drawback of the method is that the effective penetration depth is typically about 50 mm and thus the method is ineffective for detecting internal MC from very thick structures. Also, for example, timber bridges are frequently treated with creosols or other chemical compounds, which have an effect on the electrical properties of the treated wood. The treatment eliminates the possibility of using the standard electrical methods for moisture content measurement. EIS has not been been comprehensively tested for chemically treated wood.

Today MG can be measured non-destructively by using laboratory equipment based on X-rays, gamma rays or nuclear magnetic resonance (NMR; Maunu, 2002; Pang and Wiberg, 1998; Tiitta *et al.*, 1993). The effect of density on radiation-based methods and the complexity and costs of the advanced techniques such as computerised tomography (CT) and NMR are the most limiting factors concerning their applications in practical use. Several electrical techniques have been applied on MG measurement. Resistance measurements were used by inserting electrodes in different depths (Forrer, 1984; Forrer and Vermaas, 1987). Also, there have been studies on dielectric measurement systems using multiple or scanning electrode configuration and single frequency excitation (Jazayeri and Ahmet, 2000; Sobue and Yokotsuka, 2003). EIS-based subsurface gradient analyses have been reported for different applications, including skin, concrete and wood (Martinsen *et al.*, 1999; McCarter and Garvin, 1989; Tiitta *et al.*, 1999).

4.4 Equipment and procedure

Many measurement methods can be used to evaluate electrical impedance (Ackmann and Seitz, 1984; Grimnes and Martinsen, 2000; MacDonald, 1987). The measurement method can be chosen according to the needed

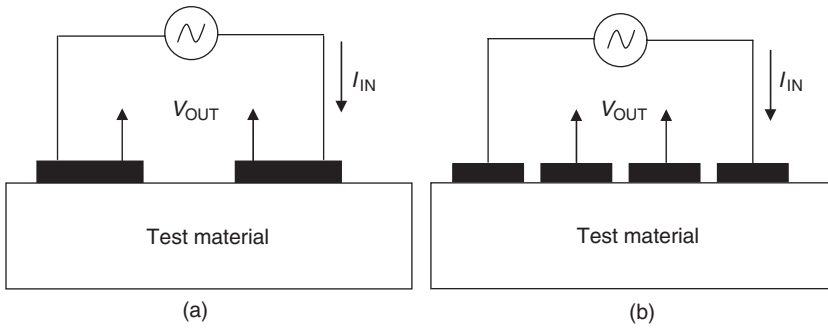
measurement accuracy, frequency region and impedance range. The ease of the operation is also an important factor in many applications. The most common electrical stimulus technique is to use sine waves and measure the impedance at a number of frequencies to obtain a frequency spectrum. Types of electrical stimuli functions other than sine waves are also used in EIS. The methods include step function, impulse and random noise signals. Typically these techniques have certain disadvantages including lower accuracy and the lack of the phase information. On the other hand, frequency responses can be quickly evaluated using Fourier transform.

The electrical bridge method is a well-known measurement technique, where electronic bridge elements are used. It is typically used as an accurate standard laboratory method and has the advantages of high resolution and accuracy. The main disadvantage is that it is slow. The measurements can be done from DC (if the bridge is directly coupled) to the MHz region. Automatic equipments have been developed to ease the use of the method.

The electrical impedance can be determined from measured voltage and current values (current–voltage method). Constant current AC excitation can be used and the resulting voltage is then monitored or vice versa. Then the complex impedance may be determined from the measured phase shift and amplitude values. When using voltage-excitation, the current can be calculated, e.g. from voltage value across an accurately known impedance, which is in series with the unknown impedance. The applicable frequency range is up to 100 MHz.

Lock-in amplifiers are commonly used for impedance measurements. The amplifiers can be divided into digital and analogue amplifiers. Digital lock-in amplifiers use two sine waves, one being a reference signal and another one carrying the amplitude modulated signal. When using two amplifiers and one signal in phase and another 90° out of phase with the excitation signal, the complex impedance can be determined by multiplication of the reference and the modulated signals. The analogue lock-in amplifier can be constructed from a synchronous rectifier, including phase-sensitive detector and a low-pass filter. Digital lock-in amplifiers cover a frequency range from μHz to 200 MHz. Typically, the lower limit of the analogue lock-in amplifiers is about 1 Hz and the upper limit 100 kHz. The auto-balancing bridge method is also widely used in EIS. The method uses ‘virtual ground’ to determine the unknown impedance. Typically the auto-balancing bridge method covers frequency ranges in the Hz to MHz region.

In EIS, electrodes are used to convert the AC electrical current in a wire to ionic current in a material. If the material is dielectric, there will be an electric field inside the material. Many types of electrodes have been tested and examined for EIS. The electrode polarisation may dominate the measurement when low frequencies are used. The polarisation can be consider-



4.4 Basic connections for two-electrode (a) and four-electrode (b) arrangements.

ably reduced using non-polarisable electrode materials such as AgCl and paste. The electrode polarisation decreases rapidly with increasing frequency and thus high frequencies are preferred in many practical applications. The electrode polarisation is low if the material is dielectric and thus there are very few free ions. Reasonably good results can be achieved using metal electrodes including stainless steel if using frequencies above 1 kHz.

Many different types of electrode systems have been used in EIS. Two frequently used systems are two- and four-electrode configurations (Fig. 4.4). A two-electrode system is a simple and widely used technique. It can be effectively used in many applications where the highest accuracy is not needed. The effect of electrode polarisation is very high at low frequencies and thus model analyses are frequently used to get accurate and reliable results from the studied material. The electrode cable compensation is highly important because the electronic properties of the cables are part of the measurement system. Four-cable systems using grounded coaxial cables are frequently used to improve the signal to noise ratio in a two-electrode configuration. In that arrangement, the same potential leads are connected in electrodes. The four-electrode system uses separated current and voltage electrodes. The technique reduces the effect of electrode polarisation because the signal current electrodes are separated from the measurement voltage electrodes, which are thus not externally polarised.

Open and short circuit compensations are needed to achieve accurate results in EIS. In the short circuit compensation, the electrodes are short-circuited and the residual impedance of the system can be determined. In open loop compensation the electrodes are placed in the measurement position without the sample and thus any stray admittances from the system can be measured and compensated.

Many mathematical methods can be used for the complex model fits. Among the most frequently used methods are complex non-linear least

Table 4.1 Basic steps in electrical impedance spectroscopy-based material analysis

1.	Study the basic electrical properties of the material (e.g. conductor or dielectric)
2.	Test and choose electrode materials (e.g. electrode polarisation, durability)
3.	Develop electrode configuration (e.g. through-transmission or one-sided measurement, size of the electrodes, two or four electrodes)
4.	Examine reliable frequency range (e.g. low frequencies might give erroneous results)
5.	Examine different models and choose the one best suited to empirical measurements and also in agreement with the theoretical background
6.	Study the relations between the material properties and the electrical model parameters
7.	Use multiparameter analysis to develop a method to evaluate one or more material properties using EIS

squares (CNLS), Gauss–Newton and the Nelder–Mead simplex method. The choice of the method is based on *a priori* information about the object, the complexity of the model and the accuracy needed. Typically all the methods are effective if the measurement range of the studied electrical properties is known and the model is properly chosen.

The basic steps of a typical EIS application in practice are given in Table 4.1. Learning the basics concerning the electrical properties of the studied material is one of the most important tasks because the model and the experimental studies are based on their properties. The electrodes chosen must be suitable for the application. The properties of electrodes include durability and polarisation, and their size and separation from each other can be altered to produce a certain electric field inside the material. Typically the most informative part of the frequency spectrum is near the dispersion frequencies, which should be carefully examined to achieve the most informative results. One of the most demanding tasks in EIS study is to choose a proper model, which should be done by an experienced researcher in order to obtain the best results. As in other spectroscopic techniques, multiparameter analyses can be used effectively to achieve the best solution for the application. Multiple regression, principal component analysis, partial least squares and neural networks are among the potential techniques.

4.5 Wood moisture gradient inspection

MC is an important factor affecting the properties of wood (Kollman and Cote, 1984; Skaar, 1988; Torgovnikov, 1993). MC influences, for example, strength properties, stiffness, hardness, abrasion resistance, machinability,

heat value, thermal conductivity, yield and quality of pulp and resistance of wood against biodegradation. If MC is above 20% wood is available for biodegradation including decay. The determination of MC is therefore of the utmost importance. Also, MG is typically involved in wood in both dried and green state. The moisture content is defined as the weight of water contained in the wood, expressed as a percentage ratio to the weight of the oven-dry wood:

$$\mathrm{MC}\% = 100[(w_\mathrm{m} - w_\mathrm{d})/w_\mathrm{d}] \qquad [4.9]$$

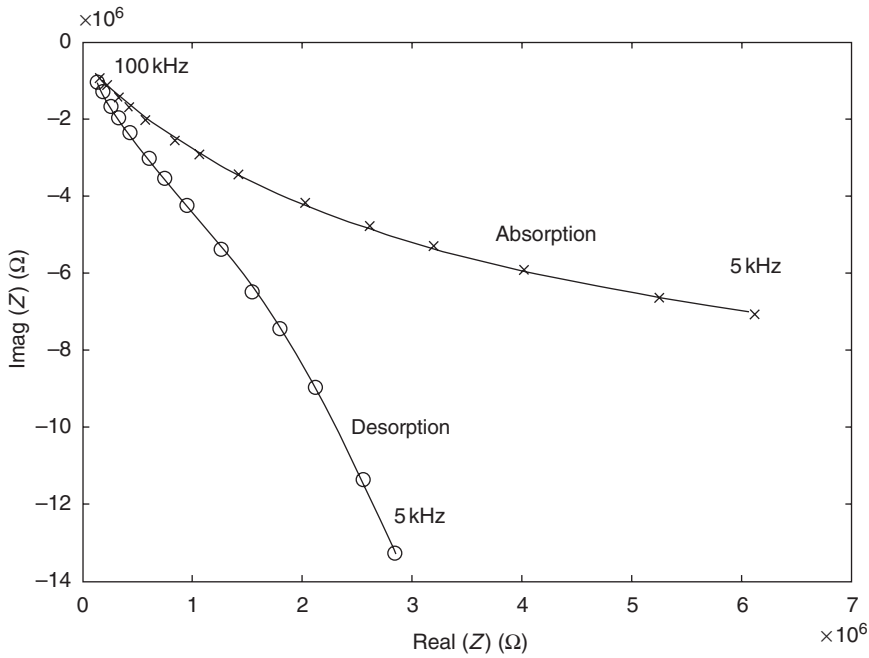
where w_m is the weight of a specimen at the measurement stage and w_d is the oven-dry weight after drying at 103 ± 2 °C.

The fibre saturation point (FSP) is defined as the moisture content at which cell cavities contain no liquid water, but the cell walls are fully saturated with moisture. FSP is experimentally difficult to obtain accurately. Extractive content and density affect the FSP. The strength properties of wood generally decrease with increasing moisture content below FSP while above FSP there is no essential change with MC. Capillary or free water in the cell cavities has no effect on strength when the fibres are fully saturated with water.

Moisture content predominately affects the electrical properties of wood when moisture content is below the FSP. A lot of studies have been conducted using the direct current electrical resistance, and resistance moisture meters are frequently used in wood moisture content inspection. The meters are compact and relatively accurate when moisture content is low (Forsen and Tarvainen, 2000). Though MC has the most significant effect on electrical resistance, other material properties such as temperature and extractives also have significant effects.

The dielectric properties of wood are also greatly affected by its MC. Density, temperature, grain orientation and frequency also have an effect on dielectric properties. Moist and dry wood can be considered as polar dielectrics. The general polarisation of wood can be regarded as a total of two components, instant polarisation and relaxation polarisation (Torgovnikov, 1993). The instant polarisation is the sum of the electronic and atomic polarisation, which follow the electric field. Dipole, interfacial and electrolytic polarisations affect the relaxation component, which lags behind the changes of the field strength. Dipole and interfacial polarisation are the main factors in the polarisation of wood.

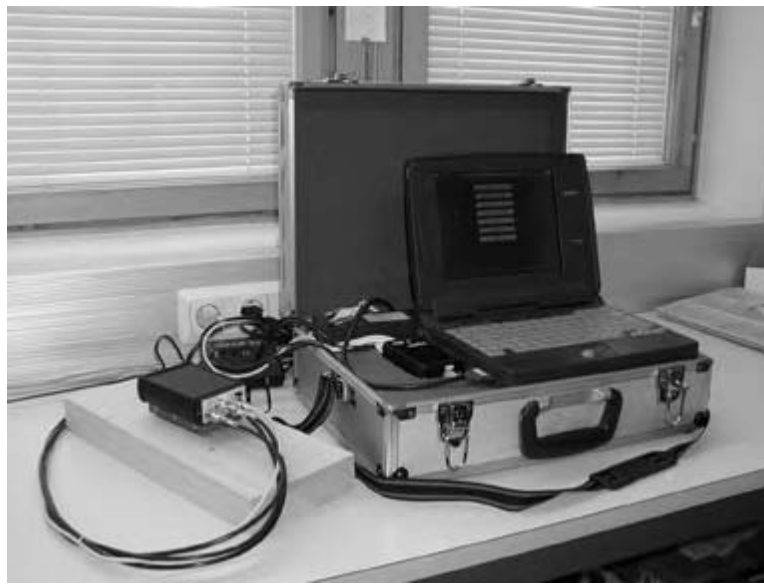
To analyse the electrical spectral properties of wood, a model based on CPE was constructed. In the model a CPE element based circuit forms a slightly flattened semicircle at the upper end of the frequency spectrum (ZARC-Cole element; MacDonald, 1987) and another CPE element forms a direct line at the lower end of the frequency spectrum in the impedance graph. The MG of wood can be analysed with the aid of parameters obtained from the CPE models.



4.5 Examples of impedance spectra and the best fits for wood moisture gradient measurement. One-sided measurement using stainless steel plate electrodes. Both wood samples have the same average moisture content near the surface.

The model fits the empirical data measured from wood samples well (Fig. 4.5). The wood MG calibration measurements were made using $40 \times 50\,\text{mm}^2$ stainless steel plate electrodes, which were fastened on the measuring probe at a distance of 5 mm from each other. The measurements were carried out in such a way that the electrical field was formed in the longitudinal direction of the sample and the probe was laid on the sample.

To be able to use the EIS technique in the field, a portable EIS device has been developed (Tiitta and Olkkonen 2002; Fig. 4.6). The electronics of the spectrometer were optimised especially to measure wood specimens with a large variation in MC, including high impedances. The EIS device consists of a measurement probe and a control unit, which are connected via coaxial and power cables. The hand-held probe consists of a measuring card and plate electrodes. A buffer amplifier produces a sine wave current signal through the electrodes and the current signal is determined by measuring the voltage across the reference impedance. The hand-held probe is laid against the surface of wood during measurement. In the measurement, a changing electrical field is induced into the material by the electrodes. The transverse moisture gradient of the material is determined from the effect



4.6 Electrical impedance equipment for wood moisture gradient measurement.

of dispersive characteristics of the material evaluated from the electrical impedance spectrum. In the continuous measurement, a graph of transverse moisture gradient and estimates of minimum, maximum, surface and average MC are displayed on the screen. A more detailed description of the method and EIS device can be found in Tiitta *et al.* (1999) and Tiitta and Olkkonen (2002).

4.6 Wood decay inspection

As a hygroscopic material, wood is subjected to several types of micro-organisms including mould, blue stain, decay fungi and bacteria when humidity and temperature conditions are suitable for their growth (Viitanen, 1996; Zabel and Morell, 1992). The degradation of wood is affected by the interaction of wood cell and ambient microclimate. Different decay types of wood have been detected and the chemical and physical structure of the wood cell and ambient moisture conditions have a major effect on the decay type and also on the intensity of decay. During the decay process, a wide range of changes in the mechanical, physical and chemical properties are involved. These include drastic reduction in wood strength and biomass loss. Changes to density, hygroscopicity, permeability and electrical conduction

are also present. Typical chemical changes include degradation, metabolism and depolymerisation of the cell wall constituents. All the changes are highly affected by the type of decay fungi and degree of decay.

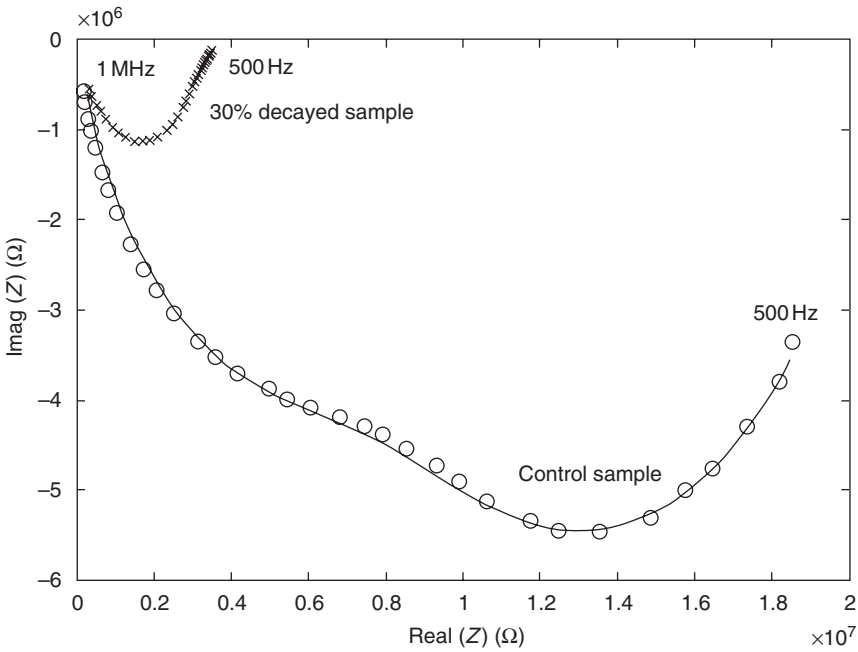
The main types of decay fungi can be classified as white rot, brown rot and soft rot. White rot fungi mainly decompose all the major components of wood including lignin and carbohydrates. Brown rot fungi produce organic acids and enzymes, which mainly decompose the carbohydrates, hemicellulose and cellulose, leaving the lignin modified but not metabolising it. The hyphae of soft rot fungi penetrate the cell wall, producing cavities. Soft rot fungi primarily decompose the carbohydrates but, unlike brown rot fungi, they metabolise some lignin as well.

Soft rot fungi are often the main degrading factors in wood in ground contact or wet conditions. Often bacterial decay is also involved. For decay development, high humidity or wet conditions for longer periods (weeks or months) are needed: RH above 95% and temperature between 0 and 50 °C. Active decay fungi can also affect the moisture content of wood. For the optimum activity of several brown rot fungi, the wood moisture content should be between 60 and 80%. As the decay process continues, the porosity of wood will be higher and more water can be absorbed in the wood. For soft rot fungi and bacteria, the wood moisture content after decay process can be above 200–300% as compared with moisture content of sound wood (max. 170–180%) in pine sapwood. In dried decayed wood, the equilibrium moisture content is often lower than that of sound wood, owing to loss of hemicellulose and cellulose since the equilibrium moisture content of lignin is lower.

Decay inspection from wet or living wood using electrical pulsed current has been used for decades (McGinnes and Shigo, 1975; Shortle, 1982). The measurement is highly dependent on the increased moisture content in intact areas and thus the method has not been succesfully applied to dried wood (Piirto and Wilcox, 1978). On the other hand, decay has an effect on both moisture content and the structure of wood and thus EIS was tested for decay inspection of dried wood.

In the EIS decay study the wood specimens (Scots pine, sapwood) were exposed in unsterile conditions using different organisms, mainly soft rot fungi (e.g. *Chaetomium globosum*) and bacteria (Tiitta *et al.*, 2001b). After the decay treatment the specimens were conditioned at two different relative humidities (RH 76% and 90%) for six weeks to achieve the equilibrium MC in the specimens. Both decayed and control specimens were conditioned in the same chamber to make sure that all specimens had the same environmental conditions. The electrical model used was constructed from two parallel R-CPE circuits in series.

The shape of the impedance spectrum changed as a result of wood decay and with increasing MC (Fig. 4.7). The distribution coefficient ψ decreased



4.7 Examples of impedance spectra and the best fits for decayed and control wood samples. Through-transmission measurement from small samples.

with increasing decay rate in both RH conditions. On the other hand, the effect of MC on model parameters was significant. No obvious effect of decay on conductance or capacitance could be found, but capacitance and conductance increased with increasing MC in all treatments. It was concluded that a good estimate for both MC and the degree of soft rot decay could be achieved by using multiparameter analysis including model parameters and conductance/capacitance values.

4.7 Future research and development

Today electrical measurement applications for wood inspection in field are almost entirely based on the moisture measurement. Moisture and moisture gradient are the main factors affecting electrical properties of wood in both direct current and alternating current applications. In DC analysis, electrode pins have to be pushed inside the wood to evaluate moisture content below surface. On the other hand, it has been shown that the electrical impedance spectroscopy and tomography can be used to determine moisture gradients inside the wooden structures.

To make the advanced electrical techniques available for field use, a portable EIS analyser prototype was developed. Today research is continuing to develop small handheld EIS equipment for advanced *in situ* analyses of structures. By using moisture gradient evaluation, it would be possible to increase the reliability of a fully non-destructive wooden structure inspection. Combined methods could be used to get more information from the wooden structures, e.g. the efficiency of ultrasonic inspection to detect biodegradation would increase if MC and MG are known because ultrasonic propagation is affected by moisture content and moisture gradient.

It has been shown that biodegradation has an effect on electrical properties of wood. The effect depends on the type of biodegradation and its extent, and is thus quite a complex research area, which should be comprehensively examined before it can be applied to field measurements. There is a need for a low-cost and compact biodegradation analyser, which could be used for *in situ* evaluation of wooden structures such as bridges and civil structures. Electrical impedance spectroscopy is one of the potential techniques for that.

4.8 Conclusions

Electrical impedance spectroscopy is an electrical measurement technique in which spectral and model analyses are used. In the test, electrodes are used to induce changing electric field into the material and the responses are evaluated. Numerous successful applications include wood moisture gradient test, corrosion test, coating test and electrical impedance tomography. In wooden structure evaluation, detection of high moisture content and biodegradation are highly important. It has been shown that EIS can be used for the analyses and thus it is among the powerful future techniques for *in situ* analyses because the technique is relatively low cost and it is possible to develop compact instruments for field measurements.

4.9 References

Ackmann, J.J. and Seitz, M.A. (1984), 'Methods of complex impedance measurements in biological tissue', *CRC Cri Rev Biom Eng* **11**, 281–311.

Emerson, R.N., Pallack, D.G., McLean, D.J., Fridley, K.J., Ross, R.J. and Pellerin, R.R. (1999), 'Nondestructive testing of large bridge timbers', *Proc 11th Int. Symp on NDT of Wood*, Forest Products Society, Madison, Wisconsin, 175–184.

Forrer, J.B. (1984), 'An electronic system for monitoring gradients of drying wood', *Forest Prod J* **34** (7/8), 34–38.

Forrer, J.B. and Vermaas, H.F. (1987), 'Development of an improved moisture meter for wood', *Forest Prod J* **37** (2), 67–71.

Forsen, H. and Tarvainen, V. (2000), *Accuracy and Functionality of Hand Held Wood Moisture Content Meters*, VTT Publications 420, Otamedia Oy, Espoo, Finland.

Grimnes, S.G. and Martinsen, O.G. (2000), *Bioimpedance and Bioelectricity Basics*, Academic Press, London.

James, W.L. (1986), 'The interaction of electrode design and moisture gradients in dielectric measurements on wood', *Wood and Fiber Sci* **18** (2), 264–275.

Jazayeri, S. and Ahmet, K. (2000), 'Detection of transverse moisture gradients in timber by measurements of capacitance using a multiple-electrode arrangement', *Forest Prod J* **50** (11/12), 27–32.

Kollman, F.F.P. and Cote, W.A. (1984), *Principles of Wood Science and Technology I. Solid Wood*, Springer-Verlag, Berlin.

MacDonald, J.R. (1987), *Impedance Spectroscopy*, John Wiley & Sons, New York.

Mackay, J.F.G. (1976), 'Effect of moisture gradients on the accuracy of power-loss moisture meters', *Forest Prod J* **26** (3), 49–52.

Martinsen, O.G., Grimnes, S.G. and Haug, E. (1999), 'Measuring depth depends on frequency in electrical skin impedance measurements', *Skin Res and Tech* **5**, 179–181.

Maunu, S.L. (2002), 'NMR studies of wood and wood products', *Prog in NMR Spectr* **40**, 151–174.

McCarter, W.J. and Garvin, S. (1989), 'Dependence of electrical impedance of cement-based materials on their moisture condition', *J Phys D: Appl Phys* **22**, 1773–1776.

McGinnes, E.A. Jr and Shigo, A.L. (1975), 'Electronic technique for detecting discoloration, decay, and injury-associated ring shake in black walnut', *Forest Prod J* **25**, 30–32.

Pang, S. and Wiberg, P. (1998), 'Model predicted and CT scanned moisture distribution in a *Pinus radiata* board during drying', *Holz als Roh- und Werkstoff* **56**, 9–14.

Piirto, D.D., Wilcox, W.W. (1978), 'Critical evaluation of the pulsed-current resistance meter for detection of decay in wood', *Forest Prod J* **28**, 52–57.

Ross, R.J., Pellerin, R.F., Volny, N., Salsig, W.W. and Falk, R.H. (1999), *Inspection of Timber Bridges Using Stress Wave Timing Nondestructive Tools*, USDA FPL-GTR-114, Forest Products Lab., Madison.

Shortle, W.C. (1982), 'Decaying Douglas-fir wood: ionization associated with resistance to a pulsed electric current', *Wood Sci* **15** (1), 29–32.

Skaar, C. (1988), *Wood–Water Relations*, Springer-Verlag, Berlin.

Sobue, N. and Yokotsuka, M. (2003), 'Estimation of moisture gradient in structural timbers by capacity measurement in RF range while scanning electrodes', *5th Int Conf on Electromagnetic Wave Interaction with Water and Moist Substances*, Industrial Research, New Zealand.

Tiitta, M. and Olkkonen, H. (2002), 'Electrical impedance spectroscopy device for measurement of moisture gradients in wood', *Rev Sci Instr* **73** (8), 3093–3100.

Tiitta, M., Olkkonen, H., Lappalainen, T. and Kanko, T. (1993), 'Automated low energy photon absorption equipment for measuring internal moisture and density distributions of wood samples', *Holz Roh-Werkstoff* **51**, 417–421.

Tiitta, M., Beall, F.C. and Biernacki, J.M. (1998), 'Acousto-ultrasonic assesment of internal decay in glulam beams', *Wood and Fiber Sci* **30/3**, 24–37.

Tiitta, M., Savolainen, T., Olkkonen, H. and Kanko, T. (1999), 'Wood moisture gradient analysis by electrical impedance spectroscopy', *Holzforschung* **53**, 68–76.

Tiitta, M., Biernacki, J.M. and Beall, F.C. (2001a), 'Classification study for detecting

internal decay in glulam beams by acousto-ultrasonics', *Wood Sci Technol* **35**, 85–96.

Tiitta, M., Repo, T. and Viitanen, H. (2001b), 'Effect of soft rot and bacteria on electrical properties of wood at low moisture content', *Mat Org* **33** (4), 271–288.

Torgovnikov, G.I. (1993), *Dielectric Properties of Wood and Wood-based Materials*, Springer-Verlag, Berlin.

Viitanen, H. (1996), '*Factors affecting the development of mould and brown rot decay in wooden material and wooden structures*,' Diss, The Swedish Univ of Agric Sci, Dept of Forest Products, Uppsala, Sweden.

Webster, J.G. (1990), *Electrical Impedance Tomography*, Adam Hilger, Bristol.

Zabel, R.A. and Morrell, J.J. (1992), *Wood Microbiology: Decay and its Prevention*, Academic Press, San Diego.

5

Detecting decay in wood components

R.J. ROSS,
USDA Forest Products Laboratory, USA and
X. WANG and B.K. BRASHAW
Natural Resources Research Institute, USA

5.1 Introduction

Wood deterioration is one of the most common damage mechanisms in timber bridges and other wood structures and often inflicts damage internally. This may occur without visible signs appearing on the surface until a member's load-bearing capacity has been largely destroyed. Determining an appropriate load rating for an existing timber structure and establishing rational rehabilitation, repair, or replacement decisions can be achieved only when an accurate assessment of its existing condition is made. Knowledge of the condition of the structure can lead to savings in repair and replacement costs by minimizing labor and materials and extending its life.

In wood structures, the degradation of a load-bearing (in-service) member may be caused by any one of several organisms that derive their nourishment or shelter from the wood substrate in which they live. For example, several types of fungi attack wood. The hyphae of these fungi secrete enzymes that depolymerize the chemical components of wood, thereby lowering the density, strength, and hardness of a member. This results in a significant reduction in load-carrying capacity, which in turn may result in the member's failure. Accurate detection of decay in wood structures is therefore critical to ensuring the safety of the public and extending the service life of the structures.

Recently, we prepared a comprehensive manual on the inspection of wood structural elements titled *Wood and Timber Condition Assessment Manual* (Ross *et al.* 2004). It was prepared at the request of the American Forest and Paper Association to assist field engineers and other inspection professionals. It is published by the Forest Products Society and includes chapters on visual inspection techniques, ultrasound or stress wave based inspection tools, and probing type techniques. A chapter on post-fire inspection and assessment is included in addition to a sample inspection report and summaries from numerous inspections. Detailed descriptions of the

various available tools, guidelines on their use, and interpretation of data obtained from them are included.

This chapter presents a summary of the *Wood and Timber Condition Assessment Manual*. It focuses on current inspection techniques for decay detection and provides guidelines on the use of various non-destructive evaluation (NDE) methods in locating and defining areas of deterioration in timber bridge components and other civil structures.

5.2 Conventional methods

Conventional methods for detecting deterioration in bridges are divided into two categories: those for exterior deterioration and those for interior deterioration. In both cases, specific techniques or tools are appropriate for certain types of damage, and their usefulness varies depending on the type of structure. Although a variety of inspection methods may be employed, in practice the inspector uses only a few tools. The methods or tools are often dictated by budget, previous experience, and the types of problem that are encountered.

5.2.1 Methods for determining exterior deterioration

Exterior deterioration is the easiest to detect because it is often readily accessible to the inspector. The ease of detection depends on the severity of damage and the method of inspection. Commonly used methods include visual inspection and probing. When areas of exterior deterioration are located by these methods, further investigation by other methods is required in order to confirm and define the extent of damage.

Visual inspection

Visual inspection is the simplest method for locating deterioration in timber structures. The inspector observes the structure for signs of actual or potential deterioration, noting areas for further investigation. Visual inspection requires strong light and is suitable for detecting intermediate or advanced surface decay, water damage, mechanical damage, or failed members. Visual inspection cannot detect early stage decay, when remedial treatment is most effective. The following paragraphs describe signs of deterioration that should be noted during an investigation.

Fruiting bodies provide positive indication of fungal attack but do not indicate the amount or extent of decay. Some fungi produce fruiting bodies after small amounts of decay have occurred, whereas others develop only after decay is extensive. Fruiting bodies are not common on bridges, and they almost certainly indicate serious decay problems when they are present.

Sunken faces or localized surface depressions can indicate underlying decay. Decay voids or pockets may develop close to the surface of the member, leaving a thin, depressed layer of intact, or partially intact, wood at the surface. Staining or discoloration indicates that members have been subjected to water and potentially high moisture contents suitable for decay. Rust stains from connection hardware are also a good indication of wetting.

Insect activity is visually characterized by holes, frass, powder posting, or other signs previously discussed. The presence of insect activity may also indicate the presence of decay. Plant or moss growth in splits or cracks, or soil accumulation on the structure indicates that adjacent wood has been at relatively high moisture content suitable for decay for a sustained period of time.

Probing

Probing with a moderately pointed tool, such as an awl or knife, locates decay near the wood surface by revealing excessive softness or a lack of resistance to probe penetration. Although probing is a simple inspection method, experience is required to interpret results. Care must be taken to differentiate between decay and water-softened wood that may be sound but somewhat softer than dry wood. It is also sometimes difficult to assess damage in soft-textured woods such as western red cedar.

In addition to probing with simple tools, some mechanical devices, such as the Pilodyn, can also be used to detect surface damage. The Pilodyn is a spring-loaded pin device that drives a hardened steel pin into the wood. The depth of pin penetration is used as a measure of the degree of decay. The Pilodyn is used extensively in Europe, where soft rot attack is more prevalent. It is also used to measure the specific gravity of wood for tree improvement programs. Where surface damage is suspected, the Pilodyn can produce an accurate assessment, provided corrections are incorporated for moisture content and the wood species tested.

5.2.2 Methods for detecting interior deterioration

Unlike exterior deterioration, interior deterioration is difficult to locate because there may be no visible signs of its presence. Numerous methods and tools have been developed to evaluate internal damage that range in complexity from sounding the surface with a hammer to sophisticated X-ray or radiographic evaluation. In addition, tools such as moisture meters are also used to help the inspector identify areas where conditions are suitable for development of internal decay.

Sounding

Sounding the wood surface by striking it with a hammer or other object is one of the most commonly used inspection methods for detecting interior deterioration. Based on the tonal quality of the ensuing sounds, a trained inspector can interpret dull or hollow sounds that may indicate the presence of large interior voids or decay. Although sounding is widely used, it is often difficult to interpret because factors other than decay can contribute to variations in sound quality. In addition, sounding provides only a partial picture of the extent of decay present and will not detect wood in the incipient or intermediate stages of decay. Nevertheless, sounding still has its place in inspection and can quickly identify seriously decayed structures. When suspected decay is encountered, it must be verified by other methods, such as boring and coring.

Drilling and coring

Drilling and coring are the most common methods for detecting internal deterioration in bridges. Both techniques are used to detect the presence of voids and to determine the thickness of the residual shell when voids are present. Drilling and coring are similar in many respects and will be discussed together.

Drilling is usually done with an electric power drill or hand-crank drill equipped with a 10–19 mm (3/8 to $^{3}/_{4}$ inch) diameter bit. Power drilling is faster, but hand drilling allows the inspector a better feel and may be more beneficial in detecting pockets of deterioration. Generally, the inspector drills into the structure, noting zones where drilling becomes easier (torque releases) and observing the drill shavings for evidence of decay. The presence of common wood defects, such as knots, resin pockets, and abnormal grain, must be anticipated while drilling and must not be confused with decay. If decay is detected, the inspection hole can also be used to add remedial treatments to the wood.

Coring with increment borers also provides information on the presence of decay pockets and other voids, and coring produces a solid wood core that can be carefully examined for evidence of decay. Where appropriate, the core can also be used to obtain an accurate measure of the depth of preservative penetration and retention. Where structures are not yet showing signs of decay, cores can be cultured to detect the presence of decay fungi. The presence of such fungi usually indicates that the wood is in the early or incipient stage of decay and should be remedially treated. Culturing provides a simple method for assessing the potential decay hazard, and many laboratories provide routine culturing services. Because of the wide variety of fungi near the surface, culturing is not practical for assessing the hazard of external decay.

Drilling and coring are generally used to confirm suspected areas of decay identified by the use of moisture meters or other methods. When decay is detected, drilling and coring are also used to further define the decay's extent and limits. Inspectors may find drilling best for initial inspection until some evidence of decay is found. When decay is detected, coring may be preferred for defining the limits of the infection and extracting samples for further examination and analysis. It is important to use sharp tools for both drilling and coring, and the inspector should always carry extra bits or increment borers. Dull tools tend to crush or break wood fibers and cause excessive core or shaving breakage that may be confused with decay.

Shell-depth indicator

A tool that is useful when drilling or coring is the shell-depth indicator. This tool is a metal bar, notched at the end and inscribed in inches or centimetres, that is inserted into the inspection hole and pulled back along the hole sides. As it moves along the wood, the hook will catch on the edges of voids. In this way the inspector can note the depth of the solid shell, which can be used to estimate residual wood strength.

Shigometer

The Shigometer, a device that has been compared to the moisture meter, uses a pulsed current to measure changes in electrical conductivity associated with decay. A small hole is drilled into the wood, and a twisted wire probe connected to a meter is inserted into the hole. As the probe encounters zones of decreased resistance, the meter reading drops. Zones of large meter declines (50–75% of that indicated for sound wood) are then bored or drilled to determine the nature of the defect. The Shigometer has performed very well in detecting decay in living trees, but wood in service is normally too dry to permit the use of this instrument. Nevertheless, several studies show that the Shigometer is a reasonable method for detecting decay if it is used under proper conditions by trained operators who understand its operation and interpretation.

X-rays and tomography scanners

X-rays were once commonly used for detecting internal voids in wood. As the X-rays pass through the wood, the presence of knots or other defects alters the density of the resulting radiograph. X-ray technology has advanced considerably since the first field units were developed; however, the high cost of equipment, safety factors associated with the use of ionizing

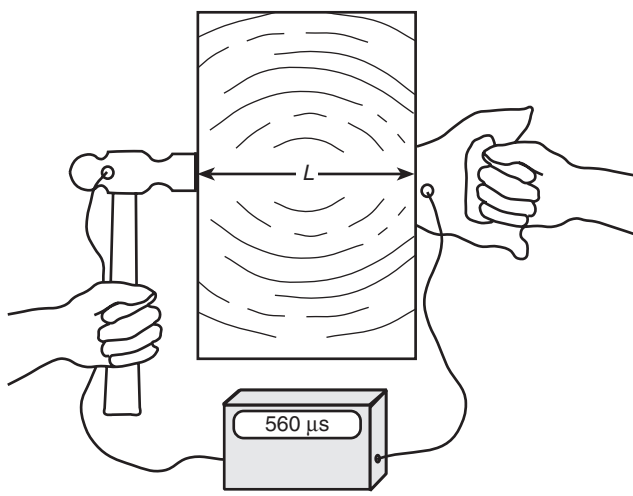
radiation, and the need for expert interpretation of results have largely eliminated its use in wood. Despite these problems, X-rays are particularly useful for detecting insect and marine borer infestations in wood.

5.3 Stress wave propagation method

Another method that has been successfully used for decay detection in wood structures is the inducement of a stress wave in a structural member and measurement of attenuation and time required for the stress wave to propagate through the member (Pellerin and Ross 2003). If decay is present in the member, the attenuation and propagation time of the stress wave passing through the member is increased. Propagation time in decayed wood may be as much as several times the propagation time in solid wood.

5.3.1 Concept and limitations

As an introduction to this stress wave concept for detecting decay in wood structural members, a schematic of the stress wave measurement in a rectangular timber is shown in Fig. 5.1. A stress wave is induced by striking the member with an impact device that is instrumented with an accelerometer that in turn emits a start signal to a timer. A second accelerometer, which is coupled to the timber, then responds to the leading edge of the propagating stress wave and sends a stop signal to the timer. The elapsed time for the stress wave to propagate between the accelerometers is displayed on

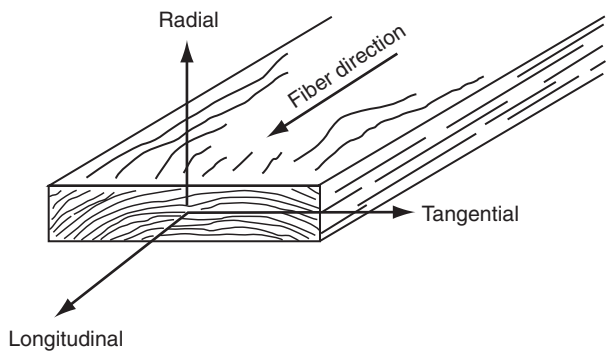


5.1 Schematic of stress wave measurement in a rectangular timber.

the timer. The underlying premise for this technique is that the speed, and hence the transmission time, at which a stress wave travels through a wood member is indicative of the member's condition.

The use of stress wave velocity to detect wood decay in timber bridges and other structures is limited only by access to the structural members under consideration. It is especially useful on large timbers or glulam timbers ≥89 mm (≥3.5 inches) for which hammer sounding is not effective. Access to both sides of the member is required. Because timber is an organic substance, material properties and strength vary in accordance with the direction timber is hammered relative to the cell structure orientation. Hammering the end grain of a beam or post will cause a primarily longitudinal shock wave along the length of the cell structure in the timber. Hammering the side or top of the beam will cause a wave across or transverse to the timber cells. The timber cells are arranged in rings around the center of the tree. The velocity at which a stress wave propagates in wood, as well as other physical and mechanical properties, is a function of the angle at which the fibers of wood are aligned. For most structural members, fibers of the wood align more or less with the longitudinal axis of the member (Fig. 5.2).

Stress wave transmission times on a per length basis for various wood species are summarized in Table 5.1 (Ross *et al*. 2004). Stress wave transmission times are shortest along the grain (with the fiber) and longest across the grain (perpendicular to fiber). For Douglas fir and southern pine, stress wave transmission time parallel to the fiber is approximately 200 µs/m (60 µs/ft). Stress wave transmission time perpendicular to the fiber ranges from 850 to 1000 µs/m (259 to 305 µs/ft). When the stress wave propagation method is used to detect localized decay in timbers, measurements should be made in transverse paths (perpendicular to grain). Parallel-to-grain travel paths (longitudinal direction) can bypass regions of decay and therefore are not effective.



5.2 Three principal axes of wood with respect to grain direction and growth rings.

Table 5.1 Summary of research on stress wave transmission times for various species of non-degraded wood

Species	Moisture content (% OD)[a]	Stress wave transmission time (μs/m (μs/ft))	
		Parallel to grain	Perpendicular to grain
Sugar maple	12	256–194 (78–59)	–
Yellow birch	11	230–180 (70–55)	–
White ash	12	252–197 (77–60)	–
Red oak	11	262–200 (80–61)	–
Birch	4–6	213–174 (65–53)	715–676 (218–206)
Yellow poplar	4–6	194–174 (59–53)	715–676 (218–206)
Black cherry	4–6	207–184 (63–56)	689–620 (210–189)
Red oak	4–6	226–177 (69–54)	646–571 (197–174)
Several	11	203–167 (62–51)	–
Red oak	12	302–226 (92–69)	–
Several	–	272–190 (83–58)	–
Sitka spruce	10	170 (52)	–
Southern pine	9	197 (60)	–
Douglas fir	10	203 (62)	–
Southern pine	10	197–194 (60–59)	–
Douglas fir	12	–	1092–623 (333–190)
Douglas fir	11	–	850–597 (259–182)
Douglas fir	–	–	1073 (327)
Southern pine	9	200–170 (61–52)	–
Live oak	12	–	613–1594 (187–486)
Northern red and white oak	Green	–	795 (242)

[a] OD is oven dry.
Source: Ross *et al.* (2004).

5.3.2 Effect of decay

The presence of decay greatly affects stress wave transmission time in wood. Table 5.2 summarizes stress wave transmission values obtained from field investigations of various wood members subjected to degradation from decay (Ross *et al.* 2004). Stress wave transmission times perpendicular to the grain are drastically reduced when the member is degraded. Transmission times for non-degraded Douglas fir are approximately 800 μs/m (244 μs/ft), whereas severely degraded members exhibit values as high as 3200 μs/m (975 μs/ft) or greater.

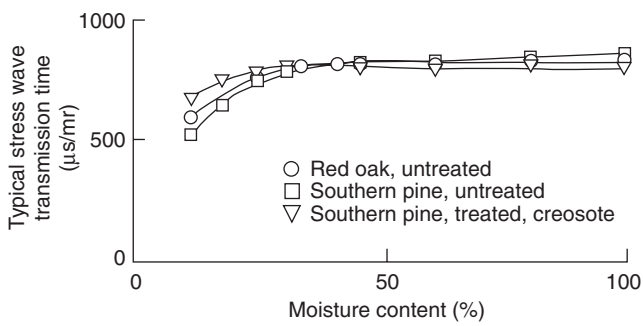
5.3.3 Effect of moisture content

Several studies have revealed that stress wave transmission times perpendicular to the grain of wood follow a relationship to moisture content (Fig. 5.3). At moisture contents less than approximately 30%, transmission

Table 5.2 Summary of research on use of stress waves for detecting decay in timber structures

Structure	Wood product	Test	Analysis
Bridge	Douglas fir glulam, creosote pressure treated	Stress wave transmission time perpendicular to grain, across laminations at 0.3 m (0.98 ft) intervals	Sound wood: 1279 μs/m (390 μs/ft) Moderate decay: 1827 μs/m (557 μs/ft) Severe decay: 2430 μs/m (741 μs/ft)
Football stadium	Solid sawn Douglas fir, creosote pressure treated	Stress wave transmission time perpendicular to grain, near connections	Sound wood: 853 μs/m (260 μs/ft) Incipient decay: – Center of members: 1276 μs/m (389 μs/ft) – 38 mm thick solid wood shell: 2129 μs/m (649 μs/ft) Severe decay: >3280 μs/m (1000 μs/ft)
School gymnasium	Douglas fir glulam arches	Velocity of stress wave transmission time perpendicular to grain, near end supports	Sound wood: 1073 μs/m (327 μs/ft) Decayed wood: 1574 μs/m (480 μs/ft)

Source: Ross *et al.* (2004).



5.3 Relationship between transverse stress wave transmission time and moisture content.

Table 5.3 Stress wave transmission time adjustment factors for temperature at various moisture contents for Douglas fir

Moisture content (%)	Adjustment factors			
	–18 °C (0 °F)	3 °C (38 °F)	27 °C (80 °F)	49 °C (120 °F)
1.8	0.94	0.95	0.97	0.98
3.9	0.95	0.96	0.98	0.99
7.2	0.96	0.98	1.00	1.01
12.8	0.97	0.99	1.00	1.01
16.5	0.99	1.01	1.03	1.05
23.7	1.05	1.07	1.09	1.14
27.2	1.07	1.10	1.12	1.17

time decreases with decreasing moisture content. Corrections for various moisture content values are summarized in Table 5.3. At moisture content values greater than approximately 30%, little or no change in transmission time occurs. Consequently, there is no need to adjust the measured values for wood that is tested in a wet condition.

5.3.4 Effect of preservative treatment

Treatment with waterborne salts has almost no effect on stress wave transmission time. Treatment with oil-borne preservatives increases transmission time by about 40% over that of untreated wood. Round poles are usually penetrated to about 37–61 mm (1.5–2.5 inches), except at their ends, where the treatment fully penetrates the wood. Table 5.4 was calculated to show expected travel time for round poles treated with oil-borne preservatives. Although these data illustrate the effect oil-borne treatments have on transmission time, these values should not be used to estimate the level of penetration.

5.3.5 Measurement of stress wave transmission time

Several techniques can be used to measure stress wave transmission time in wood structural members. The most common technique utilizes simple time-of-flight measurement systems. With these systems, a mechanical or ultrasonic impact is used to impart a wave into the member. Piezoelectric sensors are placed at two points on the member and are used to detect passing of the wave. The time required for the wave to travel between

Table 5.4 Stress wave transmission times for round poles treated with oil-borne preservatives

Pole diameter	Stress wave transmission time (μs) for various levels of penetration		
(mm)	37 mm	61 mm	Full penetration
294	222	240	300
343	254	271	350
392	286	305	400
441	321	338	450
490	350	370	500
539	386	403	550
588	422	436	600

sensors is then measured. The commercial equipment options available for stress wave measurements are shown in Table 5.5. Field use of equipment should be conducted in accordance with the instructions provided by equipment manufacturers.

5.3.6 Field considerations

Before venturing into the field, it is useful to estimate stress wave transmission time for the size of the members to be inspected. Preceding sections provided information on various factors that affect transmission time in wood. This information can be reflected in a baseline transmission time of 1300 μs/m (400 μs/ft). Transmission time, on a per length basis, less than this value would indicate sound material. Conversely, transmission time greater than this value would indicate potentially degraded material. Using this value, one can estimate the transmission time for a member by knowing its thickness (path length) and the following formula:

$$T_{\text{baseline}}(\mu s) = 1300 \times \text{WTD}$$

where T_{baseline} is baseline transmission time (μs), and WTD is wave transmission distance (path length) (m). By knowing this number for various thicknesses, field work can proceed rapidly.

The baseline values provided here serve as a starting point in the inspection. It is important to conduct the test at several points at various distances from the suspect area. In a sound member, little deviation is observed in transmission times. If a significant difference in values is observed, the member should be considered suspect.

In the field, extra batteries, cables, and sensors are helpful. Testing should

Table 5.5 Commercial equipment for measuring stress wave transmission time in wood structural members

Name	Manufacturer	Method of wave generation	Contact information
Metriguard Model 239A Stress Wave Timer	Metriguard, Inc.	Impact	Metriguard, Inc. PO Box 399, Pullman, WA 99163, USA www.metriguard.com
FAKOPP Microsecond Meter	FAKOPP Enterprise	Impact	FAKOPP Enterprise H-9423 Agfalva, Fenyo Str. 26, Hungary www.fakopp.com
Electronic Hammer	IML, Inc.	Impact	IML, Inc. 1275 Shiloh Road, Suite 2780, Kennesaw, GA 30144, USA www.imlusa.com
Sylvatest Duo	Concept Bois Technologie	Ultrasonic pulse generator	Concept Bois Technologie Jordils Park Ch. Des Jordils 40, CH-1025 Saint-Sulpice, Switzerland www.cbs-cbt.com
James 'V' Meter	James Instruments Inc.	Ultrasonic pulse generator	James Instruments Inc. 3727 North Kedzie Ave., Chicago, IL 60618, USA www.ndtjames.com

be conducted in areas of the member that are highly susceptible to degrading, especially in the vicinity of connections and bearing points.

5.4 Cases studies

5.4.1 Timber bridges

A report by Hoyle and Rutherford (1987) describes the evaluation of wood bridges for the Washington State Department of Transportation using speed-of-sound transmission as an index of deterioration. The

previously described stress wave propagation method was used. Of 12 bridges evaluated, only one revealed signs of decay. Similarly, Aggour *et al.* (1986) used ultrasonic techniques to evaluate the residual compression strength of timber bridge piles. A good correlation was found between stress wave transmission time and the residual compressive strength.

5.4.2 USS *Constitution*

The USS *Constitution*, known as 'Old Ironsides,' is the oldest floating, commissioned ship in the world and still a part of the US Navy. Launched on 21 October 1797, the ship was recently in dry dock. At the time of dry dock, an intensive condition assessment of the ship's timbers was conducted. Stress-wave-based techniques were utilized to assess many of the ship's timbers (Ross *et al.* 1998). All deck beams (four decks of approximately 32 beams each), various knees, the stern post, the stem keelson, and keel were examined. Baseline stress wave transmission times for sound live oak wood (the species used in original construction of the ship) were calculated for the thickness of various members. Inspection of these members after they were removed from the ship revealed that the severity of degradation corresponded to increases in transmission times.

5.4.3 TRESTLE

Another structure evaluated with stress wave propagation method was TRESTLE, located at Kirkland Air Force Base, New Mexico. Constructed between July 1976 and February 1979, TRESTLE is one of the largest known glue-laminated structures in the world. It was built as a test stand for aircraft that weigh 250 000 kg (550 000 lb). It has a $15 \times 120\,m^2$ ($50 \times 394\,ft^2$) access ramp and a $61 \times 61\,m^2$ ($200 \times 200\,ft^2$) test platform, and the top surface is 36 m (118 ft) above the ground. In the early 1980s, the US Air Force wanted to test aircraft that were considerably heavier than had previously been tested, so they requested a structural evaluation of TRESTLE. One evaluation method relied upon stress wave propagation measurements. Measurements were taken both longitudinally and transversely to the length of the laminated beam. Neal (1985) and Browne and Kuchar (1985) reported that a total of 484 glulam members, representing approximately 5% of the structural members, were evaluated. They concluded that the structural framework of TRESTLE had not measurably degraded, but the exposed deck system was significantly degraded.

5.5 Future research and development

Several non-destructive inspection methods discussed here, such as sounding, resistance drilling, and stress wave propagation, offer great potential as means of locating internal decay in wood structures. However, the sensitivity of these methods to the detection and quantification of incipient decay is relatively low. Future research should be directed to improve the precision and sensitivity of existing NDE methods and also develop new technologies that are capable of detecting wood decay at the earliest possible stage when remedial treatments are most effective. Recently, several European universities have developed computer-aided tomography scanners for wood poles. The scanners move up or down a pole and provide an image of internal wood conditions. Prototypes of these devices are in the early stages of development, and further refinements are necessary to speed up the process of data evaluation.

Current inspection methods for wood structures are limited to evaluating each structural member individually, which is a labor-intensive, time-consuming process. A more efficient strategy would be to evaluate structure systems or subsystems in terms of their overall performance and serviceability. From this perspective, examining the dynamic response of a structural system might provide an alternative way to gain insight to the ongoing performance of the system. Deterioration caused by any organism or any type of physical damage to the structure reduces the strength and stiffness of the materials and thus could affect the dynamic behavior of the system. Research is currently being conducted at USDA Forest Products Laboratory and other research institutions to investigate the effectiveness of global dynamic testing methods for identifying deteriorated wood structures (Ross *et al.* 2002).

5.6 Conclusions

This chapter has reviewed current inspection techniques for decay detection and provided guidelines on the use of various NDE methods in locating and defining areas of decay within wood structural members. Visual inspection and probing techniques are commonly used for locating exterior deterioration of wood members. When suspect decay areas are located by these methods, further investigation by coring or drilling is suggested to confirm and define the extent of damage. Internal decay of wood structural members can be detected by a variety of means. Among the most effective and cost-efficient techniques for field applications are coring, resistance drilling, and stress wave propagation method. But the sensitivity of these methods to detection and quantification of early stage of decay is limited. New technologies are yet to be developed

for more efficiently identifying deteriorated wood structures and detecting incipient decay in individual structural members before significant strength loss occurs.

5.7 References

Aggour, M.S., Hachichi, A. and Meyer, M.A. (1986), 'Nondestructive evaluation of timber bridge piles', in: *Proceedings of the American Society of Civil Engineers Structural Congress. Special publication on evaluation and upgrading of wood structures, Structural Congress' 86*, 15–18 September, New Orleans, LA. New York: American Society of Civil Engineers: 82–95.

Browne, C.M. and Kuchar, W.E. (1985), 'Determination of material properties for structural evaluation of TRESTLE', in: *Proceedings, 5th International Nondestructive Testing of Wood Symposium*, 9–11 September, Pullman, WA. Pullman, WA: Washington State University: 361–384.

Hoyle, R.J. and Rutherford, P.S. (1987), 'Stress wave inspection of bridge timbers and decking', Final report for research project Y-3400, Pullman, WA: Department of Civil and Environmental Engineering, Washington State University.

Neal, D.W. (1985), 'Establishment of elastic properties for in-place timber structures', in: *Proceedings, 5th International Nondestructive Testing of Wood Symposium*, 9–11 September, Pullman, WA. Pullman, WA: Washington State University: 353–359.

Pellerin, R.F. and Ross, R.J. (2003), *Nondestructive Evaluation of Wood*, Madison, Wisconsin: Forest Products Society.

Ross, R.J., Soltis, L.A. and Otton, P. (1998), 'Assessing wood members in the USS Constitution using nondestructive evaluation methods,' *APT Bulletin, The Journal of Preservation Technology*, **XXIX** (2), 21–25.

Ross, R.J., Wang, X., Hunt, M.O. and Soltis, L.A. (2002), 'Transverse vibration technique to identify deteriorated wood floor systems,' *Experimental Techniques*, **July/August**, 28–30.

Ross, R.J., Brashaw, B.K., Wang, X., White, R.H. and Pellerin, R.F. (2004), *Wood and Timber Condition Assessment Manual*, Madison, Wisconsin: Forest Products Society.

6

Testing timber pile length in bridges

A.K. PANDEY
EDM International Inc. and
R.W. ANTHONY
Anthony & Associates Inc., USA

6.1 Introduction

During the late 1980s, attention in the USA was directed toward bridge failures due to scour. Recognizing the need to uniformly evaluate bridge scour, the Federal Highway Administration (FHWA) published a Technical Advisory on the scour of bridges (Federal Highway Administration, 1988). This Technical Advisory was used to address the effects of bridge scour in the design process and inspection of existing structures within the National Bridge Inspection Standards Program. In 1991 it was apparent that scour calculations could not be conducted adequately on bridges with unknown foundations. A lack of available technology for determining unknown foundations, including timber piles, resulted in a change in FHWA procedures (Federal Highway Administration, 2001). A review by the FHWA of European practices revealed that scour was as significant in the UK as it was in the USA and similar problems were found in Germany and Switzerland (Federal Highway Administration, 1998).

Knowledge of pile length is a vital component in calculating the scour resistance of a bridge. However, records of timber pile lengths may, in many cases, be non-existent or incomplete owing to construction practices for timber piles. Piles are typically driven until they reach a predetermined resistance, and then trimmed at the end to provide a solid, level surface for substructure construction. Records that specify initial pile length, depth of driven pile or length of pile trim are often not available, especially in older structures. Thus, it is difficult to obtain timber pile length data for scour evaluations.

6.2 Background

Limited research has been conducted on evaluating the length of embedded timber piles. Davis (1994) described use of sonic echo and parallel seismic methods for estimating pile length. The sonic echo method is based on

impacting the head of the pile and measuring the time for the reflected stress wave to reach an accelerometer, also mounted on the head of the pile. Davis reported several difficulties using this method when a structure is resting on the pile: (a) damping of the stress wave and multiple reflected waves made determination of the echo from the pile tip difficult; (b) attaching the accelerometer to the side of the pile was difficult; and (c) delivering a direct impact to the side of the pile was difficult.

The parallel seismic method used by Davis (1994) avoids the difficulty of not having access to the head of the pile. An access hole is drilled in the ground parallel to the pile, lined with a plastic tube, and filled with water. The water acts as a couplant for a transducer (typically a geophone or hydrophone) submerged in the tube to detect the transit time of impacts delivered near the top of the pile. By lowering the transducer at known increments it is possible to determine the length of the pile from a plot of transducer depth versus transit time. Cost is a primary limitation to conducting the parallel seismic test on timer piles. The parallel seismic method has achieved acceptance for concrete structures and a modified sonic echo technique (termed ultraseismic) also shows promise for higher-value structures (Jalinoos and Olson, 1996).

Douglas and Holt (1993) used analysis of bending waves in timber piles to estimate length. A signal processing technique, termed the short kernal method, was developed to allow for processing of dispersive bending waves. Dispersive waves have frequency components that travel at different velocities and, therefore, render signal processing more difficult, particularly when dealing with unknown geometries. Nonetheless, these researchers were able to evaluate lengths of 26 piles with reported accuracies of approximately ±10%.

Research on timber poles and piles (Anthony and Phillips, 1989; Anthony *et al.*, 1992) resulted in non-destructive evaluation (NDE) techniques based on longitudinal stress wave propagation that provided the means to evaluate the length of timber piles. To adapt the technology for pile length determination, modifications to existing impact methods and sensor attachments were necessary, coupled with further testing on piles of known lengths. Field testing of the technique was conducted to identify the accuracy, limitations, and the means of applying the pile length determination technology. Details of this development were provided in the report to the Timber Bridge Information Resource Center (Engineering Data Management, 1992).

Work at the Tennessee Technological University (TTU), funded by the Tennessee Department of Transportation, has led to the development of field equipment for the measurement of pile lengths. This work began with the analysis of acoustic signals sent through aluminum piles,

a homogeneous medium. The signals were generated using an actuator at one end, and recorded with an accelerometer at the other. Theoretical models using this system were developed, and accurately predicted length (by ±5%). The theoretical models were then further advanced to cover homogeneous piles embedded in soil and surrounded by water (Darvennes and Pardue, 2001), and to cover non-homogeneous piles constructed of wood (Pardue and Houghton, 1998). No tests were conducted on *in-situ* timber piles.

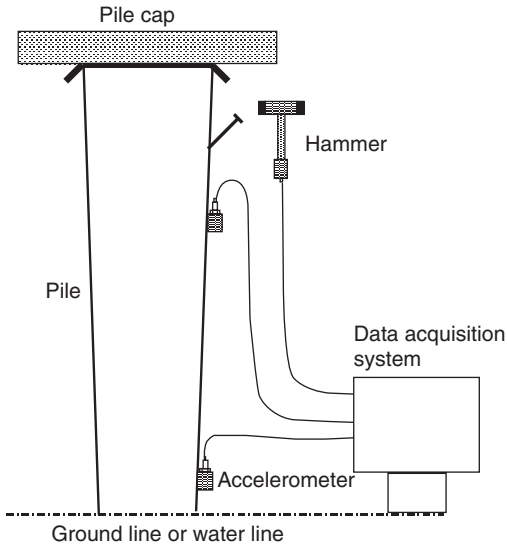
The field equipment developed at TTU has been in the process of improvement (Pardue *et al.*, 1999). The current equipment is developed to measure the velocity of stress waves moving through the piles and the natural frequency of the pile. The natural frequencies of timber piles are then used to determine the frequency response function of each pile by autocorrelation. Pile length is calculated from the combination of wave velocity and the frequency response function. In addition to pile length, there are indications that this technique can be used to determine the presence and location of flaws in piles (Henderson *et al.*, submitted). The most pressing problem identified by Henderson with the development of this technique for *in-situ* applications is the placement of the actuator and accelerometer; the same problem noted by Davis (1994) and Anthony *et al.* (1992).

6.3 Use of longitudinal stress waves

6.3.1 Basis of pile length determination

Stress waves, produced from a hammer impact, travel along the length of a pile and are reflected at boundaries until dissipation of the impact energy. The stress waves travel at a velocity that is dependent on the timber pile density, moisture content and material quality. Pile length can be evaluated by measuring the reflection time required for the stress wave to travel down to the base of the pile and return. The reflection time is related to the resonant frequency of the pile. The measurement of resonant frequency or reflection time and stress wave velocity enable the calculation of pile length.

By inducing a stress wave in the pile with a hammer and measuring the resulting echoes with sensors attached to the pile, a computerized data acquisition system can collect and process the information to determine pile length. The three components of the data collection process are the excitation source for inducing the stress wave, sensors for measuring the pile response and a data acquisition system for recording and processing the stress wave data. Figure 6.1 provides an illustration of the equipment and the setup for collecting data for determining pile length.



6.1 Hammer impact and sensor locations on a typical pile.

6.3.2 Excitation

To excitate the pile, a stress wave of sufficient energy must travel the length of the pile and back. It is crucial for the determination of pile length that the induced stress wave is aligned primarily along the longitudinal axis of the pile, avoiding transverse excitation of the pile as much as possible. The impact must occur below the pile cap through an attachment on the side of the pile since the end of the pile is generally not accessible. The attachment must be positioned such that the operator can easily swing a hammer without the interference of the bridge deck stringers or other components near the pile cap. Further, the attachment must be simple to install and not result in any damage that would decrease the service life of the pile.

A lag screw mounted at an angle of less than 45° from the longitudinal axis produces adequate stress waves for pile length determination. Best results are obtained with a 19 mm × 200 mm (0.75 inch × 8 inch) lag screw. This larger screw is necessary to prevent driving the screw into the pile when delivering the impacts. Installation of the lag screw is simple; a small pilot hole is drilled, then the lag screw is mounted with an electric impact wrench. Installation time is approximately three minutes.

Studies were conducted to determine the effect of lag screw placement along the length of the pile. The best results were obtained by placing the lag screw as near to the pile cap as possible. Placement of the lag screw

away from the pile cap created multidirectional stress waves at the impact point, making the interpretation of the sensor information difficult. Other impact methods, such as striking the top of the bridge deck directly above the pile cap with a sledge hammer, showed less success than the lag screw at the top of the pile. Less energy was transferred to the pile through the deck compared with the lag screw. Although this impact method was not preferable, it may be required when the amount of pile exposed below the cap is too small to swing a hammer.

Several types of impact hammers were investigated, ranging from a common construction hammer to a modally tuned, instrumented hammer. Various hammer tips, from soft to hard, were examined to produce stress waves with minimal attenuation. Harder tips were found to produce high-energy signals at higher frequencies. High-energy impacts were found to cause distortion of the sensor signal because of the electronic limitations of the sensor. Softer tips, on the other hand, produced lower energy signals at lower frequencies which attenuated quickly. A 1.4 kg (3 lb) modally tuned sledge hammer with a medium density plastic tip provided the best combination of signal energy with minimal signal attenuation.

6.3.3 Sensors and attachment methods

A piezoelectric quartz accelerometer was chosen to measure pile response to an impact because of its high sensitivity over a broad range of frequencies. Shorter piles will generally have a higher resonant frequency than longer piles of similar quality. The accelerometer provided the flexibility to measure the stress wave response of varying pile lengths with equal sensitivity.

Attachment of the accelerometer to the pile is critical to establish good transfer of stress wave energy from the pile to the side-mounted sensor. Poor attachment methods result in unrepeatable, low-energy measurements which give inconsistent pile length estimates. The attachment method must be quick and simple to avoid prolonged set-up times. Two attachment devices, a steel pin and a sheet metal screw attached to a metal block, were investigated.

The steel pin was the simpler of the two attachments. Initial studies showed that the steel pin tended to loosen over time, causing poor transfer of stress wave information. As a result, the wave reflections from the pile tip measured by the sensor were not as detectable as with the sheet metal screw attachment. Because the waves reflected from the tip of the pile are low energy and critical to the determination of pile length, the sheet metal screw attached to an aluminum block was chosen as the appropriate sensor attachment for this project. The metal screw is easy to install and remove, requiring only a cordless drill.

A lag screw for delivering the hammer impact and three sensors are attached to the pile to collect all the necessary non-destructive information to estimate pile length. Two sensors, aligned with each other along the axis of the pile and a fixed distance apart below the impact point, are used to measure the transit time between each other to obtain a stress wave velocity. The third sensor, not seen in Fig. 6.1, is attached to the pile to measure the resonant frequency of the pile or reflection time for the stress wave to travel to the base of the pile and return. This sensor is placed near the pile cap opposite the hammer impact.

6.3.4 Data acquisition system

The hammer impact and pile response from the two sensors are recorded using a field-rugged data acquisition system. The data acquisition system consists of the hardware and software needed for collecting and storing the stress wave data. Post-processing of the data is required to determine pile length.

6.4 Pile length determination

6.4.1 Stress wave relationships

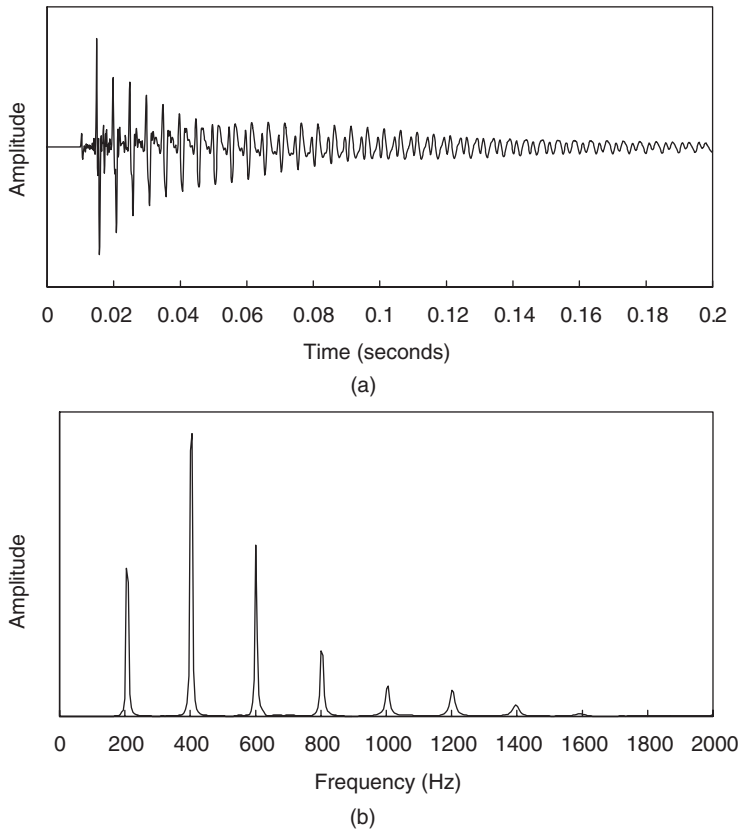
Stress waves induced from the hammer impact travel through the pile and are reflected at the ends of the pile. From the information recorded by the two sensors, located a fixed distance apart, an estimate of stress wave velocity (V) is obtained. Total pile length, L_t, is calculated from stress wave velocity and the reflection time. Reflection time (T) is the time taken for the stress wave to travel from the impact point to the bottom of the pile and back. Thus, pile length can be obtained through the following relationship:

$$L_t = \frac{(\beta * V * T)}{2} \qquad [6.1]$$

where β is a velocity adjustment factor.

The resonant frequency (F) of the pile is the inverse of the reflection time required for the stress wave to travel twice the length of the pile. The resonant frequency of a pile is related to pile length and stress wave velocity. Thus, the length of the pile can also be estimated using the resonant frequency of the pile:

$$L_t = \frac{(\beta * V)}{(2 * F)} \qquad [6.2]$$

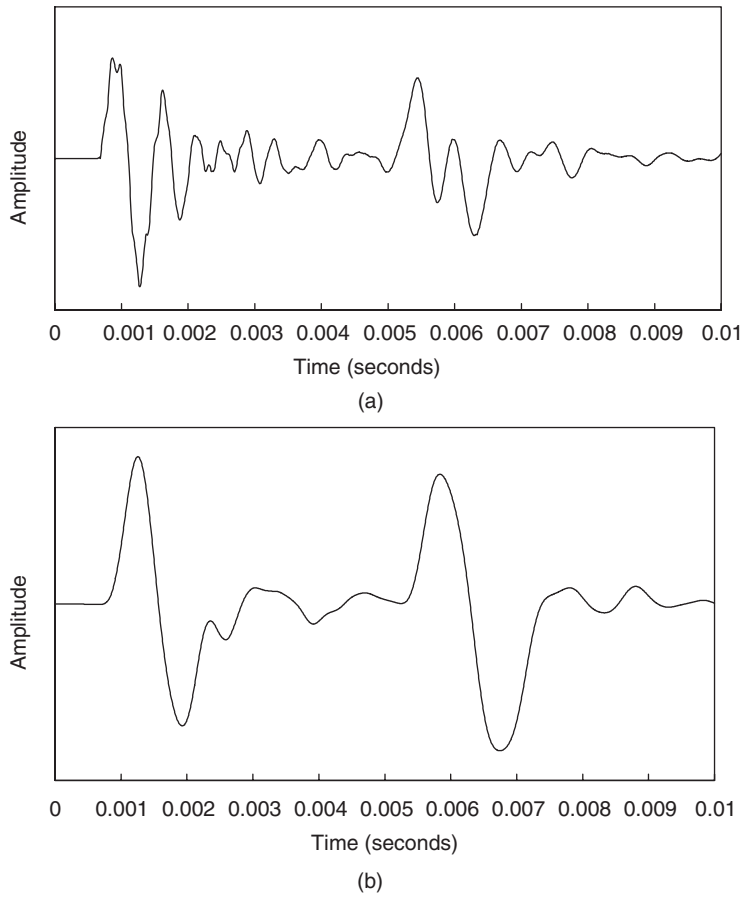


6.2 Time-domain (a) and frequency-domain (b) representation of data collected on a 12 m (40 ft) pile before driving.

Previous studies (Sansalone and Carino, 1986) have shown the resonant frequency to be a factor of 0.9 times the inverse of the reflection time, for materials such as concrete. A velocity adjustment factor, β, of 0.9 worked well in estimating length of timber piles as well. Pile length can be measured by knowing stress wave velocity and reflection time or resonant frequency.

6.4.2 Estimation of reflection time

The sensor data collected by the data acquisition system recorded a time record as shown in Fig. 6.2(a) on a pile before driving. Note the echoes that occur as the stress wave returns to the butt of the pile after reflecting off the tip. The time between echoes is the reflection time of the stress wave.



6.3 Time-domain (a) and filtered time-domain (b) representation of data collected on a 12 m (40 ft) pile before driving.

Figure 6.3(a) shows the time-domain representation of the stress wave for a 12 m (40 ft) pile described above. In Fig. 6.3, only a small portion from the beginning of the signal from Fig. 6.2(a) is shown. Using filtering techniques, the time-domain representation of Fig. 6.3(a) can be transformed into a much cleaner time domain representation as shown in Fig. 6.3(b).

The filtered time-domain representation clearly identifies the onset of the stress wave and the arrival of the stress wave reflection from the tip of the pile. Measurement of the time between these two events provides an accurate estimate of the reflection time. This reflection time represents the time for the stress wave to travel from the location of the accelerometer to the tip and back. For this 12 m pile, the reflection time is 0.004 585 s for an accelerometer mounted 1.2 m from the butt.

6.4.3 Resonant frequency determination

The time record shown in Fig. 6.2(a) can be transformed into a frequency representation through a fast fourier transform (FFT). The FFT produces a frequency record that represents the amount of energy at each of the frequencies contained within the signal. The frequency record reveals information about the resonant frequency of the pile and its harmonic content. Figure 6.2(b) illustrates a frequency record for a pile with a resonant frequency of 200 Hz and harmonics at 400, 600, and 800 Hz. The interval spacing between harmonics reveals the resonant frequency of the pile. For example, Fig. 6.2(b) represents a pile 12 m in length with a resonant frequency of 200 Hz.

The locations of the impact and sensor attachments are designed to maximize the harmonic content of the signal to facilitate measurement of the resonant frequency of the pile. The soil surrounding the pile, the high water content of the wood and soundness of the wood itself can significantly alter the time and frequency representation of the signal. A shift in the frequencies with similar spacing is due to the presence of soil at the bearing tip; the broadening of the peaks is due to the dampening of the signal by the surrounding soil, resulting in fewer echoes.

Degradation of a pile at the water line will also affect the signal. The harmonic content of the signal becomes inconsistent and may indicate the presence of decay at the water line, although this cannot be verified using this method because the actual pile length is unknown. Decay and other environmental factors such as soil pressure and moisture can influence the harmonic content of the signal.

6.4.4 Factors affecting the determination of resonant frequency and reflection time

One of the effects of water in wood is that it reduces the velocity of the stress wave. A typical timber pile contains three zones of water content: a dry zone above the water or soil line up to the pile cap; a transition zone at the water line where the wood contains an increasing amount of water; and finally a saturated zone which is the buried or below-water-line portion of the pile. Because the velocity of the stress wave affects the resonant frequency, the equation for pile length can account for the differing velocities in the pile by defining ‘wet’ and ‘dry’ velocities of the pile. The dry velocity of the pile is measured by the transit time between two sensors and the wet velocity is estimated because it cannot be measured easily. Wet velocity is estimated to be 90% of the calculated dry velocity.

To include the effects of wet and dry velocity into equation 6.2, an assumption must be stated. This assumption is that the resonant frequency

of the pile is a product of stress waves traveling at a collective velocity, which is weighted by the amount of the pile that is dry compared with that which is wet. By defining a dry velocity V_d and wet velocity V_w, the weighted average velocity V_a can be expressed as:

$$V_a = \left(\frac{L_d}{L_t} * V_d\right) + \left(\frac{L_w}{L_t} * V_w\right) \quad [6.3]$$

where L_d is the length of pile containing dry wood, L_w is the length of pile containing wet wood, and L_t is the total length of pile. Unfortunately, the length of pile buried or under water (L_w) is unknown. The relationship:

$$L_t - L_d = L_w \quad [6.4]$$

can be substituted into equation 6.3.

Equation 6.2, modified by equations 6.3 and 6.4 for the moisture profile in the wood simplifies to:

$$L_t = L_d + \left(\frac{(\beta * V_w)}{(2 * F)}\right) - \left(\frac{V_w}{V_d} * L_d\right) \quad [6.5]$$

6.5 Case studies

6.5.1 Verification of pile length technique

A total of 33 piles from different bridge sites in the USA were initially selected for equipment evaluation and verification testing of the pile-length technique. The bridge sites were in four different states. Table 6.1 lists the number of piles tested, the age, and condition of the piles for the different sites. The Colorado piles were used during the initial stages of the project to evaluate multiple sensor configurations and hammer impact methods. The Louisiana, Tennessee, and Minnesota bridge sites each contained piles of various lengths that had been recorded during construction. The piles were evaluated by the stress wave technique, and then compared with construction records for verification of length.

Pile lengths from Colorado and Louisiana were estimated using only the resonant frequency method whereas piles from Tennessee and Minnesota were evaluated using both the resonant frequency method and the reflection time method described above.

The advantage of using both the resonant frequency and the reflection time is that it is possible to evaluate and predict lengths for a greater percentage of piles tested. There are some piles for which an estimate of the length cannot be obtained using resonant frequency because of difficulties in interpreting the frequency record. In many such cases, it is possible

Table 6.1 Sites for equipment evaluation and verification testing

Location of test site	Number of piles	Age of piles (yr)	Condition of piles
Colorado	13	46 to 59	Decayed to good
Louisiana	9	0 or unknown	Good to new
Tennessee	7	0	New
Minnesota	4	Unknown	Good

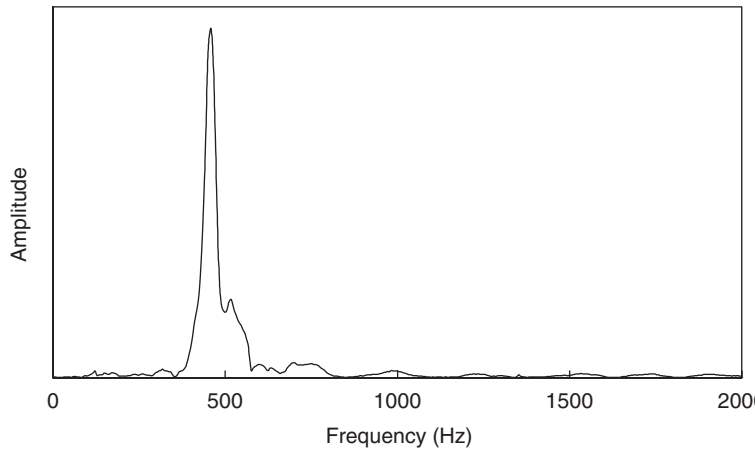
to obtain an estimate of the length using the reflection time. In general, the reflection time method provides a more accurate estimate for the length of piles.

As an example, a frequency record that is difficult to interpret is shown in Fig. 6.4. This frequency record has only one dominant peak (at approximately 500 Hz). It is difficult to obtain an estimate of the resonant frequency from a single peak because spacing between peaks is used as a measure of the resonant frequency. For the same pile, a time domain record of the stress wave and its representation after filtering are shown in Fig. 6.5. From Fig. 6.5(b), an estimate of the reflection time is obtained as the time between the two marked points. Using reflection time, the length of this pile was estimated to be 9.1 m (30 ft). The actual length, obtained from the construction records, is 9.4 m (31 ft).

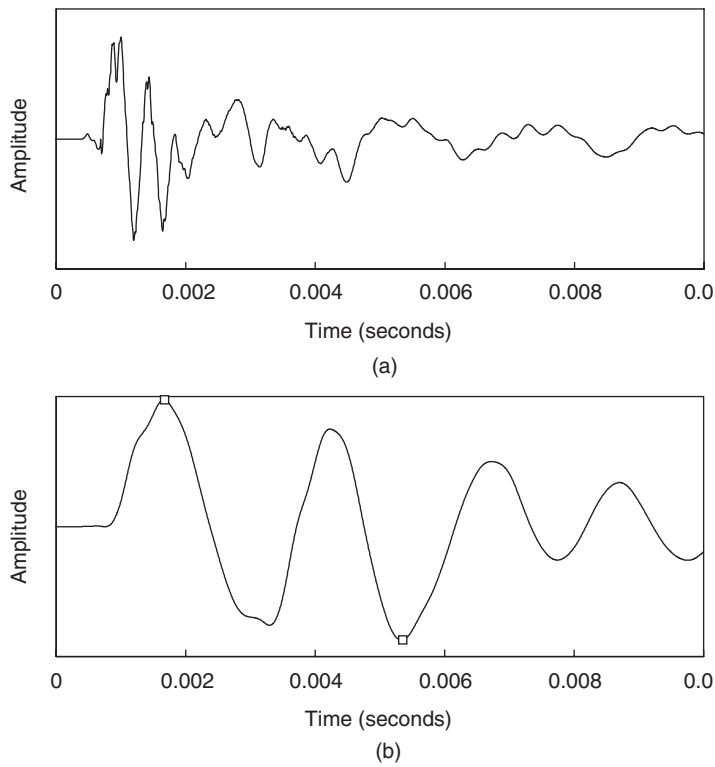
Figure 6.6 depicts the relationship between the actual and estimated pile length for the 33 piles in Table 6.1. Points on the figure marked with a filled circle represent the piles from Tennessee and Minnesota. These piles were evaluated using both resonant frequency and reflection time. As shown in Fig. 6.6, the range of pile length estimates in the verification study falls within ±15% of the actual pile length as defined by the two lines. For cases requiring conservative length estimates, pile length can be adjusted by reducing the estimated length up to 15%.

6.5.2 Clallam County bridge testing

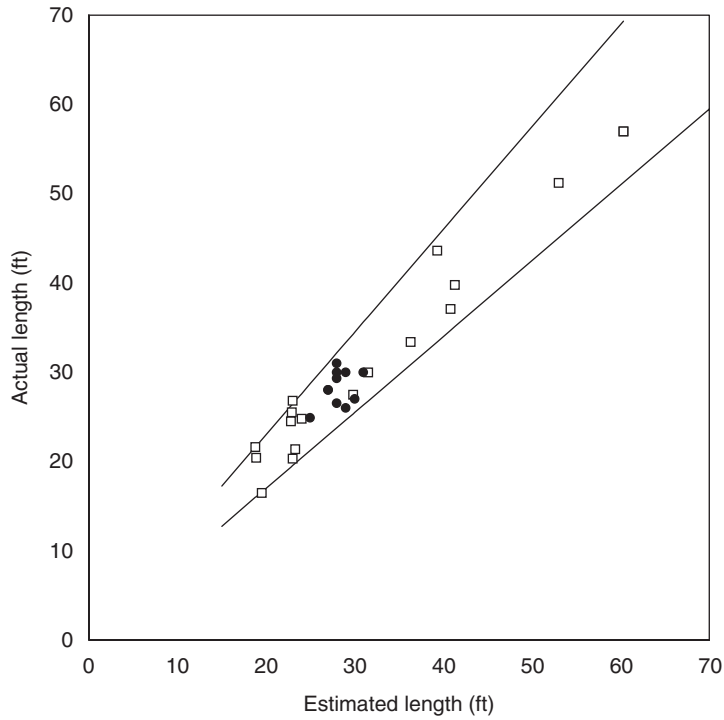
The Clallam County Road Department, located in Washington State, USA, needed to inspect timber piles from 10 bridges as outlined in Table 6.2 and described in detail in Pandey *et al.* (1998). Pile length was determined on all accessible piles listed using longitudinal stress wave analysis. Piles that could not be inspected by wading or had insufficient headroom for conducting tests were considered inaccessible. Pile condition was determined using the longitudinal stress wave data (on piles where length was evaluated) and visual inspection with NDE on accessible sections of the piles above water



6.4 Frequency record for a 9 m (30 ft) pile.



6.5 Time-domain (a) and filtered time-domain (b) representation of data for a 9 m (30 ft) pile.



6.6 Plot of actual and estimated pile lengths for 33 piles of known length in Table 6.1. (1 foot = 0.3048 m.)

Table 6.2 Accessibility and type of inspection performed on the 10 bridges in Clallam County

	Bridge	Structure number	Number of piles	Type of inspection[a]	Accessibility[b]
1	Trout Creek	91460BR4	16	1 & 2	A
2	Charley Creek	18670BR1	12	1 & 2	A
3	Weel	18760BR1	26	1 & 2	B
4	Lower Lake Creek	15610BR1	20	1 & 2	B
5	Salt Creek	22990BR1	32	2	B
6	Dry Creek	93110BR1	18	1 & 2	C
7	Meadowbrook (S)	95250BR2	10	1 & 2	D
8	Meadowbrook (M)	95250BR3	10	1 & 2	D
9	Meadowbrook (N)	95250BR4	10	1 & 2	A
10	Jimmycomelately	56830BR1	10	1 & 2	A

[a] 1, determine pile length; 2, determine pile condition.
[b] A, all piles are fully accessible; B, some piles may not be accessible by wading; C, piles are fully accessible but headroom is limited; D, piles are fully accessible but headroom is limited, and knee-deep mud hinders mobility.

line. For piles where length evaluation was not required, only visual inspection and NDE above water line were used.

Piles in the 10 bridges were first inspected using Sylvatest to identify regions suspected of having decay. Sylvatest measures wave propagation speed. Resistance drilling was done where Sylvatest readings indicated the possibility of voids or decay. Resistance drilling provides a printout of the relative resistance of a pile as a small-diameter needle penetrates the wood.

Although, in general, visual inspection was unable to determine whether the piles were decayed, the piles did exhibit various degrees of degradation when inspected using the NDE technologies. Four of the bridges, Charlie Creek, Salt Creek, Dry Creek and Meadowbrook (South), exhibited no decay in the piles inspected. Evidence of incipient decay was detected at the center and at the top of one pile from the Meadowbrook (Middle) bridge. Intermediate decay was detected in two of the piles from the Weel bridge and one pile from the Meadowbrook (North) bridge. Advanced decay was found in one pile from the Meadowbrook (North) bridge, one pile from the Lake Creek bridge and two piles from the Trout Creek bridge.

In addition to the decay investigation, longitudinal stress wave data collected in the field were processed and analyzed to determine pile length. Pile length was estimated using both time domain and frequency domain methods. From the predicted lengths for individual piles, an average length for the piles in a bent was calculated. The individual pile lengths and the average length for piles in a bent are provided in Table 6.3.

Pile length data could not be collected on some of the inaccessible piles. The Dry Creek bridge had very limited headroom and, therefore, data could be collected only on two piles in the middle bent of the bridge. A few of the piles on the Meadowbrook (S) and the Meadowbrook (M) bridges could not be tested because of limited headroom and knee-deep mud, which hindered mobility. These bridges had piles with less than 0.6 m exposed length above ground. Limited exposed length increases the uncertainty in the stress wave velocity estimation, possibly resulting in increased error in the pile length prediction. Based on known ranges of pile length by Clallam County, even with the increased error, the predicted pile lengths appear to provide a good indication of the actual length of these piles.

6.5.3 UP Railroad Bridge, Denver, Colorado

Ten piles from a Union Pacific Railroad Bridge in Denver, Colorado, were tested to determine the length of timber piles. Piles were selected for evaluation to represent the range of lengths which might be expected along the length of the pier. Stress wave records were processed to determine timber

Table 6.3 Estimated pile lengths for the Clallam County bridges

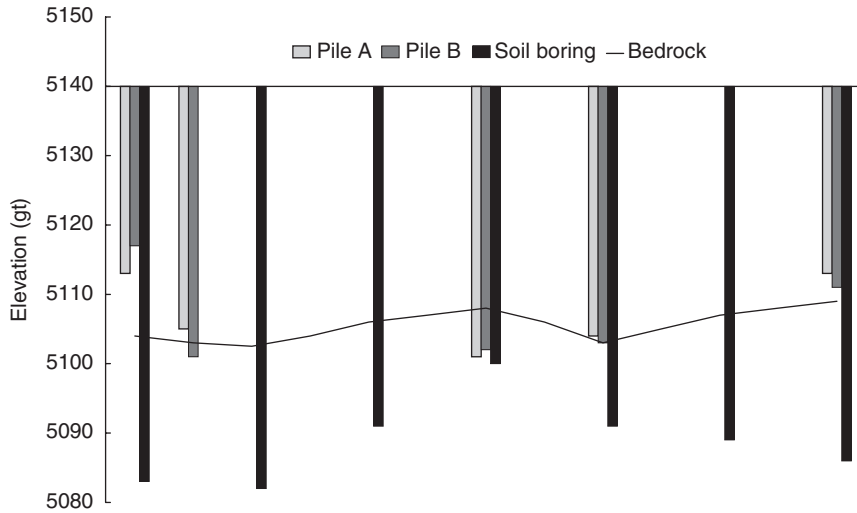
Structure no.	Bridge	Bent no.	Estimated length (ft)						Average length in bent (ft)
			Pile A	Pile B	Pile C	Pile D	Pile E	Pile F	
1	Trout Creek	1	19	24	20	A			21
		2	21	27	26	25			25
		3	23	23	21	22			22
		4	A	19	20	A			19
2	Charley Creek	1	18	19	17	20	23	21	20
		2	21	20	23	22	20	20	21
3	Weel	1	25	27	24				25
		2	25	27	29	26	28		27
		3	29	A	A	A	30		29
		4	A	A	A	31	31		31
		5	A	A	29	26	27		27
		6	23	23	24				23
4	Lower Lake Creek	1	21	20	20	22	20		21
		2	26	28	30	28	29		28
		3	22	20	24	20	22		22
		4	22	19	24	20	20		21
6	Dry Creek	2	A	A	A	A	18	20	19
7	Meadow-brook (S)	1	22	A	A	20	20		21
		2	19	17	A	A	19		18
8	Meadow-brook (M)	1	18	20	20	19	A		19
		2	19	21	20	19	17		19
9	Meadow-brook (N)	1	17	20	19	17	20		19
		2	21	19	22	18	21		20

A, pile not evaluated.

pile lengths. For this bridge, a soils company had performed borings and determined the location of bedrock underneath the bridge. This information was made available after the pile length predictions. The predicted pile lengths when compared to the bedrock information clearly showed that the piles were driven to the bedrock, as shown in Fig. 6.7.

6.6 Future research and development

A number of factors can affect the wave characteristics used to determine pile length. Decay and fractures at the mudline from excessive bending loads were found to influence the harmonic content of the frequency record. For one pile with a decayed section, the harmonic content was inconsistent. No specific information could be collected on the decayed pile because the section of interest was under water. One fender pile with severe fractures



6.7 Comparison of predicted pile lengths to bedrock location from soil boring for the UP Railroad Bridge, Denver, Colorado.

near the mud line was accurately evaluated and recommended for replacement. Damage that may occur during pile driving, such as severe bending of the pile, separation of annual growth rings near the surface and brooming or crushing of the tip were not evaluated in this project. Thus, if such conditions are encountered, the length estimate may be altered.

The estimate of the wet velocity of the wood below the water or mud line is subjective. Sandoz (1991) reported that for sound timber, the wet velocity will be approximately 90% of the dry velocity. However, the authors are aware of wet velocities of 2540 m/s (8333 ft/sec) on very saturated, older piles, which is well below the commonly known dry velocity range of 3170–5580 m/s (10 400 to 18 300 ft/sec). Misjudging the wet velocity adds to the error of the pile length estimation. The unknown wet velocity in this project may have contributed to the errors in pile length estimation.

The calculation of resonant frequency is affected by wide harmonic peaks due to the rapid attenuation of the stress waves. Wider peaks give less accurate frequency spacing compared with sharply defined harmonic peaks and add to the error in calculating resonant frequency.

A key to rapid pile length assessment is automation of the data collection and data processing operations. The ability to determine the length of a pile while in the field would make the technology more practical for bridge inspectors.

6.7 Conclusions

An NDE method now exists to evaluate the length of timber piles. The method requires post-processing of data collected in the field. Field-rugged hammer impact methods and sensor attachments are available that are simple to install and employ. The stress wave technique was proven to reliably estimate pile lengths between 6 and 18 m (20 and 60 ft) with an identified accuracy of ±15% of pile length.

It is recommended that a trained technician coordinate the data collection and personally review the frequency records of each pile at the time of testing. Comparisons should be made of pile length estimations within a single bent to minimize erroneous data. The technician should discuss with bridge maintenance personnel the local geotechnical conditions to further validate the pile length estimations. Given the recent advances in computerized data acquisition system and sensors, approximately 20 piles per day could be evaluated with a trained technician and assistant once dedicated equipment and analysis software are developed for determining pile length.

Engineers and maintenance personnel who require knowledge of pile length to evaluate the effects of scour on pile capacity will find the stress wave pile length estimation technique a unique opportunity to acquire information previously unavailable. Applied NDE technology can effectively provide the required information to make a more sound engineering decision.

6.8 References

Anthony R.W. and Phillips G.E. (1989), 'Nondestructive strength assessment of in-situ timber piles', in *Proceedings of the First International Conference on Wood Poles and Piles*, Engineering Data Management, Inc. and Colorado State University, Fort Collins, CO.

Anthony R.W., Bodig J., Phillips G.E. and Brooks R.T. (1992), *Longitudinal NDE of New Wood Utility Poles*, Report TR-100864, Electric Power Research Institute Report, Palo Alto, CA.

Darvennes C.M. and Pardue S.J. (2001) 'Boundary effect of a viscous fluid on a longitudinally vibrating bar: theory and application', *Journal of Acoustical Society of America*, **110** (1), 216–224.

Davis A.G. (1994), 'Nondestructive testing of wood piles', in *Proceedings*, *Second International Conference on Wood Poles and Piles*, 21–23 March, Fort Collins, CO.

Douglas R.A. and Holt J.D. (1993), *Determining Length of Installed Timber Pilings by Dispersive Wave Propagation Methods*, Report for the Center for Transportation Engineering Studies, North Carolina State University, Raleigh, NC.

Engineering Data Management (1992), *Determination of Timber Pile Length Using Stress Waves*, Report prepared for the Timber Bridge Initiative Special Projects Program, Timber Bridge Information Resource Center, Morgantown, WV.

Federal Highway Administration (1988), 'Technical Advisory 5140.20, Scour at Bridges', Federal Highway Administration, Washington, DC.

Federal Highway Administration (1998), 'Summary of 1998 Scanning Review of European Practice for Bridge Scour and Stream Instability Countermeasures', Federal Highway Administration, Washington, DC.

Federal Highway Administration (2001), 'Memorandum on Revision of Coding Guide, Item 113 – Scour Critical Bridges', Federal Highway Administration, Washington, DC.

Henderson R.C., Pardue S., Ariam A., Rossillon, J.A. and Chambers J.P. (submitted), 'Determining the length of wooden bridge piles using random vibration excitation', *Journal of Performance of Constructed Facilities*, ASCE.

Jalinoos F. and Olson L.D. (1996), 'Determination of unknown bridge foundations using nondestructive testing methods', in *Proceedings*, *the Structural Materials Technology – An NDT Conference*, 20–23 February, 1996 San Diego, CA.

Pandey A.K., Tyler, R., Arnette, C.G. and Anthony, R.W. (1998), 'Assessment of Timber Piles in Clallam County, Washington', in *Proceedings of Structural Materials Technology Conference*, San Antonio, TX.

Pardue S.J. and Houghton J.R. (1998), 'Wave speed: the key to insitu wooden pile length assessment', in *16th International Model Analysis Conference Proceedings*, Society for Experimental Mechanics, Bethel, Connecticut, 1560–1566.

Pardue S.J., Houghton, J.R. and Renfro, M. (1999), 'Experiences with in-situ bridge wooden pile length measurement using random vibration', Transportation Research Board, 78th Annual Meeting, Washington, DC, January.

Sansalone M. and Carino N. (1986), *Impact-Echo: A Method for Flaw Detection in Concrete Using Transient Stress Waves*, US Dept. of Commerce, National Bureau of Standards, Report, NBSIR 86–3452, Gaithersburg, MD, 137.

Sandoz J.L. (1991), 'Nondestructive evaluation of building timber by ultrasound', in *Proceedings of the Eighth International Nondestructive Testing of Wood Symposium*, Washington State University, Pullman, WA.

7

Ultrasonic testing of structural timber components

T.L. SHAJI
College of Engineering – Trivandrum, India

7.1 Introduction

Wood is one of the oldest building materials and its long-term performance can be observed in buildings that are several centuries old. From ancient times wood has been used as a multipurpose material in construction and has played a continuous and significant role in the history of buildings as a primary material and often in a secondary role. It has been through the utilization of the inherent advantage of wood that major architectural traditions have been established. Early Egyptian architecture associated with the Greek step-pyramid of Sakkara (around 3900 BC) had its origin in a domestic architecture based on wood and reeds (Kemp 1982). The Greek Parthenon, representing perfection in architecture, is the epitome of the traditional system based upon the earlier timber-framed megaron house. Roman buildings were enclosed with vaults or domes with wood roof trusses. One of the most spectacular uses of timber in medieval buildings is the stone-sheathed timber spire in Salisbury cathedral, which rises to a height of 123 m (404 feet). Exquisite examples of houses, churches, commercial structures dating from the 18th century built with wood can be found along the east cost of the USA. The 160 m (530 feet) diameter Tacoma Dome built in 1982–83 in the state of Washington is both the largest wood dome structure and one of the longest clear roof spans in the world (Freas 1986). Timber has been the traditional construction material all over India since the Vedic time.

Timber building components may deteriorate due to environmental factors, neglect, lack of maintenance, improper renovation efforts and lack of understanding of material behaviour. Routine inspections of timber elements can identify potentially damaging problems. Without a proper inspection and maintenance procedure, wooden members are prone to decay, leading to member failure or structural collapse (Shaji *et al*. 1993). Visual observations should be combined with non-destructive techniques in inspection programme (Freas 1982).

This chapter presents a summary of detailed laboratory and field investigations carried out with the ultrasonic test technique for inspection and evaluation of timber elements in buildings.

7.2 Properties of wood

7.2.1 Physical properties

The main physical properties of timber, such as knots, checks and splits, density and moisture content, which affect the strength of wood are described herein. The fibres around the knots deviate from the direction of major axis thereby reducing the overall strength in bending tension and compression parallel to grain. The amount of reduction depends on the size of the knot.

Wood dries faster on its surface than in its interior. Shrinkage of the surfaces of wood results in tensile stresses across the grain that cause a fracture along the grain which resulted in the formation of checks and splits. Both the defects decrease the resistance to shear stress. Low-density wood has a larger percentage of voids than high-density wood. The density varies from 320 to 721 kg/cm^3. Denser wood is stronger and stiffer.

Wood contains moisture. Cell walls within the wood fibers are able to absorb moisture equal to about 30% of the wood by weight (the fibre saturation point). When wood dries below the fibre saturation point, the fibres begin to shrink and the dimensions are reduced (Stamm and Loughborough 1942). When the moisture content rises above the fibre saturation point, the fibres begin to swell and the dimensions are increased. Wood shrinks and swells very little in the longitudinal, more in radial, and the most in tangential direction. The transverse shrinking/swelling may range from 10% to 15% compared with 0.1% in the longitudinal direction. Cellulose has high affinity to water because of the presence of a large number of OH groups. However, water cannot enter into the cellulose crystalline regions within the microfibril. Thus the water is confined to the amorphous region on the exterior of the microfibril. Because of the long axis of the crystalline region of the microfibril, the microfibril decreases in diameter, and draws closer together when the water is removed, thus decreasing the cell wall thickness. When water is absorbed, the microfibril increases in diameter, thus increasing the cell wall volume. High-density wood shrinks more than lower-density wood. As wood dries, it also became stronger and stiffer. If wood is not exposed to rain or direct water sources, it will gather moisture content in equilibrium with the average relative humidity (Sherwood 1986).

Dry wood (below 20% moisture content) will not decay. In a few species the heartwood contains toxic extractives that impart good resistance to decay. The sapwood has very low resistance regardless of species.

7.2.2 Mechanical properties

Wood is an anisotropic material so the elastic constant and other mechanical properties may vary with the direction of grain. Small elastic deformations imposed for a period of time may return to plastic deformations. If the deformations increase, structural members may fail since there is no yielding of stress. The moduli of elasticity in tension, compression and bending of wood are approximately equal, but the elastic limit is considerably lower for compression than for tension.

The tensile strength of wood parallel to grain is extremely high and may reach a maximum of 3000 kPa/cm^2 for some species in air-dry condition (12% moisture content). The tensile strength of separated wood fibres is even higher. Wood cannot be extensively used in structures under tension. Such usage may result in crushing of ends due to shear stress to which wood is quite vulnerable. The maximum crushing strength parallel to grain is only 50% of the tensile strength along the grain. The ratio is variable and is influenced by moisture content. The compressive strength of wood along the grain increases with density.

The difference between the tensile strength and the compressive strength of wood determines the characteristic behaviour of wood in bending. Wood withstands static bending well, thus it is widely employed for elements such as trusses and rafters. Shape and size, grain angle, density and moisture content will influence the shock resistance of wood.

Wood has low shear strength along the fibres. Resistance of wood to cutting across the fibres is three to four times greater than that along the fibres, but no pure shear generally takes place, since the fibers are subjected to crushing and bending. The strength and stiffness along the grain are about 20 times greater than perpendicular to the grain. Most of the engineering materials are isotropic and for efficient utilization it is made anisotropic by fabrication of ribs, corrugations or the like. Wood is surprisingly efficient and as a material has never been replaced by any synthetic microstructural engineering (Geimer *et al*. 1974).

7.3 Wood deterioration

Timber can decay and deteriorate in service. Decay can be caused by bacteria, fungi and insects such as termite and woodborers. Most of the wood-degrading organisms require oxygen (air), proper temperature, moisture and food to survive (Degroot and Esenther 1982). Elimination of one of these factors will generally prevent decay or destruction, except by wear and fire. Bacteria and fungi require free water to grow, whereas the requirements of insects can vary from saturation to an air dry condition.

Weathering is the combined effect of heat (atmospheric temperature), light and water. The principal cause of weathering is the frequent exposure to rapid changes in moisture content (Fiest 1982). It has little influence on most of the strength properties, but some changes in physical properties are expected. In addition, changes in surface characteristics, cupping, warping and pulling away from fasteners are also attributed to weathering (Fiest 1988).

Bacterial infestation produces a marked increase in the permeability of wood. Generally the properties of wood are unaffected, except that wood may became absorptive. Wood exposed to excessive wetting, but that is not completely waterlogged (in which case oxygen is unavailable), is subject to decay from fungal attack. Practically all wood is exposed at one time or another to fungal attack (Walters 1981). Fungi can be divided into two types: stain and mould fungi and decay-causing fungi. The first causes stains and spots or molds, and the second is responsible for decay, which can be of two types: brown rot and white rot. The decay condition in which only the cellulose and associated carbohydrates are affected is brown rot (*Wood Handbook* 1987). It is characterized by brown colour, cracks across the grain and collapse of cracked pieces. In white rot, both lignin and cellulose are removed, and the wood looks white after losing its colour. The most familiar lignin-degrading fungi are the mushrooms, brackets and other saprophytes that form on decaying trees, wood and other materials (Kirk *et al*. 1992).

Decay-causing fungi can destroy the wood completely, almost totally reducing the strength and toughness after losses in mass of only 5–10% (Lyon 1982). Compared with white rot fungi, brown rot fungi cause more rapid loss of mechanical properties (Degroot and Esenther 1982). Limited test results have shown that the strength and mass losses for brown rot fungi are linearly related (Winandy and Morrell 1993).

7.4 Ultrasonic pulse velocity technique

The assessment of the condition of timber elements in service is of great importance with respect to the inspection and monitoring of timber building components. No comprehensive guideline is currently available for inspection and evaluation of timber structures. Destructive evaluation techniques are not feasible as they may affect the structural integrity.

Because of their advantage over conventional destructive testing methods, non-destructive testing methods have gained much popularity in the field of inspection and evaluation of concrete structures. A comprehensive review on non-destructive testing of wood members is given by Ross and Pellerin (1991). The writers conclude that the laboratory investigations on validating the fundamental hypothesis for establishing predictive relationship for

biologically degraded wood have been limited. Bodig and Goodman (1988) have suggested a method for the evaluation of timber by measuring the velocity of sonic stress waves. Sayal and Gulati (1979) proposed another method – measuring ultrasonic pulse velocity parallel to the grain. Acoustic emission techniques and research related to their application to wood structures are reviewed by Beall (1987). Being a biological material, wood has much inherent variability which can cause wide variation in properties among individual elements. It is very important to develop a non-destructive technique for the *in-situ* assessment of quality and strength properties of timber elements, as conventional destructive techniques are not particularly suited for on-site measurement of strength of elements in service and may weaken the structural integrity.

When an impact load is applied to any body, it produces elastic waves that propagate inside the body. Studies on wave propagation have shown that longitudinal waves (P-waves), shear waves (S-waves) and surface waves (R-waves) are the three wave modes in infinite isotropic elastic media. Of the three, P-waves are the fastest.

The ultrasonic pulse velocity technique involves determining the velocity of an ultrasonic pulse through a solid material. The pulse is generated at one side of a test object and is transmitted through the body of the object. The speed (or velocity) at which the pulse travels depends on the density and elastic properties of the material. The quality of material is related to its elastic stiffness, and hence the measurement of the ultrasonic pulse velocity can be used to assess the quality and the extent of decay, as well as some elastic properties of the material.

The ultrasonic test method employs the principles of measuring the travel velocity of ultrasonic pulses through a material medium. The pulse velocity equipment consists of an emitter (generating transducer) from which ultrasonic pulses are transmitted, receiver (or receiving transducer) where the pulses are received, and a device for indicating the time of travel from the transmitter to the receiver. The ultrasonic pulse is created by applying a rapid change of potential from a transducer placed in contact with the material so that the vibrations are transferred to the material. The vibrations travel through the material and are picked up by the receiver. The wave velocity is calculated using the time taken by the pulse to travel the measured distance between the transmitter and the receiver.

When using the equipment, the contact surfaces of transducers are covered with sufficient grease to ensure good contact. Grease is also applied to the surfaces of the test specimens where the transducers are being placed. Then the transducers are held tight to the surfaces of the specimens, and the digital display indicates the time of travel of the sonic wave to an accuracy of $\pm 0.1\,\mu s$. The pulse velocity can be determined from the following equation:

$$V_1 = L \times 10/t \quad [7.1]$$

where V_1 = pulse velocity (km/s); L = path length (cm); t = transit time (μs); and 10 = constant to adjust the unit.

7.5 Laboratory investigations

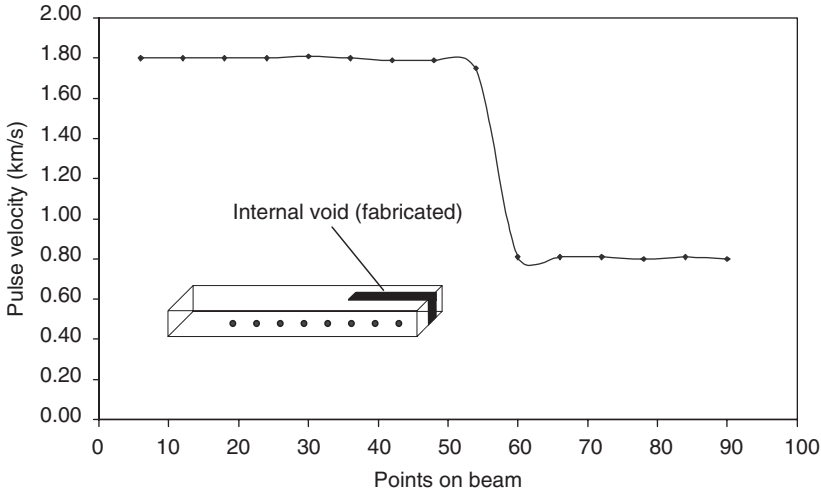
In order to assess the validity of using the ultrasonic pulse velocity to evaluate timber elements in buildings, a series of experiments were conducted to establish the pulse velocity characteristics in various species of wood (Shaji 1994). Six species of timber – *Tectona grandis* (teak; two varieties), *Atocarpus hirsutus* (aini), pine, *Magnifera indica* (mango), *Heavea brasilienisis* (rubber wood) – were selected for carrying out the experiments in the laboratory, Straight-grained clear specimens free from all defects and of size $10 \times 10 \times 45\,cm^3$ were prepared from each species.

Points 5 cm from the centres were marked and the transducers were placed for direct transmission of the pulse perpendicular to the grain of the specimen. Lubricating grease was applied on probes and the test points, and the transducers were placed at opposite points for direct transmission and reception of pulses. The time recorded in the display was recorded. Readings were taken for all sets of points marked on all the specimens. Ultrasonic pulse velocities for the clear wood specimen were calculated from equation 7.1. The average pulse velocities for the test specimens are shown in Table 7.1.

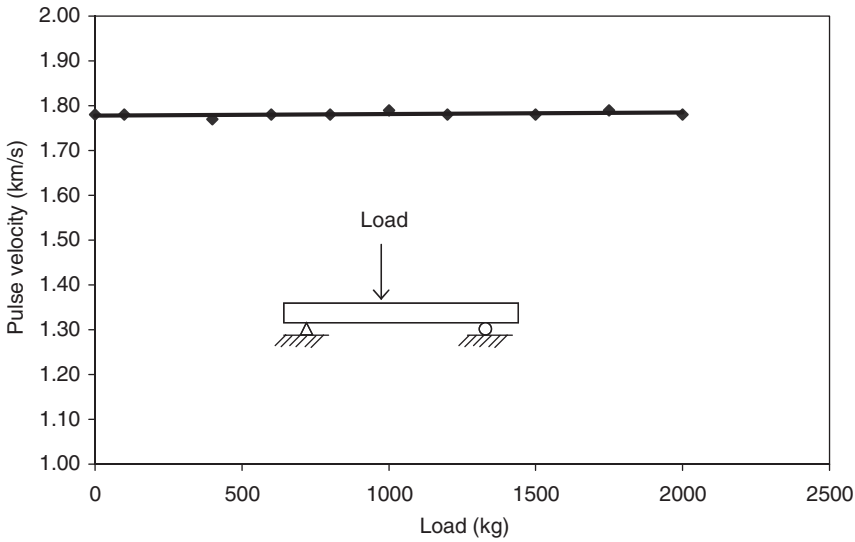
To find out the effect of the discontinuities in internal structure, and of the voids created by decay on pulse velocity, tests were carried out on about 4 m long specimens made hollow by removing, at one end, a 3 cm thick and

Table 7.1 Average ultrasonic pulse velocities for clear wood specimens

Species	Common name	Ultrasonic pulse velocity (km/s)		
		Average	Standard deviation	Coefficient of variation
Tectona grandis (old)	Teak	1.92	0.012	0.006
Pine	Pine	1.62	0.015	0.009
Artocarpus hirsutus	Aini	2.02	0.019	0.009
Tectona grandis (new)	Teak	1.85	0.005	0.002
Magnifera indica	Mango	1.52	0.014	0.009
Heavea brasiliensis	Rubber wood	1.42	0.009	0.006



7.1 Effect of void on ultrasonic pulse velocity.



7.2 Effect of load on ultrasonic pulse velocity.

60 cm long strip and measuring the pulse through its width at different points (Fig. 7.1). Structural elements in a building carry external loads and thus are subjected to stress of various magnitudes. To establish the effect, if any, of stress on pulse velocity, measurements were made in a wooden beam specimen of clear wood subjected to increasing load. Typical results for a point on beam close to the bottom fiber are shown in Fig. 7.2.

Table 7.2 Average properties of some clear wood specimens

Species	Common name	Tests			
		Moisture content (%)	Specific gravity (oven dry)	Compressive strength parallel to grain (kg/cm^2)	Compressive strength perpendicular to grain (kg/cm^2)
Tectona grandis (old)	Teak	10.99	0.65	563	186
Pine	Pine	11.08	0.56	390	120
Artocarpus hirsutus	Aini	16.60	0.90	607	216
Tectona grandis (new)	Teak	12.35	0.61	543	162
Magnifera indica	Mango	14.80	0.56	310	112
Heavea brasiliensis	Rubber wood	16.00	0.54	270	98

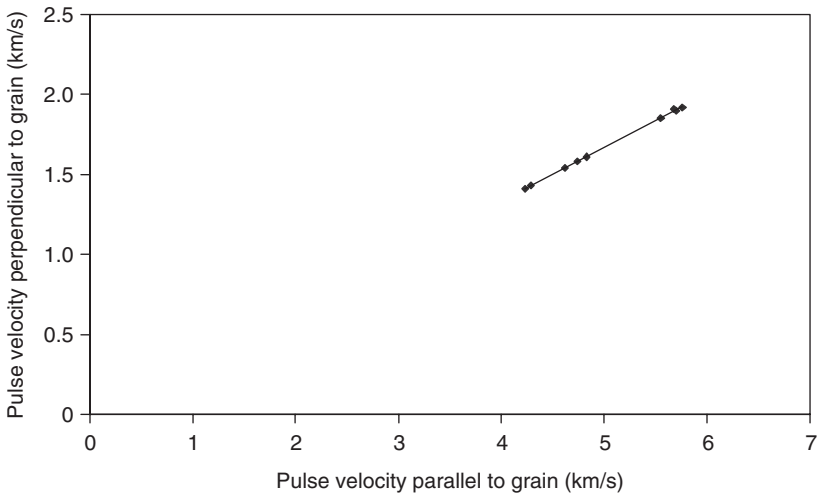
$1\,kg/cm^2 = 0.0981\,MPa$.

The laboratory investigation results indicate that the pulse velocity is independent of the applied load or the stress level. It can thus be concluded that the technique can be used to assess the extent of damage in timber elements subjected to different loading or stresses.

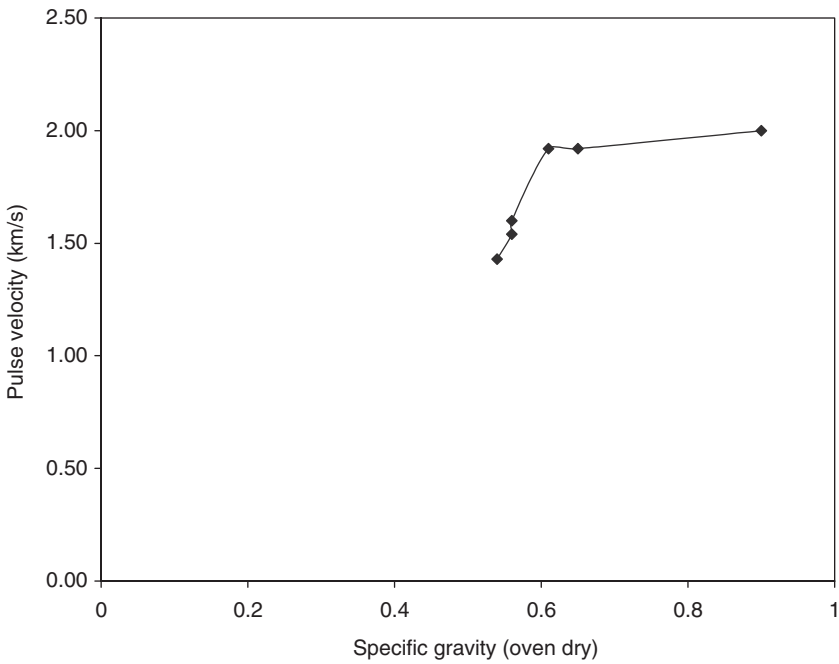
Tests were conducted in a number of wood samples to establish the effect of moisture content, specific gravity and compressive strength parallel to grain on the pulse velocity. Table 7.2 gives the average properties of the test samples. Figure 7.3 gives the relationship between the pulse velocity parallel to grain and perpendicular to the grain. This provides a basis for assuming that the perpendicular to the grain velocity can be used to establish the relationship between the parallel to grain strength properties and the perpendicular to the grain pulse velocity readings.

7.6 In-service evaluation

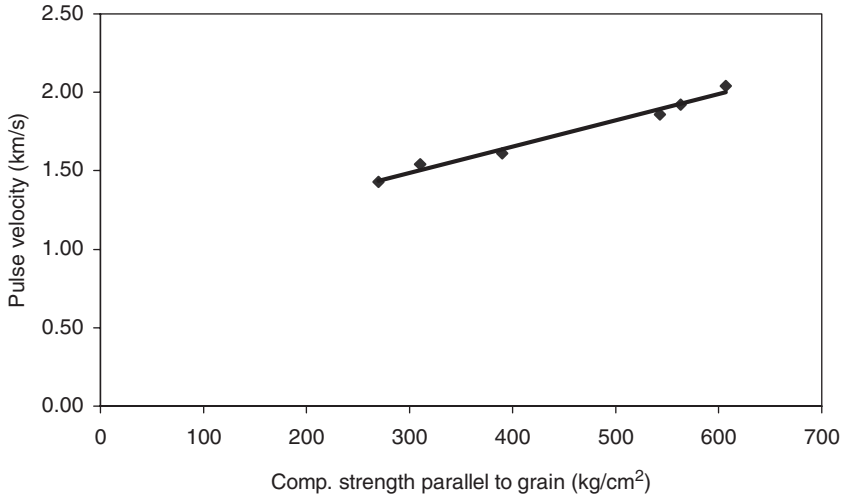
The results of various tests conducted on clear wood specimens show that the pulse velocity perpendicular to grain increases with an increase in specific gravity or compressive strength perpendicular to the grain (Figs 7.4 and 7.5). The data for Fig. 7.4 were obtained by measuring the pulse



7.3 Relationship between ultrasonic pulse velocity parallel and perpendicular to grain.



7.4 Relationship between ultrasonic pulse velocity perpendicular to grain and specific gravity.



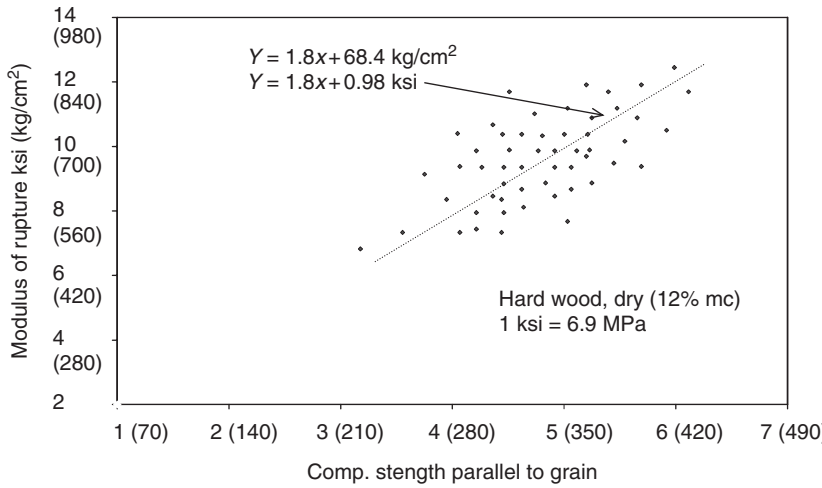
7.5 Relationship between ultrasonic pulse velocity perpendicular to grain and compressive strength parallel to grain.

velocities of clear wood samples cut from lumber of different sizes belonging to the six species of timber shown in Table 7.1. A point on the graph may represent more than one measurement (1 to 7). A pulse takes a longer path to travel through internal voids, discontinuities and cracks present in the wood. In a specimen of uniform dimensions and grade, a sudden drop (as in Fig. 7.1) in the pulse velocity indicates the possibility of internal voids. The studies show that there does not seem to be any influence of external load on pulse velocity.

Based on the extensive tests on various species of wood, a correlation was established between the compressive strength parallel to grain and the ultrasonic pulse velocity perpendicular to the grain (Fig. 7.5). Using the method of least squares, a best fit relationship was established:

$$X = (V - 1) \times 625 \qquad [7.2]$$

where X = compressive strength parallel to grain (kg/cm^2) and V = ultrasonic pulse velocity (km/s). From the above relationship, compressive strength parallel to the grain of any species can be estimated by measuring the ultrasonic pulse velocity of a clear wood specimen. Using this relationship, a condition-rating system, with respect to compressive strength parallel to the grain, can be formulated. The procedure, which involves the establishment of a relation between pulse velocity and compressive strength of known timber species followed by the development of the condition-rating system, can be used to assess the extent of damage or the decay in



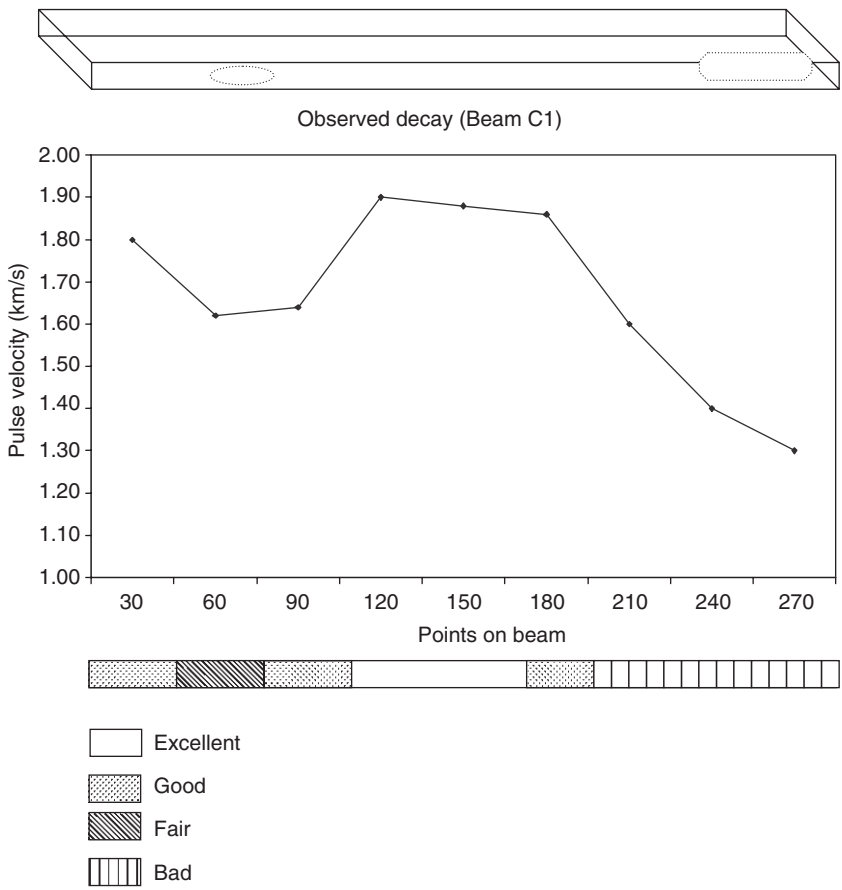
7.6 Relationship between modulus of rupture and compressive strength.
(*Sources*: points from *Wood Handbook* 1987, Table 4.2; line from Rajput *et al.* 1991.)

timber components. The condition-rating system for structural assessment of timber elements of common species (hardwood) was developed from the pulse velocity–compressive strength relationship shown in Fig. 7.5. It is based on the assumption that compressive strength parallel to grain, in a relative sense, is a measure of the load-carrying capacity of a wooden member.

The most common use of wood in buildings is in the form of floor and roof rafters. Decay in these members is on the top portion that is in contact with flooring material and also at the ends. The members are subjected to flexure, and the structural assessment of these members should be related to the reserve bending capacity. The average values of the modulus of rupture and compressive strength parallel to grain for clear wood samples of several species of hardwood (dry condition) are plotted in Fig. 7.6 (*Wood Handbook* 1987). The relationship between the two properties proposed by Rajput *et al*. (1991) based on tests conducted on 60 species of wood is also shown in the figure. A general linear relationship exists between the two properties, and one could assume that the compressive strength parallel to grain estimated from the pulse velocity readings could be used for relative comparison of reserve load-carrying capacity between various portions of a timber component. Accordingly, using the pulse velocity readings, a rating system was developed to estimate the reserve capacity (as the percentage of the

Table 7.3 Condition-rating system for in-service evaluation

Ultrasonic pulse velocity perpendicular to grain (% of basic velocity)	Compressive strength parallel to grain (% of basic compressive strength)	Rating
100	100	Excellent
$(80 + 20/V_b) - 100$	80–100	Good
$(70 + 30/V_b) - (80 + 20/V_b)$	70–80	Fair
Below $(70 + 30/V_b)$	Below 70	Bad



7.7 Mapping of decay pattern – both ends decayed.

capacity of undamaged portion) as well as the structural condition of the wood member (from excellent to bad). A summary of the rating system is shown in Table 7.3, where the term basic velocity (V_b) refers to an average of velocities measured at undamaged portions of similar elements.

A rating of 100% of the basic compressive strength, or the strength of the undamaged portion, is used to identify wood members that are in excellent condition. This rating is assigned for the portion of members that are expected to have a maximum or nearly maximum compressive strength and with no sign of deterioration. A 'good' rating is for portions that are expected to possess strength between 80 and 100% of the basic compressive strength. These portions are not expected to have the potential for serious structural problems such as internal decay or insect attack. Also some kind of a maintenance scheme needs to be considered. A 'fair' rating (between 70 and 80% of the basic strength) occurs when some deterioration has taken place. Structural weakening due to localized decay or reduction in cross-section from insect attack is highly probable. Maintenance, repair or strengthening may be required urgently. A 'bad' rating (below 70% of the basic strength) indicates that a major deterioration has occurred in portions of members due to severe decay or termite attack greatly affecting the load-carrying capacity or the load transfer capacity at supports. Immediate attention is required to strengthen the member or to replace it.

To assess the validity of the condition rating system developed from laboratory investigations, field tests were conducted on several timber elements. Typical results from the field study are shown in Figs 7.7 and 7.8. They show the observed damage pattern in the beam and the assigned rating as per the proposed rating system. Good agreement was found to exist between the actual decay pattern and the measured velocity readings, supporting the conclusion that this non-destructive test technique can be used effectively for inspection and in-service assessment of damaged or decayed timber elements.

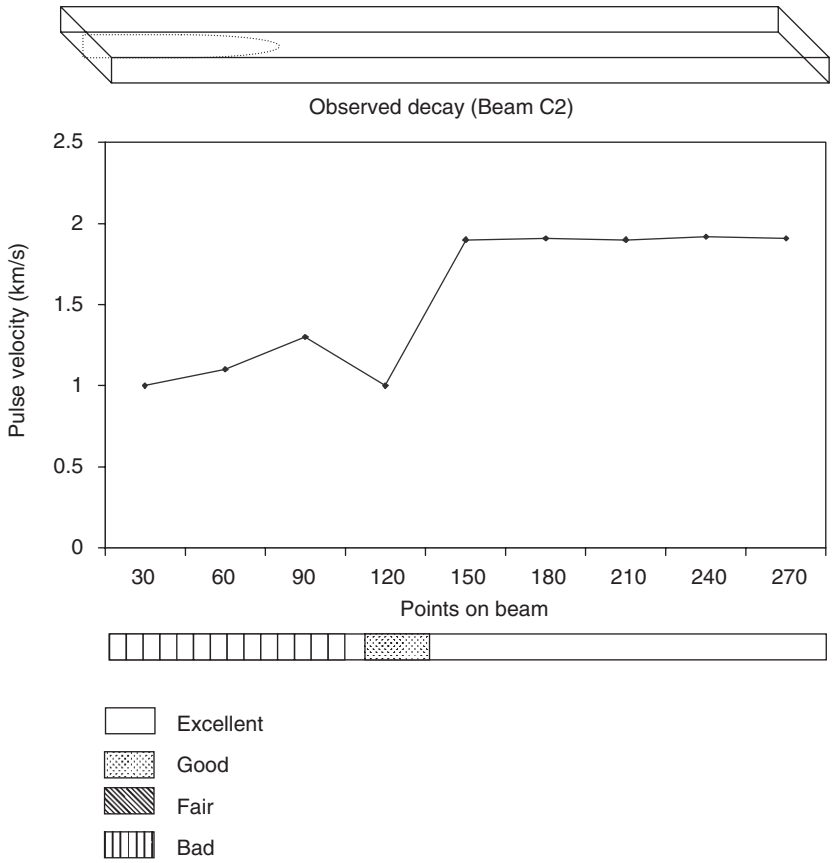
7.7 Future research and development

Research on the following aspects, which have not been considered in the present study, would provide useful information:

- Study of the effect of knots, cross-grain on ultrasonic pulse velocity.
- Study of the various *in-situ* repair methods of timber components.
- Strength evaluation of repaired wooden members.

7.8 Conclusions

Wood is an efficient material for construction if built and maintained properly. Tests on several species of timber elements show that the specific



7.8 Mapping of decay pattern – decay at external support.

gravity and compressive strength parallel to the grain of the wood are proportional to the pulse velocity. The effect of internal voids, cracks and discontinuation reduce the velocity. The pulse velocity measured perpendicular to the grain of a flexural member can be used to detect decay and to estimate the reserve load-carrying capacity.

The ultrasonic pulse velocity test can be an effective tool for the inspection and structural assessment of timber elements in buildings. A condition-rating system described could be used for mapping the deterioration or decay pattern in structural timber.

7.9 Acknowledgements

This chapter is based on the paper by T.L. Shaji, S. Somayaji and M.S. Mathews (2000) 'Ultrasonic pulse velocity technique for inspection and

evaluation of timber', *J. Materials in Civil Engineering*, ASCE, vol. 12, No. 2, pp. 180–185 (reproduced by permission).

7.10 References

Beall, F.C. (1987). 'Fundamentals of acoustic emission and acoustic ultrasonics.' *Proc., 6th Non-destructive Testing of Wood Symp.*, Washington State University, Pullman, Washington, 3–28.

Bodig, J. and Goodman, J.R. (1988). 'NDE for performance of wood structures.' *Proc., Int. Workshop on Non-destructive Evaluation for Perf. Evaluation of Civil Struct.,* M.S. Agbabian and S.F. Masri, eds., University of Southern California, Los Angeles, 203–215.

Degroot, R.C. and Esenther, G.R. (1982). 'Insects, fungi, and other organisms that affect wood'. '*Wood Structures*', ASCE, New York, 126–135.

Fiest, W.C. (1982). 'Structural use of wood in adverse environments.' *Wood*, R. Mayer and W. Kellogg, eds., Van Nostrand Reinhold, New York, 156–178.

Fiest, W.C. (1988). 'Outdoor wood weathering and protection.' *Proc., 196th Meeting of Am. Chem. Soc., Archeological Wood: Properties, Chemistry and Preservation, Adv. In Chem.* Ser. 225, R.M. Rowell and J.R. Barbour, eds., Washington, DC, 263–298.

Freas, A.D. (1982). 'Inspection.' *Wood Structures: A Guide and Commentary,* ASCE, New York.

Freas, A.D. (1986). 'Wood.' *Engineering Design Concepts*. Clark C. Heritage memorial series on wood, Vol 4. R.C. Moody and L.A. Soltis, eds., Pennsylvania State University, University Park, PA.

Geimer, R.L., Lehmann, W.F. and McNatt, J.D. (1974). 'Engineering properties for structural particle board from forest residues.' *Proc. 8th Washington University Symposium on Particle Board*, 119–143.

Kemp, E. (1982). 'Old wood structures.' *Wood Structures: A Guide and Commentary,* ASCE, New York, 24–39.

Kirk, T.K., Lamer, R.T. and Glaser, T.A. (1992). 'The potential of white-rot in bioremediation.' *Biotechnology and Environmental Science Molecular Approaches*, S. Mongkolsuk, P.S. Lowett and J.E. Tempy, eds., Plenum, New York, 131–137.

Lyon, D.E. (1982). 'Degradation of wood in use and wood protection.' *Wood as Structural Material,* Clark C. Heritage memorial series on wood, Vol. 2, Pennsylvania State University, University Park, PA.

Rajput, S.S., Shukla, N.K., Gupta, V.K. and Jain, J.D. (1991). *Timber Mechanics*, Indian Council of Forestry Research and Education, Dehra Dun, India.

Ross, R.J. and Pellerin, R.F. (1991). 'Non-destructive testing for assessing wood members in structures.' *General Tech. Rep. FPL-GTR70*, Forest Products Laboratory, Madison, WI.

Sayal, S.N. and Gulathi, A.S. (1979). 'Compressive strength of timber by ultrasonic pulse technique.' *Indian Forester*, **105**(2), 180–185.

Shaji, T.L. (1994). 'Non-destructive evaluation of timber components in historic buildings.' M. Tech. thesis, Civ. Engrg. Dept., IIT Madras, Chennai, India.

Shaji, T.L., Mathews, M.S. and Somayaji, S. (1993). 'Inspection and restoration of timber in historic buildings.' *Congr. on Traditional Sci. and Technol. of India,* abstracts, IIT Bombay, Bombay, 2–19.

Sherwood, G.E. (1986). 'Technology of preserving wood structures.' *Building Performance: Function*, *Preservation and Rehabilitation*, ASTM STP 901.6, G. Davis, ed., American Society for Testing and Materials, Philadelphia, 121–125.

Stamm A.J. and Loughborough, W.K. (1942), *Transactions*, Vol. 64, ASME, New York, 379–385.

Walters, C.S. (1981). 'The chemical treatment of wood for end use.' *Wood: Its Structures and Properties,* F.F. Wangaard, ed., Clark C. Heritage Memorial Ser. on wood, Vol. 1, Pennsylvania State university, University Park, PA, 272–320.

Winanady, J.E. and Morrell, J.J. (1993). 'Relationship between incipient decay strength and chemical composition of Douglas fir heartwood.' *Wood and Fiber Sci.*, **25**(3), 278–288.

Wood Handbook (1987). *Agric. Handbook No. 72*, Forest Products Lab., US Department of Agriculture, Washington, DC.

8

Digital radioscopy analysis of timber structures

R.W. ANTHONY
Anthony & Associates Inc., USA

8.1 Introduction

In 1870, Sir William Crookes found that passing an electric current through a glass vacuum bottle with wires embedded at each end produced a purple light inside the bottle and a green glow outside (Wisehart, 1928). This phenomenon was simply another unexplained scientific curiosity until Wilhelm Conrad Roentgen at the University of Würzburg in Germany began experimenting with several types of vacuum tube, including the 'Crookes tube' in the early 1890s (Brown, 2002). Roentgen formally announced his discovery of X-rays in December of 1895 (Brown, 2002). His paper was originally sent to the Würzburg Physical-Medical Society, but by 1 January 1896, he had sent the report to scientists across Europe. By mid-January, newspapers in the USA had reported on the new discovery.

In the USA, Thomas Edison took up the investigation in an attempt to develop X-ray equipment that could be widely used. He eventually developed a hand-held fluoroscope but was unable to develop a commercial X-ray lamp. Other investigators quickly followed, and by the early decades of the 20th century, X-rays were being used widely not only for medical purposes, but also for a large variety of industrial uses, such as steel manufacture, foundry practices, railroading, and the production of electrical equipment. X-rays were even used to fit shoes, find grit in chocolates, and sort fresh eggs (Wisehart, 1928). Unfortunately, the radiation hazard present in many of these uses, especially medical uses, was unrecognized. For instance, a discussion of medical uses in 1928 showed that often the patient was in front of an X-ray tube for extended periods while doctors watched the movements of the digestive organs or a beating heart (Wisehart, 1928).

Fluoroscopy provided a two-dimensional image of an object of interest immediately on a screen. Because of its portable nature and ability to produce 'real-time' images, fluoroscopy, unlike film X-ray techniques, allows for easy manipulation of the test material during inspection, thereby

enabling better examination. Fluoroscopy had two primary disadvantages which have limited its use: although somewhat portable there were safety concerns with the X-ray source and there was no means to store the image for later processing. Digital radioscopy does not have these disadvantages; advances in the technology make it safer to operate and it has the ability to store images. Perhaps, though, the most useful feature is the ability to post-process the X-ray image to focus on particular details or use image enhancement techniques to change contrast, brightness or position.

Traditional X-ray technology using film and high-energy X-ray sources has been used to examine wood structures for over 40 years. However, owing to safety concerns and the high costs involved, use has been quite limited in timber structure evaluation. As opposed to traditional film X-ray technology, use of digital real-time X-ray technology for structure investigation has shown considerable promise for use on timber bridges. X-rays emitted from traditional high-energy electromagnetic radiation sources are capable of penetrating most materials used for bridge construction. Depending on the material properties of the object being inspected, a photographic image is produced that reflects the density, thickness, energy absorption, and chemical properties of the material.

8.2 Physics of X-rays

X-rays are simply another form of electromagnetic radiation, just like light and heat. In the 1860s, James Clerk Maxwell produced the four equations that define electrodynamics. These equations brought together for the first time the study of electricity, magnetism, and light. Maxwell showed that all types of electromagnetic radiation were simply mutually perpendicular, fluctuating electric and magnetic fields. This radiation is characterized by both a wavelength (λ) and a frequency (f), related to the speed of light in a vacuum (c is equal to 3×10^8 m/s) as:

$$c = \lambda f \qquad [8.1]$$

This equation shows that the wavelength of light is inversely proportional to its frequency. Radio and infrared radiation have wavelengths longer than that of visible light, and the energy of individual photos is lower, while X-rays and gamma rays have shorter wavelengths (and thus greater frequencies), and also have higher amounts of photon energy.

This energy relationship is defined as:

$$E = hc/\lambda \qquad [8.2]$$

where h is Planck's constant, and the energy (E) of individual photons is measured in electron-volts (eV). The smaller the wavelength (and thus greater energy), the more likely the radiation is to penetrate matter. If you

hold your hand up to a bright light, you can see some light coming through the edges. The hand appears to be translucent. Low-energy X-rays easily penetrate human bodies, while high-energy X-rays and gamma rays can be stopped only by a meter or more of concrete or several centimeters of lead. This differential absorption is what makes X-rays useful for structural investigations. X-rays of a given wavelength (or small range of wavelengths) may easily penetrate a wood beam, but are preferentially absorbed by the nails attaching the beam to the rest of a structure. Thus the final image (produced either on film or a fluorescent screen) will have light areas corresponding to less dense material, where most of the beam is transmitted, and darker areas corresponding to heavier materials, where most of the beam is absorbed.

X-rays are subdivided by wavelength, with soft (or lower-energy) X-rays having wavelengths around 1–10 angstroms (one Å angstrom is 10^{-10} m) while very hard X-rays have a wavelength around 10^{-3} Å. The X-rays used in digital radioscopy are soft X-rays, produced at 150 kV, with wavelengths of highest intensity at about 0.13 Å. This energy is approximately equivalent to that produced by medical X-ray equipment, which typically produces X-rays at 40–140 kV, and so safety issues using this X-ray source are reduced.

The intensity of a beam of X-ray photons is a measure of the energy per unit time per unit area produced by the beam of X-rays (for example in W/m^2), and can be calculated in a variety of ways. Closely related to this is the radiation dose, or units of radiation exposure, usually defined as the energy deposition per gram of absorber (such as human tissue). Both the RAD (radiation absorbed dose) and REM (Roentgen equivalent man) are units typically used in the USA to define appropriate limits for exposure to radiation. The RAD is equivalent to 100 ergs of energy per gram of absorber. The REM is equal to the RAD multiplied by the QF (quality factor). This factor accounts for the relative biological effectiveness of different types of radiation (including alpha and beta radiation, which are not electromagnetic radiation). The QF for X-rays is 1, however, so the units are equivalent.

There are limits to the amount of radiation exposure, to protect individuals from radiation damage. The Whole Body Occupational Dose limits for an adult are set by the US Environmental Protection Agency as 5 REM (5000 milli-REMs or mREM) per year. For comparison, a typical adult living in Colorado in the mountainous USA (at an elevation between 1500 and 1800 m, 5000 and 6000 feet), who takes at least three airline flights per year and watches television, receives a typical dosage of about 400–450 mREM per year (EPA website, 2004). A dental X-ray is usually 2–3 mREM, while the author's experience is that the total exposure of a technician conducting radioscopy in the field is typically less than 20 mREM per year.

8.3 History of wood building radiography

Radiography has been used for field investigations of wood products since the 1960s. Prior to the development of digital radioscopy, investigators used high-energy X-ray sources for examining timber structures. Mothershead and Stacey (1965) conducted X-ray studies on wood poles to identify the presence of internal deterioration. Using film to capture the images, they were able to observe variations in X-ray density, which corresponded to wood decay.

Hart (1974) used X-ray analysis to examine the Narbonne House in Salem, Massachusetts. The goals of the examination were to determine the presence and configuration of wall bracing, possibly identify original window framing, and determine whether some of the framing had once been an exterior wall. Hart used a portable X-ray generator and Polaroid camera in the field to conduct the examination. The examination successfully identified the configuration of hidden structural braces. Further, the technique showed the type of fasteners used and that the wood had no signs of decay. By examining exterior walls Hart was able to determine that no original window framing was present. The question of whether some of the framing had once been part of an exterior wall was inconclusive owing to limited access with the X-ray equipment and modifications to the structure.

An X-ray examination of the House of Seven Gables was described by Wrenn (1976). Based on work conducted by Hart, Wrenn discussed the merits of using X-rays to assess the structural condition of wood in historic buildings. The ability to determine material conditions and construction without disturbing the fabric of the structure was seen as the primary benefit. However, Wrenn noted that the technique was limited by the inability to take an X-ray straight through an object and get a clear image.

Interest in the construction of the Delorme dome at Thomas Jefferson's Monticello led to an X-ray examination described by Harnsberger (1981). A Polaroid camera was used to record images taken through the domed roof. A portable X-ray emitter was mounted on a tripod near the dome ceiling while a receiver was placed above the exterior of the dome. The X-ray inspection revealed the type and pattern of fasteners used in the timber ribs supporting the dome. The examination allowed for an interpretation of Jefferson's use of Delorme's innovative timber framing system.

Radiography can also be used to determine the location or extent of deterioration in wood due to insects or decay. Frames of historic artwork have been examined with X-rays to show the presence of wood rot and insect damage (Lang and Middleton, 1997). The success of traditional X-ray imaging for this application shows promise for digital radioscopy once the capabilities and limitations of the technology have been more fully explored.

8.4 Equipment for investigating timber structures

To produce digital radiographs, several different systems are available, two of which will be discussed here. These systems use the same source of X-rays, but have different imaging systems. The first imaging system (the RTR-4™ imaging system from SAIC®) produces real-time digital radiographs, with technology somewhat equivalent to a digital camera. The second imager is a plate which creates fluorescence when X-rays impinge on the surface, similar to X-ray film. This imager plate then is scanned for 3–7 min to produce the digital radiograph (the EPIX Digital Imaging System by Logos Imaging). The source and both types of imagers are discussed below.

8.4.1 XR200® X-ray source

The X-ray source used for wood investigation is the XR200®, manufactured by Golden Engineering, Inc. This model is a single packaged, pulsed source, producing X-ray pulses of short duration (60 nanoseconds or 6×10^{-8} s each) and minimal dose (3.1 milliroentgens for each pulse at a distance of 30.5 cm from the front of the unit), with energy up to 150 kV. The source size is 3 mm, and the beam produced by this source has a 40° beam angle, so that X-rays taken about 0.6 m (2 feet) from the source have a spread equal to the width of the imager. For each X-ray, the number of pulses can be set from 1 to 99. One or two pulses are required to penetrate paper; and four to ten are typically used to penetrate most wood building walls.

The source is portable and easy to use in the sometimes confined spaces characteristic of timber bridges. It is 11.5 cm wide, 19 cm tall, 31.8 cm wide, and weighs 5.5 kg. It is operated by a 14.4 V removable, rechargeable nickel–cadmium battery pack that can be used in buildings or bridges with no source of electrical power. The base of the source unit has a threaded tripod mount, which can be used with a standard photographic tripod.

Safety issues are always a concern when using X-rays. This X-ray source has a variety of safety features. The unit does not rely on a radioactive source. Rather, X-rays are generated through the introduction of an electrical potential across the vacuum tube (just as light is only produced when the electricity is turned on for a fluorescent fixture). The low dose of each pulse and the ability to create a specific number of pulses allow for an individual to work with the minimum amount of energy necessary to accomplish the investigation. Leakage from the unit while it is working is limited to 10 milliroentgens per 100 pulses on the sides of the unit, 7.6 cm from the center, and three milliroentgens per 100 pulses 5.1 cm behind the

unit. Since X-ray radiation has an inverse-squared relationship between energy and distance, individuals standing in a safety zone more than 1.5 m behind the unit when it is working are protected. The XR200® will work only when a key is inserted in the top. This allows the operator to always have the key in his or her possession, so that the unit will not accidentally discharge while shots are being set up.

8.4.2 RTR-4™ imager

The RTR-4™ portable digital X-ray imaging system is manufactured by SAIC® (Science Applications International Corporation). This system is a fully digital imaging system that includes its own image modification tools. The system is composed of a control unit (a laptop computer), the imager, and cables that connect the imager to the controller. The imager is a compact, solid state camera with a 20.3 by 27.2 cm^2 field of view. The imager measures 17.8 by 29.8 by 37.3 cm^2, and weighs 4.6 kg. It is typically mounted on a tripod or placed directly against the surface of the object of interest, opposite to the source, so that access to both sides of the object is required. The imager's electro-optical system captures the images and transmits them to the control unit, where they are stored as tagged-image file format (TIFF) images.

This imaging system has an advantage in that it produces digital radiographs in real time, so that the images are instantly available. It is easy to shift the imager if needed when the area of concern was not included in the image, or to shift the imager along an object (such as a beam or joist) to make sequential radiographs. Having the cables in place to connect the imager to the control unit can limit the ability to investigate hard-to-reach areas of a bridge. However, a cordless option for this imaging system is available which can address these concerns.

These images, since they are TIFF files, can be manipulated by any standard photographic-enhancement software. The control unit (or the software that is included for the laptop) includes a package that can also be used to enhance the images so that subtle details of the X-ray can be investigated. This software includes not only the standard image-enhancement techniques (such as image sharpening and contrast stretching), but also features designed to assist specifically with X-ray enhancement (such as the ability to transmit all the grey tones of the X-ray into a full spectrum of colors, and edge detection algorithms).

8.4.3 EPIX scanner and imaging plates

The second imaging system is the EPIX Digital Imaging System by Logos Imaging. This system is composed of the EPIX imaging plates, the EPIX

scanner, and a laptop with software to import and save the scanned image. The imaging plates are reusable, photostimulatable phosphor imaging surfaces, either 20.3 cm by 25.4 cm, or 20.3 cm by 43.2 cm in size. They are composed of flexible plastic sheets coated with a very thin layer of tiny storage phosphor crystals bonded together. X-ray images are created on these imaging plates as the phosphor crystals capture the energy of X-rays passing through the object of study. This energy is stored in the crystals, and released by the process of scanning. However, the scanning process does not completely erase the image from the plate, so the plates need to be exposed to light (usually about 2 min in the direct light of a 100 W bulb or light table) before they can be used again. With care to keep the imaging plates stored out of the light, and in their cases (to avoid scratching the coating), these plates are reusable indefinitely.

The second component of the EPIX Digital Imaging System is the EPIX scanner. This machine, often referred to as the 'bread-maker', is 39.4 cm high, 49.3 cm wide and 27.4 cm deep, and weighs 14.7 kg. To mount the imaging plates and insert them in the scanner, two carousels (one for each imaging plate size) are available. After exposure, the imaging plate is mounted on the cylindrical carousel (with care not to expose the photosensitive surface to much light) and inserted into the scanner. The scanner uses red laser light to cause the crystals to release their stored energy, which is released as blue light captured by the scanner. The scanning process can capture the image at either high or low resolution. The high-resolution image, which takes about 7 min to process, is 300 DPI, 85 microsquare pixels. The scanned image of the larger plate at high resolution is about 24 MB. The low-resolution image is half that, and takes half the time to process.

8.4.4 Monitoring devices

Two types of monitoring devices are typically used during structure investigation with X-rays. The pocket or pen dosimeter (also known as a Pocket Ionization Chamber) is used to determine exposure during individual X-ray operations. These 11.4 cm cylinders can clip on shirt pockets, and are easy to use. They read dosages up to 200 mREM and can be manually reset to zero for each X-ray session. They are used to monitor background radiation and any leakage near the source, one being stationed right behind the source for each X-ray session. They are easily calibrated, and should be read at least at the beginning and end of each session.

Long-term exposure to radiation should be monitored for all staff using X-ray equipment. Thermoluminescent dosimeter (TLD) badges can be used for this type of monitoring. The TLD badges are more accurate than a pocket dosimeter and are checked periodically to determine the cumulative level of radiation exposure.

8.5 Case studies

Digital radioscopy has not yet been used extensively to investigate bridges. A number of applications of digital radioscopy to wood structures have been reported by Anthony (2004). The wood connections in covered bridges, metal rods or bolts in modern timber bridges can all be inspected using digital radioscopy. To demonstrate the capabilities of this technology, several examples are given below. The examples show the use of radioscopy to identify the type, location and condition of metal connectors; corrosion of iron tension rods; yield damage in connections; and wood deterioration.

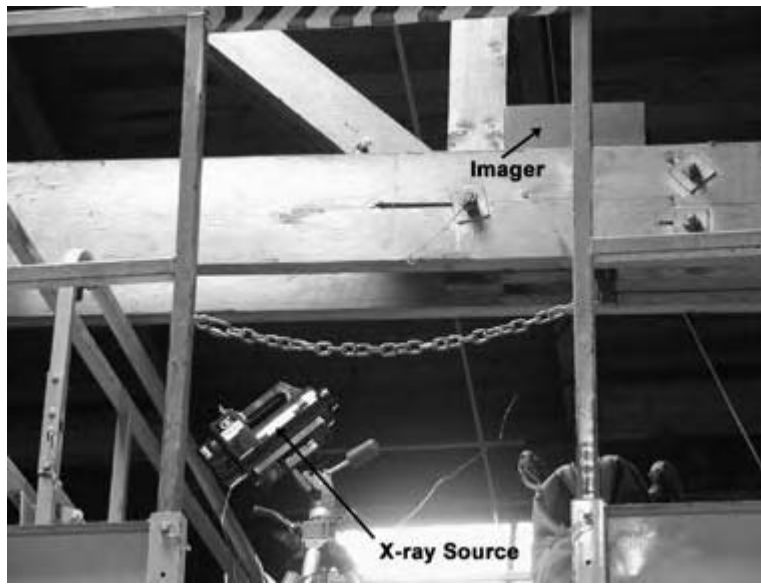
8.5.1 Investigation of connections in built-up timber trusses

Concerns about load-carrying capacity led to an examination of connections in trusses in large military warehouses built prior to 1950. The original structural framing in the buildings consists of timber frames with built-up timber trusses as roof supports. Cracks present in some of the truss chords, diagonals, and verticals initiated the investigation to verify whether any metal fasteners exist in the connections between wood members that make up the trusses.

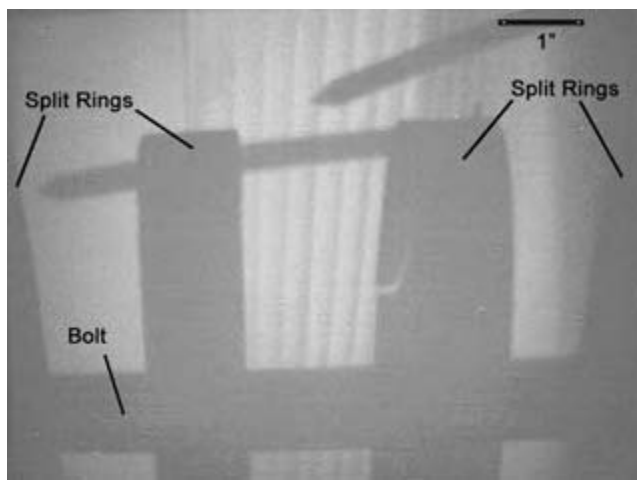
A key question regarding the structural integrity of the warehouses was whether metal fasteners were present in the connections in the built-up timber trusses. Although drawings of repairs to one warehouse were found that indicated split ring connectors were present, it was not known whether this joint detail had been used in other warehouses. Therefore, digital radioscopy was used to examine the connections in selected warehouses to determine the presence of split rings; their size, number, and condition; and the condition of the surrounding wood.

A test configuration for the bottom chord with a single-bolted connection is shown in Fig. 8.1. This configuration was used for similar connections between horizontal truss chords and vertical and diagonal web members.

The radiograph resulting from the single-bolted connection is shown in Fig. 8.2. Four split ring connectors are visible in the radiograph. Although a scale is shown in Fig. 8.2 (and in other radiographs), direct measurement of a component on the radiograph is not precise. Radioscopy essentially projects a three-dimensional object onto a two-dimensional image, resulting in somewhat distorted sizes. Precise dimensions can be obtained using stereo-radioscopy and by measuring the distances between the X-ray source, the imager and the object of interest. The bolt, visible in Fig. 8.2, showed no evidence of corrosion as determined by observing the smooth, parallel



8.1 Test configuration for digital radioscopy of bottom chord with a single-bolted connection.



8.2 Radiograph of bottom truss chord, view from below.



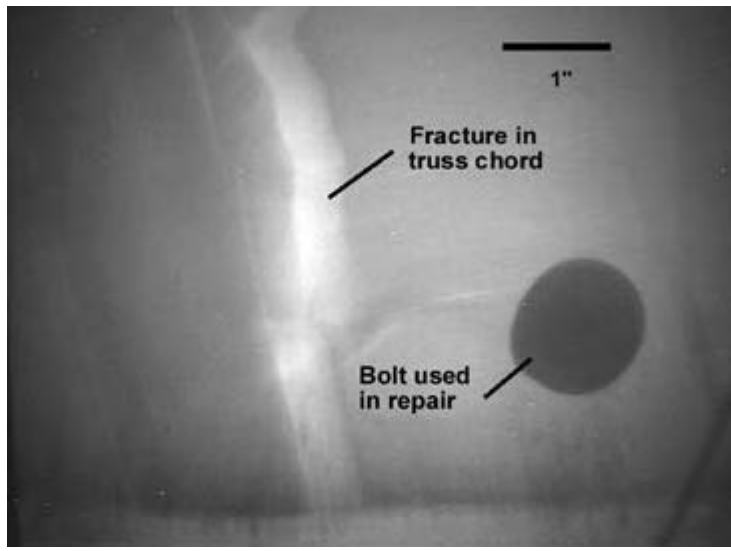
8.3 Imager attached to repaired bottom truss chord.

edges of the bolt. The connections in the roof trusses used 4-inch (10 mm) split ring connectors. Joints with diagonal web members used four split rings while splices in bottom chords used only two. As was observed on the bolts, the radiographs showed that the split rings are in good condition and do not exhibit signs of corrosion or failure. Further, based on the radiographs, the wood adjacent to the fasteners is in good condition and has not deteriorated.

Figure 8.3 shows the bottom chord of a repaired truss. The accompanying radiograph, given in Fig. 8.4, showed that no split ring connectors were used in the repair. Further, the reason for the repair can be seen as a vertical fracture in one of the timbers. The head of the bolt securing the repair timber to the original truss chord is also visible in the radiograph.

8.5.2 Investigation of threaded rods embedded in timber beams

In 1997 the balcony on Pavilion I at Thomas Jefferson's Academical Village at the University of Virginia collapsed. The cause of the failure was determined to be a corroded iron rod. Four rods supported the balcony from



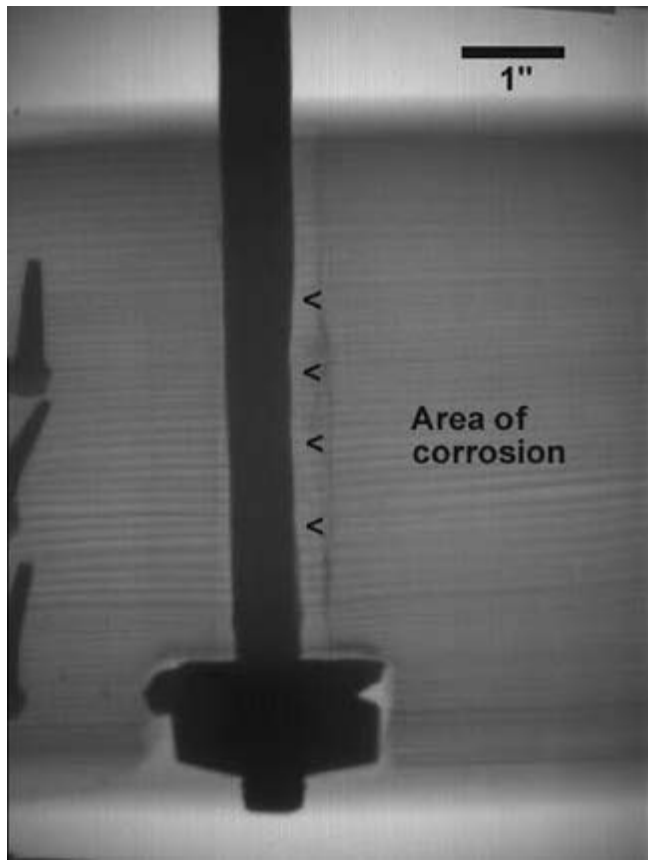
8.4 Radiograph of repair to bottom truss chord, side view. Note the fracture in the original timber (bright area).

above. The ends of the rods were embedded in timber beams and not accessible for visual inspection.

Post-failure, digital radioscopy was used to determine whether corrosion of the iron rods could be detected. Figure 8.5 shows an iron rod embedded in a timber beam in the same configuration used on Pavilion I. The rod was shown to have minimal surface corrosion as evidenced by the reduced cross-section of the rod within the beam. The remaining cross-section of the rod could be measured during post-processing of the radiograph data stored on a computer. Note the lack of a void in the wood surrounding the rod; a condition that might be expected if the corrosion was due to the presence of moisture.

8.5.3 Examination of double shear joint tests

Digital radiography has been used to evaluate joints subjected to double shear loading, tested in the laboratory in accordance with ASTM D 5652 (1995). Radioscopy provided the means of assessing the failure mode of nails and bolts without dismantling the joints. While inspecting joints in a bridge after a seismic event or a vehicle impact would be more cumbersome than imaging test specimens in the laboratory, the brief study verified that radioscopy could be used to aid in assessing seismic damage.



8.5 Radiograph of a corroded rod embedded in a timber beam.

8.5.4 Examination of mortise and tenon joints

Finding and determining the condition of metal fasteners embedded in wood is possible, in part, because of the different densities of wood and metal. For wood connections, such as mortise and tenon joints (common in covered bridges), the interpretation of the radiographs is more challenging.

Laboratory research conducted on a mortise and tenon joint showed that differences in the grain orientation of the mortise and tenon were visible. A cross-hatched pattern is typically visible where the two pieces of wood overlap as the tenon penetrates the mortise. Field studies on joints in a historic granary in Loveland, Colorado, corroborated the laboratory studies.

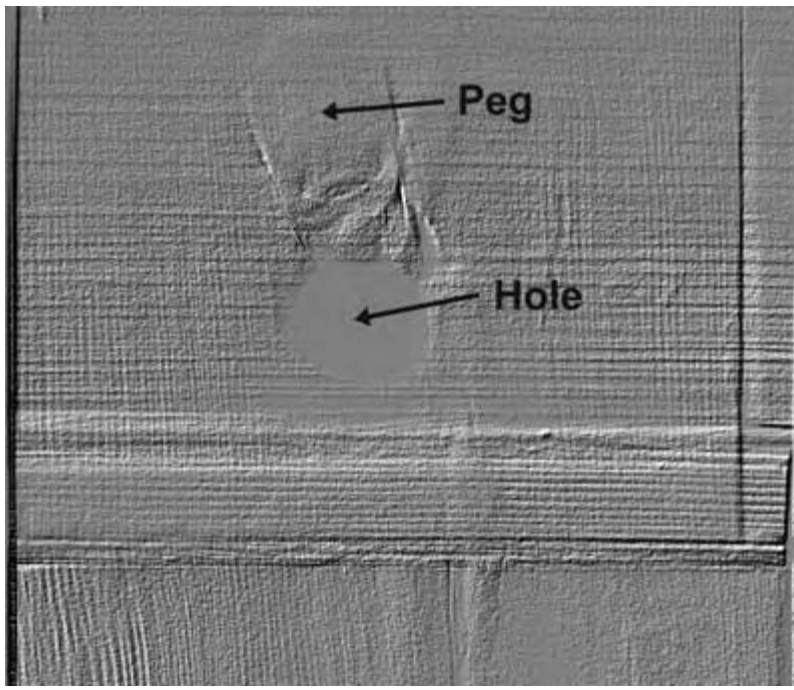


8.6 Mortise and tenon joint showing placement of X-ray source.

Figure 8.6 shows the X-ray source in position to provide an image of a mortise and tenon joint in the attic of the granary. Visible moisture stains raised concerns about the condition of the joint. Figure 8.7 is an enhanced version of the radiograph that better illustrates the cross-hatch pattern indicative of two pieces of wood with the grain perpendicular to one another. Note the flat spot near the center of the radiograph, corresponding to a mis-drilled hole through the tenon. Further image enhancement was able to show the wood grain in the beam with the mortise, verifying that the mis-drilled hole was in the tenon.

8.5.5 Investigation of decay and termite damage

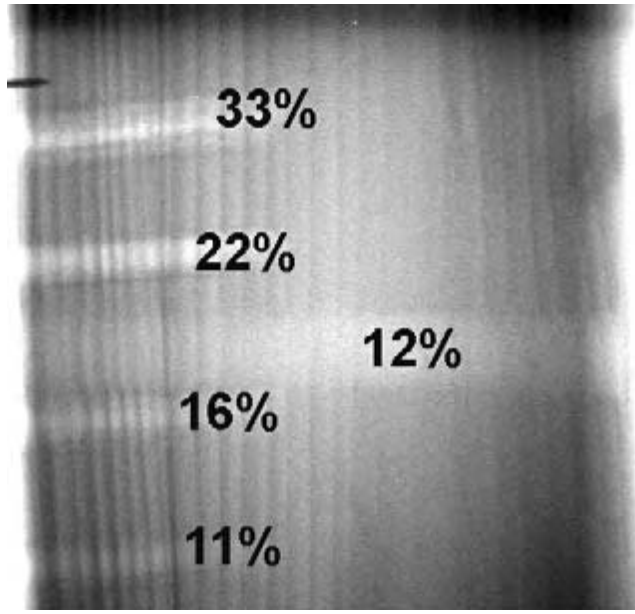
Termite activity can result in catastrophic damage in timber structures. Infrared thermography and acoustic non-destructive methods have been used to detect termite activity but no suitable technique has yet been established to quantify the loss of material in a structural timber. Knowledge of the remaining sound cross-section is crucial for determining load-carrying capacity and structural safety. Preliminary laboratory work has been conducted to determine the feasibility of using digital radioscopy to quantify termite damage.



8.7 Radiograph using image enhancement to better illustrate the wood grain of the tenon and the beam with the mortise.

Quantifying deterioration can be accomplished using imaging processing techniques to distinguish subtle differences in measured X-ray intensity. Transmitted X-ray energy is recorded as intensity. Greater intensity measured at a given point implies less wood substance to absorb the X-ray energy. The loss of wood substance can be due to deterioration. By comparing the measured intensities on a radiograph, the extent of deterioration in wood members can be quantified.

Holes were drilled into a timber to simulate termite damage profiles of known cross-section. Radiographs taken of the test section were initially examined visually to determine whether variations in intensity due to the different volume of wood at each plane could be distinguished. The radiograph, shown in Fig. 8.8, reveals that it is difficult to visually distinguish subtle differences in intensity. However, using digital imaging techniques it may be possible to identify differences in intensity that correspond to the remaining cross-section at each plane. Similarly, Fig. 8.9 is a radiograph of a timber beam with a void due to wood decay fungi. Using an inverted greyscale, the darker zones are areas where either a void or deteriorated wood is present.



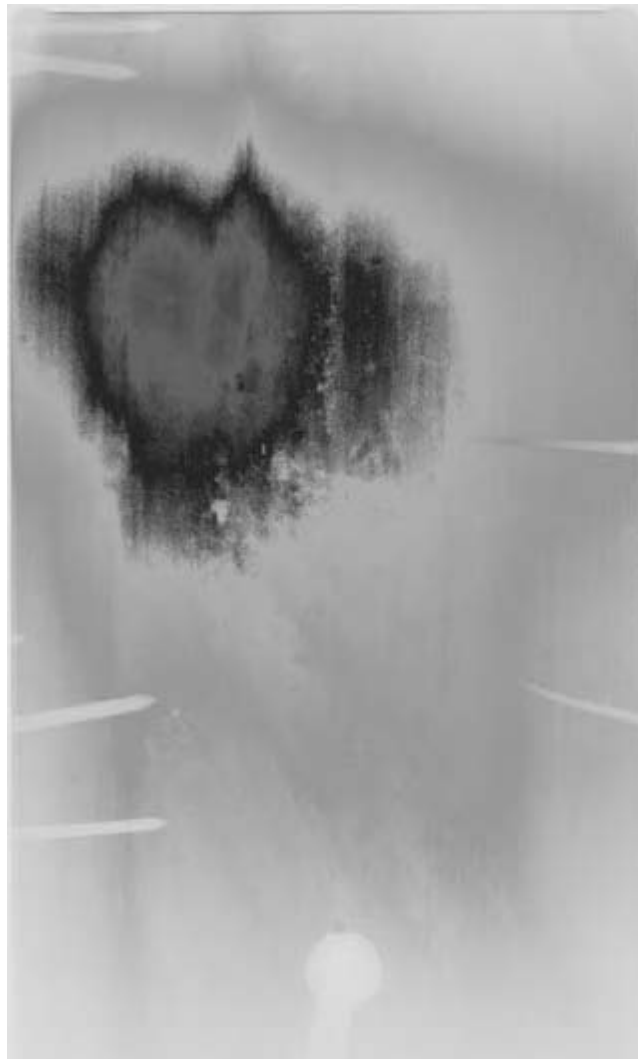
8.8 Radiograph of simulated termite damage showing measured loss of cross-section at various locations.

8.6 Future research and development

Using image enhancement techniques, effort is underway to enhance digital images to detect areas of deterioration due to decay fungi or insect activity. Techniques being investigated include digital filters that are standard with commercial photography software packages, such as PhotoShop® or PaintShop™ Pro®. Use of stereo-imaging is also being researched so that items (nails, pins) within an image can be properly placed within the thickness of the object.

8.7 Conclusions

Digital radioscopy provides investigators with the means to assess connections and deterioration in timber structures without costly or damaging destructive testing. The type, location, and condition of fasteners can readily be determined. Quantifying the remaining cross-section in timber damaged by termites, decay, or other deterioration is feasible, but additional research is needed for the technique to be more useful to practitioners.



8.9 Radiograph showing the location and size of an internal void in a timber.

8.8 References

American Society for Testing and Materials (1995), 'ASTM D 5625-95, Standard Test Methods for Bolted Connections in Wood and Wood-Based Products', Philadelphia, PA.

Anthony, R.W. (2004), 'Condition assessment of timber using resistance drilling and digital radioscopy', *APT Bulletin* **35**(4), 'Special Focus on Covered Bridges'.

Brown, G.I. (2002), *Invisible Rays: A History of Radioactivity*, Phoenix Mill, UK, Sutton Publishing Limited.

EPA website (2004), http://www.epa.gov/radiation/index.html

Harnsberger, D. (1981), 'In Delorme's manner', *APT Bulletin* **13**(4), 2–8.

Hart, D. (1974), 'X-ray analysis of the Narbonne House', *APT Bulletin* **6**(1), 78–98.

Lang, J. and Middleton, A. (1997), *Radiography of Cultural Material*, Oxford, Butterworth-Heinemann.

Mothershead, J.S. and Stacey, S.S. (1965), 'Applicability of Radiography to Inspection of Wood Products', in *Proceedings of the Second Symposium on Nondestructive Testing of Wood*, Spokane, WA, April.

Wisehart, M.K. (1928), *Marvels of Science: Modern Discoveries and Inventions and the Part They Play in Our Everyday Life,* New York, London, The Century Co.

Wrenn, G. (1976), 'Questions of preservation and a new X-ray investigative technique', in *Preservation and Conservation: Principles and Practices*, *Proceedings of the North American Regional Conference*, Williamsburg, VA, 10–12 September.

9

Visual inspection techniques for bridges and other transportation structures

B.M. PHARES
Iowa State University Bridge Engineering Center, USA

9.1 Introduction

Visual inspection (VI) is the most basic and also the most common method by which bridges and other transportation structures are evaluated. However, although very basic in nature the results of a VI are relied upon at many different decision making levels. As such, these inspections are expected to result in an accurate assessment of a bridge's ability to meet both the safety and serviceability requirements of the traveling public; clearly an important aspect of any bridge management system.

9.2 History of structural inspection in the USA

The first major, concerted bridge construction effort in the USA started with the extensive road construction program mandated by the Federal Highway Act of 1956, which was initiated when President Eisenhower signed the bill creating the National System of Interstate and Defense Highways [1]. During this time, the primary emphasis was placed on the economical construction of new bridges. Consequently during this period, very little effort was put toward safety inspection or preventive maintenance of bridges. In the late 1960s the safety of the bridge network first came into question when the US Highway 35 Silver Bridge, a 2235 ft (680 m) pin-connected link suspension bridge connecting Point Pleasant, West Virginia, and Kanauga, Ohio, suddenly collapsed on 17 December 1967 [2]. This sudden catastrophic collapse, which was the first major failure of a structure since the historic wind-induced failure of the Tacoma Narrows Bridge in 1940, prompted the nationwide recognition of the deterioration of the national bridge network and the need for periodic and consistent bridge evaluations and training of bridge inspectors. As a result, in 1970 the Federal Highway Administration (FHWA) established the National Bridge Inspection Program (NBIP) requiring State highway agencies to inspect their bridges every two years and to submit the inspection results to the

FHWA where they are maintained in the National Bridge Inventory (NBI) database. In the following year, the first National Bridge Inspection Standards (NBIS) were established in cooperation with the American Association of State Highway Officials (AASHO) under the Federal-Aid Highway Act of 1971. This landmark legislation was enacted on 27 April 1971 and set, for the first time in the USA, uniform national standards for bridge inspection and safety evaluation including a national policy related to frequency and qualifications of bridge inspectors, report formats, and inspection and rating procedures [2].

The collapse of the Silver Bridge was certainly a catastrophic disaster that resulted in the loss of 46 lives and disrupted commerce in the Midwestern US for several months. Nonetheless, it was the catalyst for what became a comprehensive bridge safety inspection program that was mandated by the NBIS. Engineers became more knowledgeable about bridge deterioration and, therefore, bridge structures were designed and maintained for better quality and with at least some consideration for future evaluation and maintenance. Also, the Silver Bridge catastrophe highlighted the need to replace and/or rehabilitate bridges or members of bridges before they failed. In response, the Special Bridge Replacement Program (SBRP) was also established under the Federal-Aid Highway Act of 1971 to provide funds to help states replace bridges. It was later expanded for rehabilitative activities and replaced with the Highway Bridge Replacement and Rehabilitation Program (HBRRP) in the Surface Transportation Assistance Act of 1978.

Despite the efforts of these bridge evaluation programs, other unforeseen events resulting in the collapse of bridges continued and periodically necessitated expansion of the bridge evaluation effort. In June 1983, the collapse of a 100-foot (30 m) section of the Mianus River Bridge on Interstate 95 in Greenwich, Connecticut killing three people and critically injuring three others, caused elevated concern regarding fatigue and fracture-critical bridges. The National Transportation Safety Board (NTSB) determined that the failure of the span was caused by an undetected lateral displacement of the hangers in the pin and hanger suspension assembly by corrosion-induced forces that went undetected following the state-of-the-practice inspection procedures. Following this incident, and further investigation, significant research regarding fatigue of steel connections was conducted and special fracture-critical inspections were recommended to be mandated.

Scour-induced failures at the Schoharie Creek Bridge in New York in April 1987 and at the Hatchie River Bridge in Tennessee in April 1989 [2] showed the importance of designing bridge piers to resist scour and illustrated the need to better understand and design for scour effects. Consequently, guidance for scour assessment was provided and an under-

water bridge inspection program for all structures at risk and susceptible to scour damage was initiated.

Since the Federal-Aid Highway Act of 1971, the development of the NBIS and other associated bridge programs has incrementally enhanced bridged evaluation. Overall, approximately $55 billon in HBRRP funding and other sources of funding from Federal and State bridge programs has been allocated and used to improve the condition and safety of the nation's bridges. The following summarizes the major bridge inspection and funding programs and the notable associated changes [3]:

- Federal-Aid Highway Act of 1971
  - Inventory requirements for all bridges on the Federal-aid system
  - Established minimum data collection requirements
  - Established minimum inspector qualifications and inspector training programs
  - Established SBRP
- Surface Transportation Assistance Act of 1978
  - Established HBRRP
  - Extended inventory requirements to all bridges on public roads in excess of 20 feet (6 m)
  - Provided $4.2 billion for the HBRRP over four years
- Highway Improvement Act of 1982
  - Provided $7.1 billion for the HBRRP over four years
- Surface Transportation and Uniform Relocation Assistance Act of 1987
  - Provided $8.2 billion for the HBRRP over five years
  - Added requirements for underwater inspections and fracture critical inspections
  - Allowed increased inspection intervals for certain types of bridges
- Intermodal Surface Transportation Efficiency Act of 1991 (ISTEA-1991)
  - Provided $16.1 billion for the HBRRP over six years
  - Mandated state implementation of a quantitative computerized bridge management system
- National Highway System Designation Act of 1995
  - Repealed mandate for management system implementation
- Transportation Equity Act for the 21st Century (TEA-21, 1998–2003)
  - Provided $20.4 billion in HBRRP funding over six years

In addition to these bridge programs, many standards, manuals, and technical advisories have been developed with respect to bridge inspection. Most of these were developed by the FHWA or the American Association of State Highway and Transportation Officials (AASHTO), formerly known

as the AASHO. A list of the major publications related to bridge inspection and their issue dates follows [2]:

- AASHO *Manual for Maintenance Inspection of Bridges* (1970)
- AASHTO *Manual for Maintenance Inspection of Bridges* (1974, 1978, 1983, and 1993)
- AASHTO *Manual for Condition Evaluation of Bridges* (1994)
- FHWA *National Bridge Inspection Standards* (1971, 1979, and 1988)
- FHWA *Recording and Coding Guide for the Structure Inventory and Appraisal of the Nation's Bridges* (1972, 1979, 1988, 1991, and 1995)
- FHWA *The Bridge Inspector's Manual for Movable Bridges* (1977)
- FHWA *Bridge Inspector's Training Manual 70* (1979)
- FHWA *Culvert Inspection Manual* (about 1979)
- FHWA *Inspection of Fracture Critical Bridge Members* (1986)
- FHWA *Scour at Bridges, a technical advisory* (1988)
- FHWA *Hydraulic Engineering Circular No. 18* (about 1988)
- FHWA *Bridge Inspector's Training Manual 90* (1991)
- FHWA *Engineering Concepts for Bridge Inspectors* (1994)

Areas of concern and emphasis related to bridge safety issues are ever changing and expanding as new problems become apparent and newer bridge types and materials become more common. Yet, one factor remains constant: the ability to effectively evaluate bridge components and materials and to make sound evaluations with accurate ratings is critical to maintaining the safety and efficiency of the transportation system.

9.3 Types of visual inspection

The AASHTO *Manual for Condition Evaluation of Bridges* [4] serves as the standard by which bridges in the USA are evaluated in terms of physical condition, maintenance needs, and load capacity. This manual was developed to provide guidance to bridge owners on establishing a bridge inspection program that conforms to the NBIS. One of the seven chapters describes, in detail, the types of inspection that are typically performed and what the minimum qualifications of inspection personnel must be.

Just as the condition of a bridge changes over its useful life, so too do the type and level of inspection required. In basic terms, the different types of inspections normally completed represent differing levels of intensity and associated frequency. Each of the five general types of inspections commonly called for is described below. It should, however, be pointed out that, depending on the depth of inspection required, some of these inspections may require testing (either non-destructive or destructive) beyond a traditional VI.

9.3.1 Initial inspection

An initial inspection is the first inspection that takes place once an agency takes ownership of a bridge (either following new construction or transfer of ownership from one agency to another). The results of the initial inspection are used to collect the required Structure Inventory and Appraisal (SI&A) data and to establish the baseline condition of the bridge. These are two very important aspects of an initial inspection as they usually become part of the permanent bridge file. It is also usually expected that the initial inspection will identify fracture critical elements and other members that may require special attention in the future.

9.3.2 Routine inspection

Routine inspections are, by far, the most common types of inspections completed on highway bridges. The general goal of a routine inspection is to determine, quantify, and note the general physical condition of the bridge being inspected. Further, a routine inspection is expected to yield information on the functionality of the bridge and to identify any changes that may have occurred since previous inspections. Generally conducted from the deck or from ground level, these inspections must satisfy all the requirements of the NBIS in terms of information collected and the qualifications of the inspection team. Although the entire bridge is generally inspected during a routine inspection, the inspector is expected to focus on those areas identified during previous inspections or through calculations to be critical elements or in need of continued observation. The results of a routine inspection are summarized in brief inspection reports. These inspection reports consist of standard information that is collected and supplemented by photographs and written descriptions. Following an inspection, an inspector may also recommend maintenance or repair actions.

9.3.3 Damage inspection

When a bridge is known to have been damaged, a damage inspection is usually called for to assess the severity of the damage and to determine the need for load restrictions or complete closure. The level of inspection detail needed during a damage inspection is dependent upon the severity and extent of the damage. If significant damage is found, the inspector can generally be expected to make detailed measurements of the damaged members (e.g. level of misalignment, section loss). It is highly desirable for the inspector to have the ability to make engineering calculations in the field specifically related to the need for load restrictions or closure.

9.3.4 In-depth inspection

In-depth inspections, commonly referred to as 'arms-length' inspections, can either be a scheduled inspection or are sometimes called for after a damage inspection. Quite simply the goal of an in-depth inspection is to identify important structural attributes that would not, or could not, be detected during a routine or damage inspection. An in-depth inspection usually, although not always, requires special equipment to allow the inspector to get near the locations to be inspected. Most frequently, the access equipment used will include either a snooper truck or a bucket truck. As such, traffic control is often also needed. When necessary to fully understand the condition of an element, the inspector may need to employ some type of non-destructive testing (magnetic particle test, dye-penetrate test, ultrasonic testing, etc.). Because of the importance of the results of an in-depth inspection, the procedures and results of the inspection must be documented with care and a great deal of detail.

9.3.5 Special inspection

The final category of inspection, a special inspection, is generally very focused in nature and typically used to monitor the condition, or change in condition, of a known or suspected problem. Examples of the need for a special inspection include monitoring foundation settlement and bearing corrosion. A special inspection is generally very limited and precise in scope, consisting of only assessing the problem. To ensure uniformity in the data collected during a special inspection, written guidelines and tasks should be established that explicitly instruct the inspector.

9.4 Qualifications of inspectors

The normal hierarchy of the unit given the responsibility of bridge inspection has at least three levels. The person in charge of the entire inspection unit is typically referred to as something equivalent to an Inspection Program Manager. This person is responsible for the overall operation of the unit. Most highway bridge inspections are completed by teams of inspectors and most of the time the team consists of two members. The team is led by a person designated as the Inspection Team Leader. The Inspection Team Leader is responsible for the conduct of the field inspection and is typically assisted by either an Inspector, an Assistant Inspector, or an Inspection Helper.

9.4.1 Inspection Program Manager

The Inspection Program Manager is the person responsible for the overall bridge inspection unit. This person serves as a supervisor to all other

members of the unit and should also be the technical leader of the group. In general, the person in this position should have a good understanding of bridge engineering with specific knowledge of highway bridge design, load rating, maintenance, and other areas. In some cases, the Inspection Program Manager may need to make immediate, engineering-based decisions to ensure the safety of the traveling public. The Inspection Program Manager must have the following minimum qualifications:

- be a registered professional engineer (PE); or
- be qualified to be a PE in the state in which the inspection is completed; or
- have a minimum of 10 years of bridge inspection experience and have also completed a training course based on the *Bridge Inspector's Training Manual* [2].

9.4.2 Inspection Team Leader

The Inspection Team Leader is the person in charge of the on-site inspection activities and is responsible for the reporting of inspection results. Generally, the Inspection Team Leader plans the inspection (including needed traffic control, etc.) and dictates the procedures that will be followed and techniques that will be used. At least one person with the qualifications of an Inspection Team Leader should be present at the bridge at all times. The minimum qualifications for an Inspection Team Leader are as follows:

- have the qualifications necessary to be the Inspection Program Manager; or
- have a minimum of five years of bridge inspection experience and have also completed a training course based on the *Bridge Inspector's Training Manual*; or
- be certified at either the NICET Level III or IV for bridge safety inspection.

9.5 Inspection tools

One might assume that the only inspection tools that a visual inspection requires would be the inspector's eyes. While it is true that the vision of the inspector is the main tool used, there are other common tools that are also very important. It is interesting to note, however, that although the inspector's most commonly used tool is his or her eyes, there really are no requirements for bridge inspectors to have a minimum level of visual acuity. Further, there do not appear to be any requirements related to color vision deficiencies.

Although each inspector will develop an individual 'tool bag', the general types of inspection tools used by most inspectors are summarized in the *Bridge Inspector's Training Manual* [2]. The following summarizes some of the typical tools that a visual inspector would commonly employ. Because bridges operate in the natural environment, they are exposed to all types of dirt, debris, and plant growth that can inhibit an inspector's ability to visually observe portions of a bridge. As a result, an inspector must be prepared with field-durable cleaning tools such as wisk brooms, wire brushes, small scrapers, and shovels.

Sometimes deterioration that should be identified by an inspector lies just below the surface; as such, the inspector should always be prepared to do some light probing with hand tools. Typical probing activities might include using a knife or a probe to investigate the soundness of a material, using a small drill or a boring device to check for internal deterioration of timber, and using a masonry hammer for concrete sounding (note: concrete sounding is one example of when an inspector must rely upon a sense other than vision).

Bridges are large objects that cover large amounts of land area and usually cross some type of an obstruction. Thus, visual inspectors frequently find that some areas of a bridge are not sufficiently visible without some type of visual aid or enhancement. Tools used to improve the inspector's ability to view a structure generally fall into three general types: those that enhance an inspector's view from a large distance (e.g. binoculars), those that improve an inspector's close-up view of a small area (e.g. magnifying glass), and those that generally improve an inspector's ability to view the object (e.g. flashlight, inspection mirrors).

Besides identifying areas of a bridge that present a potential safety hazard to the traveling public and also recommending needed maintenance actions, some of the most critical information that an inspector can collect is direct measurements of the overall bridge and individual elements. To make the needed measurements, the inspector will typically need to rely on a variety of measurement tools including a short (less than 25 ft) (7.5 m) tape measure, a long (usually 100 ft) (30 m) tape measure, callipers, crack width gage, tiltmeter and/or protractor, thermometer, and a level (either 2 or 4 ft (0.6/1.2 m) in length). In addition, the inspector may find a plumb bob useful for assessing vertical alignment.

Without proper and complete documentation, the results of an inspection are basically useless. As such, a bridge inspector should always have the tools needed to provide full and complete documentation. Typically, an inspector will need a place to keep written descriptions of the observations made, places to make detailed and rough sketches, and will need a camera(s) to provide visual documentation (the inspector needs to be able to take long-term documentation photographs and also be able to take photographs of situations requiring immediate attention). To increase

the efficiency and comfort of an inspector, a variety of other tools may be needed. Items such as clamps and penetrating oil may be useful in various situations.

9.6 Reliability and accuracy of visual inspection of highway bridges

Because the physics and concepts associated with VI are relatively easy to understand (an inspector visually observes a bridge and notes information specifically related to the bridge's condition), a study of the reliability of VI of Highway Bridges [5] will be used to summarize the capabilities and limitations of a VI. This study, conducted from 1998 to 2001 at the FHWA Nondestructive Validation Center (NDEVC), aimed to quantify the reliability of VI because no other critical examination existed. This study was deemed to be important because VI is relied upon very heavily to assess the condition of the nation's bridges and also because VI is the baseline technique which other inspection methods should improve upon. During this study, 49 practising bridge inspectors from 25 states were asked to inspect the same set of bridges. The bridges that were the subject of the study were thought to be representative of the general types of bridges in the USA with conditions that varied from 'like new' to 'heavily deteriorated'. During the study the inspectors were asked to complete both routine and in-depth inspections following the general definitions given previously. The inspectors were observed, but not assisted, by trained research engineers. These research engineers noted the types of inspection activities conducted as well as the manner in which they completed them. To ensure that inspectors would not be influenced by previous inspection results, they were not provided with previous inspection reports and were asked to not alter the condition of the bridges as they completed their inspection.

9.6.1 The 'typical' inspector

Because one of the goals of the VI reliability study was to try to identify attributes of the inspector and/or the inspection environment that influence the reliability of inspections, a significant amount of information was collected about the inspectors participating in the study. This information, which was collected through both written questions and vision tests, was very important as the researchers evaluated the inspection results. When the sample of inspector characteristics are considered together, one can get a sense of what the 'typical' inspector is like. Although the study could not definitively show this, it is believed that the group of inspectors

participating in the study was generally typical of the inspectors within an individual state.

The inspectors participating in the case study averaged 41 years of age (range of 28 to 54) and nearly all considered themselves to be in 'average' to 'superior' physical condition. However, approximately 35% indicated that they had some type of orthopedic ailment which could generally be classified as having bad knees, bad shoulders, or a bad back. When asked how frequently they felt so 'tired or winded' during an inspection that they needed to work slower or temporarily stop working, 18% indicated 'Never', 69% indicated 'Very Rarely', and 13% indicated 'Sometimes'.

When asked if they 'assess the importance to public safety' of the inspections they perform, over 93% indicated 'yes'. However, 7% responded 'no', which indicates that some inspectors may have other motivations. Similarly, when asked to assess how important their work was to public safety, 59% indicated 'Essential', 39% indicated 'Very Important', and 2% indicated 'Important'. In this case, no inspectors indicated either 'Not at all' or 'Slightly Important'. Generally, the inspectors participating in the study indicated that they were generally 'Somewhat Focused' during an inspection and found inspection work to be either 'Somewhat Interesting' or 'Very Interesting'.

Because bridge inspections must generally be completed near traffic, from high places, and in various types of weather conditions, a series of situations were presented to the participating inspectors. Generally, it was found that inspectors are concerned, although not terrified, with working from access equipment when it is windy. Similarly, most inspectors appear to be unaffected by working in enclosed spaces where there is limited light available. The inspectors were, by far, most concerned about the dangers associated with passing traffic.

Thirty-seven inspectors indicated that they had completed some type of State-run bridge inspection training program and 32 inspectors indicated that they had received 'apprentice' type training from experienced inspectors. Ten inspectors indicated some type of 'other' State training. One inspector listed the Internet as a source of training. Twenty-eight inspectors indicated that they had completed the Bridge Inspector's Training Course Part I, while 35 indicated that they had completed Part II. Thirty-five inspectors indicated that they had also completed the course on the inspection of fracture-critical members. Only 21 inspectors had completed the refresher course, while 25 had completed the training course on the use of nondestructive testing (NDT) for steel bridges. Eleven inspectors indicated that they had completed the FHWA training course on culvert design and six inspectors listed some type of 'Other' FHWA training. Table 9.1 summarizes the highest completed traditional education level of the inspectors participating in the study.

Table 9.1 Inspector general education level

Education level	Number of inspectors
Some High School	0
High School Degree or equivalent	10
Some Trade School	2
Trade School Degree	0
Some College	9
Associate's Degree	
CE Technology	3
Other	7
Bachelor's Degree	
Civil Engineering	12
Other	4
Some Graduate Work	
Civil Engineering	1
Other	0
Master's Degree	
Civil Engineering	1
Other	0
Terminal Degree	
Civil Engineering	0
Other	0
Other	0

The average inspector indicated having just over 10 years of experience in bridge inspection (standard deviation of 6.1 years) and approximately 11.5 years of experience in the general area of highway structures (standard deviation of 7.6 years). The minimum experience that any inspector indicated was under 1 year and the maximum was 26 years in bridge inspection and 32 years in highway structures. Eleven of the participating inspectors also indicated that they had been an inspector in another industry.

In general, inspectors had what could be considered 'normal' near and distance visual acuity. Note that inspectors were allowed to use corrective lenses that they ordinarily would use. However, there was enough variation in the vision test results to be able to say that inspector vision is not necessarily 20/20. In two cases, an inspector had very poor visual acuity (i.e. 20/160 or worse) in one eye. However, those two inspectors had better than 20/20 vision (both near and distance) in the other eye.

Approximately 10% of the general population exhibits some form of color vision deficiency. Consistent with this, the results of the color vision tests administered for this study indicated that 5 of the 49 inspectors showed signs of a color vision deficiency. Of these five inspectors, two showed signs of protan (i.e. red) color vision deficiency, one showed signs of deutan (i.e. green) color vision deficiency, one showed signs of tritan (i.e. blue) color

vision deficiency, and one showed signs of all three types of color vision deficiencies.

9.6.2 Routine inspections

To study the reliability and accuracy of routine inspections, the 49 inspectors were asked to complete seven routine inspections on seven bridges located in Pennsylvania and Northern Virginia. These bridges ranged from approximately 60 years old to nearly new condition. In terms of construction type, the bridges had both concrete and steel superstructures with bridge types that could be classified as rigid frame, t-beam, or girder plus slab. One bridge was considered fracture critical with traffic volumes ranging from nearly zero to heavy and continuous. In all cases, the inspectors were asked to provide condition ratings for the primary bridge components (i.e. deck, superstructure, and substructure) within a prescribed time limit.

Inspection procedures observed during the study could be summarized in three broad classifications. First, the inspector's ability to identify important structural attributes and probable structural deterioration modes was examined. This was accomplished through a series of questions posed to each inspector prior to the inspector completing each task that asked the inspectors to describe the bridge and to identify expected deterioration modes. The inspectors were generally able to identify the overall structure type. However, most inspectors did not indicate the existence of important structural attributes that may influence how each bridge should be inspected (skew, support conditions, fracture critical members, etc.). In addition, most inspectors indicated that they expected to find some type of general concrete and/or steel deterioration. However, there was little consistency on how the deterioration would specifically be manifested. In some cases the inspectors had no expectations on the possible forms of deterioration they might find.

The second inspection procedure category related to the inspector's methods for completing the inspection. In general, most inspectors visually examined all the primary bridge components (although there was a notable difference in the intensity of the examinations). Inspection tool use was minimal and, as a result, few detailed examinations were completed (sounding, measurement, etc.). Although typically used by fewer than 50% of the inspectors, the most common inspection tools used during the routine inspection tasks included a masonry hammer, flashlight, tape measure, and binoculars.

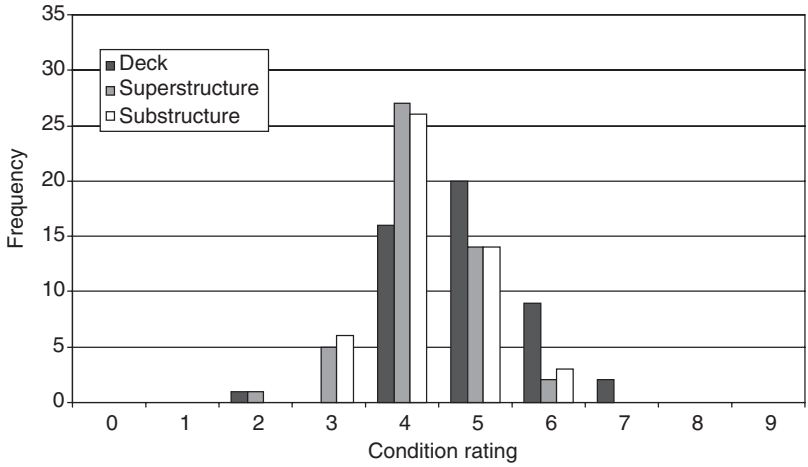
The final inspection procedure category focused on the differences between an inspector's normal practices and those used during these performance trials. Although the inspection tasks were completed in a

somewhat artificial manner (e.g. under observation, within prescribed time limits), the participating inspectors indicated that the tasks were administered and completed in a manner similar to normal routine inspections. Furthermore, the inspectors generally indicated that they were about as thorough as usual and that they exerted a typical amount of effort to complete the tasks. The implication of this is that the inspections completed during this study were completed in a manner similar to the manner in which the inspectors would normally complete an inspection.

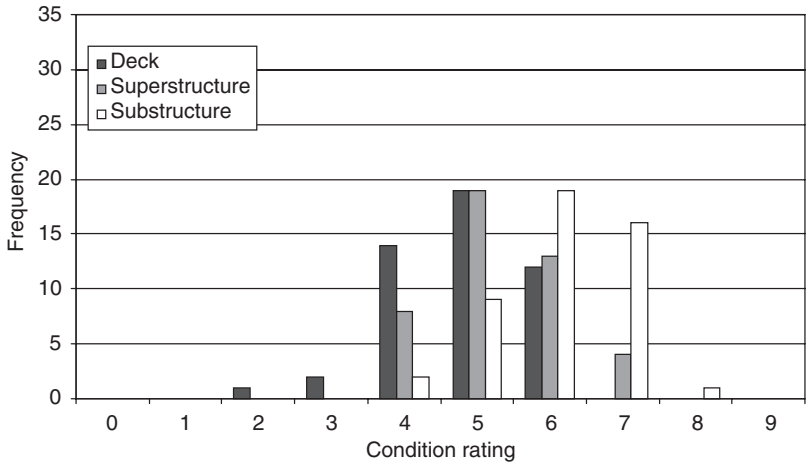
On average, there were between four and five different condition rating values assigned to each primary element. Examples of condition rating assignment frequency are given in Fig. 9.1. In addition, it was found that, even if one does not know what the correct condition rating is, at least 48% of the individual condition ratings for the primary elements were assigned incorrectly, and if the Condition Ratings assigned by the NDEVC staff are considered to be correct, then 58% of the individual ratings were assigned incorrectly. As expected, the distribution of assigned primary element condition ratings was found to be normal, and as a result, it is likely that 95% of the primary element condition ratings assigned by the entire bridge inspector population will vary within approximately two rating points from the average. In other words, 95% of inspection results for the same bridge would be distributed across five different condition ratings. Similarly, only 68% of the population would vary within approximately one rating point from the average (i.e. distributed across three condition ratings).

Overall, primary bridge elements in 'better' condition were rated lower than the condition ratings assigned by the NDEVC staff and 'poorer' condition primary elements were rated higher. In addition, it was found that the greatest dispersion in inspection results resulted from assessments of the bridge substructures and 'poorer' condition elements. Generally, it was also found that inspectors who rated one primary element type higher than the condition ratings assigned by the NDEVC staff also tended to do so for the other element types. A similar relationship was also found to exist between condition rating assignment on 'poorer' and 'better' condition primary elements. Finally, it was also found that as the severity of the deficiencies rises, so does the difficulty in assessing the severity. This difficulty was found to be most prevalent in the assessment of bridge decks.

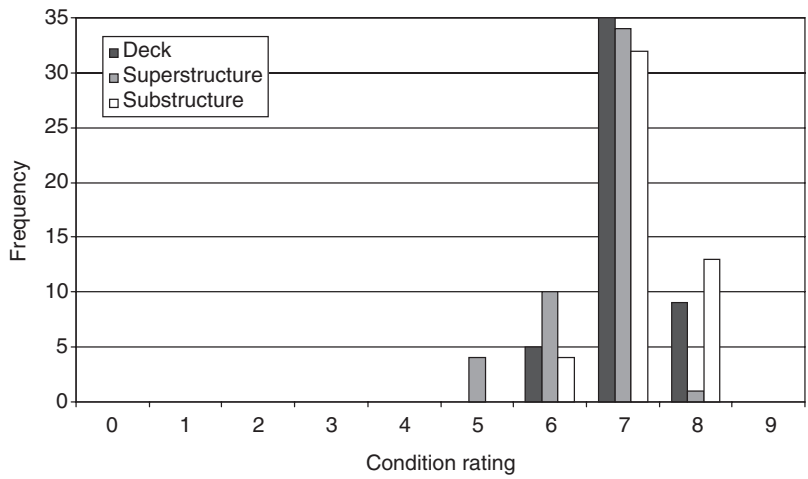
During one inspection the inspectors were provided with a camera with which they could photographically document their observations. The use of photographic documentation varied significantly – both in terms of the number of photographs taken and the items photographed. The most common photographs were of joint deterioration, deterioration of the parapet, an overall elevation view, and a general approach view. All other photographs were taken by fewer than half the inspectors. Interestingly it



(a) Bridge 1



(b) Bridge 2



(c) Bridge 3

9.1. Example cross-section of condition rating assignment for three bridges.

was found that neither the amount nor type of photographic documentation captured appeared to influence the assignment of condition ratings. Inspector documentation was also studied in terms of the specific written field notes the inspectors recorded. Of the investigated field notes describing moderate to severe deficiencies, most were taken by more than half the inspectors. However, there was much less consensus on notes describing lower levels of deterioration.

9.6.3 In-depth inspections

To study the accuracy of in-depth inspections, the participating inspectors were asked to complete two partial in-depth inspections. The first inspection was of a portion of the superstructure of a moderately deteriorated steel girder/concrete slab bridge. This bridge had both broad-based deterioration (corrosion, loss of section, etc.) as well as specific, localized deterioration (fatigue crack indications, impact damage, etc.). The second inspection was of a portion of a good condition steel girder/concrete slab bridge with difficult access. This bridge had fewer general types of deterioration but had a larger number of fatigue crack indications and loose/missing bolts. To give the inspectors the appropriate access required to complete the inspections, both inspections were completed, at least in part, from a manlift. The first bridge was approximately 35 ft (10 m) high and the second bridge was approximately 55 ft (17 m) high.

Because less quantifiable information was collected about these inspections, the results presented here are quite brief. In general, it was observed that an in-depth inspection will probably reveal coating types of deficiencies in a steel superstructure bridge. This is more likely to be true if the coating deficiency is more severe.

With regard to the more localized, specific defects present in the subject bridges, results show that it is unlikely that an inspector will note the types of deficiencies examined in this study. In every case, fewer than 8% of the inspectors noted these types of defects. In terms of the specific types of defects, it was found that the overall correct identification rate for weld crack indications was approximately 3.9%. Identification of missing/loose bolts was higher, but was correctly identified by only approximately 25% of the participating inspectors.

9.7 Conclusions

VI is relied upon very heavily to ensure the continued safety of the nation's bridges. As there are relatively few bridge failures every year, it appears that VI, as it is currently practised, is part of an effective bridge management system. However, the findings of the study presented above illustrated

some alarming features of VI. First, routine inspections appear to be conducted in many different manners. This tends to result in a wide variety of inspection results. The variability is most obvious, and most important, in the assignment of condition ratings for the primary bridge elements where it was found that condition ratings were found to vary over a range of five (out of a possible ten). In terms of in-depth inspections, it appears that, more often than not, these inspections may not identify the types of deterioration/damage for which they are typically prescribed. For example, it appears unlikely that an in-depth inspection of a steel girder bridge would identify fatigue crack indications that are significant enough to warrant further NDT.

Even considering the limitations of VI illustrated in the NDEVC study, bridge owners should continue relying upon VI as an integral part of the overall management system. However, it is important for bridge owners to realize that VI is not an exact science and that actual conditions may, in some cases, be significantly different from what is reported in an inspection report. Realizing this, the bridge owner should ensure that inspectors are well trained in what features they should be looking for and how the structural characteristics of the bridge influence where damage/deterioration is most likely to occur. It may also be advantageous to implement a process where inspectors do not inspect the same bridges during consecutive inspection cycles. Also, performing regular 'calibration' of all inspectors by having them inspect the same bridge (or better, a group of bridges) and then comparing the inspection results with detailed discussion about differences in the results may help to reduce inconsistency in inspection procedures and results.

9.8 Acknowledgements

The study conducted at the FHWA NDEVC which provided much of the information contained herein was funded by the FHWA through a contract with Wiss, Janney, Elstner Associates. Many individuals were involved in, and contributed significantly to, that study and, as such, deserve special acknowledgement: Mr Mark Moore, Mr Benjamin Graybeal, Mr Dennis Rolander, Dr Glenn Washer, Mr Richard Walther, and Dr Steven Chase.

9.9 References

1. *America's Highways 1776–1976*, Federal Highway Administration, Washington, DC, 1976.
2. *Bridge Inspector's Training Manual/90*, Federal Highway Administration, Washington, DC, 1991.
3. *Status of the Nation's Highways, Bridges, and Transit: Conditions and Performance*, Federal Highway Administration, Washington, DC, 2002.

4. *Manual for Condition Evaluation of Bridges*, American Association of State Highway and Transportation Officials, Washington, DC, 1994.
5. Moore, M.E., Phares, B.M., Graybeal, B.A., Rolander, D.D. and Washer, G.A. 'Reliability of Visual Inspection of Highway Bridges', Federal Highway Administration, Report FHWA-RD-01-020, Washington, DC, 2001.

10

Acoustic emission testing of bridges

K.M. HOLFORD and R.J. LARK
Cardiff University, UK

10.1 Introduction

The theme of this chapter is an overview of the use of the non-destructive technique known as acoustic emission (AE) in the inspection and monitoring of bridge structures. The first section deals with the role of AE in bridge monitoring, firstly outlining the fundamental properties of AE that enable the techniques to be used successfully for this application, followed by a discussion of the major issues involved in the use of this technique and finally a review of applications.

The second section provides an insight into the theoretical aspects of AE that are pertinent in bridge inspection, namely wave modes, attenuation and source location. This section is not intended to fully cover the theory of AE, and the reader is advised to consult the many sources of information listed in Section 10.5 for further theory. This section concludes by outlining how modal AE analysis can provide more information about both the location and the orientation of an AE source.

The third section offers some practical advice for implementing AE inspection, including sensors and instrumentation, procedures and analytical techniques as well as listing sources of advice and some information on standards. Finally conclusions are drawn regarding the current state of the art of the AE technique, its potential in this field and projected trends.

10.2 The role of acoustic emission in bridge monitoring

10.2.1 Fundamental AE

Acoustic emissions are stress waves generated by the mechanical deformation of materials. AE techniques have been widely studied since the pioneering work of Kaiser in 1950. A comprehensive review of the history of AE is given by Droulliard (1996).

In general use, the term 'acoustic emission' is used to describe both the practical technique and the phenomenon upon which it is based. AE differs from other methods of investigating material deformation processes in three significant respects. Firstly, the energy that is detected originates from the specimen itself, rather than being supplied from an external source as in ultrasonic testing. Secondly, AE is capable of detecting the dynamic processes associated with the degradation of structural integrity. Thirdly, a sensor located anywhere in the vicinity of an AE source can often detect and locate the resulting emission: this contrasts with other methods, which largely depend on prior knowledge of the probable location of a discontinuity. The technique cannot, however, be used to provide an instant measure of the level of damage present in a structure.

A vast range of microscopic and macroscopic mechanisms generate AE and emission is often classified into two categories: primary and secondary. The term 'primary' is used to describe emission from sources internal to a material and is commonly associated with microstructural mechanisms such as the dislocation movement and inclusion fracture that can accompany fatigue crack development. 'Secondary', or 'pseudo', emission originates from stress wave sources that are external to a material surface, and describes a vast range of mechanisms, often associated with frictional activity. For example, secondary sources from fatigue are commonly the result of crack face closure, and include crack face fretting, debris grinding and re-weld unsticking. The term 'noise' is often used to describe the presence of secondary AE that impedes detection or isolation of primary sources. In fact, the definition of noise as it is widely used in AE practice is more subjective and usually describes the presence of any emission of no interest or relevance to the study.

Structural AE monitoring has two basic objectives: to detect the presence of emission sources and to provide as much information as possible about the sources originating from damage mechanisms. In the presence of background noise, this is possible only if the emission of interest can be identified and analysed. The key procedures are:

- source location;
- source identification;
- severity assessment.

The predominant method of AE source location is the time-of-arrival (TOA) technique. This develops the arrival delay, based on first threshold crossing, of a particular signal between a network of two or more sensors at different distances from the source and uses a measure of the propagation velocity in a material to derive the source location in one, two or three dimensions. The procedure is well established and is described further in Section 10.3.1. The TOA method is, however, subject to several limitations

that affect its suitability to certain aspects of structural monitoring; these are primarily considerations of accuracy, reliability, cost and logistic complexity.

The process of source identification attempts to determine the origin of an emission source; this is addressed by source characterisation techniques. Two approaches to AE source characterisation have emerged. The deterministic, or fundamental, approach attempts to develop quantitative relationships between source parameters and physical measurements of the AE transducer signal. The statistical, or stochastic, approach uses distribution, rate and correlation analysis of AE feature data from a range of different damage sources in samples of interest to compile empirical correlations with measured source properties and behaviour. This information may then be used to attempt to characterise AE data of unknown origin using a range of methods, from simple filtering and inference methods to more complex computational pattern recognition techniques.

Once damage has been located, some measure of its severity is required so that the need for subsequent maintenance can be assessed. The method of severity assessment may be qualitative or quantitative and varies depending upon the nature of the damage. If the damage is visible, one measure of severity is a measure of its size by visual inspection. This size may then be assessed against acceptance criteria and engineering judgement of the overall criticality of the damaged component or site. If the damage is not visible, local AE monitoring must be used. Qualitative measures of activity and intensity may be made if primary emission can be reliably identified and in some cases, if crack face closure processes generate sufficient secondary emission, it may be possible to estimate crack lengths. However, this is a particularly complex task given the difficulty of differentiating between primary and secondary emissions.

More quantitative aspects of severity assessment, such as estimation of damage growth rate, remaining fatigue life or failure prediction are extremely difficult in arbitrary structures and are an ongoing challenge to AE researchers. A wide range of studies have examined the correlation between AE feature data and fracture mechanics parameters in an attempt to provide some measure of damage, a comprehensive review of which is presented by Muravin *et al*. (1993). The common problem in this approach is that such correlations are highly specific to a particular material, specimen geometry and loading regime, and are therefore only valid for the conditions in which they were obtained.

10.2.2 AE issues for bridge monitoring

Perhaps the most important aspect of AE testing is its ability to continually monitor entire sections of a structure *in situ*. As such, the AE technique has

considerable potential for bridge monitoring systems, but any such system must be capable of producing reliable information that does not give rise to false alarms or fail to highlight potential areas of concern. Appropriate methods of AE detection, source location and characterisation are central to this aim.

The validity of the emission data collected governs all subsequent analysis procedures and results. Successful AE monitoring requires a thorough understanding of all the factors that govern the AE process. Simply attaching sensors arbitrarily to a structure and recording the subsequent data is not sufficient. If suitable raw data are to be acquired, the specification and configuration of an AE monitoring system must be tailored around the detection of sources of interest and the requirements for source analysis. The methodology and equipment choice and configuration will vary widely among applications, especially so between local and global studies, where the key objectives differ greatly. Knowledge of the following is vital:

- AE wave propagation and structural acoustics.
- The implications of structural details.
- Identification of the key AE sources of interest.
- The properties of these key AE sources.
- Environmental and structural noise effects.
- The capabilities and limitations of the AE equipment and processing software.

Location methods may be applied in two ways:

- To establish the position of an AE source.
- For spatial discrimination (rejecting/accepting AE from specified regions).

Both of these methods may be used in either global or local monitoring. Source location in global monitoring attempts to identify a particular zone of the structure where suspect emission is present. In local monitoring, source location may be used to attempt to locate specific damage, especially if this is subsurface and cannot be located by visual methods. Conversely, if the position of the damage is known, a source location algorithm may be used in reverse as a discrimination method, whereby only emission from a specific area is accepted as valid damage growth data. The most significant challenge of source location is in global monitoring. Most AE sources can be readily located if data are received on the requisite number of sensors. However, in light of economic constraints, it is desirable to minimise the number of sensors used to monitor the structure. This limits the hardware investment and the expense of mounting and maintaining the equipment; it also reduces the logistic complexity of installing the instrumentation.

A reduction in the number of sensors used may be achieved in two ways: by carefully targeting critical zones of the structure where the flaws of interest are most likely to occur, or by increasing the sensor spacing. Both methods require a thorough understanding of the history and behaviour of the structure in question, all aspects of source detection and the capabilities of the source location algorithms used. Therefore, in global monitoring, sensor configuration is a carefully judged compromise between system sensitivity and cost. This is not usually the case in local monitoring where the sensors are in much closer proximity to a source and can be used for source location with a high degree of confidence.

10.2.3 Review of applications

One of the first applications of modern AE monitoring to bridges was that reported by Pollock and Smith (1972), in which a portable military bridge was tested by the British Army. During the test, a bridge girder was instrumented with seven transducers configured for linear discontinuity location. Emission during loading and load hold periods was recorded, and an analysis of AE amplitude distributions and source location was made. AE sources were attributed to locations where plastic deformation had occurred. Tests during the 1970s highlighted the problem of mechanical noise interference, but the feasibility of a central monitoring system to perform AE signature analysis from sensors located around a bridge was demonstrated by work undertaken for the Federal Highway Administration (FHWA) (Hutton and Skorpik 1975, 1978).

From 1982 the Kentucky Transportation Research Program used an Acoustic Emission Weld Monitor (AEWM), originally developed to monitor in-process welding operations, to detect local crack activity in steel bridges (Prine and Hopwood 1985; Hopwood and Prine 1985). The system subjected consecutive AE events to statistical characterisation methods, based on simple filtering of feature data, rate and time of arrival criteria. Over a four-year period, 13 tests were conducted on nine different bridges. During these tests, the AEWM was used to monitor visible cracks, ultrasonic subsurface discontinuity indications, stress intensifying weld details and bolted joints. The system detected AE activity from visible cracks on three occasions, and in one case from a subsurface ultrasonic discontinuity indication. Preliminary data indicated a correlation between fatigue crack activity, vehicle loading and AE activity. In some instances, extended monitoring of large surface cracks did not reveal any crack growth AE activity, an observation that was confirmed by long-term visual inspection.

Widely varying noise levels were encountered during the tests, and were found to depend on the structural details present near the monitoring site

and the nature of the traffic loading. Traffic-related noise was found to depend not only on the volume, but also on the speed and weight of a vehicle. Heavy vehicles travelling at speeds generated high noise levels, but were best at triggering AE activity. The AEWM was generally successful in rejecting the large amounts of mechanical noise arising from traffic loading and environmental effects, although the fact that the noise rejection model may exclude some valid emission data was recognised.

A series of tests conducted by Physical Acoustics Corporation for the FHWA examined the use of AE for testing the effectiveness of retrofits and finding new cracks. This study highlighted the need for source location and guard sensors to reject unwanted noise emission (Carlyle and Leaird 1992; Carlyle 1993; Carlyle and Ely 1993) and has provided the foundations for standard guidelines for the application of AE to the in-service inspection of steel bridges (Physical Acoustics corp. 1995). In the UK, similar procedures have been investigated and developed by Carter and Holford (1996, 1998), Pullin *et al*. (1999a,b) and Watson *et al*. (2000), and what now exists is an established approach for both the global and local structural integrity monitoring of steel bridges.

For concrete structures there is not such a wealth of established precedence, and what there is is primarily based on the work of Ohtsu and Yuyama in Japan (Yuyama *et al*. 1999). This includes using AE to diagnose concrete failure mechanisms (Ohtsu 1987), quantifying microfracture (Yuyama *et al*. 1988) and assessing the condition of damaged or repaired concrete structures (Murakami and Yuyama 1986; Yuyama *et al*. 1992; Matsuyama *et al*. 1994; Kamada *et al*. 1996).

As the world's concrete bridge stock has begun to age and assessment tools have become increasingly important, the amount of research into the use of AE for monitoring concrete has increased. Landis and Shah (1995) examined signal attenuation through concrete, work that has been continued by Bradshaw (2003) and Beck (2004). Paulson and Elliott (2000) and Cullington *et al*. (2001) have used the technology to monitor the condition of post-tensioned cables in prestressed concrete bridges and Beck *et al*. (2003) and Pullin *et al*. (2003, 2004) describe the application of AE monitoring to both reinforced concrete laboratory specimens and in-service reinforced concrete bridge structures. The latter clearly demonstrate the potential of the technique, but a number of practical issues remain to be resolved if it is to be generally accepted as reliable.

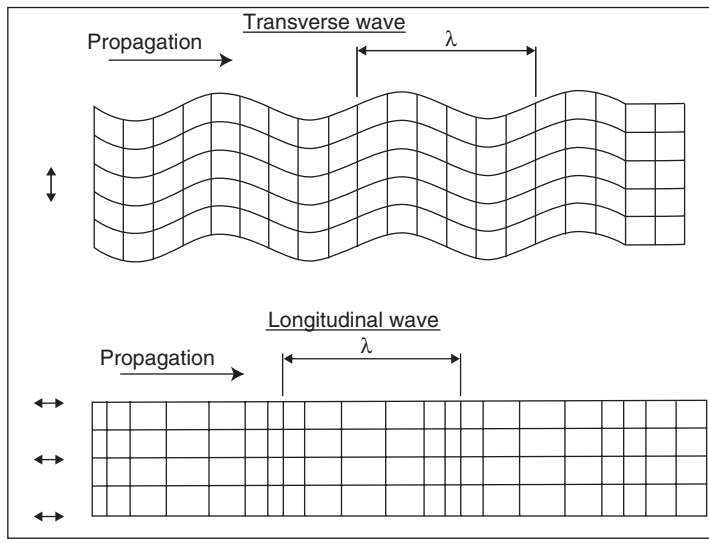
Another application of AE to concrete bridges has been the inspection of reinforcement corrosion. Dun *et al*. (1984) looked at the possibility of this application of the technique, but it has only been more recently that attempts have been made to develop the approach into a practical tool (Ing *et al*. 2003).

10.3 Acoustic emission theory

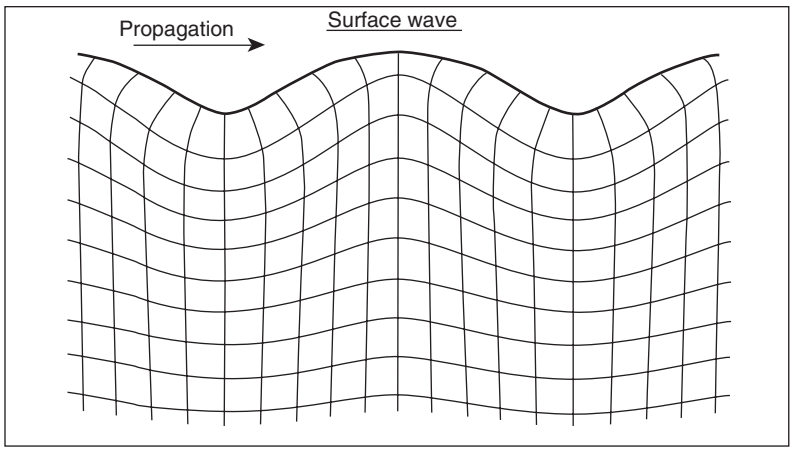
10.3.1 Wave modes

The propagation of acoustic waves in solid media is highly complex, but can be categorised into four principal modes according to the way in which the particles oscillate; namely, longitudinal (compression), transverse (shear), surface and plate waves. In an infinite medium elastic waves propagate as bulk waves in two basic modes; longitudinal waves and transverse waves, each with a characteristic velocity that can be calculated from the density and elastic constants of the solid. The particle motion in a longitudinal wave is parallel to the direction of propagation, whereas transverse waves are characterised by a particle motion perpendicular to the direction of propagation. Longitudinal waves can be generated in liquids, as well as solids because the energy travels through the atomic structure by a series of comparison and expansion (rarefaction) movements. Transverse (shear) waves are not effectively propagated in liquids or gasses; they are relatively weak when compared with longitudinal waves and, in fact, are usually generated in materials using some of the energy from longitudinal waves. These two basic forms are illustrated in Fig. 10.1.

If a surface or boundary is introduced, the longitudinal and transverse waves that propagate in the bulk of the material combine in the region close to the surface; a compression produces a transverse displacement in accordance with Poisson's ratio of the material so that the overall particle



10.1 The two basic wave modes in a solid (Rindorf 1981).

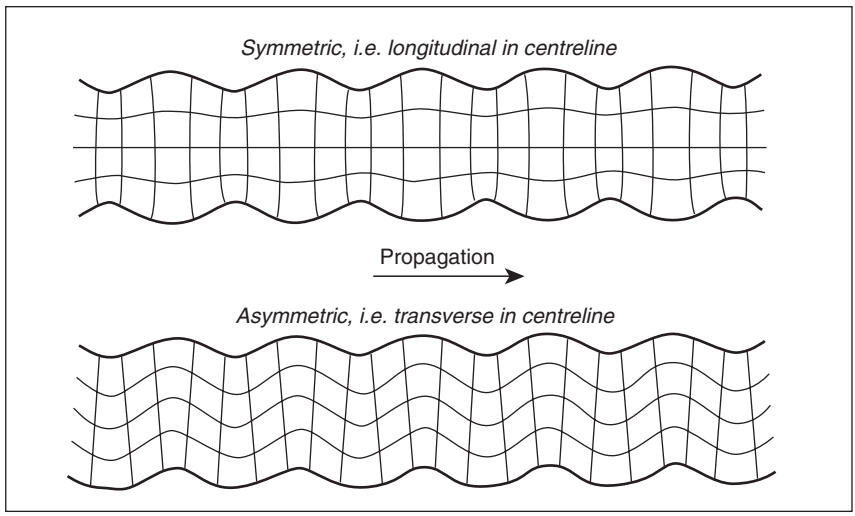


10.2 Rayleigh wave particle motion (Rindorf 1981).

motion is neither purely longitudinal nor transverse. This type of surface wave, shown in Fig. 10.2, is called a Rayleigh wave. The characteristic velocity of Rayleigh waves can also be calculated from the physical constants of the propagation medium and is generally slower than either of the bulk wave velocities. Rayleigh waves travel the surface of a relatively thick solid material penetrating to a depth of one wavelength. Rayleigh waves are useful in ultrasonic inspection because they are very sensitive to surface defects and, since they will follow the surface around, can be useful in examination of areas that other waves might have difficulty reaching.

In a medium bounded by two surfaces, i.e. a plate, at distances greater than a few centimetres from an AE source, surface waves can couple to produce more complex propagation modes called plate waves. These can be Love waves (particle vibration is parallel to plane layer and perpendicular to wave motion) or Lamb waves (particle vibration has a component perpendicular to the surface, i.e. an extensional wave). Lamb waves are commonly used in ultrasonic techniques, where practitioners have the ability to select the frequency of propagation. Lamb waves occur in two basic modes: *symmetric* (S_o) or *extensional* and *asymmetric* (a_o) or *flexural*, although higher order modes can exist (a_1, S_1, etc.). The basic Lamb wave modes are illustrated in Fig. 10.3.

Propagation of Lamb waves depends on density, elastic and material properties of the component, and their behaviour is complex and characterised by dispersion, which depends on the thickness of the plate and the frequency of the wave. For a fixed plate thickness, wave components of different



10.3 Lamb wave modes (Rindorf 1981).

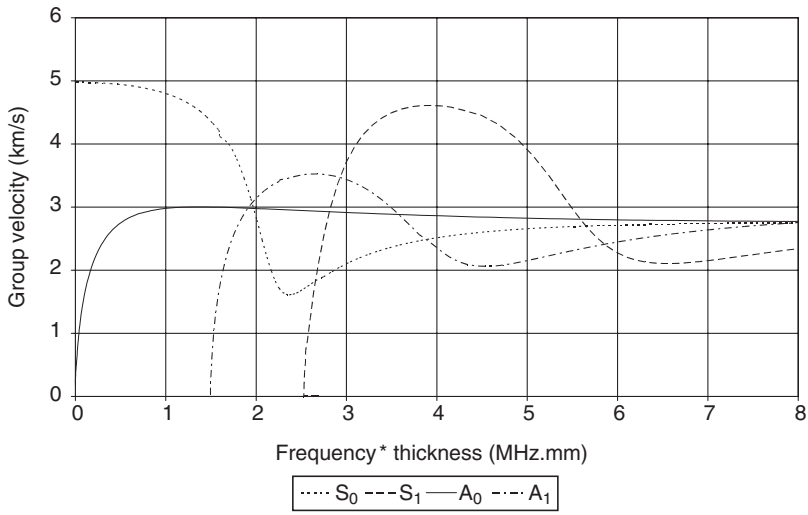
frequency travel at different velocities and a broadband impulse signal appears to separate with increased propagation distance. Dispersion curves, based on solutions to Lamb's homogeneous equation, are used to describe the relationship between velocity and the product of frequency and plate thickness. A typical dispersion curve for steel is shown in Fig. 10.4.

10.3.2 Attenuation

The reduction in AE signal amplitude as a wave propagates is termed *attenuation*. Pollock (1986) attributes attenuation to four principal mechanisms:

- Geometric spreading of the wave front.
- Internal friction.
- Dissipation of the wave into adjacent media.
- Dispersion of signal components.

In the region close to the source (the near field), the dominant attenuation mechanism is geometric spreading of the wave front. In plates, where wave propagation can be considered two-dimensional, the signal amplitude decreases inversely as the square root of the propagation distance. This can give rise to relatively high attenuation levels over the first few centimetres of propagation. Further away from the source (the far field) where the majority of structural AE monitoring measurements are made, attenuation becomes dominated by absorption or conversion of sound energy into heat.



10.4 Dispersion curves in 10 mm steel plate.

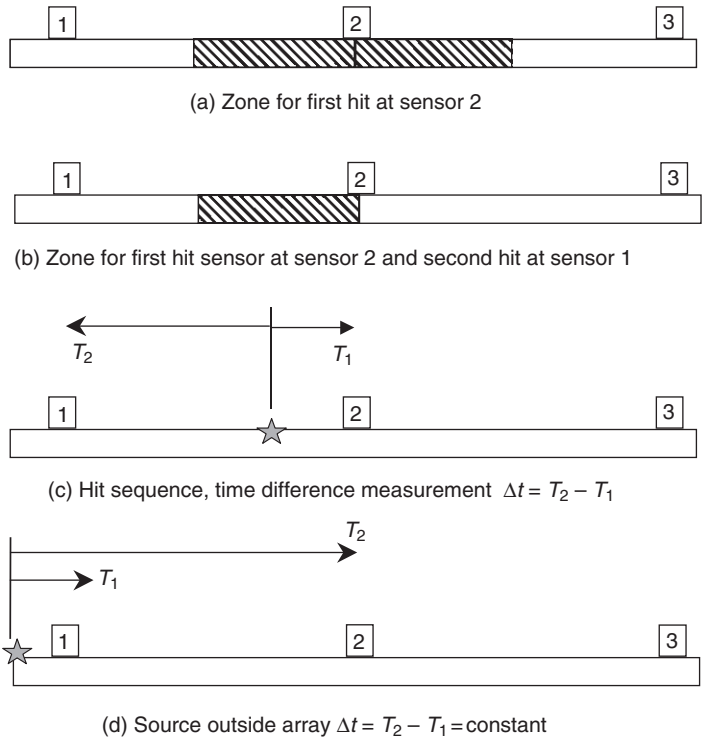
Absorption usually has an exponential relationship with distance and a far-field attenuation coefficient can be calculated, with units of dB per unit distance.

Dissipation attenuation can be caused by inhomogeneities in the propagation medium which scatter the sound wave in the same material, for example grain structure in metals. However, it is most prevalent in specimens in contact with an adjacent liquid, for example a pipe or pressure vessel where energy can propagate readily into the surrounding media.

Attenuation due to velocity dispersion is caused because the different frequency components of a broadband Lamb wave travel at different velocities and the resulting spreading in time causes a loss in amplitude. The magnitude of amplitude loss depends on the slope of the dispersion curves and bandwidth of the signal.

10.3.3 Source location

Source location techniques may be classified by the type of AE source mechanism (continuous or discrete) and include amplitude measurement techniques, such as the zone and attenuation measurement methods, and timing techniques, such as the cross-correlation, coherence and TOA approaches. Some techniques are common to both categories; however, only the pertinent TOA methods for discrete source location are considered here. For further discussion of other techniques the interested reader should consult Baron and Ying (1987). TOA source location



10.5 Linear source location technique (Miller and McIntire, 1996).

techniques are well developed and readily implemented in commercially available AE analysis software routines for use in one, two or three dimensions.

TOA source location in one dimension (linear location)

Many source location applications are concerned with one-dimensional source location, where a single position along a measurement axis is sufficient to define the location of a source, for instance if a defect is anticipated in a weld, or if the component is very long and thin. This is illustrated in Fig. 10.5. If a discrete AE event occurs somewhere along the structure the resulting stress waves propagate in both directions at the same constant velocity. The simplest form of source location would be to note the sensor that received the stress wave signal first (termed the *first-hit*). Referring to Fig. 10.5(a), if the first-hit occurs at sensor 2, then the source lies in the area from a point half-way between sensor 1 and sensor 2 to a point half way between sensor 2 and sensor 3. This area can be reduced somewhat by also

noting the second-hit sensor. If the second-hit sensor is sensor 1, then the source lies between sensor 2 and a point halfway between sensor 1 and sensor 2. For evenly spaced sensors, this halves the potential location region (Fig. 10.5b). This procedure is termed zonal source location, since it only allows identification of an encompassing zone rather than a more exact specification of the source position. However, if not only the hit sequence, but the time difference (arrival delay) between hits is measured (Fig. 10.5c) more precise location can be achieved. If the arrival delay of a signal between sensor 1 and sensor 2 is zero, it would indicate a source sited precisely midway between the two sensors. If the hit sequence is sensor 2, sensor 1 and the arrival delay is equal to the time taken to cross the entire sensor spacing, then the source is located at sensor 2. In general the linear source location is given by equation 10.1:

$$d = 0.5(D - \Delta tV) \qquad [10.1]$$

where d is the source location (measured from first-hit sensor), D is the sensor spacing, V is the wave velocity and Δt is the arrival delay.

Application of linear location is most appropriate when the sensor spacing (along the length of a specimen) is large compared with the specimen depth. As this ratio reduces, sources close to sensors can be incorrectly located if they are distant from the direct axial line through the sensors.

Source location in two dimensions (planar location)

Figure 10.6 shows two sensors mounted on an infinite plane in the presence of stress waves from an AE source. Assuming the signals travel at a constant velocity in all directions:

$$\Delta tV = r_1 - R \qquad [10.2]$$

and

$$Z = R\sin\theta$$

$$Z^2 = r_1^{\,2} - (D - R\cos\theta)^2 \qquad [10.3]$$

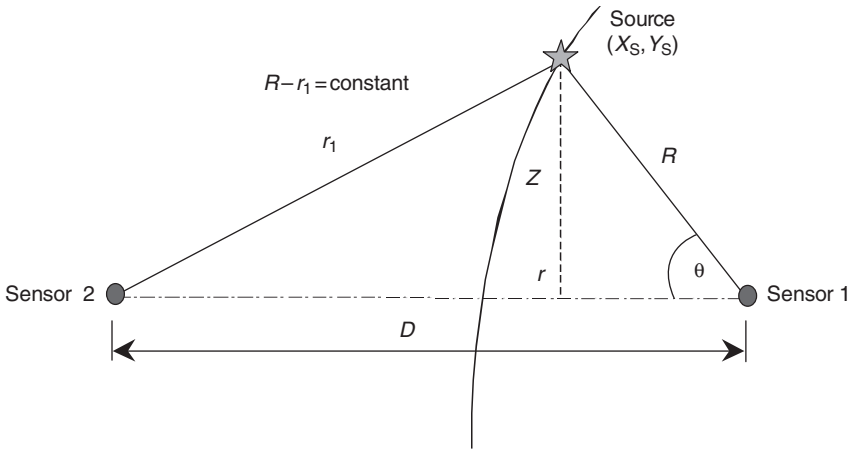
then:

$$R^2\sin^2\theta = r_1^{\,2} - (D - R\cos\theta)^2 \qquad [10.4]$$

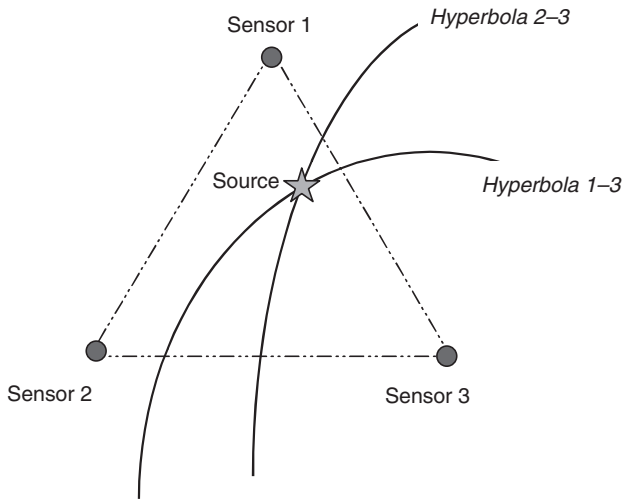
$$R^2 = r_1^{\,2} - D^2 + 2DR\cos\theta \qquad [10.5]$$

Substituting $r_1 = \Delta tV + R$ from equation 10.2 yields:

$$D = \Delta t\left(\frac{C_{\mathrm{HF}}C_{\mathrm{LF}}}{C_{\mathrm{HF}} - C_{\mathrm{LF}}}\right) \qquad [10.6]$$

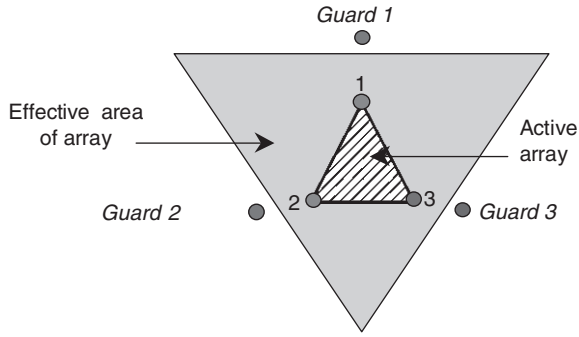


10.6 Source location using two sensors on an infinite plane (Miller and McIntire, 1996).



10.7 Intersection of hyperbolae used to define source position (Miller and McIntire, 1996).

Equation 10.6 is the equation of a hyperbola passing through the source location (X_s, Y_s), i.e. any point on the hyperbola satisfies the sensor hit sequence and arrival delay. This result is generally insufficient for practical two-dimensional source location requirements and a third sensor is necessary in order to determine the coordinates of the source from the intersection of the hyperbolae defined by the measured time delay at other sensor pairs (Fig. 10.7).



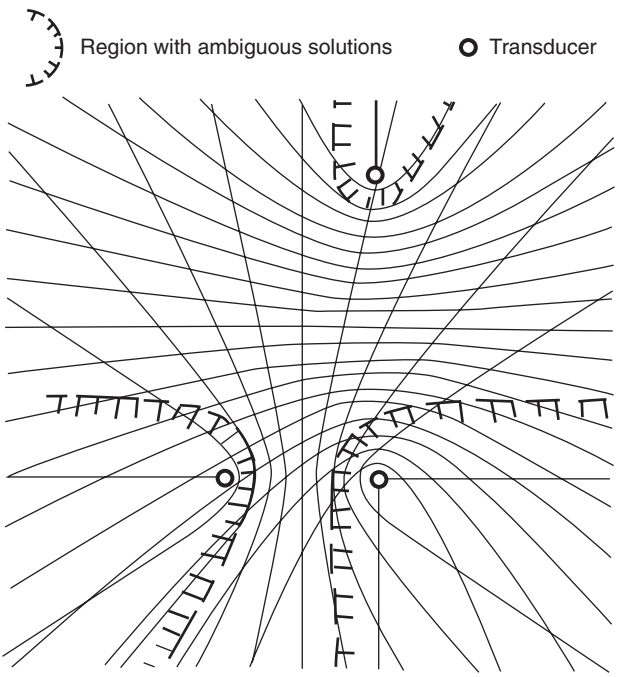
10.8 Restricting the active source location region using guard sensors (Miller and McIntire, 1996).

Source location in three dimensions

Most applications of AE source location are concerned with locating a source in an essentially two-dimensional shell-type structure. However, if the thickness of the specimen is significant relative to the other two dimensions, or if the area of interest is internal to the specimen, then three-dimensional source location is required. One approach is to extrapolate the two-dimensional technique into three dimensions. Each sensor location is defined in full spatial coordinates and the hyperbolae become surfaces. The source location solution in three dimensions is more complex than in the two-dimensional case and is not relevant to this work; the interested reader should therefore consult Tatro *et al*. (1979) for further information. In general, n transducers will yield $n-1$ arrival delay measurements and coordinates. Thus the minimum number of transducers required for linear location is two, three for planar location and four for three-dimensional location.

Restricting the active source location region

The solutions to the source location equations are theoretically valid over the entire area of the surface on which the sensors are mounted. There are practical limitations, but often the area of interest may represent a small area relative to the whole surface, such as a particular weld or fixture. Accepting and processing AE signals from the entire surface may limit the computer processing time available for data from the particular zone of interest and there are significant advantages in rejecting unwanted data as early in the computational process as possible. Also, the geometric arrangement of the structure may tend to cause false location solutions which may be avoided by effectively restricting the operational area of the sensor array. One such method is illustrated in Fig. 10.8, where each active sensor is paired with a guard sensor. If AE is detected so that the first sensor to be



10.9 Regions with ambiguous solutions (Rindorf 1981).

hit is a guard, then that signal is rejected and not processed. Only AE that first hits an active sensor is processed, limiting the operational zone to the shaded area. Note that the guard sensors are used solely to reject data; they do not participate in the source location function. Care must be taken when using guard sensors to ensure that their sensitivities are consistent with the active sensors.

Problems with TOA source location methods

The problems associated with location via time of arrival algorithms are mainly due to ambiguity or measurement error. Ambiguous solutions sometimes arise when the minimum number of transducers is used. In the region close to each transducer there is a certain area in which twin solutions occur. This is shown in Fig. 10.9. Both solutions are physically meaningful; however, to resolve the ambiguity, further information is required. This can be achieved via the addition of an extra sensor which provides a third arrival delay measurement for comparison with the computed source location.

The two main sources of error using TOA source location techniques are premature triggering of the timing measurement by a low-amplitude extensional pre-cursor and dispersion of the flexural mode components.

Dispersion effects can cause arrival timing to be triggered on different phase points of the signal at different sensors, while attenuation of the higher-frequency components can cause erroneous timing, since the lower frequencies travel at lower velocities. These effects can combine to introduce considerable inaccuracy into source location calculations. In large area or zonal source location procedures the effects may be relatively insignificant. However, in local monitoring or spatial filtering applications, which may require more accurate source location information, for example on crack tip AE movement, the degree of error can become unacceptable.

10.3.4 Source location using modal analysis techniques

The dispersion curves of Fig. 10.4 illustrate how, for a fixed plate thickness, different frequency components of Lamb waves travel at different velocities. If the wave is detected in an appropriate manner by a suitably broadband transducer, separation of the different frequency components can be achieved by band pass filtering, and the respective arrival times measured. If the two components travel at different velocities, C_{HF} and C_{LF}, and the time lapse (Δt) between their arrivals is measured, then the source to sensor distance (D) is given by equation 10.7:

$$D = \Delta t\left(\frac{C_{HF}C_{LF}}{C_{HF} - C_{LF}}\right) \qquad [10.7]$$

10.3.5 Source identification using modal AE techniques

The principles of modal AE source identification are based on analysis of the way energy released from an AE source propagates to the sensor. Analytically, it is useful to consider sources in terms of their planar origin. For example, primary AE from crack growth processes originates from sources internal to the specimen; these are broadly termed in-plane (IP) sources, whereas secondary sources, commonly associated with noise and frictional processes, are the result of external interaction with specimen surfaces and are regarded as out-of-plane (OOP) sources.

Considering the planar nature of sources in a plate-like medium, it is logical that particle motion induced by OOP sources would cause the majority of energy to propagate in the flexural mode, whereas IP sources would primarily induce an extensional mode component. Furthermore, given the nature of flexural mode particle displacement, it may be anticipated that in a plate cross-section where crack growth occurs, that the magnitude of the flexural wave will be related to the moment arm of the source with respect to the central axis. Hence, if information on AE wave propagation modes from an unknown source can be recovered from the

frequency and velocity information available from the signal waveform, both a qualitative insight into its origin and a measure of the depth of an IP source, i.e. a crack, is theoretically possible.

10.4 Practical techniques

10.4.1 Sensors and instrumentation

AE instrumentation typically consists of:

- a sensor that converts a stress wave to an electrical signal;
- a low-noise amplifier that raises the signal to a usable level;
- signal processing electronics for feature extraction and waveform capture;
- microprocessor and digital signal processing (DSP)-based parallel distributing processing instrumentation;
- knowledge-based software for easy analysis, defect correlation and development of expert systems that comply with demanding AE standards;
- decision and feedback electronics to utilise the information.

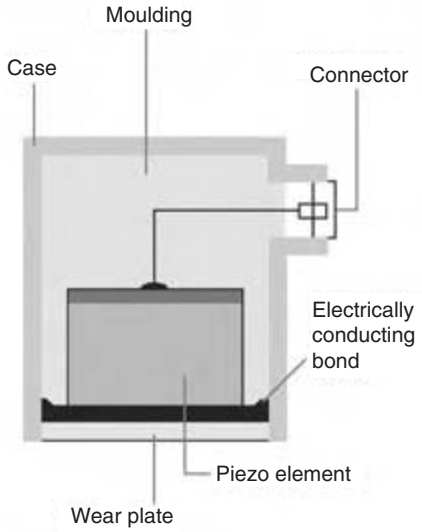
AE sensors

When an AE wave impinges on the surface of a test object, minute movements of the surface molecules occur. The function of AE sensors is to detect this mechanical movement and convert it into a useable electric signal. The main considerations in sensor selection are:

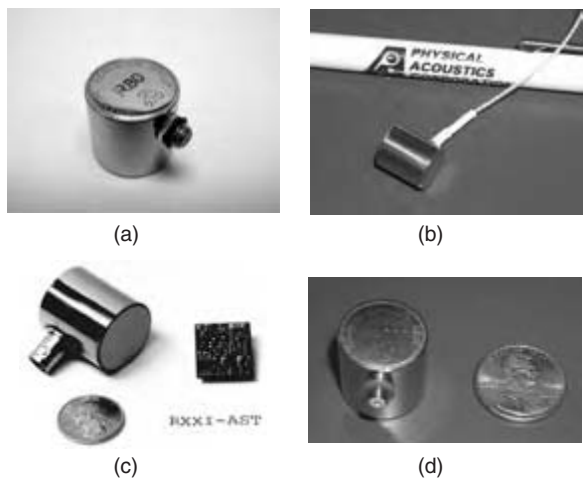
- operating frequency range;
- sensitivity;
- environmental and physical characteristics.

AE sensors can be based on several physical principles including capacitative transduction and laser interferometry; however, AE testing is nearly always performed with sensors that use piezoelectric elements for transduction. Piezoelectric sensors are sensitive and easy to apply, and are available in a wide range of response characteristics at relatively low cost. The construction of a typical AE sensor is illustrated diagrammatically in Fig. 10.10 (Vallen 2002); some commercial sensors are pictured in Fig. 10.11.

Terminology describing the performance of AE transducers is varied and sometimes confusing. The expressions ‘broadband’, ‘wideband’, ‘flat with frequency’, ‘high fidelity’ and ‘resonant’ are often applied to describe transducer performance characteristics. ‘Broadband’ and ‘wideband’ imply high sensitivity over a large frequency range. ‘Resonant’ implies high sensitivity over a narrow frequency range, while ‘flat with frequency’ and ‘high fidelity’



10.10 A typical piezoelectric sensor (Vallen 2002).



10.11 Some commercial AE sensors: (a) general purpose; (b) miniature; (c) integral pre-amplifier; (d) wideband (Courtesy of Physical Acoustics).

imply that there are no resonances over the frequency band of interest. Confusion often arises when the term 'broadband' is used in the context of being 'high fidelity' and 'resonant' is inferred as a transducer having sensitivity over a narrow range of frequencies. In practice, an AE transducer can

exhibit resonances but still be responsive to signals over a broad frequency range. A high-fidelity sensor can have flat response with frequency, but be limited to a narrow frequency range. Generally, if high sensitivity is required, a resonant type transducer is selected.

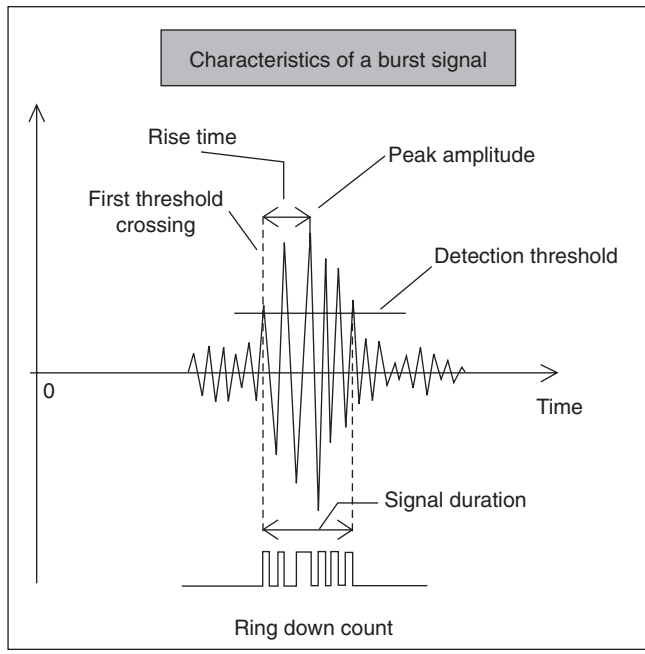
The very small voltage generated across the piezoelectric crystal is increased to a usable electric signal by a preamplifier. This provides the required filtering, gain (usually 40 dB) and cable drive capability. The preamplifier must be located close to the sensor and is often integrated into the sensor housing. In conjunction with sensor selection, filtering in the preamplifier is the primary means of defining the monitoring frequency range of an AE test, although, in modern systems, this is often supplemented by additional 'front end' filters in the signal processing hardware.

In practice, the lower frequency limit of an AE test is governed by background noise and the upper frequency limit is ultimately governed by wave attenuation that restricts the useful detection range. The most common frequency range for AE testing is 100–300 kHz.

AE feature descriptors

After sensing and pre-amplification the signal is transmitted to the main instrument which detects and processes the signal. AE monitoring is usually performed in the presence of background noise. To cope with this an acquisition 'threshold' is set above the background emission level. The threshold defines the minimum amplitude of an AE signal that will be recorded and analysed. Detection of a signal whose peak amplitude exceeds the predetermined threshold on any one channel constitutes a 'Hit', so that each source event may produce one or more hits.

The threshold is the prime variable that controls channel sensitivity. It also serves as a reference for the measurement of some waveform features used to characterise the hit. Five principal AE signal features, illustrated in Fig. 10.12, have become standardised and widely adopted during the past 20 years. AE counts are defined as the number of times the source waveform crosses the acquisition threshold. Counts are a traditional measure of AE activity and depend strongly on the magnitude of the source event, the acoustic properties of the specimen and the frequency response characteristics of the sensor. The amplitude of an AE signal is the value of the highest peak attained by the waveform. Amplitude can be related to the intensity of an AE source and directly determines its detectability. One of the most impressive attributes of AE is the wide range of signal amplitudes that are produced. This large dynamic range can present significant problems in the measurement and analysis of signals; to cope with this most modern AE systems measure the amplitude on a logarithmic scale in decibels (dB); see equation 10.8:



10.12 AE waveform features. (Source: http://www.ndt.net)

$$A = 20\log_{10}\left(\frac{V_s}{V_{ref}}\right) \qquad [10.8]$$

where A is the signal amplitude in dB, V_s is the signal amplitude in μV and V_{ref} is the reference voltage.

10.4.2 Experimental procedures

Sensors are usually supplied with a calibration certificate which should provide a measure of the response to surface displacement or velocity across the frequency spectrum. Commercially available sensors use either the NIST Transient Surface Wave Calibration (ASTM 1992) or the White Noise Continuous Sweep (ASTM 2001), otherwise known as the Face-to-Face technique. Transducers used for acoustic emission measurement are, in general, sensitive to surface motion normal to the surface to which they are attached. In practice, the measured frequency spectrum of an AE source is significantly influenced by both the sensor type and the transmission characteristics of the specimen (i.e. its geometry and acoustic properties). Therefore, a true evaluation of sensor frequency response characteristics in a given test configuration can only be achieved by an *in-situ* calibration of an AE system. A problem that has been studied in some detail is the provi-

sion of an artificial source for this type of procedure. This is important in any practical application, both to ensure results are properly comparable and to verify that the system is responding in a satisfactory way. An extensive study of the calibration of AE sensors has been carried out by the National Physical Laboratory (Esward *et al*. 2002).

A practical technique for mounted sensor sensitivity testing was proposed by Hsu and Breckenridge (1981) and exploits the remarkably repeatable fracture energy of continuous pencil lead. Using a clutch action holder and a constant length of lead, he demonstrated how a cheap and reliable standard source could be produced. In Europe, Nielsen (1980) carried out an extensive test programme and evolved a small guide attachment to the pencil holder, which allows anyone to produce about 80% of breakages within a small energy band. The method, designated the Hsu–Nielsen (H-N), or pencil lead fracture (PLF), source has been widely adopted as a convenient means of checking the frequency response and sensitivity of sensors in a multichannel system. It also provides a useful artificial source for the *in-situ* study of wave propagation effects in large structures.

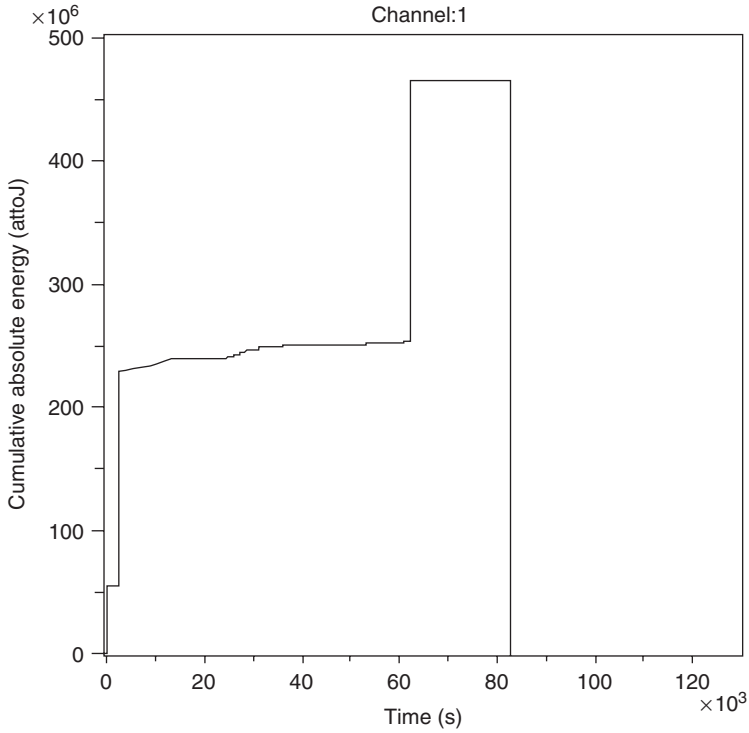
It is vital to use a couplant when mounting AE sensors. A couplant is a general term for any material that aids the transmission of acoustic waves. Care must be taken when choosing a couplant to match it to the type of application, for example, field tests on bridges and other structures that may be exposed to rain or other environmental hazards may degrade the couplant interface by washing the couplant away. If the couplant layer is too thick, or comprises an unsuitable medium that causes excess attenuation, then acoustic sensitivity will be reduced.

Sensors are commonly attached to ferrous specimens via a magnetic clamp that has a spring-loaded mechanism which holds the sensor in firm contact with the specimen surface. On concrete bridges it has proved useful to manufacture small aluminium clamps that can be screw-mounted to the concrete. Alternatively, an epoxy resin or other semi-permanent bond may be used as both an attachment and couplant; however, extreme care must be taken to avoid damaging the sensors when they are removed from the structure.

10.4.3 Analytical techniques

Graphical data displays

Modern software-based hit-driven AE systems present AE data using many types of graphic displays. The operator is not limited to that which can be observed during the test as the presentation techniques can be re-displayed, modified and refined during post-test analysis via user-configurable data filters, display types and parameters. Some of the most commonly used plots are discussed below.

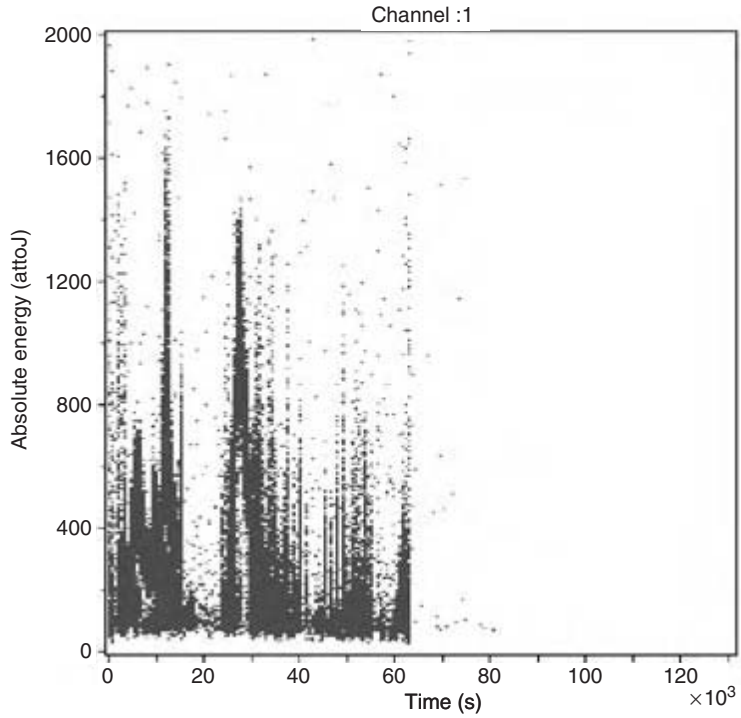


10.13 Cumulative absolute energy recorded with respect to time.

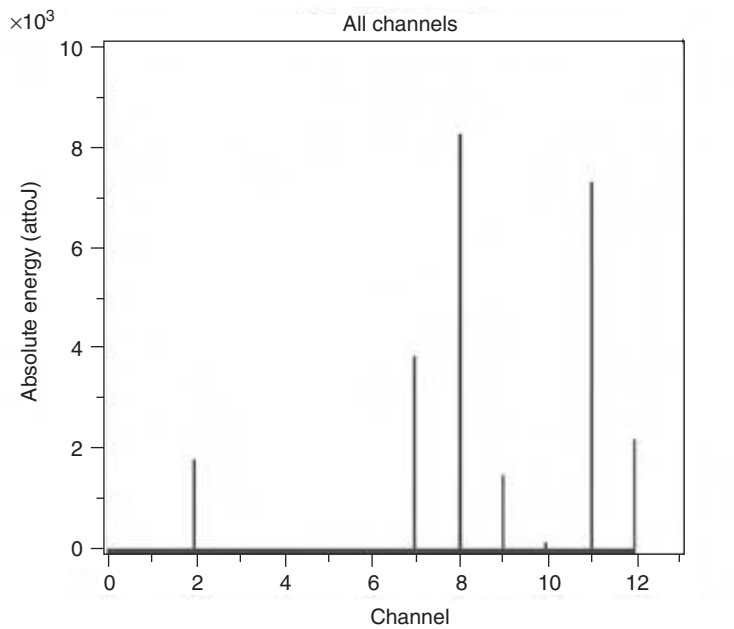
Historical plots – illustrate the change in an AE parameter with time. These are useful in indicating changes in source activity levels. Figures 10.13 and 10.14 illustrate historical plots of AE energy versus time in rate and cumulative form respectively. A cumulative plot is the more convenient format for displaying total emission quantity, while a rate plot highlights changes in activity during a test.

Channel plots – show the distribution of the detected emission on individual channels. Channel plots may be useful in highlighting the most active regions of a structure and can serve as a crude means of source location. An example of a channel-based plot is shown in Fig. 10.15.

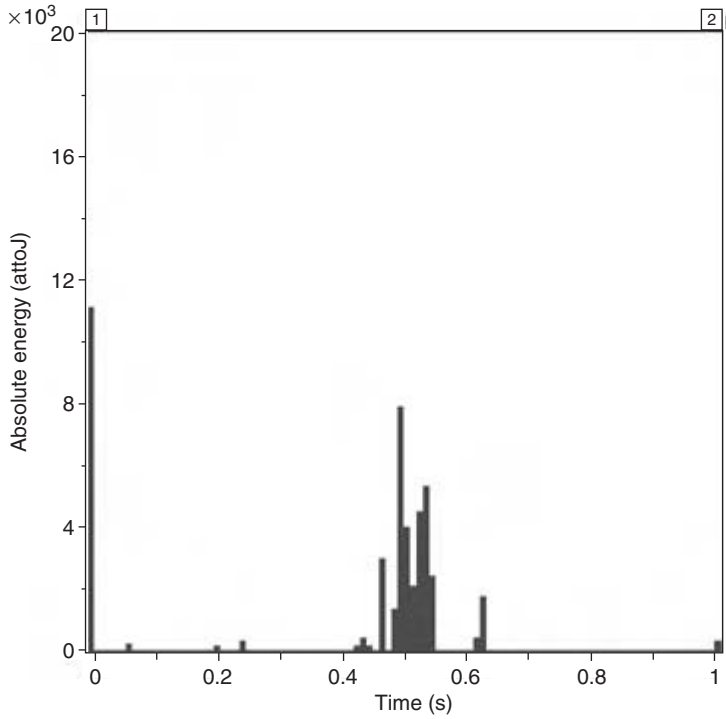
Location displays – display the calculated position of an AE source. Fig. 10.16 shows an example of a linear location plot. Linear location is a one-dimensional location mode plotting parameters of an event against position between sensor pairs. An example of an arbitrary location plot is shown in Fig. 10.17. Arbitrary location is a two-dimensional location mode obtained by plotting an event against its '*x*' and '*y*' position in a defined group of sensors. Unlike other planar location modes, arbitrary location allows the



10.14 Absolute energy recorded with respect to time.



10.15 Channel-based plot of energy.

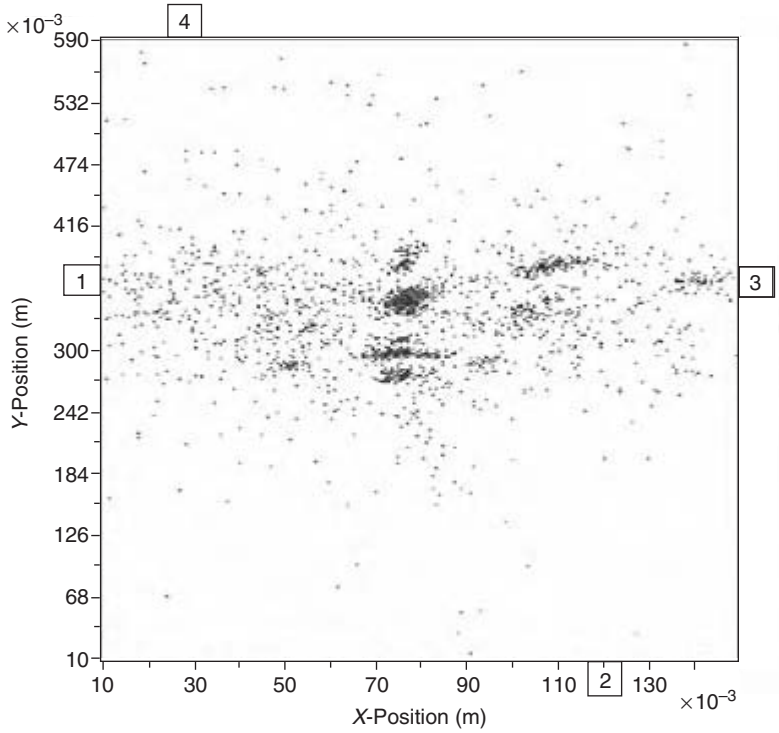


10.16 Example of a linear location plot.

user to configure multiple sensors on a structure in a flexible format, with no restrictions on the configuration of the sensor array. Figure 10.18 displays the same data in a three-dimensional plot showing the relative energy at each position.

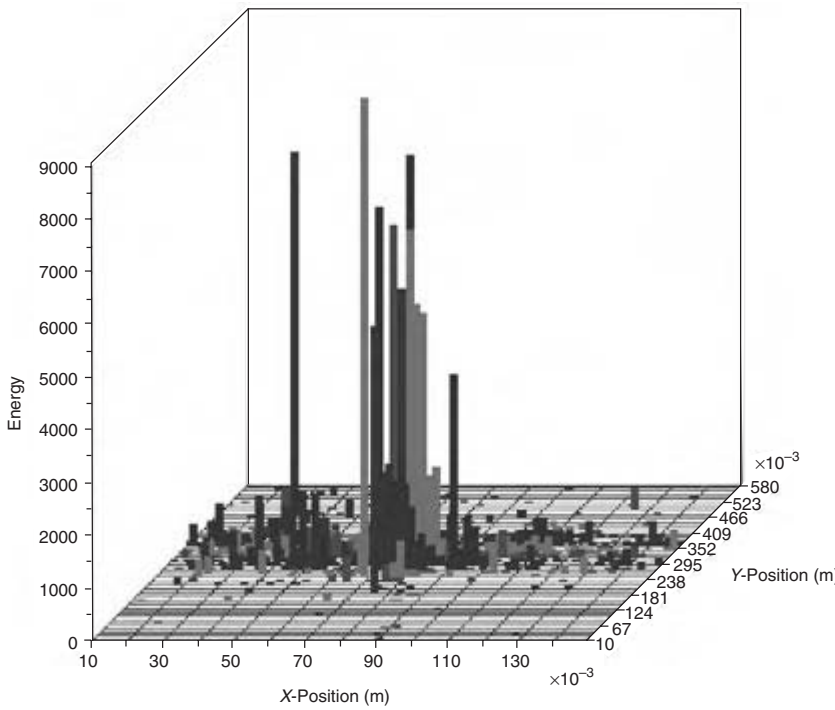
The following terminology is commonly used in AE source location procedures:

- *Hit:* the term used to indicate that a given channel has detected and processed a transient AE signal. The ASTM E-1316 definition of a hit is 'any signal that exceeds the threshold and causes a system channel to accumulate data.'
- *Event:* a single AE source produces a transient mechanical wave that propagates in all directions in a medium. The AE wave is detected in the form of hits on one or more channels. An event is the term given to a group of hits received from an AE source. In the physical sense an event is a single source phenomenon. The ASTM E-1316 definition of an event is 'a local material change giving rise to acoustic emission.'



10.17 Arbitrary location plot of events.

- *Location group:* an array of AE sensors (based on known placement between one another) for the purpose of determining the general or exact location of an event occurring near or within its detection area.
- *Lockout time:* the minimum time following the detection of an event before the analysis software resumes event processing within a location group. This is typically set to the period of time taken for an AE signal to propagate from one sensor in a group to the most distant sensor in the given group. Use of a lockout time is intended to prevent reflections from a single source event being incorrectly identified as new events by the source location algorithm.
- *Velocity:* the speed at which an AE wave propagates from one sensor to another. In some applications it is sufficient to use a velocity provided from a velocity chart for the material being tested. However, the effects of different wave propagation modes and structural geometry make it desirable to measure propagation velocity in a given source location application empirically.

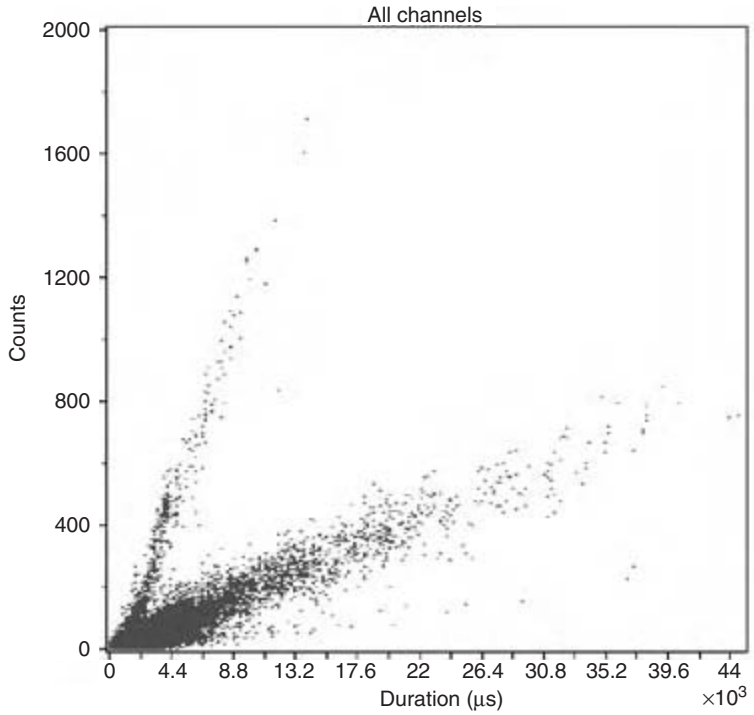


10.18 Arbitrary location plot with respect to energy.

- *Wrap:* in many source location cases the geometry of the structure is such that the sensors can be considered 'wrapped'. A simple example is the case where one-dimensional source location is performed around the circumference of a cylindrical specimen. In this case source location is also performed between the first and last sensor in the location group, i.e. in addition to the first and second sensor, the second and third, etc. In this way, source location around the entire circumference of a specimen can be achieved.

Correlation plots – point plots which show the relationship between a pair of AE parameters. Certain correlation plots, for example counts *vs* duration, as shown in Fig. 10.19, can offer an insight into the number and type of sources present, and in some circumstances may assist in source identification. Figure 10.19 shows an example of a correlation plot produced using the MI-LOC software.

Colour intensity plots – provide an 'at a glance' analysis of an emission population offering improved diagnostic capabilities from a single graph, particularly when large amounts of spurious data are present. They are

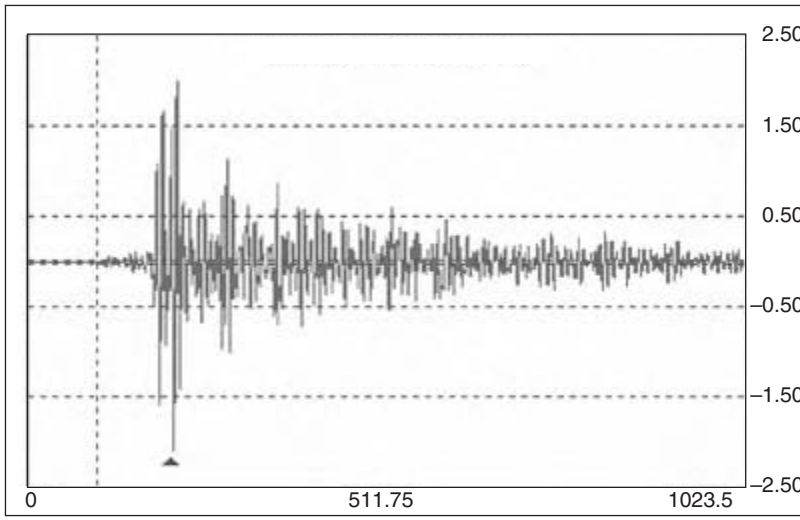


10.19 Correlation plot displaying counts versus duration.

particularly useful in presenting the spatial density of emission in a two-dimensional location plot, or for revealing how AE features are distributed in a correlation plot.

Distribution analysis – the inherently random nature of AE sources, coupled with uncertainties in the paths and wave modes during transmission from source to sensor and instrumentation limitations, forms a strong argument for statistical analysis of AE signals. One type of statistical analysis in widespread use is distribution analysis; this plays an important role in the study of trends in signal amplitude. Two main distribution functions are used to describe the statistical spread of amplitudes within an emission population; these are the differential distribution (which shows the number of hits with particular amplitude) and cumulative distribution (which shows the number of hits that exceed a certain amplitude).

Amplitude distributions can be applied to test data in a range of methods. If the amplitude distribution is presented in real time, then direct observations of the distribution trends plot can be used to provide an indicator of changes in the behaviour or the occurrence of new source mechanisms. For example, a shift towards higher-amplitude emission can indicate the onset



10.20 Time domain representation.

of fatigue crack development. More sophisticated curve fitting routines and distribution models can be used to provide quantitative descriptions of an emission population.

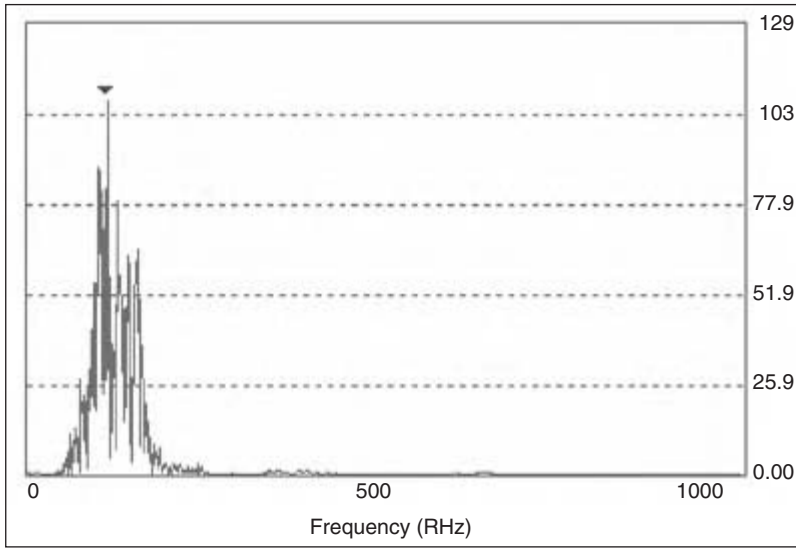
Transient records

Another important tool of AE analysis is the analysis of transient records also known as AE waveforms. Time domain representation of an AE waveform is similar to a trace captured on an oscilloscope; the vertical deflection is the amplitude of the signal in volts, and the horizontal scale is the elapsed time from the trigger point. An example of a waveform display in the time domain is shown in Fig. 10.20. Figure 10.21 shows an example of a frequency domain waveform display. This is the frequency spectrum computed from a fast Fourier transform (FFT) algorithm of the time domain representation. The vertical scale represents the amplitude in dB at that frequency.

10.5 Sources of information and advice

10.5.1 Standards

There are a number of organisations that publish standards connected with acoustic emission testing:



10.21 Frequency domain transient.

- ISO International Organisation for Standardisation
- CEN Comité Européen de Normalisation (European Standardisation Committee)
- ASTM American Society for Testing and Materials
- EWGAE European Working Group on Acoustic Emission
- AFNOR Association Française de Normalisation (French Standardisation Society)
- DGZfP Deutsche Gesellschaft für zerstörungsfreie Prüfung (German Society for Non-destructive Testing)

10.5.2 Websites

The following websites contain information that will benefit both the novice and the advanced practitioner:

- American Society for Nondestructive Testing (ASNT) www.asnt.org
- British Institute of Non-Destructive Testing (BINDT) www.bindt.org
- The Nondestructive Testing Information Analysis Center (NTIAC) www.ntiac.com
- ASTM International www.astm.org
- The e-journal of non-destructive testing www.ndt-ed.org
- Structural Integrity and Damage Assessment Network www.sidanet.org

- Structural Integrity Monitoring Network www.simonet.org
- US Department of Transportation Federal Highways Administration www.fhwa.dot.gove
- Highways Agency www.highways.gov.uk
- International Association for Bridge and Structures Engineering www.iabse.ethz.ch

10.6 Conclusions

AE differs from other methods of investigating material deformation processes in three significant respects. Firstly, the energy that is detected originates from the specimen itself, rather than being supplied from an external source. Secondly, it does not take a 'snap shot' of the condition of a specimen, but instead detects the actual dynamic processes associated with the degradation of structural integrity. Thirdly, a sensor located anywhere in the vicinity of an AE source will both detect and locate the resulting emission. The result is a truly powerful monitoring technique that has considerable potential as a tool to aid bridge inspection and assessment procedures.

In steel structures, global monitoring of emissions generated by normal traffic loading has been used to identify possible sources of damage in both the parent metal and bolted and welded connections. Local monitoring can then be used to characterise the damage, assess its severity and confirm its activity, thereby assisting with the assessment of the criticality of the damage. The presence of noise can complicate this process but the use of guard sensors, appropriate boundary conditions and careful filtering of the emissions can overcome this obstacle.

Similar procedures can be adopted for concrete although, to date, the characterisation of damage caused by the various modes of concrete fracture, bond failure and steel failure are less well defined. It is also clear that concrete severely attenuates acoustic emissions and therefore appropriate sensor selection, spacing and location require further investigation before the technique can be reliably applied to concrete structures on a regular basis.

The goal is for AE to become an integral part of regular bridge inspection regimes. Regular monitoring should enable defect growth to be identified, characterised and quantified. The significance of these defects can then be assessed and the remaining life of the structure investigated. In this way AE can be much more than just another inspection technique: it can become an integral part of asset management procedures for maintaining and extending the life of highway structures.

10.7 Acknowledgements

The authors wish to acknowledge the enormous contribution from Damian Carter, who permitted work from his PhD Thesis (Carter 2000) to be repro-

duced for this chapter. The authors would also like to thank the following researchers from Cardiff University School of Engineering: Dr Rhys Pullin (who has conducted most of the laboratory and field tests described and whose common sense attitude to work keeps it all in perspective), Mr Tim Bradshaw (now with Physical Acoustics), Mr Jon Watson (now with Physical Acoustics) and Dr Aled Davies, who initiated the civil engineering application work. The authors would also like to thank the staff at Physical Acoustics, in particular Phil Cole who has provided technical advice to our team for 20 years.

10.8 References

ASTM (1992), 'Standard Method for Primary Calibration of AE Sensors', E1106-86.

ASTM (2001), 'Standard Guide for Determining the Reproducibility of AE Sensor Response', E976-84.

Baron, J.A. and Ying, S.P. (1987), 'Acoustic emission source location', *Non-destructive Testing Handbook*, American Society for Non-destructive Testing, Columbus, OH, vol. **5** (6), 136–154.

Beck, P. (2004), 'Quantitative damage assessment of concrete structures using acoustic emission', PhD Thesis, Cardiff University, July 2004.

Beck, P., Lark, R.J. and Holford, K.M. (2003), 'Moment tensor analysis of acoustic emission in concrete specimens failed in four-point bending', *Damage Assessment of Structures. Key Engineering Materials*, 245–246, 443–450.

Bradshaw, T.P. (2003), 'Acoustic emission monitoring in concrete and composite components', MPhil Thesis, Cardiff University, September 2003.

Carlyle, J.H. (1993), *Acoustic Emission Monitoring of the I-10 Mississippi River Bridge*, *Phase Report no. R90-259*, Physical Acoustics Corporation, Lawrenceville, NJ.

Carlyle, J.H. and Ely, T.M. (1993), *Acoustic Emission Monitoring of the I-95 Woodrow Wilson Bridge*, *Phase Report no. R90-259*, Physical Acoustics Corporation, Lawrenceville, NJ.

Carlyle, J.H. and Leaird, J.D. (1992), *Acoustic Emission Monitoring of the I-80 Bryte Bend Bridge*, *Phase Report no. R90-259*, Physical Acoustics Corporation, Lawrenceville, NJ.

Carter, D. (2000), 'Acoustic emission techniques for the structural integrity monitoring of steel bridges', PhD Thesis, Cardiff University.

Carter, D. and Holford, K.M. (1996), 'I.M.A.G.IN.E.: Letting bridges do the talking', *Insight*, **38** (11), 775–779.

Carter, D. and Holford, K.M. (1998), 'Strategic considerations for the AE monitoring of bridges – a discussion and case study', *Insight*, **40** (2), 112–116.

Cullington, D.W., MacNeal, D., Paulson, P. and Elliott, J. (2001), 'Continuous acoustic monitoring of grouted post-tensioned concrete bridges', *NDT & E International*, **34** (2), 95–105.

Droulliard, T.F. (1996), 'A history of acoustic emission', *Journal of Acoustic Emission*, **14** (1), 1–34

Dun, S.E., Young, J.D., Hartt, W.H. and Brown, R.P. (1984), 'Acoustic emission characterisation of corrosion induced damage in reinforced concrete', *National Association of Corrosion Engineers*, **40** (7), pp. 339–343.

Esward, T.J., Theobald, P.D., Dowson, S.P. and Preston, R.C. (2002), *An Investigation into the Establishment and Assessment of a Test Facility for the Calibration of Acoustic Emission Sensors*, report CMAM 82, Teddington: National Physical Laboratory.

Hopwood, T. and Prine, D.W. (1985), 'Acoustic emission structural monitoring in noisy environments using event based processing', *Proceedings of International Conference on Fatigue, Corrosion Cracking, Fracture Mechanics and Failure Analysis*, Salt Lake City, UT. Metals Park, OH, American Society of Metals, December, pp. 277–282.

Hutton, P.H. and Skorpik, J.R. (1975), *Acoustic Emission Methods for Flaw Detection in Steel in Highway Bridges*, Phase I. FHWA report no. FHWA-RD-78-97, Richland, WA: Battelle Pacific Northwest.

Hutton, P.H. and Skorpik, J.R. (1978), *Acoustic Emission Methods for Flaw Detection in Steel for Highway Bridges*, FHWA report no. FHWA-RD-78-98, Richland, WA: Battelle Pacific Northwest.

Hsu, N.N. and Breckenridge, F.R. (1981), 'Characterisation and calibration of acoustic emission sensors', *Materials Evaluation*, **39**, 60–68.

Ing, M., Watson, J., Lyons, R. and Austin, S. (2003), 'Risk based investigation of steel reinforcement using the AeCORR technique', *Proceedings of the 3rd International Conference on Emerging Technologies in NDT*, 26–28 May, Thessaloniki, Greece.

Kamada, T., Iwanami, M., Nagataki, S. and Otsuki, N. (1996), 'Application of acoustic emission evaluation of structural integrity in marine concrete structures', *Progress in Acoustic Emission VII*, Japanese Society for NDI, Tokyo, pp. 355–360.

Landis, E.N. and Shah, S.P. (1995), 'Frequency-dependent stress wave attenuation in cement based materials', *Journal of Engineering Mechanics*, June, 737–743.

Matsuyama, K., Ishibashi, A., Fujiwara, T., Fukuchi, S. and Ohtsu, M. (1994), 'AE field applications for diagnosis of deteriorated concrete structures', *Progress in Acoustic Emission VII*, Japanese Society for NDI, Tokyo, pp. 361–367.

Miller, R.K. and McIntire P. (Eds) (1996), 'Acoustic emission testing', *NDT Handbook* Volume 5, Second Edition, American Society for Nondestructive Testing, USA.

Murakami, Y. and Yuyama, S. (1986), 'Acoustic emission evaluation of structural integrity in reinforced concrete beams deteriorating due to corrosion of reinforcement', *Progress in Acoustic Emission II*, Japanese Society for NDI, Tokyo, pp. 217–224.

Muravin, G.B., Lezvinskaya, L.M. and Ship, V.V. (1993), 'Acoustic emission and fracture criteria (review)', *Russian Journal of Nondestructive Testing*, **39** (8), 567–576.

Nielsen, A. (1980), *Acoustic Emission Source based on Pencil Lead Breaking*, Danish Welding Institute, Report 80–15.

Ohtsu, M. (1987), 'Acoustic emission characteristics in concrete and diagnostic applications', *Journal of Acoustic Emission*, **6** (2), 99–106.

Paulson, P.O. and Elliott, J.F. (2000), 'SoundPrint ® Acoustic Monitoring to confirm the integrity of stressed wire in bridges, structures and water pipelines', *Proceedings of the 15th World Conference on NDT*, Rome.

Physical Acoustics Corporation (1995), *MISTRAS 2001 Users Manual*, Princeton, NJ.

Pollock, A.A. (1986), 'Classical wave theory in practical AE testing', *Progress in AE III, Proceedings of the 8th International AE Symposium*, Japanese Society for NDI, Tokyo, pp. 708–721.

Pollock, A.A. and Smith, B. (1972), 'Acoustic emission monitoring of a military bridge', *Nondestructive Testing*, **5** (6), 164–186.

Prine, D.W. and Hopwood, T. (1985), 'Improved structural monitoring with acoustic emission pattern recognition', *Proceedings of the Fourteenth Symposium on Nondestructive Evaluation* San Antonio, TX.

Pullin, R., Carter, D.C., Holford, K.M. and Davies, A.W. (1999a), 'Bridge integrity assessment by acoustic emission – global monitoring', *Proceedings of the 2nd International Conference on Identification of Engineering Systems*, Swansea, pp. 401–409.

Pullin, R., Carter, D.C., Holford, K.M. and Davies, A.W. (1999b), 'Bridge integrity assessment by acoustic emission – local monitoring', *Proceedings of the 2nd International Conference on Identification of Engineering Systems*, Swansea, pp. 401–409.

Pullin, R., Holford, K.M., Lark, R.J. and Beck P. (2003), 'Acoustic emission assessment of concrete hinge joints. Damage assessment of structures', *Key Engineering Materials* **4**, 245–246, 323–330.

Pullin, R., Holford, K.M. and Lark, R.J. (2004), *An Investigation of the Use of Acoustic Emission to Monitor Hinge Joints*, *Cardiff School of Engineering Report* No. 3060, February.

Rindorf, H.J. (1981), 'Acoustic emission source location in theory and in practice', *Brüel & Kjær Technical Review*, No 2.

Tatro, C.A., Borown, A.E. and Freeman, T.H. (1979), *On-line Safety Monitoring of a Large High Pressure High Temperature Autoclave*, *ASTM STP 697*, Philadelphia PA: ASTM.

Vallen, H. (2002), **'**AE Testing Fundamentals, Equipment, Applications', http://www.NDT.net – September 2002, 7 (09)

Watson, J.R., Holford, K.M., Davies, A.W. and Cole P.T. (2000), 'BOXMAP – non-invasive detection of cracks in steel box girders', *Proceedings of the 4th International Bridge Management Conference*, University of Surrey, Guildford, pp. 80–87.

Yuyama, S., Imanaka, T. and Ohtsu, M. (1988), 'Qualitative evaluation of microfracture due to disbonding by waveform analysis of acoustic emission', *Journal of the Acoustical Society of America*, **83** (3) 976–983.

Yuyama, S., Okamoto, T. and Nagataki, S. (1992), 'Acoustic emission evaluation of structural integrity in repaired concrete beams', *Materials Evaluation*, **52** (1), 86–90.

Yuyama, S., Okamoto, T., Shigeishi, M., Ohtsu, M. and Kishi, T. (1999), 'A proposed standard for evaluating structural integrity of reinforced concrete beams by acoustic emission', *Acoustic Emission: Standards and Technology Update*, *ASTM STP 1353*, 25–40.

11

Bridge inspection using virtual reality and photogrammetry

D.V. JÁUREGUI and K.R. WHITE
New Mexico State University, USA

11.1 Introduction

This chapter is divided into three major sections: Bridge inspection via virtual reality (Section 11.2); Bridge monitoring via photogrammetry (Section 11.3); and Potential impact and future developments (Section 11.4). Section 11.2.1 briefly covers the current regulations set by the Federal Highway Administration (FHWA) and United States Department of Transportation (USDOT) for conducting routine bridge inspections. It also highlights important results from a research study conducted by the FHWA Non-Destructive Evaluation Validation Center (NDEVC) related to the accuracy and reliability of visual inspections. The FHWA-NDEVC study raised several important issues in need of further action to improve routine bridge inspections, one of which is the collection and management of inspection data. In Section 11.2.2, an approach using QuickTime Virtual Reality (QTVR) is described for recording bridge inspection data at a high level of photographic detail. The section covers the basic equipment (hardware and software) and procedures for documenting the physical condition of a bridge using virtual reality techniques. The virtual reality development process is illustrated by means of different bridge inspection projects conducted by the authors and consists of three fundamental phases: (1) planning and taking of photographs; (2) creation of panoramas; and (3) rendering of virtual reality records with hot spots.

Section 11.3.1 provides a brief overview of photogrammetry including basic definitions, instruments, procedures, and applications. Topics discussed include aerial versus terrestrial photogrammetry; the central perspective projection; measurement by triangulation; photogrammetric camera types, characteristics, and calibration; and photogrammetric analysis fundamentals. The overview is written in general terms for non-photogrammetrists and structural engineering applications (in particular the field of bridge engineering) are emphasized. Several references are also provided for the reader to pursue a broader and more technical coverage of the subject.

Section 11.3.2 covers the four major tasks of the photogrammetric measurement process for monitoring bridge deformation: (1) set-up and calibration of camera-lens system; (2) target layout and camera stations; (3) control survey and image acquisition; and (4) image preparation and analytical processing. These tasks are illustrated referencing a commercially available photogrammetry software program and a professional-grade digital camera commonly used for close-range photogrammetric measurement.

Sections 11.4.1 and 11.4.2 provide concluding comments regarding the potential impact of virtual reality and photogrammetry, respectively, for the inspection and monitoring of bridges. Advantages and limitations of the two technologies are addressed as well as areas for future development.

11.2 Bridge inspection via virtual reality

11.2.1 Traditional inspection

Since the early 1970s, the safety inspection of bridges has been regulated in the USA by the National Bridge Inspection Standards (NBIS). These standards set national policy for bridge inspection practice in matters such as inspection and rating procedures, frequency of inspections, qualifications of inspectors, and inspection report formats (NBIS, 1996). For the most part, the type of inspection performed to satisfy NBIS regulations is routine inspection, which is described as 'Regularly scheduled inspections consisting of observations and/or measurements needed to determine the physical and functional condition of the bridge, to identify any changes from initial or previously recorded conditions, and to ensure that the structure continues to satisfy present service requirements' (AASHTO, 2000). In a routine inspection, the bridge is visually examined for evidence of damage and/or deterioration such as (White *et al.*, 1992; FHWA, 1995a): collision damage; concrete spalls, cracks, and delaminations (with, possibly, exposed rebar); corroded steel; fatigue cracks; malfunctioning or damaged bearing devices; member section loss; and scour and undermining. Based on these field observations, condition ratings are assigned using the rating system given in Table 11.1 to describe the general condition of each bridge subsection (i.e. deck, superstructure, and substructure). As shown in the table, there are ten condition states ranging from Failed to Fair to Excellent. Handwritten notes, sketches, measurements, and/or photographs are utilized to document the bridge condition and support the assigned condition states.

In lieu of the NBIS rating system given in Table 11.1, many state highway departments in the USA are now using the AASHTO Guide for Commonly Recognized (CoRe) Elements (1998) which provides more quantitative definitions of the various bridge condition states. This guide breaks down

Table 11.1 Standard condition rating system

Condition state and rating	Description of condition state
Not applicable (N)	
Excellent (9)	
Very good (8)	No problems noted
Good (7)	Some minor problems
Satisfactory (6)	Structural elements show some minor deterioration
Fair (5)	All primary structural elements are sound but may have minor section loss, cracking, spalling, or scour
Poor (4)	Advanced section loss, deterioration, spalling, or scour present
Serious (3)	Section loss, deterioration, spalling, or scour have seriously affected primary structural members; local failures possible; fatigue cracks in steel or shear cracks in concrete may be present
Critical (2)	Advanced deterioration of primary structural members; fatigue cracks in steel or shear cracks in concrete may be present or scour may have removed substructure support
Imminent failure (1)	Major deterioration or section loss present in critical structural members or obvious vertical or horizontal movement affecting structure stability
Failed (0)	Out of service; beyond corrective action

Source: condition states and ratings provided in FHWA (1995b).

the deck, superstructure, and substructure into individual elements (as defined by CoRe element descriptions) and a rating ranging from 5 to 1 (with 1 being the best) is assigned to each element based on its condition. For example, a condition state of 4 in the AASHTO CoRe Guide for a concrete deck or slab (with or without coated reinforcement) represents the case where patched areas and/or spalls/delaminations exist and the combined area of distress is between 10% and 25% of the total deck surface area. The same condition state has a different meaning for prestressed concrete girder, stringer, or floor beam element(s) of a superstructure. For this type of CoRe element, a condition state of 4 represents the following situation:

> Delaminations, spalls and corrosion of non-prestressed reinforcement are prevalent. There may also be exposure and deterioration of the prestress system (manifested by loss of bond, broken strands or wire, failed anchorages, etc.). There is sufficient

concern to warrant an analysis to ascertain the impact on the strength and/or serviceability of either the element or the bridge. (AASHTO, 1998)

As shown in this comparison, the AASHTO CoRe Guide (1998) provides descriptions of condition states that are more quantitative and element specific than those given in the NBIS rating system. Another important difference of note is that there are ten NBIS condition states (see Table 11.1), which rate from 0 to 9 with the higher number being the best condition. Both of these procedures, however, primarily utilize visual evaluation of the bridge components and are very subjective. As a result, the quality of the reported field inspection depends upon the training, experience, and dedication of the inspection teams. Consistent and uniform inspections are difficult to achieve as shown by Phares *et al*. (2000).

A series of studies related to highway bridge inspection was completed by the FHWA. In one study, Rolander *et al*. (2000) surveyed 42 state highway departments, 72 county highway departments (in the state of Iowa), and six bridge inspection contractors. Two important findings from the survey were (1) visual inspection was the most common technique used to evaluate the condition state of highway bridges and (2) a professional engineer is rarely on-site during the inspections. All the survey participants also indicated that inspectors are allowed to review old inspection reports. In another study, Phares *et al*. (2000) investigated the reliability of routine bridge inspections; participants in the study included 49 state highway inspectors from 25 different states in the USA. Each participant inspected six different bridges without the aid of previous inspection reports and then assigned NBIS condition ratings for the deck, superstructure, and substructure of each bridge. Findings from the study showed that on average, between four and five different ratings were assigned to each primary bridge element (with a minimum of three and a maximum of six). Based on a statistical analysis of the results, approximately 58% of the individual ratings were assigned incorrectly (compared to reference ratings established by the FHWA); bridge elements in poorer condition were assigned fewer correct ratings. The statistical results also showed that the ratings varied ±2 points (at a 95% confidence interval) and ±1 point (at a 68% confidence interval) from the average inspector rating.

11.2.2 Virtual reality inspection procedures

The two FHWA studies just summarized were performed by the NDEVC and raise several important issues in need of further action to improve routine bridge inspections, one of which is the collection and management of inspection data. In this section, an approach using QTVR is described for recording bridge inspection data at a high level of photographic detail.

High-resolution photography also provides an excellent management tool for the review of inspection reports by supervisors. Virtual reality technology has been previously used to create virtual worlds of various settings such as art museums, archaeological sites, city attractions, and natural surroundings, to name a few. There are many other ways in which QTVR has been employed; however, prior to this application for bridge inspection little has been done to address a specific engineering problem.

In QTVR, photographic images are moved from the flat, two-dimensional world into a more immersive, three-dimensional environment complete with interactive components (Apple, 2004). Thus, this technology provides the capability for an inspector or engineer to explore and examine a bridge's physical condition as if he/she were actually in the field, with the simple use of a computer mouse in lieu of virtual reality equipment such as goggles, headsets, or gloves (Apple, 2004). The amount of equipment needed for a virtual reality system is not extensive; a basic system (excluding a laptop computer) should include a high-resolution digital camera, a camera tripod, panoramic tripod heads, and virtual reality computer software. A list of suitable hardware and software products is provided below (Kaidan, 2004):

- Olympus C-5060 Digital Camera with wide-angle lens (including memory cards).
- Kaidan Slik Master Classic Tripod.
- Kaidan Kiwi+ Panoramic Tripod Head (with QuickTilt Leveler).
- Kaidan QuickPan III System (spherical camera bracket with universal camera mount and rotator configuration).
- VR Toolbox The VR Worx (panoramic software).
- Realviz Stitcher (panoramic software).

The virtual reality documentation process consists of three basic steps: (1) planning and taking of photographs; (2) creation of panoramas; and (3) rendering of virtual reality records with hot spots. These steps are discussed in detail in the following sections for different bridge inspection projects with reference to the equipment listed above.

Planning and taking of photographs

The time invested in planning the fieldwork will greatly improve the efficiency of the photography as well as the overall image quality. The photography plan should primarily indicate the locations to set up the camera at the bridge site; camera stations may be limited at some bridges owing to accessibility and obstructions. From each camera station, a series of individual photographs are taken and later merged into a single panorama through a stitching process discussed later. At first, the photography should

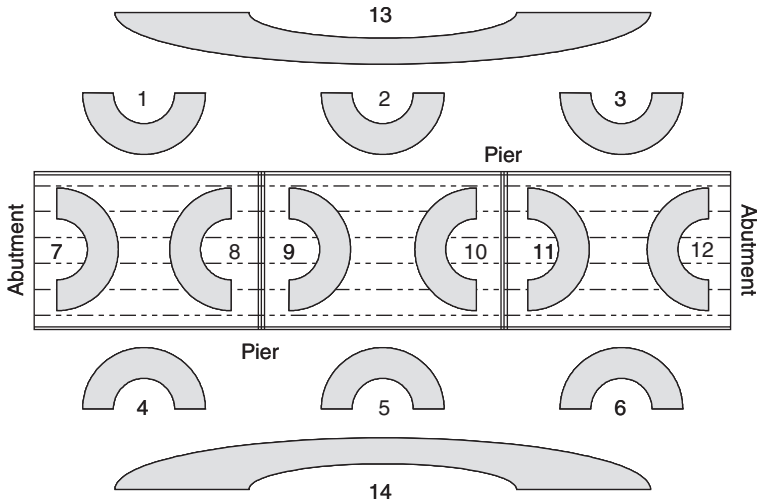
focus on producing global panoramas of the bridge from both elevation and cross-section viewpoints as outlined below.

- End spans – horizontal sweep of span elevation from the abutment to the adjacent interior pier (from each side of bridge width) and horizontal sweep of cross-section (in the direction of the abutment from the interior pier and vice versa).
- Interior spans – horizontal sweep of span elevation between interior piers (from both sides of bridge width) and horizontal sweep of cross-section (from one interior pier to the other).
- Overall bridge – horizontal sweep of bridge elevation between abutments (from both sides of bridge width).

Based on the recommendations given above, the photography of a three-span bridge, for example, would involve a total of 14 global panoramas (i.e. four panoramas per span plus two panoramas of the whole bridge) as shown in Fig. 11.1. Afterward, local areas of the bridge having damage and/or deterioration should be identified with the assistance of an experienced bridge inspector or professional engineer and photographed. If the bridge is in pristine condition, pictures should be taken of deterioration-prone areas such as bearing locations and interior piers below an expansion joint. Local photographs of existing and/or potential problem areas may be integrated into the global panoramic images to further establish a baseline for future condition assessment.

In general, proper photographic procedures should be followed by the inspector to acquire the images needed for the virtual reality record. A good quality tripod (with a tiltable head and adjustable legs) such as the Kaidan Slik Master Classic should be used in order to withstand and adapt to the bridge environment. Many features of a bridge require the use of the pan and tilt adjustment which allows the inspector to view under the superstructure as well as pan horizontally. The camera should be oriented vertically on the panoramic tripod head so that the captured photos have a portrait orientation. Having the camera in portrait orientation fills the viewing area as much as possible; however, the angle of view in the horizontal direction is reduced compared with landscape orientation. Thus, more pictures need to be taken in order to cover the panoramic area being photographed. Care should be taken to position the tripod head such that the individual pictures representing the middle region of the panoramic area are level and centered. In order to reduce errors due to parallax, the camera should be positioned on the tripod head so that it rotates horizontally about the focal point of the lens. Parallax is corrected by simply repositioning the camera so that the effect is minimized.

The panoramic tripod heads mentioned earlier have a graduated horizontal rotation scale and a detect mechanism to provide click stops when



11.1 Camera stations for global panoramas of three-span bridge.

rotating the camera in equal angle increments. Detect discs are available with 2 to 22 stops which correspond to horizontal angle increments of 180° and about 15.7°, respectively. The number of stops used depends on the lens size of the camera (or the lens equivalent in 35 mm format for a digital camera) and should provide 30–50% overlap between adjacent images. For a 35 mm lens equivalent, for example, an 18-stop detect disk with a horizontal angle increment of about 18.9° is specified. This setting results in a total of 11 images for a 180° partial panorama and 18 images for a 360° complete panorama. In general, more pictures will be required for multiple span and longer bridges. For these cases, arrangements should be made to have sufficient time, disk space, and battery power to complete the digital photography.

Regardless of the camera model, certain settings are recommended which can help in creating high quality panoramic images. The first recommendation is to adjust the camera to its highest *f*-stop in aperture priority, auto-exposure mode. This camera setting controls the aperture size and hence, the amount of light that passes through the lens. Higher *f*-stop settings will increase the depth of field which is the range of distance (measured along the lens axis) over which the subject is in sharp focus in the photograph. Without a flash, the camera will adjust the exposure time in order to get adequate images; advanced digital cameras use through-the-lens (TTL) light metering to determine the appropriate exposure. An important detail is that the white balance sensor in front of the camera should not be directly exposed to the sunlight. The use of an umbrella to cast a shadow on the

sensor, while remaining out of the view of the lens, will result in better exposure of darkened areas such as the abutments and between girders. Owing to the likelihood of long exposure times, self-timer or remote control shooting is suggested instead of manual shutter release. This allows hands-free operation of the camera during exposure, thus preventing camera movement and blurry images. The third recommendation is to set auto-focus to manual mode and use the same shooting range for all images of the panoramic picture set. If the focal length changes considerably between images, the virtual reality software may have problems stitching the individual pictures into a single panorama. Changes in lighting and moving objects are also factors that can influence the quality of the final panorama. An effort should be made to take each panoramic picture set with the level of sunlight constant throughout the duration of image acquisition. Lastly, there should be no moving object on the outer edge of any picture since the next picture in the series will not have the same object. In summary, out-of-focus pictures, non-uniform exposure, and moving objects can all hinder a project since the software may not be able to properly match pixels between images and, thus, stitching may not be possible.

Although the conditions at a bridge site are somewhat beyond control, the photographer should follow good photographic procedures taking as much care as possible. After the photography is complete, the images should be properly transferred to a laptop. The laptop should be equipped with a reasonably large hard drive and also with a writeable CD / DVD drive so that pictures can be backed up prior to leaving the bridge site. Two ways for transferring images to the laptop are flash memory cards, which plug into the digital camera, and direct wire connection between the camera and computer. Flash memory cards or microdrives range in capacity from 16 megabytes to 2 gigabytes. Direct wire connection is normally done through an IEE1394 (also known as Firewire) standard connection. For further details related to image storage and transfer, the reader should consult the manual for the digital camera.

Creation of panoramas

The two kinds of virtual reality panoramas are cylindrical and cubic. The cylindrical type are produced using single row images and provide the experience of standing in the center of a panoramic cylinder and looking straight ahead in all directions up to 360°. The vertical angle of view depends on the viewing range of the camera lens and, thus, wide-angle lens cameras such as the Olympus C-5060 are advantageous. Cubic panoramas combine multi-row images and add the capability to pan vertically up to 180° (overhead and/or underneath the focal point of the camera lens) in a spherical environment. There are various software programs available for creating

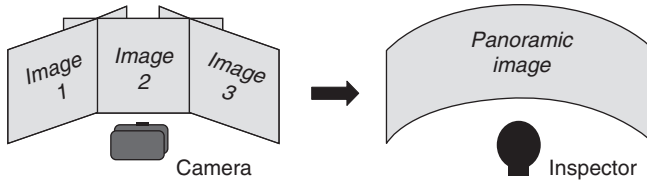
virtual reality panoramas, including Apple's QuickTimeVR Authoring Studio; VR Toolbox's The VR Worx; PhotoVista Virtual Tour Maker; iPIX's software & Panoweaver; Realviz's Stitcher; and Helmut Dersch's Panotools. The latter two stitching programs may be used to create both cylindrical and cubic panoramas, while the other programs listed are capable of only cylindrical panoramas. A brief discussion of cylindrical and cubic panorama creation using the VR Worx and Realviz's Stitcher programs, respectively, is provided in the following paragraphs.

The VR Worx (VR Toolbox, 2003) software is an IBM PC-based program which can create cylindrical panoramas of varying horizontal sweeps ranging from a partial 90° to a full 360° using the Kaidan Kiwi+ Panoramic Head mentioned earlier. Single row images must overlap by at least 30% in order for stitching to work (some programs require up to 60%). Figure 11.2 shows the general way in which a cylindrical panorama is created. A powerful feature of VR Worx is its ability to adjust the orientation and exposure of the photos to achieve uniformity across the panoramic area.

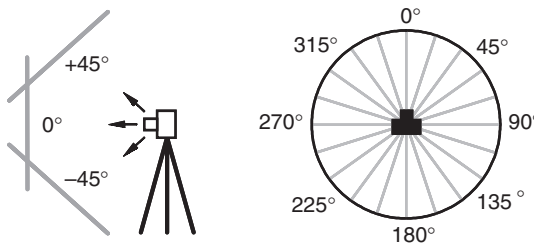
Like the VR Worx program, the Stitcher (Realviz, 2004) software operates on an IBM PC. This program has a highly developed stitching algorithm that can successfully stitch images together in difficult situations where other software programs may fail; however, one constraint is that cylindrical panoramas must be 360° and nothing smaller. As mentioned earlier, the main feature of Realviz Stitcher is its capability to create cubic panoramas. Figure 11.3 shows the camera set-up for taking the set of pictures needed for a cubic panorama. As shown in the figure, three rows of images are taken at vertical angles of –45°, 0, and +45° using the Kaidan QuickPan III System. Hence, a full cubic panorama requires three times the number of images needed for a full cylindrical panorama (e.g. 54 versus 18 images for a 35 mm lens equivalent). A final note about Realviz Stitcher is that cubic panorama creation is more complicated since images have to be manually placed into a workspace and roughly adjusted before the software can perform the automated stitching.

Rendering of virtual reality records with hot spots

Once the stitching process is complete, the cylindrical and/or cubic panoramas are rendered to an output file for viewing on the Apple QuickTime player. There are several choices in compression and playback settings for the rendered panoramas for which the reader should refer to the virtual reality software manual. One especially important setting to be aware of is the output size of the panorama, which has a direct effect on playback performance. In the final virtual reality record, hot spots are used to bring together the rendered panoramas and discrete photographs of local areas (prone to or with existing damage and/or deterioration). Generally speak-



11.2 Creation of cylindrical panorama.



11.3 Creation of cubic panorama: camera set-up.

ing, hot spots are user-defined links that connect (1) separate panoramas and/or (2) a panorama to a single picture; a nodal map defines the interaction between a single panorama and its associated links. Once linked, the panoramas and/or photographs will form a network of visual records about the bridge, which may be reviewed at the discretion of the inspector. Written explanations along with design drawings and maps may be included to fully describe the view within the virtual bridge environment and/or the specific bridge feature under observation. The amount of office time spent in the development of a virtual bridge record will depend on several factors such as (1) the number and type of panoramas; (2) the number of hot spots or links; and (3) the amount of miscellaneous material such as local pictures, text descriptors, design drawings and/or maps included in the record.

A typical movie screen has three distinct areas; the header, image, and footer area. The header area of the screen displays the name of the bridge inspection project and also contains the menu bar for the Apple QuickTime player. Below the header, the image area of the screen displays the cylindrical and/or cubic panoramas. Using the computer mouse (i.e. clicking and holding the left button and dragging the mouse), the inspector may navigate the panoramic area at his/her discretion. User-defined hot spots appear as transparent, outlined regions within the image area which link the active panorama to other panoramas and/or individual pictures. When the cursor is positioned in the delineated area of a hot spot, a narrative appears towards the bottom of the screen in the footer area to describe the link. A simple click of the computer mouse (with the cursor positioned within the

hot spot area) will show the linked panorama in the image area; this new panorama is now active and may have associated links of its own. As mentioned earlier, hot spots may also link a panorama to individual pictures of noted problem areas. Menu buttons in the footer area of the screen allow the inspector to zoom in and out of the scene, to toggle the display of the hot spots on and off, and to return to the previous panorama and/or individual picture. Further training of virtual reality development for general applications is available online at the Apple (2004) website as well as others.

11.3 Bridge monitoring via photogrammetry

11.3.1 Basic principles of photogrammetry

The American Society for Photogrammetry and Remote Sensing (ASPRS) defines photogrammetry as 'the art, science, and technology of obtaining reliable information about physical objects and the environment through processes of recording, measuring, and interpreting photographic images' (McGlone, 2004). Although the underlying concepts date back to the early 1500s, the actual practice of photogrammetry did not originate until centuries later. In the mid-18th century, the first system (camera and procedure) suitable for photogrammetric measurement was developed by Aimé Laussedat, a Colonel in the French Army Corps of Engineers, who is considered the father of photogrammetry. Since that time, there have been significant changes in the devices and techniques used in photogrammetry as well as tremendous growth in the diversity of photogrammetric applications, yet the fundamental principles of photogrammetry have remain unchanged. The following sections provide a brief over-view of photogrammetry including basic definitions, instruments, procedures, and applications. The overview is written in general terms for non-photogrammetrists and structural engineering applications are emphasized; a broader and more technical coverage of the subject can be found in numerous textbooks (Schenk, 1999; Wolf and Dewitt, 2000; Atkinson, 2001; Mikhail *et al.*, 2001) and in the manual series published by ASPRS (McGlone, 2004; Greve, 1996). The International Society for Photogrammetry and Remote Sensing (ISPRS) and the Remote Sensing and Photogrammetry Society (RSPSoc) also provide publications and conference information related to developments in photogrammetry. The home pages for the ASPRS, ISPRS, and RSPSoc websites can be found at www.asprs.com, www.isprs.org and www.rspsoc.org, respectively.

There are two broad areas of photogrammetry: interpretive (qualitative) and metric (quantitative) photogrammetry. Metric photogrammetry is the branch that deals with the use of photographs to precisely measure the

geometrical configuration (e.g. distances, angles, areas, volumes, elevations, sizes, shapes) of an object and is further classified as either aerial or terrestrial photogrammetry. Aerial photogrammetry is commonly used for topographic mapping and land surveying applications in such fields as highway engineering (planning, design, and construction) and property boundary surveying. This type of photogrammetry makes use of images taken overhead from an aircraft and has been successfully used since the beginning of modern photography and aviation. Terrestrial photogrammetry, on the other hand, is performed from camera stations situated close to or on the earth's surface. Photographs are usually taken from terrestrial stations on the side of the physical object as opposed to overhead shots such as those used in aerial photogrammetry. When the camera-to-object distance is between 100 mm (4 inches) and 100 m (330 ft), terrestrial photogrammetry is further defined as close-range terrestrial photogrammetry.

Close-range photogrammetry has found a number of applications in both the engineering and non-engineering communities. Industrial inspection, architectural documentation, and forensic analysis are three modern applications of close-range photogrammetry. In the field of structural engineering, close-range photogrammetry has been used to measure, model, monitor, and/or document the thermal deformation of steel beams (Fraser and Riedel, 2000); the local flange buckling of curved, steel box girders (Scott, 1978); the shape of soil–steel structures (Bakht and Maheu, 1994); the laboratory deformation of a closed-spandrel arch bridge up to failure (Forno *et al*., 1991); the appearance of historic transportation sites (Spero, 1983); the deformation of concrete beams and columns under laboratory loading (Woodhouse and Robson, 1998; Fraser and Brizzi, 2002; Whiteman *et al*., 2002); the characteristics of highway roadside features (Nastasia, 1998); and the shape of space structures in stationary, vibrating, and deploying conditions (Pappa *et al*., 2002). Short-term and long-term photogrammetric measurement of in-service bridges has been carried out in various bridge engineering applications by Bales (1984), Kim (1989), Johnson (2001), Albert *et al*. (2002), Cooper and Robson (1990), and Jáuregui *et al*. (2003). Further example applications of photogrammetric methods for general structural testing and monitoring are given in Cooper and Robson (1994), Kraus (1986), and Woodhouse *et al*. (1999).

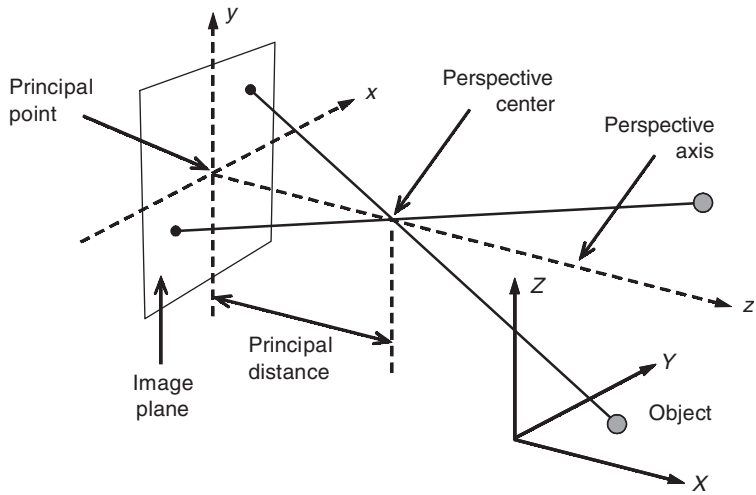
Whether used in aerial or terrestrial photogrammetry, a photograph represents a projection of a three-dimensional object onto the two-dimensional image plane of the camera. Depending on the type of camera used, the image plane contains either conventional photographic film or glass plates or in the case of a digital camera, a CCD (charge-coupled device) sensor to capture and record light transmitted from the object. The fundamental task of photogrammetry is to establish the geometrical relationship between image points on the two-dimensional photograph and real points on the

three-dimensional object. Once this image–object relationship is determined, measurements of the object can then proceed strictly from the imagery based on the principle of triangulation. The fundamental mathematical model used in photogrammetry for image formation in a camera is the central perspective projection. This model suggests that light rays travel in a straight line during exposure starting from visible points on the object and passing through the perspective center of the camera onto the image plane. As shown in Fig. 11.4, these light rays form a negative image of the object on the image plane. If the object is photographed from two different positions, the spatial location of overlapping points can be determined as the point of intersection between two rays of light as shown in Fig. 11.5.

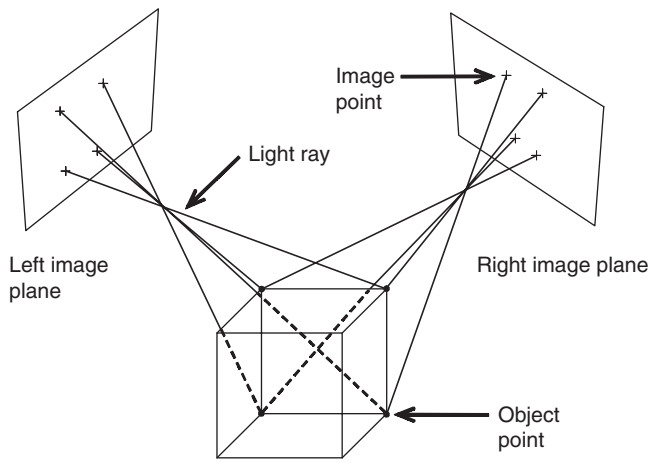
Triangulation requires knowledge of the internal geometry of the camera, including the focal length and the principal point location on the image plane through which the optical or perspective axis passes as indicated in Fig. 11.4. The focal length is also referred to as the principal distance which is the distance along the perspective axis between the camera's perspective center and the principal point. In photogrammetric terms, these parameters are referred to as the interior orientation elements of the camera. The cameras used in close-range photogrammetry are characterized according to the stability of their construction. Metric cameras, such as those produced by Geodetic Services (2004), are highly stable cameras that are designed and constructed specifically for the purpose of photogrammetry (Atkinson, 2001). These cameras have stable and repeatable lens characteristics (i.e. interior orientation) and are fully calibrated prior to use to determine calibration values for focal length, principal point coordinates, and lens distortions.

Camera calibration is the process used to 'identify why and by how much the geometry of image formation in a real camera differs from the geometry of the central perspective projection' (Atkinson, 2001). This difference is attributed mainly to imperfection of the camera lens. Fiducial marks are built into the image plane of metric cameras in order to accurately recover the coordinates of the principal point at the time of calibration. Non-metric cameras, on the other hand, are manufactured for amateur or professional photography without fiducial marks and, as a result, have a less stable construction (i.e. the interior orientation elements are completely or partially unknown and often unstable). Semi-metric is a term often used to define a non-metric camera that has been modified in some way for photogrammetric use to reduce instability of the internal orientation elements.

Digital cameras are considered semi-metric since the CCD technology provides a more stable image plane compared to conventional film cameras and is also immune to film deformation effects at the time of exposure. Kodak manufactures a series of professional-grade digital cameras



11.4 The central perspective projection. (Adapted from Woodhouse and Robson, 1998.)



11.5 Measurement of three-dimensional object from two-dimensional images by intersection. (Adapted from Bakht and Mauer, 1994.)

(DCS models) which are commonly used in close-range terrestrial photogrammetry applications (Kodak, 2004). The imaging sensors of these cameras have a high pixel resolution ranging up to 14 megapixels. Furthermore, the cameras are usually used with wide-angle lenses manufactured by Nikon for photogrammetric work. Like metric cameras, semi-metric cameras require a full calibration to determine the interior orientation and lens distortion parameters of the camera-lens system.

Although the level of photogrammetric accuracy produced by semi-metric equipment may be lower compared with metric, acceptable results can still be produced using current photogrammetric software. In addition, semi-metric cameras are much less expensive and in general, more portable than metric cameras.

Aside from interior orientation, there are four photogrammetric operations involved in calculating intersection points by triangulation which are relative orientation, block formation, absolute orientation, and bundle adjustment (Vexcel, 2000). Relative orientation is the operation that calculates the relative positions of the cameras (i.e. the distance apart and the relative directions of the perspective axes) when the photographs were exposed. This requires that common points (some having surveyed coordinates for the purpose of control) be identified and referenced in the images. In block formation, the photographs are tied together into a common image coordinate system. Absolute orientation transforms the photos from the image frame of reference (i.e. x, y, and z coordinates in Fig. 11.4) to a real world coordinate system (i.e. X, Y, and Z coordinates in Fig. 11.4) using surveyed control points to define the actual size and location of the object. The final operation is the bundle adjustment, which simultaneously computes (by least squares estimation) the camera locations and orientation angles and the spatial coordinates of referenced points along with estimates of their measurement precision. Uncertainty in the measurement arises from the different lines of sight used to determine the location of a single point. This process is performed iteratively by adjusting the camera parameters until a specified number of iterations or consistency is achieved and the overall best solution is found based on statistical techniques. A detailed discussion of these operations is outside the scope of this chapter and the reader should refer to references given earlier for that information.

11.3.2 Photogrammetric monitoring procedures

Modern photogrammetry in bridge engineering uses digital technology in the form of high-end, semi-metric cameras which are available at a fraction of the cost of a metric camera and, thus, more likely to fit within the budget of a highway agency. The photogrammetric measurement process consists of four major tasks: (1) set-up and calibration of camera-lens system; (2) target layout and camera stations; (3) control survey and image acquisition; and (4) image preparation and analytical processing. The general procedures associated with these tasks discussed in the following sections pertain to the FotoG photogrammetry software (Vexcel, 2000) using a Kodak DCS 660 professional-grade digital camera (Kodak, 2004), but are general enough to be applied to other photogrammetric systems. A few other consumer-grade software packages available for close-range photogrammetric measurement

include Australis (Photometrix Pty Ltd); PhotoModeler (Eos Systems, Inc.); and Shapecapture (Shapequest, Inc.). Before starting a photogrammetry project, the user should first become thoroughly familiar with the operation of the camera. In contrast to typical point-and-shoot cameras that are popular for general photography because of their simple designs, professional-grade cameras used in close-range photogrammetry are usually more complex, having many more settings and features.

Set-up and calibration of camera lens system

The Kodak DCS 660 digital camera has a 6-megapixel CCD sensor and should be equipped with a wide-angle lens such as the Nikon AF Nikkor 28 mm *f*/2.8D lens to be used for photogrammetric measurement. Compared with standard lenses (i.e. 50 mm in focal length) or telephoto lenses (i.e. above 85 mm in focal length), wide-angle lenses (i.e. less than 35 mm in focal length) are preferred since they provide a wider area of coverage, thus requiring fewer pictures to cover the measured object. However, lens sizes less than 20 mm in focal length are not recommended owing to significant lens distortions. High-quality images are paramount in order to obtain accurate photogrammetric measurements. The camera settings and photographic techniques used in photogrammetry are similar to those recommended earlier for creating panoramas (by stitching of individual pictures) for virtual reality playback; the reader should refer back to these suggestions for review. One setting worth mentioning again is to adjust the lens aperture to the highest *f*-stop setting (e.g. *f*/22 for the Nikon AF 28/2.8D). This setting is particularly important since it increases the depth of field and, thus, brings more of the zone in front of, behind, and around the object into sharp focus, allowing more targets to be identified and accurately marked in the images. Auto-exposure mode is also recommended so that shutter release is automatic (depending on the amount of light entering the lens) and the exposure time is optimized. At these settings, the use of a tripod and timed or remote control shutter release is recommended to avoid the undesirable effects of camera motion that may occur during slow exposure times.

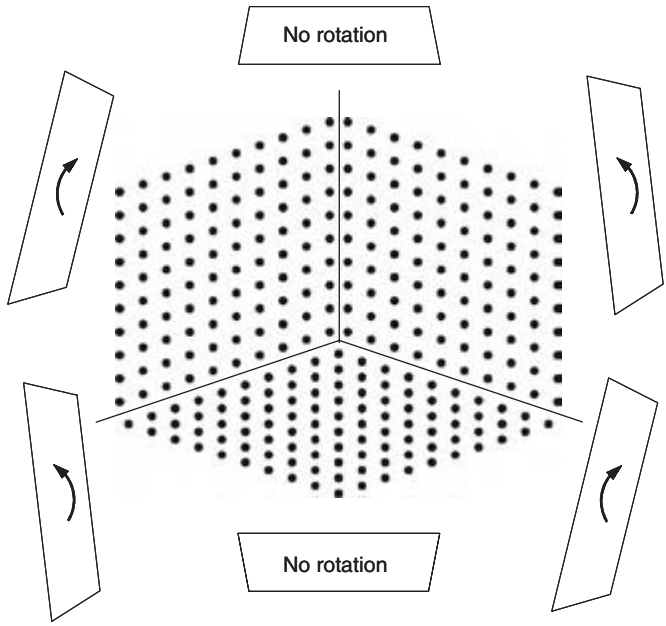
Another important camera parameter is the focus setting (lens position). The recommended choice for this setting is ∞ which maximizes the distance over which objects are in focus (approximately 1.2 m (4 ft) to ∞ for the Nikon AF 28/2.8D). It is important to note that a camera is calibrated at a fixed focal length; hence, each lens position creates a new focal length for the camera which must be determined by an independent camera calibration. Under no circumstances should the focal length be altered between camera calibration and image acquisition of the object. To ensure that the focal length is not changed by accident, the lens position of focusable lenses

such as the Nikon AF 28/2.8D should be fixed in some way (e.g. taped) at the calibrated focus setting. A final recommendation is to set the image resolution to its highest value (3048 by 2008 pixels or 6 megapixels for the Kodak DCS 660) and the saved image format to TIFF (tagged image file format). These settings result in images of the highest possible quality without loss due to data compression.

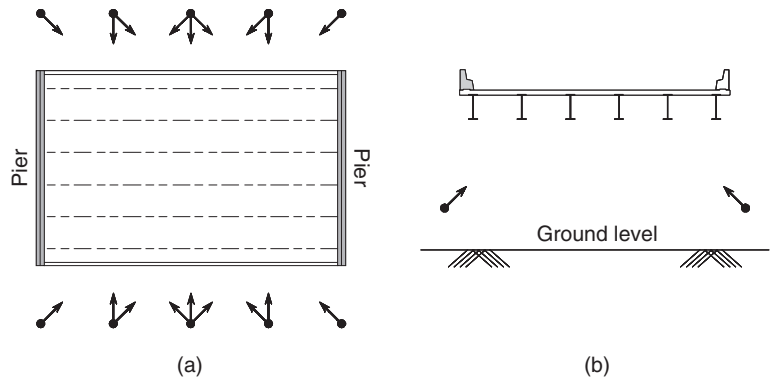
Using the FotoG software (Vexcel, 2000), a 'basic' calibration is first performed to estimate the focal length of the camera in pixels; note that the camera's focal length in millimeters can usually be found on the lens (e.g. 28 mm for the Nikon AF 28/2.8D). The remaining interior orientation elements (i.e. principal point coordinates and lens distortion parameters) are not determined in this phase of camera calibration. A simple procedure is followed to perform a 'basic' calibration. Two targets are placed on a flat wall a level distance apart and photographed with the camera mounted on a tripod. The distance in pixels between the centers of the targets (d_1) in the photograph is then measured with FotoG. Physical measurements of the distance between the two targets on the wall (D_2) and between the center of the camera and the face of the wall (D_3) are also taken in units of millimeters with a tape measure. With this information, the focal length of the camera in pixels (f) is computed as the ratio (D_3/D_2) multiplied by d_1. The result of this calibration is placed into a sensor file for later use in a low-accuracy project or an 'advanced' camera calibration.

When high-accuracy measurements are desired, an 'advanced' or full calibration of the camera lens system is necessary (Vexcel, 2000). The 'advanced' calibration process in the FotoG software is more complicated and uses the focal length determined beforehand in the 'basic' calibration as the starting point. As shown in Fig. 11.6, a calibration field is first set up, consisting of three orthogonal planes (in the corner of a room, for example), each having a uniform grid of circular targets. The target array on each planar grid should be at least 20×20 with 25 mm (1 inch) diameter targets spaced at 50 mm (2 inchs) on center. The circular targets should have a high level of contrast with the background, such as black on white or vice versa. At least four targets must be chosen to serve as control points, which are points with measured 3D coordinates in a Cartesian coordinate system; the designated control points must lie on different planes of the calibration field. Figure 11.7 shows the required camera positions and orientations for photography of the calibration field; two pictures are taken from the left side, center, and right side of the field at high and low elevations. The side of field photographs are taken with the camera rotated 90°.

Processing of the six 'advanced' calibration photographs in FotoG outputs the following interior orientation parameters (Vexcel, 2000): principal point coordinates (x_p, y_p); principal distance (f_1); radial lens distortion (k_1, k_2, and k_3); and tangential lens distortion (p_1, p_2). Radial distortion



11.6 Advanced calibration field and camera stations.



11.7 Camera station positions and pointing directions for the measurement of a single span bridge: (a) plan view and (b) cross-sectional view.

is the lens distortion component caused by the change in angle of a light ray as it enters the lens. This angle change, in turn, leads to radial shifts of projected points on the image plane either away from or towards the principal point. The direction of radial distortion in an image can be positive or negative (which creates either a 'pin cushion' or 'barrel' effect)

with the largest magnitude occurring towards the corners of the image. For standard lenses, radial distortion can be adequately described by the k_1 coefficient, while for wide-angle lenses, the higher-order k_2 and k_3 terms may be needed to account for radial distortion out to the image boundaries. Distortions caused by misalignment or decentering of the lens elements are described with the p_1 and p_2 tangential coefficients (Atkinson, 2001). Camera parameters computed in the 'advanced' calibration are saved in a sensor file in ASCII format (with .SEN suffix) for later use in high-accuracy projects.

Target layout and camera stations

In order to achieve the highest photogrammetric accuracy possible, the bridge structure should be targeted with artificial targets. Circular-type targets with high contrast (e.g. solid white circles on a black background) make good photogrammetric targets because they can be accurately located and marked in the FotoG software with the sub-pixel marking tool. Sub-pixel measurement is a standard feature in many photogrammetry software programs which can accurately calculate the center of a circular target to a fraction of a pixel. To work properly, however, sub-pixel interpolation algorithms require that photogrammetric targets have a strong contrast with the surrounding background and also an appropriate diameter so that there are sufficient pixels across the target width in the digital image. The number of pixels crossing a circular target depends on the camera resolution, the target diameter, and the camera-to-target distance.

Targets can be made out of diffuse (e.g. regular white paper) or retro-reflective (e.g. 3M reflective sheeting) material. Diffuse targets reflect light in all directions and, thus, provide a more uniform contrast from different camera angles; however, the level of contrast is quite low for this type of target, which makes target marking in the photogrammetry software difficult, particularly in dark images. Retro-reflective targets, on the other hand, reflect light at a higher intensity but not in all directions (light is reflected mostly back in the direction of the light source). As a result, this type of target provides a less uniform but stronger contrast when photographed with a flash. At any rate, this facilitates the marking of the targets in the images. Camera settings recommended for flash photography of retro-reflective targets are discussed later.

The selection of target locations depends on the type of bridge measurement. In applications involving the global measurement of bridge deformation under dead load or live load, for example, targets should be distributed on the girders at discrete locations (particularly where maximum deformation is expected) but densely spaced to define their overall deflected shape. More targets will increase the field time for installation, however,

the photogrammetry analyses are usually more successful owing to the large number of common points between photographs; in general, more targets will also result in better measurement accuracy. The targets should be positioned on the girders so that they are visible from both sides of the bridge width. When the bridge has a low vertical clearance, this may require that double-sided targets be used because of the relatively flat viewing angle; if there is a high clearance, single-sided targets may suffice. If possible, targets should also be mounted on tripods (or a scaffold) and distributed in the space between the underside of the superstructure and ground level. This completely fills the image with targeted points, which can serve to improve the photogrammetric solution; however, in some situations it may be difficult or not possible to include these space filler targets under the superstructure, such as bridges over traffic or water or a deep ravine.

To establish the actual scale and location of the bridge, targets should be situated at stable reference points near or on the structure. These control targets must be surveyed prior to the photogrammetric measurement to determine their three-dimensional coordinates in an external reference system. If the bridge site permits and targets are distributed in the area under the superstructure as discussed earlier, a chosen few of these filler targets can also be used for control purposes. Alternatively, control targets can be placed directly on substructure elements such as the abutments, wingwalls, and/or piers when negligible movement of these elements is expected under loading relative to the superstructure. The control targets should be well distributed throughout the photographed area and visible in numerous photographs; otherwise, the photogrammetry analysis may fail or produce erroneous results.

Given the target layout, the design of the photogrammetric network continues with the selection of the camera stations. An appropriate number and distribution of camera stations must be chosen to provide convergent viewing angles of the targeted structure; only targets with a clear line of sight to the camera can be measured. As mentioned earlier, the basic principle of triangulation requires that each target appear in at least two photographs to determine its spatial location; however, four or more photographs generally provide better photogrammetric measurements. A general rule of thumb is to station the cameras so that the angular separation of their optical axes from different directions is as close as possible to 90°. Vertical separation requires camera stations at elevated heights above ground level, which can be done through use of a ladder but leads to significant delays in the photography. A high camera perspective also limits or completely eliminates the view of targets installed on the underside of the girders. Instead, pictures should be taken from both sides of the bridge width to achieve the required angular separations. Sketches (a) and (b) of Fig. 11.7

show the photographic geometry plan for a single-span bridge in plan and cross-sectional view, respectively. As shown in Fig. 11.7(a), there are a total of 18 camera stations; 9 on either side of the bridge width. The bridge is divided into three regions for purposes of the photographic network: the left pier to mid-span; quarter-span to quarter-span; and mid-span to the right pier. For each portion of the bridge, there are a total of six pictures angled towards the center of the photographed region in both the horizontal (see Fig. 11.7a) and vertical (see Fig. 11.7b) directions to provide convergent viewing angles close to 90°.

Control survey and image acquisition

For small-scale or low-accuracy measurements, control targets can be measured manually to determine their spatial coordinates. It is more appropriate and feasible, however, to use a total station for the control survey in large-scale projects and when high accuracy is needed. The accuracy and reliability of photogrammetric measurements are heavily dependent on the control survey; as a result, they should be carried out carefully and preferably by a licensed surveyor. A detailed discussion of control survey procedures is outside the scope of this chapter; the reader may refer to the FotoG user's manual (Vexcel, 2000) or other basic surveying references for that information. Results of the control survey should be reported in a Cartesian coordinate system and written into a control point file (with .CTL suffix); for example, with the *X*-axis parallel to the bridge length, the *Y*-axis perpendicular to the bridge length, and the *Z*-axis in the vertical direction as determined by the right-hand rule. The origin of the coordinate system is not important; however, it, along with the designated axis orientations, must be the same in both the unloaded and loaded state of the bridge if relative deformations are desired. If possible, control surveys should be conducted prior to, during, and after loading to ensure that the control targets remain stationary. This allows adjustments to be made in the measurements should the control targets experience significant deformation under loading.

Basic camera settings should be checked before starting the photography. Ensure that the *f*-stop is at its highest setting, the focal setting is infinity, the focus mode is manual, and the image quality is at its highest resolution; these settings are the same for both non-flash and flash photography. The camera stations should be angled as designated in the photographic geometry plan but located as close as possible and at constant distances from the targeted structure to fill the image area with a maximum and uniform number of targets; peering through the viewfinder helps with this task. FotoG requires a 60–70% overlap between images (Vexcel, 2000). If diffuse targets are used, the camera should be used without a flash

and mounted on a tripod in aperture priority, auto-exposure mode as discussed earlier. Diffuse targets are hard to recognize and are virtually invisible in darker areas under the bridge. The use of a flash appears to be a solution but actually overrides the white balance feature of the camera needed for optimum exposure; instead, it triggers a shorter shutter speed, which will reduce the image quality needed for non-flash photography of diffuse targets.

If retro-reflective targets are used, the camera should be fitted with a flash; two recommended flashes that fit the Kodak DCS 660 and Nikon AF 28/2.8D lens are the Sunpak Auto DX12R ring light and the Nikon SB-28DX speedlight. The ring light transmits light primarily in the viewing direction of the camera as opposed to the wide dispersion of light transmitted by the speedlight. Determining the light intensity and shutter speed for proper illumination of the targets is often done by trial and error, and depends mainly on the camera-to-target distance. Care must be taken not to overly illuminate the targets and prevent blooming which can adversely affect the photogrammetric marking of targets. This occurs when the pixel capacity for storing light is exceeded and overflows into neighboring pixels, thus distorting the appearance of the targets in the image area (Atkinson, 2001). Because of the fast exposure, the camera does not have to be mounted on a tripod, meaning that the photography can be completed much more quickly. Furthermore, with these flash photography settings, the pictures are underexposed and the retro-reflective targets appear as very bright dots, which are easier to mark in the photogrammetry software. A final note is that the use of a flash does not mandate a different camera calibration since the interior orientation elements are mainly dependent on focal setting, not on image exposure.

The Kodak DCS 660 camera has two drives for storing digital images on removable, solid-state memory cards. As mentioned earlier, these cards are available with storage capacities ranging up to 2 gigabytes, which provides ample memory to complete the photography without the need for intermediate downloads to a laptop computer. With two 340-megabyte cards, for example, a total of about 120 images can be stored in TIFF format at the maximum resolution of 6 megapixels (each high-resolution TIFF image occupies about 5.3 megabytes of memory space). Before departing from the bridge site, however, the images should be transferred to a laptop computer using peripheral card readers or a Firewire connection and further backed up on a CD or DVD. In addition, the photographs should be properly labeled according to the camera station, particularly in large projects. Often, many photographs can be so similar in appearance that they cannot be distinguished, which can lead to confusion during the photogrammetric analysis phase of the project. The importance of successfully storing, backing up, and naming the pictures cannot be

overemphasized since lost or mistaken images will ruin a photogrammetry project. These basic suggestions also apply to the digital photographs in a virtual reality project.

Image preparation and analytical processing

There are four main modules in the FotoG photogrammetry system, each of which is designed to handle a specific task in the overall photogrammetric measurement process. These modules along with their basic function in FotoG are listed below (Vexcel, 2000):

- ControlM – generates control point coordinates for use in small-scale and/or low-accuracy projects.
- LoadM – loads the camera calibration information and converts the digital images into the proper format.
- BlockM – carries out the analytical processing of the converted images (i.e. relative orientation, block formation, absolute orientation, bundle adjustment) based on camera and control data.
- CollectM – interacts with CAD environments to extract object features and produce 3D models.

As is evident in these descriptions, the use of FotoG for bridge monitoring purposes will usually not require the ControlM and CollectM modules; thus, attention will be given only to the LoadM and BlockM modules in the remainder of this section.

The Kodak DCS 660 takes digital photographs in a proprietary version of the standard TIFF format. To be used in FotoG, the DCS images must be converted into standard TIFF format using the LoadM utility. In this software utility, the user starts by selecting the directory that contains the DCS images and for the placing of the processed images; the sensor file containing the camera calibration information and group name for the new images is also selected. The 'DCS In' process option of the software utility executes the conversion which increases the TIFF image size about threefold (i.e. 5.3 to 17.9 megabytes) and also creates a number of data files for storing image measurements and other related information.

Once the photographs are converted from DCS to FotoG ready format, analysis of the processed images is then performed with the BlockM utility. Similar to LoadM, the user starts by selecting the image directory and the sensor calibration file; in addition, the control point file and the project name/directory are selected. Next, a block of photographs is created by adding and connecting two images in the BlockM workspace. Recall that at least two images are needed for point measurement by triangulation. In each image, the user then proceeds to label and mark all the visible targets including tie (unsurveyed) and control (surveyed) points. Two linked pic-

tures must contain at least 6 points in common; however, 12 or more are recommended. The common targets can all be tie points or a combination of tie and control points. As mentioned in an earlier discussion, high-contrast circular targets (preferably retro-reflective) can be marked most accurately using the sub-pixel marking tool. Questionable targets should not be marked since considerable errors or failure of the photogrammetric analysis may result.

The relative orientation and block formation phase serve to orient the two photos in an image coordinate system based on the camera calibration parameters; the absolute orientation and bundle adjustment phase calculate and optimize the camera locations associated with the two images in an external, real-world reference system based on the control point coordinates. After each step, FotoG generates a diagnostic report in order for the user to monitor the progress of the photogrammetric solution. These reports should be reviewed routinely after the import and target marking of each image in the block and, preferably, even more frequently after a few targets have been marked and referenced between photographs. This allows the user to properly identify errors before the number of images and marked targets gets too large. Into a successfully completed block, another image can now be added, marked, and connected to preceding images and the four-stage process is repeated. A set of three linked images must have at least one common point between them. Remaining images continue to be imported in this fashion until the photographic network is complete. The final block can range from a minimum of two photographs to a maximum of 50 and there must be at least three control points in the block. With artificial targets, satisfying the FotoG requirement for the number of common points is not an issue and neither is the control point requirement if sufficient reference targets are installed and surveyed.

With the camera stations known, it is now possible to measure targets visible in at least two photographs by intersection. The measurements are three dimensional and in the real world coordinate system established by the control survey. In addition to the three-dimensional coordinates of the marked targets, FotoG also reports the measurement precision or standard deviation for the calculated x, y, and z coordinates, which allows the user to evaluate the final quality of the photogrammetric solution. Photogrammetric accuracy is influenced by many variables, including the characteristics of the camera lens system; the quality of the camera calibration; target design and distribution; the accuracy of the control survey; the design of the photographic network (i.e. camera stations); image quality and target contrast; and the sophistication of the photogrammetry software. Operator experience and the implementation of proper photogrammetric procedures and equipment, as covered in the foregoing sections, will increase

the likelihood of achieving high-accuracy measurements in bridge monitoring applications.

11.4 Potential impact and future developments

11.4.1 Virtual reality

Virtual reality can favorably contribute to bridge inspection practice in several possible ways. First of all, inspectors will often review information given in past reports to determine the type and severity of previously observed damage and/or deterioration to prepare for an upcoming bridge inspection. Design drawings, field sketches, and/or still photographs are also reviewed to further aid the inspector. Following the inspection, the observed bridge condition is then evaluated relative to that previously recorded to determine if there are any changes. This comparison may be troublesome owing to the written format and limited amount of photographic documentation given in a typical inspection report. It is important to note that the NBIS requires photographs of only the side elevation of the bridge and the top of the roadway (AASHTO, 2000). In a virtual reality system, notes and photographs can be integrated into an interactive and more realistic visual environment to aid in tracking changes from inspection to inspection.

Another powerful feature of this technology is that design drawings, overhead maps, and/or audio recordings can be integrated into the virtual reality record using programs such as those developed by Squamish Media Group (2004). In such an application, clickable node markers may be overlaid on the bridge drawing or map at different reference points. Clicking on a node marker then transports the inspector to a linked panorama. As the inspector navigates the panorama, a directional indicator on the active node marker follows the inspector's line of sight to show the position and viewing orientation of the panorama along with an audio description. This particular capability may prove quite useful to acquaint the inspector with the bridge structure and site prior to an inspection. As indicated earlier, consistent and uniform field inspections depend greatly on the experience and training of the inspection teams. The detailed, high-resolution photographic records will allow supervisors to quickly review each inspection without personally visiting every structure. Supervisors will also be able to review inspections with the field crews to improve the quality of the final reports to better determine when critical damage or deterioration has occurred.

Bridge inspector training courses that cover visual inspection could benefit greatly from virtual reality technology. In order to fulfill NBIS training requirements, inspectors must complete a comprehensive training

course based on the Bridge Inspector's Training Manual (FHWA, 1995a). These courses are offered by various agencies and cover general topics such as bridge mechanics; bridge materials; bridge types and components; fundamentals of bridge inspection; and bridge inspection reporting. Also covered in depth are the inspection and evaluation of bridge decks; timber, concrete, and steel superstructures; fracture critical bridge members; bridge bearings; and substructures. As part of the course, participants are asked to review as-built drawings, previous inspection reports, and photographs for various case studies. Alternatively, this bridge condition data could be put together for examination in a virtual reality setting, thus making the inspection exercise much more valuable and realistic. Certainly, time must be allotted in any practical-oriented training course to include hands-on field inspections at the actual bridge site; however, in the interests of time, only so many can be made. Virtual bridge inspections cannot replace field experience, but can definitely help the inspector gain valuable experience without having to leave the classroom. Also, on-the-job training by supervisors and more experienced inspectors could be accomplished by this method.

A major concern in adopting a virtual reality approach for documenting bridge inspection projects is that the size of the final output files can be quite large. Several factors influence the file size, a few of which are (1) the resolution of the digital camera; (2) the size of the panoramic image display; (3) the compression algorithm chosen for the rendering process; and (4) the number of panoramas and/or individual pictures integrated into the final output file. A possible way to address this issue is to post the virtual reality files on the Internet. When the Apple QuickTime Player is installed, plug-in drivers are automatically loaded for the Netscape and Internet Explorer browsers so that virtual reality content may be viewed over the web. This means that several smaller-sized panoramas may be linked together with a web browser rather than having all the panoramas on a single, large file. Web-based applications also make it possible to manage conventional bridge inspection forms. Internet files can also be accessed by supervisors or bridge experts when needed without visiting the site. In fact, the integration of virtual bridge inspections and the Internet provides a vast array of possibilities for further development.

An important final note about virtual reality is that the field work may be challenging for some bridges. For example, bridges located in areas of heavy traffic or crossing a river may need to be closed or require traffic control to perform the photography. Furthermore, a river crossing may require special equipment to position the inspector underneath the bridge to take pictures. Bridge sites having other forms of moving obstructions (such as those located in construction zones) are also demanding candidates for virtual reality since the photography must be carried out during periods

of either low or no construction. To summarize, situations where traffic control, bridge closure, and/or special equipment rental are needed will demand more of a time investment and also result in higher inspection costs compared with those of a typical inspection.

11.4.2 Photogrammetry

Much like virtual reality, close-range photogrammetry has tremendous potential in the fields of bridge inspection and monitoring. First of all, a major challenge in the field testing of bridges is the measurement of vertical deflection. The use of instruments such as mechanical dial gages, linear potentiometers, LVDTs (linear variable differential transformers), and other similar types of deflection transducers is often difficult since a fixed base is needed from which relative displacements are measured. This may require access under the bridge to erect a temporary support to mount the instrument or for running a wire from the instrument to the ground. Other non-traditional methods have also been employed by agencies such as the Swiss Federal Laboratories for Material Testing and Research, which have successfully used a wire-supported method, a water-leveling method, a horizontal wire-leveling method, and an electronic leveling system for vertical deflection measurement (Ladner, 1985). Compared with these measurement techniques, however, the photogrammetric method has several advantages, a few of which are (1) it is less labor-intensive; (2) it is capable of measuring difficult-to-access structures; (3) a large amount of geometric data can be extracted from the photographs; (4) additional measurements can be taken at a later time without repeating the field work; and (5) it can be used on a routine basis for various measurement applications (Bakht and Maheu, 1994). Furthermore, photogrammetry is a non-contact technique, meaning that measurements are made without having to touch the structure. Other systems are available which provide non-contact measurement capabilities using laser technology; however, at a higher cost. A photogrammetric system can operate at a fraction of the cost of a laser-based system and is thus, perhaps, more likely to fit within the budget constraints of a highway agency.

As mentioned earlier, routine bridge inspections are chiefly performed in accordance with highly-subjective visual procedures and are often carried out within high traffic corridors. One of the most time-consuming and frequently dangerous activities in a routine inspection is the measurement of vertical and horizontal clearances. Currently, inspectors must use measuring tapes or rods and often have to complete this task surrounded by high traffic volumes. As photogrammetry techniques continue to develop, clearance measurements may be made from digital photographs taken from more remote locations away from traffic. A related inspection difficulty is the

measurement of cracks, delaminations, and spalls, as well as other types of deterioration in locations where access is extremely difficult. Again, photogrammetry techniques can provide the means for a safe and accurate measurement of a deteriorated area.

Another aspect of bridge inspection that may benefit from close-range photogrammetry is the documentation of historic structures, particularly those that may need to be removed or destroyed. Federal regulations require the proper documentation of historic bridges including such aspects as overall geometry, structural deterioration, and historic features. Many photogrammetry software programs have the capability to create three-dimensional, photo-textured models as well as two-dimensional, orthographic photographs (i.e. ortho-photos). Photo-textured modeling allows natural textures to be extracted from the photographs and applied to the surfaces of the three-dimensional model, providing a truly realistic impression of the structure. These models can be exported into virtual reality format for display in still-life or animated format and may also be ultimately posted on the Internet for remote viewing by other interested parties. Ortho-photos represent the projection of a three-dimensional model onto a two-dimensional plane and, thus, provide the means for creating as-built drawings of a structure in plan, cross-section, and/or elevation view. Since perspective is removed, ortho-photos have the advantage that they may be directly used for object measurement using the appropriate scale. Both these features allow the structure to be displayed in a much more realistic format and viewed from different directions, which can serve to provide a much better understanding and appreciation of the bridge's construction and historical significance.

As with any new technology used for bridge inspection and monitoring, there are certain obstacles that must be overcome for field use, and close-range photogrammetry is no exception. Environmental factors such as temperature and humidity variations in the air may contribute to errors in photogrammetric measurement and ways to minimize and/or compensate for these variations must be investigated. One such remedy is to perform the photography close to sunset to help stabilize environmental conditions which can also serve to minimize traffic disruption. Flash photography can be performed using retro-reflective targets and equipping the digital camera with a high-intensity ring light. Another potential way to account for environmental factors is by self-calibrating the digital camera at the bridge site. In a self-calibration, optical parameters such as focal length and lens distortion of the digital camera are determined from points measured on the actual structure and based on the *in-situ* environmental conditions as well as the true object scale (Atkinson, 2001).

Another aspect of photogrammetry in need of further investigation is establishing the control network. The traditional approach of using a total

station to obtain 3D coordinate data of control points is extremely time-consuming and prone to measurement errors of its own. Some photogrammetry systems offer the option to perform the bundle adjustment using a free-network solution (with inner constraints established by calibrated scale bars). This approach could serve to reduce the time spent in the field since bars with known dimensions could be used to establish the control network instead of surveyed points; however, further investigation is needed to determine the level of accuracy of the free-network bundle adjustment. The capability of automated target recognition instead of manual point marking is also provided by some systems, which could reduce image processing time, making the use of close-range photogrammetry in bridge applications much more efficient.

Finally, professional-grade digital cameras continue to increase in pixel resolution while decreasing significantly in cost. For example, the Kodak DCS SLR Pro/n digital camera at the time of writing provides the industry's highest pixel resolution at 14 megapixels and is priced approximately one-fifth of that of the Kodak DCS 660 (6 megapixel resolution) when purchased in the year 2001. With higher-resolution cameras, the potential exists for continual improvement in photogrammetric measurement accuracy.

11.5 References

AASHTO (1998), *AASHTO Guide for Commonly Recognized (CoRe) Structural Elements*, Washington, American Association of State Highway and Transportation Officials.

AASHTO (2000), *Manual for Condition Evaluation of Bridges*, 2nd Edition, Washington, American Association of State Highway and Transportation Officials.

Albert, J., Maas, H.-G., Schade, A. and Schwarz, W. (2002), 'Pilot studies on photogrammetric bridge deformation measurement', *2nd International Symposium on Geodesy for Geotechnical and Structural Engineering*, Berlin.

Apple (2004), *QuickTime VR Authoring*, http://www.apple.com/quicktime/qtvr/, August 2004.

Atkinson, K.B. (2001), *Close Range Photogrammetry and Machine Vision*, Caithness, Whittles Publishing.

Bakht, B. and Maheu, J. (1994), 'Distress, monitoring, and repairs,' in Abdel-Sayed, G., Bakht, B. and Jaeger, L.G., *Soil–Steel Bridges: Design and Construction*, New York, McGraw-Hill Inc, Ch 10, 317–335.

Bales, F.B. (1984), 'Close-range photogrammetry for bridge measurement', *Transportation Research Record*, **950**, 39–44.

Cooper, M.A.R. and Robson, S. (1990), 'High precision photogrammetric monitoring of the deformation of a steel bridge', *Photogrammetric Record*, **13** (76), 505–510.

Cooper, M.A.R. and Robson, S. (1994), 'Photogrammetric methods for monitoring deformation: theory, practice and potential', *10th International Conference on Experimental Mechanics*, Lisbon.

FHWA (1995a), *Bridge Inspector's Training Manual 90*, Washington, Federal Highway Administration, United States Department of Transportation.

FHWA (1995b), *Recording and Coding Guide for the Structure Inventory and Appraisal of the Nation's Bridges*, Washington, Federal Highway Administration, United States Department of Transportation.

Forno, C., Brown, S., Hunt, R.A., Kearney, A.M. and Oldfield, S. (1991), 'Measurement of deformation of a bridge by moiré photography and photogrammetry', *Strain*, **27** (3), 83–87.

Fraser, C. and Brizzi, D. (2002), 'Deformation monitoring of reinforced concrete bridge beams', *2nd International Symposium on Geodesy for Geotechnical and Structural Engineering*, Berlin.

Fraser, C.S. and Riedel, B. (2000), 'Monitoring the thermal deformation of steel beams via vision metrology', *ISPRS Journal of Photogrammetry & Remote Sensing*, **55** (4), 268–276.

Geodetic Services (2004), *Picture Perfect Measurements*, http://www.geodetic.com/, August 2004.

Greve, C. (1996), *Digital Photogrammetry: An Addendum to the Manual of Photogrammetry*, Maryland, American Society for Photogrammetry and Remote Sensing.

Jáuregui, D.V., White, K.R., Woodward, C.B. and Leitch, K.R. (2003), 'Noncontact photogrammetric measurement of vertical bridge deflection', *ASCE Journal of Bridge Engineering*, **8** (4), 212–222.

Johnson, G.W. (2001), 'Digital close-range photogrammetry – a portable measurement tool for public works', *2001 Coordinate Measurement Systems Committee (CMSC) Conference*, Albuquerque, NM.

Kaidan (2004), *Photographic VR Solutions*, http://www.kaidan.com/, August 2004.

Kim, B.-G. (1989), '*Development of a photogrammetric system for monitoring structural deformations of the sturgeon bay bridge*', PhD Dissertation, Madison, University of Wisconsin.

Kodak (2004), *Professional Imaging Solutions*, http://www.kodak.com/, August 2004.

Kraus, K. (1986), 'Modern photogrammetric technology focusing civil engineering', *Photogrammetria*, **41**, 31–41.

Ladner, M. (1985), 'Unusual methods for deflection measurements', *1985 Symposium on Strength Evaluation of Existing Concrete Bridges*, Washington.

McGlone, C. (2004), *The Manual of Photogrammetry*, Maryland, American Society for Photogrammetry and Remote Sensing.

Mikhail, E.M., Bethel, J.S. and McGlone, J.C. (2001), *Introduction to Modern Photogrammetry*, New York, John Wiley & Sons, Inc.

Nastasia, L. (1998), 'Digital photo and close-range photogrammetry meet surveying tech for highway design and maintenance', *Advanced Imaging*, **13** (1), 46–48.

NBIS (1996), *Code of Federal Regulations, No. 23CFR650*, Washington, National Bridge Inspection Standards, US Government Printing Office.

Pappa, R.S., Jones, T.W., Black, J.T., Walford, A., Robson, S. and Shortis, M.R. (2002), 'Photogrammetry methodology development for gossamer spacecraft structures', *Sound and Vibration*, **36** (8), 12–21.

Phares, B.M., Graybeal, B.A., Rolander, D.D., Moore, M.E. and Washer, G.A. (2000), 'Reliability and accuracy of routine inspection of highway bridges', *Transportation Research Record*, **1749**, 82–92.

Realviz (2004), *The Stitcher User Manual*, Version 4.0, Valbonne, Realviz.

Rolander, D.D., Phares, B.M, Graybeal, B.A., Moore, M.E. and Washer, G.A. (2000), 'Highway bridge inspection: state-of-the-practice survey', *Transportation Research Record*, **1749**, 73–81.

Schenk, T. (1999), *Digital photogrammetry, volume I*, Laurelville OH, Terrascience.

Scott, P.J. (1978), 'Structural deformation measurement of a model box girder bridge', *Photogrammetric Record*, **9** (51), 361–378.

Spero, P.A.C. (1983), *The Photogrammetric Recording of Historic Transportation Sites*, Report VHTRC 83-R35, Charlottesville, Virginia Highway and Transportation Research Council.

Squamish Media Group (2004), *VR Enhancement Suite*, http://www.smgvr.com/, August 2004.

Vexcel (2000), *The FotoG User Manual*, Version 5.1, Boulder, Vexcel.

VR Toolbox (2003), *The VR Worx User Manual*, Version 2.5, Pittsburgh, PA, VR Toolbox.

White, K.R., Minor, J. and Derucher, K.N. (1992), *Bridge Maintenance, Inspection, and Evaluation*, 2nd Edition, New York, Marcel Dekker, Inc.

Whiteman, T., Lichti, D.D. and Chandler, I. (2002), 'Measurement of deflections of concrete beams by close-range digital photogrammetry', *2002 Symposium on Geospatial Theory, Processing and Applications*, Ottawa.

Wolf, P.R. and Dewitt, B.A. (2000), *Elements of Photogrammetry with Applications in GIS*, New York, McGraw-Hill Co., Inc.

Woodhouse, N.G. and Robson, S. (1998), 'Monitoring concrete columns using digital photogrammetric techniques', *11th International Conference on Experimental Mechanics*, Oxford.

Woodhouse, N.G., Robson, S. and Eyre, J.R. (1999), 'Vision metrology and three dimensional visualization in structural testing and monitoring', *Photogrammetric Record*, **16** (94), 625–641.

12

Discontinuity in masonry walls

M. PIERACCINI
University of Florence, Italy

12.1 Introduction

Masonry civil structures form a large portion of the building stock, and as they increase in age, there is considerable interest in maintaining and extending their lives. Furthermore, a considerable number of masonry buildings are part of the cultural heritage, so their maintenance and conservation are also priorities, apart from their serviceability. On the other hand, the definition of cultural heritage has been considerably extended recently, therefore even relatively recent buildings are objects of diagnosis and restoration instead of demolition and reconstruction. Diagnoses and maintenance of masonry bridges are of particular importance because they are often in service despite the fact they were not designed and built for heavy modern traffic loads. Many old masonry bridges and civil structures do not have any reliable records of construction or repair details, so it is often difficult to obtain suitable knowledge of the physical external and internal structure, and possibly the presence of discontinuities, in order to identify structural problems and to plan remedial action to be taken.

Unfortunately masonry is an inhomogeneous material for which all techniques applicable to homogeneous materials seem to fail. Furthermore, faults and discontinuities are often located at joints in marginal zones, where geometry does not cooperate with inspection. In recent years, a great amount of scientific and technical work has been done in the field of masonry non-destructive testing (NDT), but in spite of this effort, the application of NDT techniques to the solution of civil engineering problems has sometimes been disappointing. This has arisen from either using a method that lacked the precision and reliability required in a particular structural investigation, or by specifying a method that was inappropriate to the problem under consideration. The latter is a common problem in NDT investigation; the inspection technician dreams of a sort of 'universal instrument', like the X-ray of comic superheroes, able to penetrate and image any sort of material, and able to ignore all non-significant inhomogeneities.

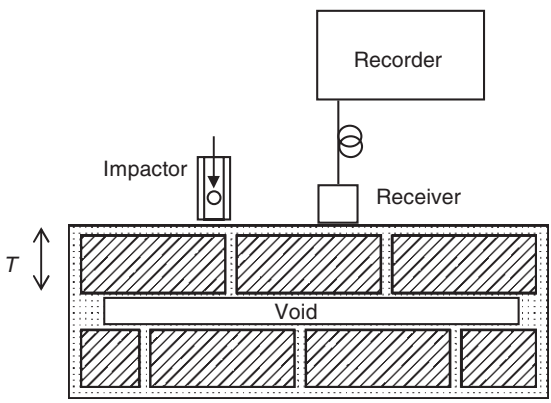
These expectations are systematically disappointed, particularly for masonry structures. This gap between unrealistic expectations and physical reality can be avoided by a deeper knowledge of the available monitoring tools before initiating the survey. The aim of this chapter is to provide a critical review of the most popular NDT techniques used in masonry investigation.

First of all, a dutiful specification; visual inspection remains the predominant and most useful NDT technique for detecting discontinuities in masonry walls. Indeed, if visual inspection is applicable, that is discontinuity in masonry causes visible cracks on the surface, no other technique is more effective and reliable than the eyesight of an expert technician. Problems arise when discontinuities are internal or in not easily accessible locations. In these cases, more advanced tools are necessary.

12.2 Impact echo

The simplest tool for detecting hidden discontinuities in masonry is obviously just a hammer; a skilled inspector, by simply beating on the masonry surface, can qualitatively evaluate the presence of detachment and superficial cavity. The direct technological evolution of the hammer is the IE (impact echo) technique [1,2]. The IE technique is traditionally used to locate defects within concrete structures; however, this technique is potentially suitable for integrity evaluation of masonry structures. Indeed, the application of IE to masonry structure has been recently evaluated [3].

The basic principle of the IE method involves impacting the surface of the material with a small diameter impactor and detecting and recording the response (see Fig. 12.1). The Fast Fourier transform (FFT) of the



12.1 Impact echo working principle.

detected signal is related to the thickness between the external surface and an inner interface by the following relationship:

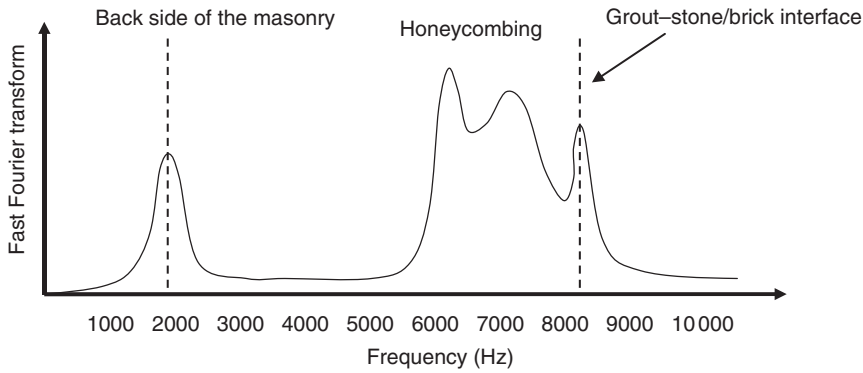
$$T = \frac{\beta C}{2 f_{\mathrm{p}}} \qquad [12.1]$$

where β, the geometrical factor for planar discontinuity is 0.96, f_{p} is the frequency peak, and C is the speed of the mechanical P-wave in masonry. C should be evaluated *in situ* by measuring on selected points of known thickness with no internal defects. A typical speed for stone/brick masonry is about 3000–3500 m/s, lower than the typical speed in concrete (about 4000 m/s). As detectable thickness is typically between 0.1 and 1 m, the detected peak frequencies range from about 1500 to 15 000 Hz. Because of the lower speed and lower consistence of masonry with respect to concrete specimens, masonry has a pattern in frequency domain at lower frequencies: it is smoother with less evident peaks.

The prominent feature detectable using IE is the lack of grouting between stones or bricks. When there is no grouting behind the masonry, the entire signal can be reflected back from the stone/brick–grout interface. Hence, the maximum peak amplitude in the frequency spectrum indicates the thickness of the stone/brick. In the case of more consistent masonry, the mechanical wave is able to impinge on the back of the masonry and it gives a low-frequency peak. If the thickness of the wall is known, it is possible to evaluate C by using equation 12.1; otherwise, if the speed of the mechanical wave was previously evaluated, equation 12.1 gives the thickness of the masonry at the investigated point. The presence of voids, discontinuities and honeycombs within the core will result in reflection frequencies with values ranging from the wall thickness frequencies (the lowest) and reflections from stone/brick–grout interface. The honeycombing is identified when there are multiple peak frequencies at close range in the frequency spectra (see Fig. 12.2).

Finally, it is important to qualify the bonding condition for the constituents of the structure. To qualify the bonding conditions, the peak frequencies between the thickness and reflected anomalies are compared. If the frequency amplitude for the full thickness is smaller than the defect peak frequency, it indicates that not much of the energy has passed through the structure and most of the impact energy has been reflected from the anomaly. On the other hand, if the signal reflections from the opposite side of the structure are stronger or equal to the internal reflections, it indicates that the bonding is good or fair.

Impact echo produces good data for reading wall thicknesses and the overall integrity. In particular, it provides excellent results in detecting stone cracking parallel to the surface. Its optimal use is when working with homogenous stone materials; it does not produce good results with complex



12.2 Impact echo frequency response.

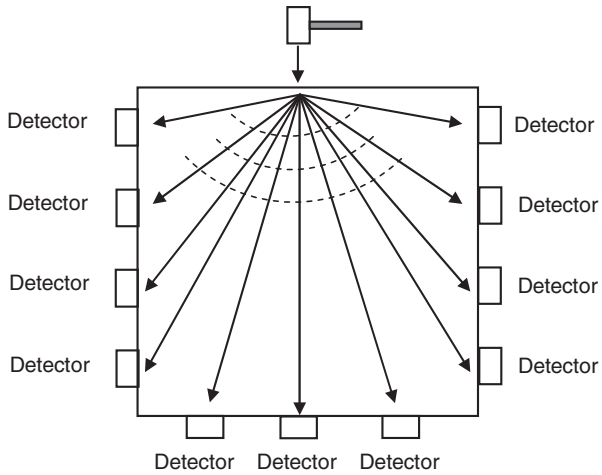
geometry and multiple layers of material. Therefore, brick arches and beams have not been well investigated, and the presence of energy-absorbing materials such as plaster or incoherent materials proves an impediment.

A notable feature of IE is that it is not adversely affected by the presence of steel reinforcing bars that can sometimes have a masking effect for electromagnetic sensors such as penetrating radar. In any case, it should be noted that depth of steel bars cannot be calculated by equation 12.1; it is no longer valid for a discontinuity filled with material with acoustic impedance higher than the propagation medium [4]. The following relationship has to be taken into account:

$$T = \frac{\beta C}{4 f_{\mathrm{p}}} \qquad [12.2]$$

12.3 Sonic tomography

Sonic tomography represents the ultimate improvement in the development of the sonic test method. By using an array of sensors, the mechanical wave is recorded at a great number of external points, ideally at any accessible points of the structure covering a close surface sampled of at least a quarter of the shortest sonic wavelength detected (Fig. 12.3). The masonry section under test is thus crossed by a dense net of ray paths, each of which relates to a specific travel time between the sonic source and receiver through the structure For a tomographic reconstruction, the test area is first divided into a number of pixels, each of which is assumed to have its own 'average' velocity. The travel time for a ray between two points on the perimeter of the area is then the sum of the transit times across each of the



12.3 Sonic tomography.

pixels that form the path. The simplest analytical technique assumes that each incident stress wave travels in a straight line between the transmitter and receiver. The most frequently used method in engineering tomography is an iterative algorithm. This algorithm gradually corrects the error between the measured travel time and the estimated travel time for each ray. This approximation is adequate for propagation in uniform homogeneous materials. However, if velocities for adjacent regions vary by more than approximately 20%, refraction and bending of the waves become significant, and more complex algorithms are required. The resulting image is a three-dimensional reconstruction of the velocity distribution across the structure or selected cross-section so that local variations in velocity can be identified and correlated with zones of weakness or flaws in the internal fabric of the structure.

In spite of its theoretical enormous potential, experimental tests on masonry are rather rare and results often not definitive. The best results are obtained when a structural element can be accessed from all sides, as in the case of the pillars of churches. The tomographic results can be more precise because the acquisition can be designed to ensure a dense and regular distribution of rays within the horizontal sections. Very good results were obtained by Binda *et al.* [5].

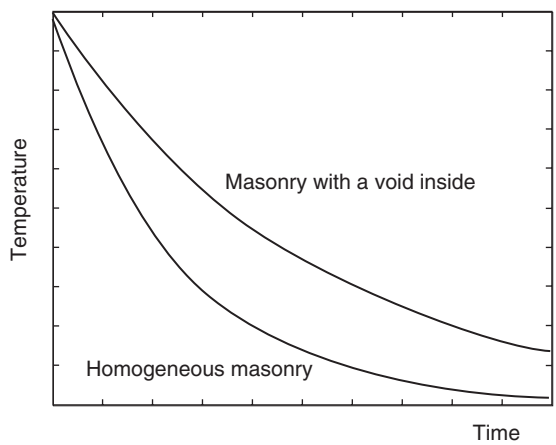
Sonic images currently suffer from lack of contrast and resolution, and are more suitable for material characterization than for detecting discontinuity. Results depend strongly on the elaboration techniques that are again rather rough: presumably, there will be significant advances in the future to the physical limits of this technique.

12.4 Thermography

Thermography is based on differential cooling of different materials in masonry. During the cooling process of a structure, for example at night, a thermo-camera takes an infrared image of the masonry that reflects the heat pattern on the wall. As different materials have different cooling times, the temperature pattern shows the hidden structure of the masonry. In particular, from the cooling behaviour at different positions on the surface, structural inhomogeneities in the near surface region can be located if the thermal conductivity, the specific heat capacity, or the density causes a measurable temperature difference. The void acts as an insulator and thus can be detected as a localized high temperature spot. Figure 12.4 shows the typical cooling behaviour at two points on a masonry.

In general, thermography is useful in locating hidden pipes and flues within masonry walls. The images of deteriorated brick masonry (water and salt damage) and patched areas of exterior granite walls clearly show as anomalies.

In masonry walls, this imaging technique is able to detect detachment of plaster, status of finishing, brick pattern, covered windows or doors. It should be noted that thermography based on natural heating during the day is not able to give information about the depth of the detected discontinuities. An alternative technique is based on the active heating of the surface using, for example, a bank of lamps [6,7,8]. Heating can be carried out through an impulse of several minutes (IT, impulse tomography) or through a sinusoidal modulation of the heating source (LT, lock-in tomography). The two methods give theoretically the same information, the first in the time domain, and the latter in the frequency domain. As heating is



12.4 Thermography.

controlled, it is possible to obtain information about the depth of the detected discontinuity. In fact, the depth can be determined as the maximum observation depth for a given frequency ω is given by the thermal diffusion length μ that can be expressed by the following formula:

$$\mu = \sqrt{\frac{2K}{\omega \rho C}} \qquad [12.3]$$

where ω is the modulation frequency of the infrared, K is the thermal conductivity, ρ is the density and C is the heat capacity. The thermal diffusion length indicates the length at which the amplitude of the thermal wave has been reduced by the l/e factor (where e is Neper's number). Approximately up to this depth, the thermal wave has enough energy to give a signal (measurable temperature difference) on the surface.

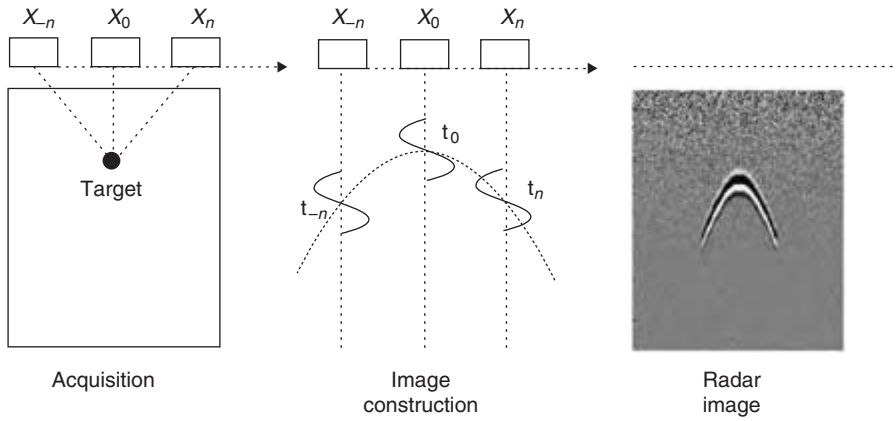
Active thermography is a more sophisticated investigation tool than passive thermography, but for large structures, the controlled heating is often impractical. Furthermore, as active thermography makes use of a very limited source of thermal energy compared with natural heating, investigation depth is usually limited to several centimetres; for example, voids up to a depth of approximately 10 cm can be detected after a heating duration of 5–10 min.

12.5 Penetrating radar

Penetrating radar techniques are based on the capability of electromagnetic waves to penetrate materials such as ground/soil, concrete and masonry. Generally speaking, a microwave transceiver is able to detect a discontinuity inside an investigated medium by measuring the time of flight of the electromagnetic wave from the transceiver that impinges on the discontinuity and is back-reflected. By scanning a surface as in Fig. 12.5, a punctual discontinuity is detected at different times of light. If single time traces are arranged by forming a bi-dimensional figure, a punctual discontinuity appears in the radar image as a hyperbola.

Technical literature reports [9,10] a number of successful applications of penetrating radar employed in masonry: determination of the structural thickness of masonry; determination of kind, location and size of voids and unfilled joints in masonry; location of inclusions of different materials such as steel and wood; checking the effectiveness of repair by injection techniques, detection of the internal structure of the wall section in multiple-leaf stone and brick masonry structures (multi-shell construction), and determination of moisture and salt content and distribution.

The radar equipment can be based on two different working principles: pulse or continuous wave. The pulse systems produce a short pulse (several ns) and with sampler acquisition electronics they detect the received



12.5 Surface penetrating radar (GPR). Image formation.

waveform (see Fig. 12.6). These systems are very popular and rather affordable but have a significant drawback; they are not able to generate a very large bandwidth. Generally speaking, the range resolution in radar image depends on bandwidth through the following equation:

$$\Delta R = \frac{v}{2B} \qquad [12.4]$$

where ν is the speed of electromagnetic waves in the investigated medium and B is the bandwidth. For a pulse system, the bandwidth is approximately given by the inverse of pulse duration. As the speed of electromagnetic waves in a masonry is about 1.5 m/ns, if, for example, a system is able to produce pulse of 5 ns and the range resolution is 15 cm, that cannot be compliant with the size of the smallest discontinuities of interest in masonry. Unfortunately, pulse durations shorter than 1–2 ns can be very difficult to sample and acquire.

Very large bandwidths can be provided by continuous wave systems. They operate in frequency domains, provide a single frequency at a time and can scan a band frequency by frequency (see Fig. 12.7). Because the measurement band for each frequency step is very small, electronics can easily manage very large bandwidths. In spite of their better band performance, these systems have two main drawbacks:

- The speed of acquisition is much lower than for pulse systems. As these systems often have an acquisition speed lower than 1 cm/s they are not suitable for large surfaces and may need a mechanical positioner.

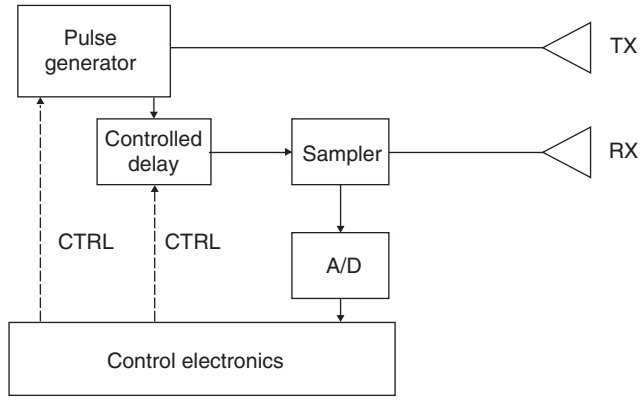
Recently, new high-speed continuous wave (CW) radar based on direct digital synthesis has been proposed [11].

- Energy on target (EOT) is typically lower than for pulse systems. CW operation is not able to manage very high power because receive electronics can be blinded by directly transmitted power.

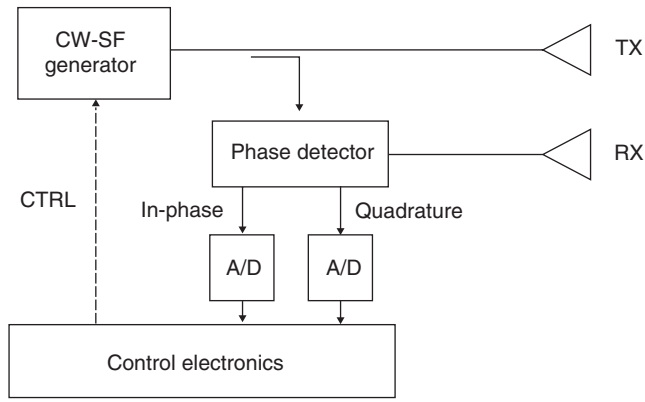
The antenna is a critical component in penetrating radar. The main problem in antenna design is that the target is always in near field, so antenna behaviour depends on the characteristics of the investigated medium, which can vary greatly. No-contact antennae are used if the surface can be damaged (e.g. a historic painted wall [12]), or if a very fast scan is necessary (e.g. in asphalt monitoring [13]). The electromagnetic behaviour of a no-contact antenna is less sensitive to characteristics of the investigated medium (depending on operation distance), but they lose about 10–25% of radiated energy because of the reflection on the air–wall interface. Furthermore, signals of airborne targets can be very evident and can make the interpretation of the radar image difficult. It should be noted that no-contact radar requires some mechanical positioning system that can prove to be a logistic problem in many applications. Contact antennae are more practical, but their electromagnetic performance is often low. Typically, they are of low efficiency, are asymmetrical and have no regular radiation pattern – it is strongly dependent on the investigated medium. In masonry investigation practice, array contact antennae are a significant improvement because they reduce scan time and provide spatially dense data.

The polarization characteristics of antennae are also important in radar image quality. In general, by employing linearly polarized antennae (e.g. bow tie or horn), a target with prevalent orientation along the polarization direction gives stronger signals. This property can be useful for detecting the disposition of bricks in a masonry [9].

Processing techniques of radar acquisition can be on-line and off-line. On-line processing is fairly standard and consists mainly of equalization and windowing. The most popular off-line processing technique is the focusing that is based on the sum of all signal contributions, taking into account their phase history [14]. It should be noted that in order to obtain radar images without angular ambiguity (i.e. phantom images at particular view direction) it is necessary to use spatial sampling smaller than a quarter of the wavelength. Focusing algorithms are able to transform the hyperbola shape in points and in general to focus the spread back-radiated energy in target points. Figure 12.8 shows an application on test masonry that exemplifies the effect of the focusing in real data acquired in order to detect a cavity in a brick wall. Radar data were acquired using a contact CW-radar operating in the band 500–1500 MHz. The antennae are bow-ties and they scanned



12.6 Pulse GPR. (CTRL, control; A/D, analogue/digital converter; TX, transmit; RX, receive.)

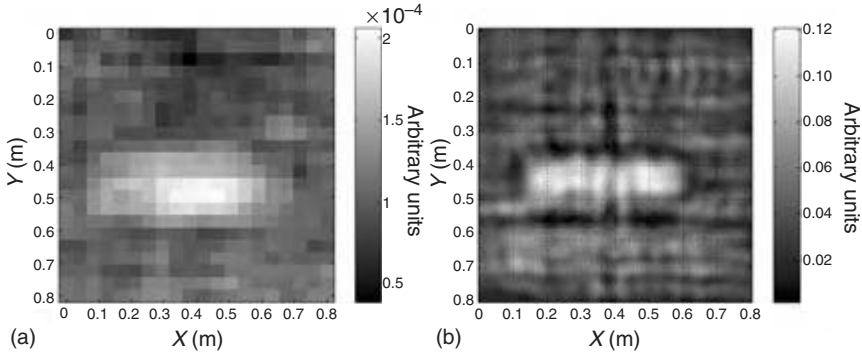


12.7 Continuous wave SPR. (CW-SF, continuous wave step frequency.)

the whole of the masonry vertical plain with a planar matrix with steps smaller than a quarter of the wavelength in order to obtain focused images without angular ambiguity.

Figure 12.8 shows an unfocused and a focused image. The focusing procedure was applied to both planar directions. In the focused image, the edges of the cavity are more clearly detected compared with the unfocused one. It should be noted that the scale of the greycode bar highlights the bigger dynamics in the focused image given by the focusing of the spread energy.

Focusing techniques for non-contact operation require some additional processing in order to take into account that the electromagnetic signal propagates through two different media from air to wall. Generally speak-



12.8 Radar images of the masonry test facility: (a) unfocused image; (b) focused image.

ing, the air–wall interface causes a change in path due to reflection (Snell's law) and a change in the speed along the path according to the relative dielectric constant. Both effects have to be taken into account by the focusing algorithm. Figure 12.9 shows a no-contact penetrating radar with operation frequency 10 GHz and bandwidth 4 GHz, that was applied to scan a historical painted wall in order to detect a possible discontinuity between the masonry wall and the stone wall below [12]. Because of the priceless worth of the painting, contact was inappropriate. The focused images obtained are shown in Fig. 12.10. The discontinuity between masonry and stone walls is clearly detected at about 15 cm depth.

In engineering practice, it is often necessary to detect closely spaced layers inside masonry. In these applications, resolution appears to be a critical requirement and the classical time domain resolution given by equation 12.4 can be unsatisfactory. Methods based on direct frequency domain analysis are able to detect layers that are very closely spaced; indeed, because of multiple reflections inside a possible cavity in masonry, the radar response in frequency exhibits resonance frequency that is strictly related to the thickness of the cavity. With reference to Fig. 12.11, the multiple reflections give resonances at the following frequencies:

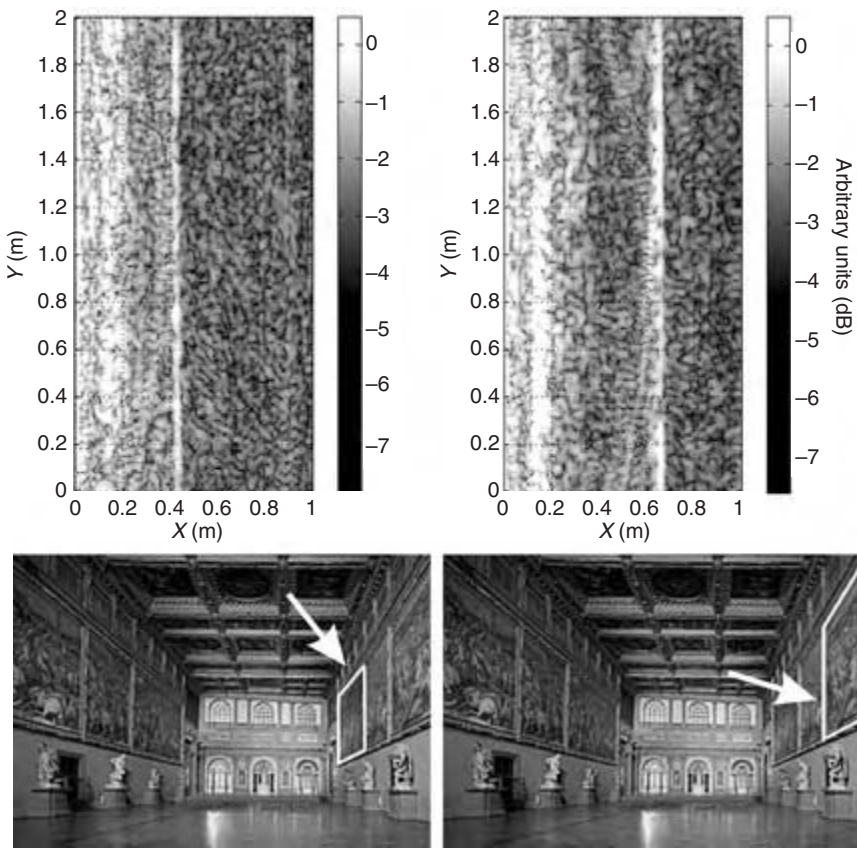
$$f_m = (2m-1)\frac{c}{4d} \qquad m = 1, 2, 3\ldots \qquad [12.5]$$

where d is thickness of an air-filled cavity and c is speed of light in a vacuum. Unfortunately, standard frequency domain methods need some *a priori* knowledge of internal geometry such as the number of interfaces and maximum depth. In contrast, in time domain, time gating allows for separate contributions of different portions of the structure under

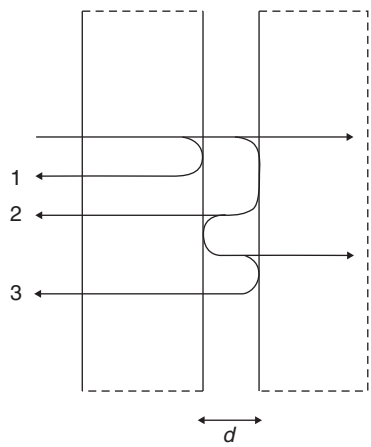


12.9 Radar acquisition on a historical painted wall [12].

test providing an easier physical interpretation of the radar signal. This is the reason time domain is often preferred in practical cases. An interesting advanced processing technique, the joint time frequency analysis (JTFA), can combine resolution and high S/N (signal to noise) of the frequency analysis with the effectiveness of time domain.



12.10 Radar images of two historical painted walls. The wall on the left is 40 cm thick. The wall on the right is 70 cm thick, as can be noted by the two focused radar images [12].



12.11 Resonance frequencies in a cavity inside masonry.

JTFA can be performed by using different mathematical tools, and the simplest is the short-time Fourier transform (STFT). STFT is basically a sliding window Fourier transform in time. By taking the Fourier transform of the windowed time data as the window is shifted in time, a two-dimensional time–frequency image is obtained. The STFT of a time signal *f(t)* is defined as

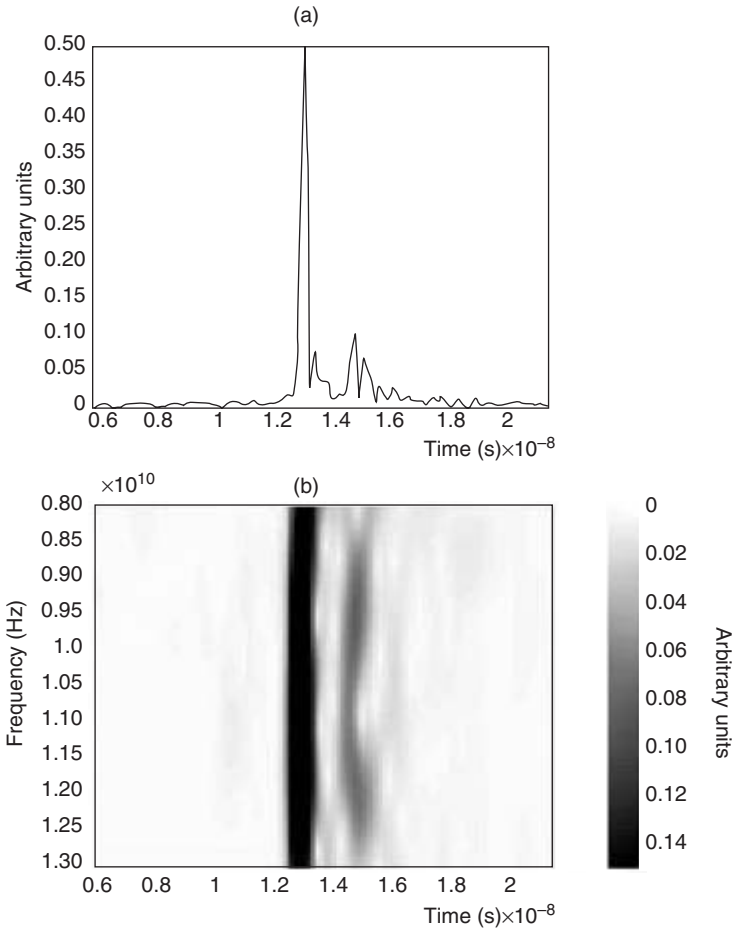
$$S(\tau,\Omega) = \int f(t)g(t-\tau)\mathrm{e}^{-j\Omega t}\mathrm{d}t \qquad [12.6]$$

where *g(t)* is a time window function. For example a hamming window can be used as *g(t)*. In the case of CW radar, *f(t)* is the inverse FFT of the experimental data. The unique feature of this kind of processing is the possibility of performing a local frequency analysis and simultaneously having a time representation of the signal. In other words, JTFA can combine the unique advantages of the frequency analysis and the effectiveness of time domain. Figure 12.12 shows an experimental radar acquisition on a test masonry facility with a controlled discontinuity [15]. Figure 12.12 (a) is the time domain trace: the peak at about 12.5 ns is the signal due to the first air–wall interface, the second peak at about 15 ns can be associated with a cavity, but from the time domain trace it is not evident because a cavity should be identified by two peaks (wall–air interface and air–wall interface). In the time-frequency plot obtained by STFT, at about 15 ns, two resonance frequencies are detectable, and equation 12.5 can be used to give the effective thickness of the cavity.

12.6 Thermal, mechanical or electromagnetic: what kind of energy for detecting discontinuity in masonry?

Generally speaking, in order to obtain information, some kind of energy has to be employed and the investigated medium must not be completely opaque to the employed energy. Thermal, mechanical, and electromagnetic energies are suitable for investigating masonry.

Thermal waves are undoubtedly the most penetrating. Furthermore, the amount of available energy for investigation can be huge compared with other kinds of energy and the sensitivity of modern thermo-cameras can detect very small temperature variations. Unfortunately, thermal sources are difficult to control. In most cases, the thermal source is natural heating during the day, and therefore the obtained images can be only qualitative. If an artificial source is employed, only a small zone can be investigated and, because of low propagation speed of thermal waves, a long time is needed (in half hour steps) for each investigated portion. In any case, thermal waves are not able to give direct depth information about the detected discontinuity directly, even in a controlled environment. The physi-



12.12 (a) Time analysis and (b) JTFA.

cal cause is that thermal waves are more diffusive than propagating waves such as sound or light. Depth information can be obtained only indirectly, for example by using equation 12.3, which gives the penetration depth of the exponentially damped wave diffusing in the investigated medium.

In order to obtain depth information (three-dimensional information about the investigated masonry), it is necessary to employ a propagating form of energy: mechanical or electromagnetic waves. Although the mathematics is very similar for sonic and electromagnetic waves, the effective values of the propagation characteristics are obviously very different, so the following main differences should be noted.

12.6.1 Wavelength

Propagation characteristics of any kind of wave depend mainly on wavelength λ, given by the following general relationship:

$$\lambda = \frac{\nu}{f} \qquad [12.7]$$

where ν is speed of wave and f is frequency. Electromagnetic waves propagate in masonry at about 1.5×10^8 m/s, with frequencies ranging from 100 MHz to 10 GHz (radar for structures mostly operates between 500 MHz and 2 GHz), therefore wavelengths range between 1.5 and 150 cm (with a typical value of about 15 cm). Sonic waves propagate in masonry at about 3000 m/s, frequencies range from 1 to 100 kHz, therefore wavelengths range between 3 and 300 cm.

It should be noted that, although sonic and electromagnetic waves operate at very different frequencies (so they need completely different electronics), they have comparable wavelengths. On the other hand, because a wave is able to detect only targets with dimensions comparable to its wavelength, both sonic and electromagnetic waves must have comparable wavelengths when employed to detect discontinuity in masonry.

12.6.2 Attenuation

Generally speaking, the intensity I (W/m^2) of a wave propagating in an attenuating medium is exponentially damped as follows:

$$I(R) = I_0 e^{-\alpha R} \qquad [12.8]$$

where I_0 is the intensity for $R = 0$ and α is an attenuation coefficient that depends strongly on material and especially on small inhomogeneities and discontinuities. Typically α is bigger for sonic waves, especially for inhomogeneous materials such as masonry, but for electromagnetic waves, α is dramatically increased by moisture, therefore such waves cannot be used in a number of practical cases when damp masonry (for example the foundations of a building) has to be investigated.

For both waves α increases with frequency, so it is a matter of fact that for penetrating it is necessary to use lower frequencies. On the other hand, resolution improves with bandwidth (see equation 12.4), which has to be a fraction of operation frequency. Therefore investigation depth and resolution are contrasting requirements: you can see a small object at a small distance or, in other words, you can see a large target at a large distance.

12.6.3 Back-reflection

The fraction R of energy back-reflected by a discontinuity has the same mathematical expression for mechanical and electromagnetic waves:

$$R = \left| \frac{1 - \frac{z_1}{Z_2}}{1 + \frac{Z_1}{Z_2}} \right|^2 \qquad [12.9]$$

For mechanical waves, Z_1 and Z_2 are the acoustic impedances of the two media separated by the interface. For electromagnetic waves, Z_1 and Z_2 have to be substituted by $\sqrt{\varepsilon_r^{(1)}}$ and $\sqrt{\varepsilon_r^{(2)}}$ with ε_r relative electric permittivity. The difference in acoustical impedance between air and masonry is very high, and therefore the back-reflected energy is practically all energy impinging the discontinuity. In contrast, the ratio between the square root of permittivity of masonry and air ranges between 2 and 3 and therefore the reflected energy ranges between 10% and 25%.

This is the main difference between mechanical and electromagnetic waves in the NDT of masonry. If a mechanical wave impinges a discontinuity filled with air it is completely reflected and is unable to detect other discontinuities behind. Masonry usually has voids, honeycombs, or detachments that prevent mechanical waves from propagating inside. In other words, an excess of sensitivity in detection of discontinuity prevents the discontinuities of interest being detected in a number of cases.

Finally, how can we answer the question about what kind of energy? The answer is obvious: all, if possible. Thermal, sonic and electromagnetic energies are substantially different, being based on completely different physical principles, so they give different and complementary information. Indeed, this conclusion is well known to technicians involved in the engineering practice of this kind of investigation. They consider they must be equipped and skilled in three kinds of completely different instrumentation and obviously they consider it an exciting aspect of their profession.

This sort of triad that constitutes the fundamentals of NDT practice is again far from the dreamed of 'universal instrument' able to penetrate and image any sort of masonry, able to detect the discontinuities of interest and able to ignore all non-significant inhomogeneities, but the three instruments are able to cover a significant part of common applications.

12.7 References

1. Sansalone, M. and Streett, W.B. (1997), *Impact-Echo Nondestructive Evaluation of Concrete and Masonry*. Bullbrier Press, Ithaca, NY.

2. Motz, M. and Haller, P. (2003), Impact-echo: new developments regarding hardware and software, *International Symposium (NDT-CE 2003) Non-Destructive Testing in Civil Engineering*.
3. Sadri, A. (2003), Application of impact-echo technique in diagnoses and repair of stone masonry structures, *NDT&E International* Vol. 36 pp. 195–202.
4. Kim, D.S., Kim, H.W., Seo, W.S., Choi, K.C. and Woo, S.K. (2002), Feasibility study of the IE-SASW method for nondestructive evaluation of containment building structures in nuclear power plants, *Nuclear Engineering and Design* Vol. 219 pp. 97–110.
5. Binda, L., Saisi, A. and Zanzi, L. (2003), Sonic tomography and flat-jack tests as complementary investigation procedures for the stone pillars of the temple of S. Nicolò l'Arena (Italy), *NDT&E International* Vol. 36 pp. 215–227.
6. Grinzato, E., Vavilov, V. and Kauppinen, T. (1998), Quantitative infrared thermography in buildings, *Energy and Buildings* Vol. 29 pp. 1–9.
7. Clark, M.R., McCann, D.M. and Forde, M.C. (2003), Application of infrared thermography to the non-destructive testing of concrete and masonry bridges, *NDT&E International* Vol. 36, pp. 265–275.
8. Maierhofer, C., Brink, A., Rollig, M. and Wiggenhauser, H. (2003), Detection of shallow voids in concrete structures with impulse thermography and radar, *NDT&E International*, Vol. 36, pp. 257–263.
9. Maierhofer, C. and Leipold, S. (2001), Radar investigation of masonry structures, *NDT&E International* Vol. 34, pp. 139–147.
10. Binda, L., Lenzi, G. and Saisia, A. (1998), NDE of masonry structures: use of radar tests for the characterisation of stone masonries, *NDT&E International* Vol. 31, pp. 411–419.
11. Parrini, F., Pieraccini, M. and Atzeni, C. (2004), A high-speed continuous wave GPR, *Proceedings of Tenth International Conference on Ground Penetrating Radar (GPR 2004)*, 21–24 June, Delft, The Netherlands, pp. 183–186.
12. Pieraccini, M., Mecatti, D., Luzi, G., Seracini, M., Pinelli G. and Atzeni, C. (2005), Non-contact intrawall penetrating radar for Heritage survey: the search of the 'Battle of Anghiari' by Leonardo da Vinci, *NDT&E International*, Vol. 38, pp. 151–157.
13. Hugenschmidt, J. (2002), Concrete bridge inspection with a mobile GPR system, *Construction and Building Materials* Vol. 16, pp. 147–154.
14. Pieraccini, M., Tarchi, D., Rudolf, H., Leva, D., Luzi, G., Bartoli, G. and Atzeni, C. (2000), Structural static testing by interferometric synthetic radar, *NDT&E International* Vol. 33, pp. 565–570.
15. Pieraccini, M., Luzi, G., Noferini, L., Mecatti, D. and Atzeni, C. (2004), Joint time-frequency analysis for investigation of layered masonry structures using penetrating radar, *IEEE Transactions on Geoscience and Remote Sensing* Vol. 42, pp. 309–317.

Index

AAR reactions 23
AASHTO 168–9, 217–19
AC impedance spectroscopy 8–10
accelerometers 74, 105–6, 119–20
accuracy of visual inspections 174–80
ACDS *see* automated chain drag system (ACDS)
acoustic emission (AE) testing 183–212
  amplitude of signal 191, 201, 209–10
  attenuation 191–2
  counts 201
  modal techniques 198–9
  monitoring systems 185–7
  noise levels 187–8
  primary emissions 184
  and reinforcement corrosion 188
  secondary (pseudo) emissions 184
  sensors 186–7, 199–203
  severity assessment 185
  source identification 185, 198–9
  source location 184–5, 192–8
    terminology 206–8
  standards 210–11
  threshold 201
  time-of-arrival (TOA) technique 184–5, 192–4, 197–8
  transient record analysis 210
  wave modes 189–91
  websites for information 211–12
  see also graphical data displays
acoustic testing 64–80
  chain dragging
    automated 69–80
    manual 66, 80
  coin-tap test 64, 65–6, 79–80
  electro-mechanical sounding devices 68–9
  global tests 64
  ground penetrating radar (GPR) 65, 67–8
  impact echo technique 65, 67–8, 248–50
  infrared thermography 65
  manual techniques 65–8
  rotary-percussion sounding system 68
  and wood decay 103
active thermography 253
aerial photogrammetry 227
aggregates 23
  alkali-reactive 25
alkali-carbonate reaction (ACR) 23
alkali-silica reaction (ASR) 22–59
  conditions for 24–6
  core samples 30–1, 33–4, 43
  crack and expansion measurements 35–7
  diagnosis 26–7, 54–6
  fast expansive reactions 23
  field inspections 27, 28
    assessment of results 40
  information sources 58–9
  laboratory investigations 27, 28–35
    assessment of results 40
    damage assessment 31–4
    microstructural analysis 31, 33, 54–5
  mapping of cracks 30
  monitoring methods 35–40
  Norwegian survey 41–3
  in railway sleepers 49–51
  reaction mechanism 24
  and relative humidity 25–6, 37–9, 47–9
  resistance to accepting 57
  rest expansion test 34–5
  slow/late expansive reactions 23
  and strength and stiffness 34
  ultrasonic pulse velocity (UPV) testing 34
  uranyl acetate test 28–9
amplitude of signals 191, 201, 209–10
anodic reactions 1–2
antennae 255
arms-length inspections 171
attenuation 191–2, 262
automated chain drag system (ACDS) 69–80
  accelerometers 74
  delamination maps 75–9
  hardware 70–1
  multiple systems 79
  signal processing 74–5
  and traffic noise 73–4, 79

back-reflection 263
bacterial infestation 135, 136
bending waves analysis 116
bonding condition of masonry 249
Bridge Inspector's Training Manual 173
brown rot fungi 95, 136

calcium hydroxide 24
calibration certificates for sensors 202
camera settings 222–3, 228, 231–4, 236–8
  see also photogrammetry; photography
carbonation testing 17–18
cathodic reactions 2
cement
  alkali content 25
  raw materials 23
chain dragging
  automated 69–80
  manual 66, 80
channel plots 204
chloride ion content analysis 16–17
Clallam County bridge 125–8
close-up photogrammetry 227, 242
coin-tap test *see* hammer sounding
color vision tests 176–7
colour intensity plots 208–9
concrete
  acoustic testing 64–80
  cracks in 30, 34, 35–7
  delaminations 64, 65–6, 75–80
  raw materials 23
  relative humidity 25–6, 37–9, 45–9
  resistivity measurements 15–16
  see also alkali-silica reaction (ASR); reinforcement corrosion
Concrete Petrography 54–5
condition rating system 142–5, 178, 218
constant phase element (CPE) 85–6, 92
Constitution, USS 112
control surveys 236
core samples 30–1, 33–4, 43
  damage rate index (DRI) 33–4
  Norwegian crack counting method 34
  rest expansion test 34–5
  and wood decay inspections 103–4
correlation plots 208
corrosion potential mapping 2–5
corrosion rate measurements 5–14
  AC impedance spectroscopy 8–10
  galvanostatic pulse technique 10–13
  linear polarization resistance (LPR) 5–8
  Tafel extrapolation 13–14
counter electrodes (CE) 5–7
cracks
  expansion measurements 35–7
  mapping 30
  Norwegian crack counting method 34
Crookes, Sir William 149
cubic panoramas 223–4
cylindrical panoramas 223–4

damage inspections 170
damage rate index (DRI) 33–4
decay inspections 94–6, 100–14, 135–6
  bacterial infestation 135, 136
  coring 103–4
  drilling 103–4
  electrical impedance spectroscopy (EIS) 94–6
  fungi 95, 100, 101, 103, 135, 136
  hammer sounding 103, 106
  insect activity 102, 135, 161–2
  interior deterioration 102–5
  pile decay 123, 129–30
  plant/moss growth 102
  probing 102, 173
  shell-depth indicator 104
  Shigometer 104
  sounding methods 103, 106
  staining and discoloration 102
  stress wave propagation 105–11
  termite damage 161–2
  tomography scanners 104–5
  ultrasonic testing 136–46
  visual inspections 87, 101–2
  weathering 136
  X-rays 104–5
delaminations 64, 65–6, 75–80
Delamtect 69
delayed ettringite formation (DEF) 51
Delorme dome 152
density of wood 134
Denver Union Pacific railway bridge 128–9
detect discs 222
dielectric analysis 83–4
digital cameras 228–9, 237–8, 244
digital radioscopy analysis 149–64
  EPIX scanner 154–5
  equipment 153–5
  history of wood building radiography 152
  monitoring devices 155
  RTR-4 imager 154
  safety issues 153–4
  XR200 X-ray source 153–4
  see also X-rays
dissipation attenuation 192
distributed models 85
distribution analysis 209
documentation 173–4, 178–80, 220
  of historic structures 243
drilling 103–4
dry velocities 123–4, 130

Edison, Thomas 149
electric bridge 89
electrical impedance spectroscopy (EIS) 83–97

advantages and limitations 87–8
constant phase element (CPE) 85–6, 92
and decay inspection 94–6
and dielectric analysis 83–4
distributed models 85
electrode configuration 90
equipment and procedure 88–91
impedance plane representation 85
lock-in amplifiers 89
lumped models 85
moisture content measurements 88, 91–4
polarisation 87, 89–90
portable devices 93–4, 97
voltage excitation 89
electrical impedance tomography (EIT) 83
electro-mechanical sounding devices 68–9
electrochemical testing 1–15
electromagnetic waves 260–3
Elgeseter bridge 43–9
EPIX scanner 154–5
event (in AE tests) 206
excitation of piles 118–19

Federal Highway Act (1956) 166
Federal Highway Administration (FHWA) 17, 166, 168–9
FFT (fast Fourier transform) 123, 248–9, 260
fibre saturation point (FSP) 92
field inspections *see* visual inspections
flash memory cards 223, 237
flash photography 243
floor rafters 143
fluoroscopy 149–50
focal length 228, 231–2
focusing techniques 255–7
FotoG software 232, 238–40
fungi 95, 100, 101, 103, 135, 136

galvanic corrosion tests 15
galvanostatic pulse technique 10–13
graphical data displays 203–10
channel plots 204
colour intensity plots 208–9
correlation plots 208
distribution analysis 209
historical plots 204
location displays 204, 206
ground penetrating radar (GPR) 65, 67–8

hammer sounding
and delamination 64, 65–6, 79–80
standards 65
and wood decay 103, 106
Hatchie River Bridge 167
historical plots 204
hit (in AE tests) 206
hot spots 224–6
humidity *see* relative humidity

imaging systems 154–5
impact echo technique 65, 67–8, 248–50
in-depth inspections 171, 180, 181
infrared thermography 65
initial inspections 170
insect activity 102, 135, 161–2
inspectors
color vision tests 176–7
Program Managers 171–2
qualifications 171–2
Team Leaders 172
training courses 240–1
typical inspector study 174–7
see also visual inspections
interpretive photogrammetry 226–7

Jefferson, Thomas 152
joint tests 159–61
JTFA (joint time frequency analysis) 258–60

King City Bridge 22
Kirkland Air Force Base 112
knots 134

laboratory investigations 27, 28–35
assessment of results 40
damage assessment 31–4
microstructural analysis 31, 33, 54–5
ultrasonic testing 138–40
lag screw placement 118–19, 120
Lamb waves 190
legislation 168
linear polarization resistance (LPR) 5–8
location displays 204, 206
location group (in AE tests) 207
lock-in amplifiers 89
lockout time (in AE tests) 207
longitudinal stress waves 117–24
accelerometer attachment 119–20
data acquisition systems 120
dry velocities 123–4, 130
excitation of piles 118–19
impact hammer types 119
lag screw placement 118–19, 120
and pile decay 123, 129–30
and pile length determination 117
reflection time estimation 121–2, 123–4
resonant frequency 120–1, 123–4, 130
sensors 119–20
stress wave relationships 120–1
wet velocities 123–4, 130
longitudinal waves 189–90
Love waves 190
lumped models 85

Manual for Condition Evaluation of Bridges 169
mapping of cracks 30
masonry structures 247–53
  attenuation 262
  back-reflection 263
  bonding condition 249
  depth information 261
  energy type 260–3
  impact echo technique 248–50
  non-destructive testing 247–8
  penetrating radar 253–60
  sonic tomography 250–1
  thermography 252–3
  visual inspections 248
  wavelength 262
Maxwell, James Clerk 150
measurement
  of concrete resistivity 15–16
  of corrosion rate 5–14
  of cracks 35–7
  of moisture content 88, 91–4
  of relative humidity 37–8, 45–6
  tools 173
  of vertical and horizontal clearances 242
mechanical waves 260–3
memory cards 223, 237
metric cameras 228
metric photogrammetry 226–7
Mianus River Bridge 167
microstructural analysis 31, 33, 54–5
moisture content 107–9, 134
  measuring 88, 91–4
  see also relative humidity
mortise joints 160–1

Narbonne House 152
National Bridge Inspection Program (NMIP) 166–7
National Bridge Inspection Standards (NBIS) 168, 217, 219
National Bridge Inventory (NBI) 167
Norwegian crack counting method 34
nuclear magnetic resonance (NMR) 88

ortho-photos 243
Oslo, Veritas House 51–4

panoramas 221, 223–4
parallel seismic method 116
Parthenon 133
Pavilion I 158–9
pen dosimeter 155
penetrating radar 253–60
photo-textured modeling 243
photogrammetry 216–17, 226–40, 242–4
  advantages 242
  aerial photogrammetry 227
  analytical processing 238–40
  camera lens calibration 228, 231–4, 236–8
  camera stations 235–6
  close-up photogrammetry 227, 242
  control surveys 236
  definition 226
  digital cameras 228–9, 237–8, 244
  documentation of historic structures 243
  focal length 228, 231–2
  history 226
  image acquisition 236–8
  image preparation 238–40
  image-object relationship 227–8
  interpretive photogrammetry 226–7
  measurement process 230–1
  metric cameras 228
  metric photogrammetry 226–7
  semi-metric cameras 229–30
  target layout 234–5
  terrestrial photogrammetry 227
  triangulation 228, 230
photographic documentation 178–80
photography 220–3
  camera settings 222–3
  detect discs 222
  flash photography 243
  panoramas 221, 223–4
  tripods 221–2
physico-chemical testing 15–18
piezoelectric sensors *see* sensors
pile decay inspections 123, 129–30
pile length testing 115–31
  bending waves analysis 116
  field equipment 116–17
  longitudinal stress waves 117–24
  parallel seismic method 116
  sonic echo method 115–16
Pilodyn 102
plant/moss growth 102
Pocket Ionization Chamber 155
polarisation 87, 89–90
potential mapping 2–5
preservative treatments 109
probing 102, 173
Program Managers 171–2

qualifications of inspectors 171–2
  color vision tests 176–7
Quebec City 56
QuickTime Virtual Reality *see* virtual reality

radar
  ground penetrating radar (GPR) 65, 67–8
  and masonry structures 253–60
radioscopy *see* digital radioscopy analysis
railway sleepers 49–51
Ramin sticks 37–8, 45–6
rate of corrosion *see* corrosion rate measurements
Rayleigh waves 190

Realviz Stitcher 224
reference electrodes (RE) 5
reinforcement corrosion 1–18
  acoustic emission (AE) testing 188
  anodic reactions 1–2
  carbonation testing 17–18
  cathodic reactions 2
  chloride ion content analysis 16–17
  concrete resistivity measurements 15–16
  corrosion potential mapping 2–5
  corrosion rate measurements 5–14
  electrochemical testing 1–15
    noise measurements 14
  galvanic corrosion tests 15
  physico-chemical testing 15–18
  remote monitoring systems 14–15
relative humidity 25–6, 37–9, 47–9
  measurements 37–8, 45–6
  see also moisture content
reliability of visual inspections 174–80
remote monitoring systems 14–15
resistivity measurements 15–16
resonant frequency 120–1, 123–4, 130
rest expansion test 34–5
rods embedded in timber beams 158–9
Roentgen, Wilhelm Conrad 149
roof rafters 143, 156–8
rotary-percussion sounding system 68
routine inspections 170, 177–80, 181, 242
RTR-4 imager 154

Sakkara pyramid 133
Salem, Narbonne House 152
scanning electron microscopy (SEM) 31
Schoharie Creek Bridge 167
scour resistance 115, 167–8
semi-metric cameras 229–30
sensors 119–20, 186–7, 199–203
  calibration certificate 202
  couplants 203
  electrical humidity sensors 37
  placement 186–7
Seven Gables House 152
shell-depth indicator 104
Shigometer 104
shrinkage of wood 134
Silver Bridge 166, 167
sliding micrometer (ISETH) measurements 35–6
soft rot fungi 95
sonic echo method 115–16
sonic tomography 250–1
sounding methods *see* chain dragging; hammer sounding
special inspections 171
standards
  acoustic emission (AE) testing 210–11
  hammer sounding 65
  for visual inspections 168, 217–19
Stanton, Thomas 22
Starkville University Street overpass 79–80
steel corrosion *see* reinforcement corrosion
STFT (short-time Fourier transform) 260
stitching programs 224
strength and stiffness
  of concrete 34
  of wood 135
stress wave propagation 105–11
  accelerometers 105–6
  concept and limitations 105–6
  and moisture content 107–9
  and preservative treatments 109
  transmission time measurement 109–10
stress wave relationships 120–1
Sylvatest 128

Tacoma Dome 133
Tacoma Narrows Bridge 166
Tafel extrapolation 13–14
Team Leaders 172
tenon joints 160–1
termite damage 161–2
terrestrial photogrammetry 227
thermal waves 260–3
thermography 252–3
TIFF files 154, 237
timber *see* wood
time-of-arrival (TOA) technique 184–5, 192–4, 197–8
TLD (thermoluminescent badges) 155
tomography scanners 104–5
tools for visual inspections 172–4
transient record analysis 210
transverse waves 189–90
TRESTLE 112
triangulation 228, 230
tripods 221–2
Trondheim, Elgeseter bridge 43–9
trusses 143, 156–8

ultrasonic pulse velocity (UPV) 34
ultrasonic testing 136–46
  condition-rating system 142–5
  in-service evaluation 140–6
  laboratory investigations 138–40
Union Pacific railway bridge 128–9
University Street overpass 79–80
uranyl acetate test 28–9

velocity (in AE tests) 207
Veritas House 51–4
vibrating wire sensors 35
virtual reality 216, 217–26, 240–2
  and bridge site 241–2
  documentation 220
  equipment 220
  file size 241

hot spots 224–6
inspector training courses 240–1
output files 224–6
panoramas 221, 223–4
photographic procedures 220–3
playback settings 224–6
posting on the Internet 241
stitching programs 224
VR Worx 224
visual aids 173
visual inspections 166–81, 217–19
accuracy 174–80
alkali-silica reaction (ASR) 27, 28, 40
color vision tests 176–7
condition rating system 178, 218
damage inspections 170
documentation 173–4, 178–80
history of structural inspections 166–9
in-depth inspections 171, 180, 181
initial inspections 170
legislation 168
Manual for Condition Evaluation of Bridges 169
masonry structures 248
photographic documentation 178–80
publications related to 169
qualifications of inspectors 171–2
reliability 174–80
routine inspections 170, 177–80, 181, 242
special inspections 171
standards 168, 217–19
tools 172–4
of wooden structures 87, 101–2
see also decay inspections; inspectors
voltage excitation 89
VR Worx 224
wave modes 189–91
weathering 136
wet velocities 123–4, 130
white rot fungi 95, 136
wood
acoustic testing 103
density 134
electrical impedance testing 83–97
fibre saturation point (FSP) 92
history as a building material 133
joint tests 159–61
knots 134
mechanical properties 135
moisture content 134
measuring 88, 91–4
physical properties 134
rods embedded in timber beams 158–9
shrinkage 134
strength and stiffness 135
ultrasonic testing 136–46
see also decay inspections; digital radioscopy analysis; pile length testing
wooden sticks (Ramin) 37–8, 45–6
wrap (in AE tests) 208

X-rays
discovery 149
exposure limits 131
physics of 150–1
uses 149
wavelength 151
and wood decay inspections 104–5
see also digital radioscopy analysis
XR200 X-ray source 153–4